MAGNETIC RESONANCE AND SUSCEPTIBILITY STUDIES OF SOME INTERMETALLIC COMPOUNDS AND RARE-EARTH ALLOYS

Thesis submitted for the Degree of

Doctor of Philosophy

at the University of London

by

STEWART ERNEST MALE

Physics Department
Imperial College of Science and Technology
London SW7

February 1976

ABSTRACT

A number of intermetallic compounds and solid solution alloys have been studied by x-band paramagnetic resonance. One system, $LaNi_5$- Gd, has also been investigated by magnetic susceptibility and electrical resistivity measurements.

The EPR behaviour of $(La_{1-x}Gd_x)Ni_5$ has been studied at various concentrations from x = 0.003 to x = 1. In the low concentration ($x < 0.1$) regime negative paramagnetic g-shifts were observed ($\Delta g = -0.128$ for $x = 0.005$), the g-shift reducing as the concentration was increased. The temperature dependence of the g-value and the linewidth have been analysed in terms of the onset of magnetic order in contrast to the previous interpretation of dynamic effects in the EPR bottleneck.

A Faraday magnetic susceptibility balance was constructed and has been used to study the magnetic properties of $LaNi_5$- Gd. The apparatus is capable of measurements ranging from 2K to room temperature, in fields up to 8.5KOe and with a force resolution of one millidyne.

Compounds with Gd concentrations greater than x = 0.1 show ferromagnetism, deviations from the Curie-Weiss law setting in at temperatures well above the ordering temperature. Resistivity measurements show a sharp maximum in the region of the ordering temperature. These effects have been interpreted in terms of an extensive region of short range order.

The linewidth and g-value have been measured for the high concentration compounds. A minimum in the linewidth was observed at temperatures well above the Curie temperature. In compounds with Gd concentrations greater than 50at.% a double resonance has been

observed between certain temperature limits.

The compound $LaAl_2$- Gd has been investigated at concentrations at which spin glass ordering is believed to occur. A temperature dependent linewidth and g-shift was observed, the latter becoming negative in the paramagnetic region. Solid solutions of Y-Gd and Sc-Gd have been examined at spin glass concentrations. The EPR measurements for the above alloys are consistant with the spin glass model.

ACKNOWLEDGEMENTS

I would like to express my sincere thanks to my supervisor, Professor B.R.Coles, for his interest, encouragement and help throughout the course of this work. I am also indebted to Dr.R.H.Taylor for teaching me how to use the electron paramagnetic resonance spectrometer and for his constant assistance.

I would also like to thank Dr.D.Griffiths for his advise on experimental matters, Dr.H.E.N.Stone for his help with many metallurgical problems and all the members of the Metal Physics Group with whom I have had many valuable discussions.

Finally, I would like to thank my wife for typing this thesis and for her patience and encouragement while this work was being written.

I am grateful to the Science Research Council for providing a studentship for this work.

CONTENTS

INTRODUCTION

Magnetism in alloys has been an intriging problem for many years, the basis of which is the formation of magnetic moments and how, once formed, they interact. This work will be concerned with the consequences of the latter - the onset, type and properties of the magnetically ordered state.

Ordering may occur in a variety of ways, depending on the interactions present, the two most well known being ferromagnetic and antiferromagnetic. Recently a new phase has been recognized, known as a magnetic or spin glass state, the magnetic behaviour of which is still not fully understood. A spin glass phase occurs in a system with spatially random moments and competing exchange interactions.

Chapter 1 deals with the formation of a local moment, chapter 2 and chapter 3 with the interaction of local moments and magnetic ordering.

The object of this work is to investigate the magnetic behaviour of certain metallic systems which contain atoms with well defined magnetic moments (Gd^{3+} and Mn^{2+}) and correlate the results with the magnetic ordering in the systems. The major part of the investigation was on the intermetallic compound $LaNi_5$- Gd which was of interest because of the dynamics of the Gd local moment and the magnetic ordering process. The remainder of the work was mainly on systems believed to be spin glasses (Y- and Sc-Gd and $LaAl_2$- Gd). Finally, the electron paramagnetic resonance (epr) of PdPt - Mn was investigated.

The intermetallic compounds and solid solution alloys studied in this work were examined by the technique of epr. This technique has been widely used for studying the dynamics of local moments and recently for investigations of magnetic ordering. The theory of

magnetic resonance is given in chapter 4.

Additional magnetic information was obtained from electrical resistivity and magnetic susceptibility measurements. The experimental techniques for all the above measurements are described in chapter 5, together with a detailed account of the construction of a Faraday magnetic susceptibility balance.

In chapter 6 the results are presented and discussed.

CHAPTER 1

THE THEORY OF LOCALIZED STATES IN METALS.

In this chapter a brief outline of the theory of magnetism in dilute alloys is presented. There are many detailed reviews of the dilute alloy problem from the mainly experimental (Heeger (01), Daybell and Steyert (02),Wohlleben and Coles (03), Rizzuto (04) and Gruner (05)) to the theoretical (Kondo (06) and Fisher (07)), therefore a detailed discussion is unecessary here.

Transition metal (3d) atoms dissolved in a metallic host show a variety of electrical and magnetic behaviour (02). Any theory attempting to explain these properties must answer two fundamental questions: "what conditions lead to the formation of a local moment?" and "what are the implications of the interaction between the local moment and the conduction electrons?". The first question has been investigated by Friedel (08) and then later by Anderson (09). The second question assumes a moment and has been attacked by the use of the s-d exchange Hamiltonian (10) (11). Under certain conditions this model can be derived from Anderson's theory.

1.1 Formation of a moment.

Friedel used the theory of resonant scattering to treat the problem of local moment formation. Anderson and also Wolff (12) treated the same problem mathematically, but based their ideas on those of Friedel. The essence of the problem is that the conduction electrons of the metallic host interact with the d-electrons of the transition atom impurity to produce a local impurity state with a finite energy width Δ.

The potential introduced into the matrix by the impurity atom acts as a scattering centre, if this potential is not quite strong enough to create a bound state then a "virtual" bound state (VBS) is produced.

This state may have the same energy as the host conduction electron states, if so then an admixture of states occurs to give rise to new states. This produces a broad region in space and energy with an energy width Δ , hence a lifetime $\tau_\Delta = \hbar/\Delta$ and an excess electron density of $\Delta\rho(r)$. This is known as a virtual bound state. The screening condition is given by the Friedel sum rule (8b),

$$Z = \frac{2}{\pi}\sum_{l}(2l+1)\delta_l(E_F) \qquad \text{.....} \qquad 1$$

where Z is the excess charge of the impurity compared with the matrix and $\delta_l(E_F)$ are the phase shifts at the Fermi surface.

Using the concept of a VBS Friedel was able to explain the residual resistivities of the first row transition metals in aluminium. He assumed that each d-shell gives rise to only one VBS with room for ten electrons. On substituting different atoms from the series Ti to Zn into the aluminium matrix the VBS is successively filled. As the actual position of the VBS relative to the Fermi energy is decided by the number of 3d electrons on the impurity atom, then for a given number of 3d electrons the VBS will fall at the Fermi level and hence give rise to an enhanced scattering, therefore maximizing the residual resistance (08).

For copper based alloys, a mechanism for allowing the VBS to become spin split and produce a double resonant peak in the density of states had to be found. Blandin and Friedel (13) derived a condition for the instability of the non-magnetic state,

$$2\,E_{ex}\rho_l(E_F) > 1$$

where E_{ex} is the average value of some effective exchange and $\rho_l(E_F)$ is the density of states for the VBS at the Fermi surface. The parameter E_{ex} needs some explanation. In Friedel's original work, the mechanism which splits the spin-up and spin-down energies was assumed to be some sort of atomic exchange (Hunds rules), although no detailed calculations were performed. E_{ex} was usually taken as a more or less empirical splitting

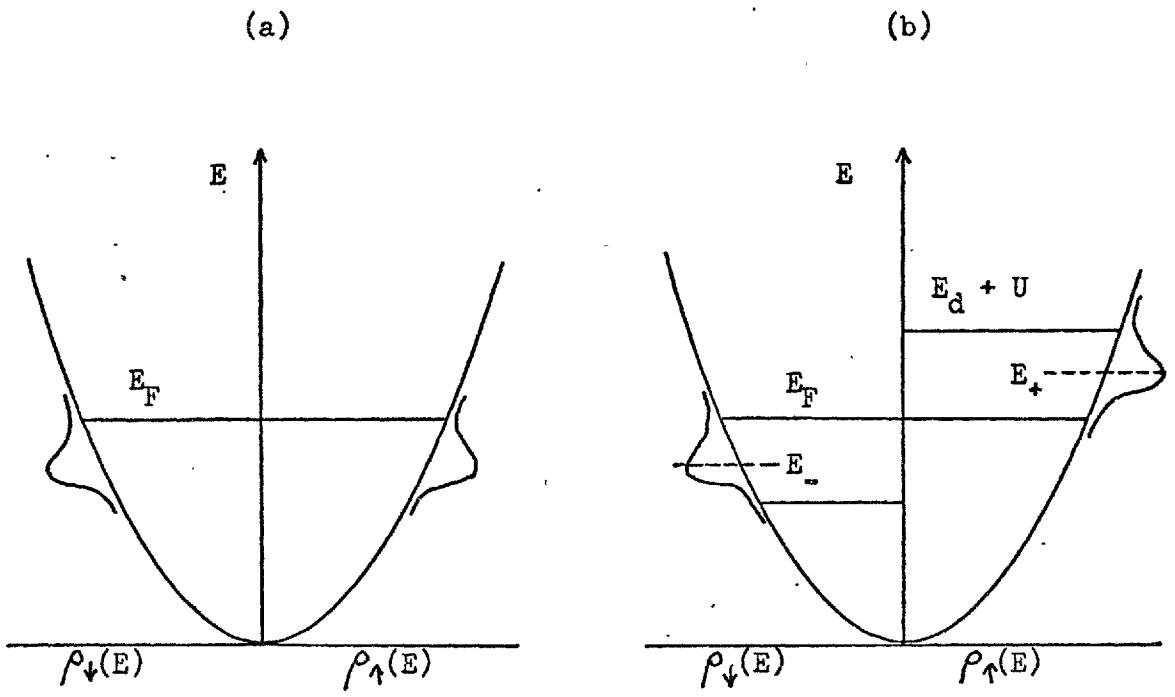

FIG.1 a. The density of states distribution for a free electron gas with the addition of a virtual bound state, (non-magnetic).

b. The density of states distribution in the magnetic case (after reference 9).
$E_+ = E_d + U\langle n_{d\downarrow}\rangle$, $E_- = E_d + U\langle n_{d\uparrow}\rangle$

factor. Subsequently it was associated with the exchange self energy of the localized state i.e. the Coulomb repulsion of opposite spin electrons on the same local orbital, this approach came mainly from Anderson (09).

He considered the impurity as a localized extra orbital embedded in a free electron sea with energy E_d, relative to the Fermi energy. Assuming a localized moment exists with an electron of say, spin-up, then if a spin down electron attempts to occupy the same level, it will see the full Coulomb repulsion U between it and the d-electron already on the localized orbital. Hence it could only occupy an energy level of value E_d+U, assumed to be empty by the initial condition that a moment exists and hence is above the Fermi level. The localized level is broadened and shifted due to the s-d mixing (see later), this pushes the high energy tail of its energy distribution above the Fermi level so that it is partially emptied; Therefore the number of localized spin-up electrons may be effectively less than one (see Fig. 1).

The Coulomb interaction which splits the local orbital into spin-up and spin-down states has the form $Un_{d\uparrow}n_{d\downarrow}$ where $n_{d\uparrow}$ and $n_{d\downarrow}$ are the number operators for the electrons with spin-up and spin-down on the localized level and U is the Coulomb integral given by the expression:

$$U = \int |\varphi_d(r_1)|^2 \frac{e^2}{r_{12}} |\varphi_d(r_2)|^2 \, d\tau_1 d\tau_2.$$

The Hamiltonian given by Anderson to describe the local impurity-conduction electron system for the case of orbital non-degeneracy is given by the following equation:

$$H = \sum_\sigma \epsilon_k n_{k\sigma} + \sum_\sigma E_d \, n_{d\sigma} + Un_{d\uparrow}n_{d\downarrow} + \sum_\sigma V_{dk}(C^*_{k\sigma}C_{d\sigma} + C^*_{d\sigma}C_{k\sigma}) \quad \ldots 2$$

the first term is the band energy, the second is the unperturbed energy

of the d-state and the last is the s-d interaction term, the so-called admixture energy. Solutions of the above Hamiltonian in the Hartree-Fock (HF) approximation have been obtained by many authors (09), (06), (14). The following is a summary of the results.

The energy width of the local state is given by a straight forward application of the Golden Rule,

$$\Delta = \pi \overline{|V_{dk}|^2} \rho(E_F) \quad \ldots\ldots\ldots\ldots\ldots\ldots \quad 3$$

where $\rho(E_F)$ is the density of states of the host evaluated at the Fermi surface and $\overline{|V_{dk}|^2}$ is the average of the squared modulus of the admixture matrix element. The density of states of the local level is Lorentzian in form and is given by,

$$\rho_{d\sigma}(E) = \frac{1}{\pi} \frac{\Delta^2}{(E - E_d)^2 + \Delta^2} \quad \ldots\ldots\ldots\ldots\ldots \quad 4$$

To preserve charge neutrality then

$$\langle n_{d\sigma} \rangle = \int_{-\infty}^{E_F} \rho_{d\sigma}(E) dE$$

which is equal to the total number of d-electrons introduced by the impurity. This is effectively a self-consistency condition which leads to the following two regimes:

(1) Non-magnetic $\langle n_{d\uparrow} \rangle = \langle n_{d\downarrow} \rangle$: $U/\Delta\pi < 1$.

(2) Magnetic $\langle n_{d\uparrow} \rangle \neq \langle n_{d\downarrow} \rangle$: $U/\Delta\pi > 1$.

The tranition between these two limits should be smooth owing to the local nature of the problem.

The Anderson Hamiltonian may be generalized to include the effects of orbital degeneracy (15) (16). If the orbital quantum number of the localized states is 1 then the condition for the appearance of magnetism is $(U + 21J)/\Delta\pi > 1$ for spin magnetism and $(U - J)/\Delta\pi > 1$ for orbital magnetism, J is the exchange integral. The existance of the intra-atomic exchange integral J helps the formation of a spin moment but opposes

the formation of an orbital moment (17). The results can be summarized on a phase diagram as shown in Fig. 2.

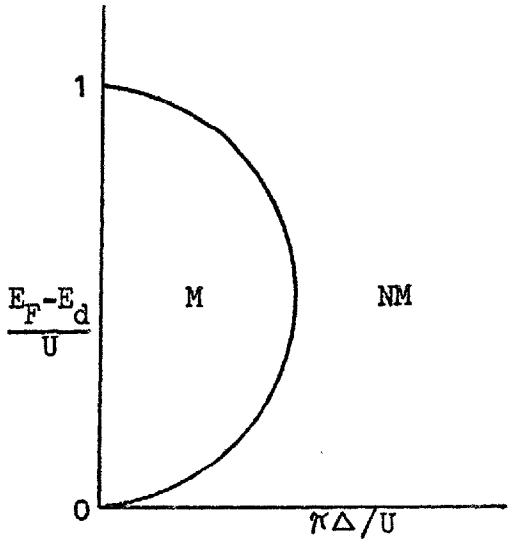

FIG.2 Regions of magnetic (M) and non-magnetic (NM) behaviour.

1.2 The s-d exchange.

In this section we shall be mainly interested in the magnetic region of the phase diagram in Fig. 2. The s-d exchange interaction is given by the equation (11) (18)

$$H_{sd} = - J_{sd}\, \underline{S}.\underline{s} \qquad \ldots\ldots\ldots\ldots\ldots\ldots\ldots\ldots \quad 5$$

where $\underline{S}$ is the impurity spin and $\underline{s}$ is the conduction electron spin. There are two contributions to J_{sd}, an antiferromagnetic covalent admixture (19) and a much smaller direct ferromagnetic s-d contribution, the overall coupling being antiferromagnetic.

The impurity is not perfectly localized, therefore H_{sd} cannot be represented as an isotropic zero range interaction. J_{sd} must be wave vector dependent and also possess the symmetry of the resonant scatterer (20), hence

$$J(\underline{k}-\underline{k}') = J_{eff}\, P_1(\cos\theta)$$

where θ is the angle between $\underline{k}$ and $\underline{k}'$ and $P_1(\cos\theta)$ is the Legendre polynomial.

The Hamiltonian in expression (5) assumes that the impurity has a well defined spin. This corresponds to $U/\Delta\pi > 1$ in the Anderson model (the strong magnetic limit). Schrieffer and Wolff (34) have transformed the Anderson Hamiltonian for the case of weak s-d coupling (magnetic limit) into a form similar to equation (5). This links the s-d exchange model with the parameters of the Anderson model:

$$J_{eff} = \frac{2|V_{kd}|^2 U}{E_{df}(E_{df} + U)}$$

$$E_{df} = E_d - E_f$$

The s-d Hamiltonian was used by Kondo (18) in an attempt to explain the anomalies found in the susceptibility, resistivity and specific heat of some dilute alloys. For example, the resistance minimum found in dilute CuFe (02); Daybell (21) and Van Den Berg (22) review in detail the experimental properties of such alloys. Essentially Kondo analysed the interaction of an impurity with spin $s=\frac{1}{2}$ with the conduction electrons by the use of scattering theory taken beyond the first Born approximation. He found the cross section acquired a logarithmic singularity as the temperature tends to zero. The magnetic contribution to the resistance is given by

$$r_m = cr(1 + N(0)J\ln(k_BT/D) + \ldots)$$

where c is the impurity concentration, r the first Born scattering term, J is the s-d exchange, N(0) is the density of states and D is a constant of the order of E_f. This logarithmic term in the resistance combined with the phonon contribution, which is proportional to the temperature, explains the resistance minimum found in some dilute alloys. Experimental results (23) (24) show that the logarithmic behaviour appears in a number of other properties.

The divergence of the scattering cross section with decreasing temperature indicates that below a certain temperature -

the Kondo temperature - the second order term is larger than the first order one and the convergence of the Born series is in doubt. The Kondo temperature is given by

$$kT_K = D\, e^{-1/\, J\, N(0)}$$

for $J<0$, the antiferromagnetic coupling case. The divergence is a result of the internal degree of freedom of the impurity which couples successive collisions, introducing indirect correlations between conduction electrons. This means that a many-body quasibound state is formed by the local moment and the conduction electrons. Below the Kondo temperature the magnetic moment disappears and any complete theory must explain this.

The exact ground state at T = 0 is still unclear. Nagaoka (25) (26) derived a self consistent solution below T_K and suggested that a long-range antiparallel spin polarization cloud would build up in the conduction electron gas, thus reducing the effective spin, with complete cancellation resulting at T = 0. Various authors have extended Nagaoka's original idea (41) (42). From the recent work of Wilson (27) it now seems likely that the ground state at T = 0 is a non-magnetic singlet. He suggested that the low temperature properties could be obtained from the limiting case of strong antiferromagnetic effective exchange coupling ($J \gg D$) between the impurity and the conduction electrons. The ground state is then a singlet in which the internal degree of freedom is frozen. This singlet may be polarized resulting in interactions amongst the conduction electrons. This gives a model similar to the local spin fluctuation theory.

Experimentally below T_K (specific to each alloy system as it depends on JN(0)) the impurity becomes non-magnetic in the sense that the measured susceptibility has little or no temperature dependence (29) (02). Therefore two regions can be defined, the high temperature region

($T > T_K$) where the impurity is magnetic and the low temperature region ($T < T_K$) where the impurity is non-magnetic, the transition between the two phases should be gradual with no critical points (30).

The weak resistance minimum found in AlMn and AlCr (31) started a new approach to the local moment problem. The physical parameters of these alloys indicate that they are a borderline case between the magnetic and non-magnetic regions in the Anderson sense ($U+4J/\Delta\pi \simeq 1$), therefore a good starting point for a theoretical description is the non-magnetic Anderson model. Rivier and co-workers (32) (33) developed such a theory by the use of local spin fluctuations.

1.3 Local Spin Fluctuations.

Essentially the question of the existence of a moment is a matter of time. For example, if the fluctuations in the spin density are sufficiently slow on the time scale of a given experimental probe then there appears (for that experiment) to be a moment (03). The effect of any finite lifetime is unobservable if $\tau_{sf} < \hbar / k_B T$; therefore as long as $k_B T > \hbar / \tau_{sf}$ the impurity behaves like a well defined local moment. τ_{sf} is known as the local spin fluctuation (LSF) lifetime.

This can be pictured as a process whereby many thermal fluctuations occur in the time occupied by one spin fluctuation, hence a thermal average moment appears. If the impurity spin fluctuates at a rate which is greater than that produced by thermal fluctuations, the impurity appears non-magnetic. The boundary between the two regions defines the LSF temperature:

$$T_{sf} = \hbar / k_B \tau_{sf}.$$

The theory of local spin fluctuations as developed for dilute alloys by Rivier et al (43) links τ_{sf} and the parameters of the non-degenerate Anderson model

$$\tau_{sf} = (1 - U/\Delta\pi)^{-1}$$

The theory of LSF is capable of explaining the disappearance of the impurity moment at low enough temperatures and also the simple power laws which are observed for many physical properties (35) (36). For example, the resistance and specific heat below T_{sf} are given by (05) (37)

$$r = r_o (1 - \pi^2 t^2 /3)$$

$$C_v = 5\pi k_B t (1 - t^2)$$

where $t = (T /T_{sf})$. For the high temperature region ($T > T_{sf}$) there are no quantative results.

This type of LSF theory is essentially different from that of Lederer and Mills (38) and others (39). In the Rivier theory the electron must scatter into the extra d-orbital before an interaction with the local spin takes place. Whereas in the Lederer and Mills theory the conduction electron-LSF interaction is a direct result of the impurity scattering. Typical applications of the latter are transition metal impurities in transition metal hosts, PdNi (38) and PtNi (40) are good examples.

The situation may now be summarized. In the magnetic region (in the Anderson sense, $U/\Delta\pi > 1$), the s-d Hamiltonian can be used giving Kondo type effects and a characteristic temperature T_K. Anomalies in resistance and specific heat appear when passing through the Kondo temperature. In the non-magnetic region local spin fluctuation theory is more appropriate; this also gives rise to a characteristic temperature T_{sf}. The question that now arises is, are the two theories different aspects of the same model?

Strictly the s-d model is valid only in the magnetic region and the LSF theory in the non-magnetic region. Both models give characteristic fluctuation times. In the spin fluctuation model it is τ_{sf}, which is determined by the d-d correlations at the impurity site. In

the s-d model it is the s-d correlation time τ_K. If these characteristic times are independent with $\tau_{sf} \gg \tau_K$, an alloy should behave differently from one with $\tau_K > \tau_{sf}$. The first case would correspond to a Kondo type system and the second to a LSF alloy. Conversely if τ_{sf} and τ_K are identical, even though the models are formulated differently, the nature of the transition and the low temperature state should be similar for all systems. The evidence seems to point to the second situation and has been summarized by Gruner (05). He compared CuFe which is usually analysed on the basis of the s-d model with AlMn usually interpreted by LSF theories, and found that there was little significant difference between the two alloys on experimental grounds.

REFERENCES CHAPTER 1

1. HEEGER, J.A., Solid St. Phys., Vol.23, edited by F.Seitz and D. Turnbull (New York: Academic Press) 1969.

2. DAYBELL, M.D. and STEYERT, W.A., Rev. Mod. Phys., 40, 380 (1968).

3. WOHLLEBEN, D. and COLES, B.R., Magnetism Vol. V, edited by H.Suhl (New York: Academic Press). (1973).

4. RIZZUTO, C., Rep. Prog. Phys., 37, 147 (1974).

5. GRUNER, G., Adv. in Phys., 23, 941 (1974).

6. KONDO, J., Prog. Theor. Phys., 28, 846 (1962); Solid St. Phys. Vol. 23 (1969), edited by F. Seitz and D. Turnbull.

7. FISHER, K., Springer Tracts in Mod. Phys., Vol. 54, edited by G. Hohler (1970).

8. FRIEDEL, J., (a) Can. J. Phys., 34, 1190 (1956);
   (b) Nuovo Cimento Suppl., 7, 287 (1958).

9. ANDERSON, P.W., Phys. Rev. 124, 41 (1961).

10. KASUYA, T., Progr. Phys., 16, 45 (1956).

11. YOSIDA, K., Phys. Rev., 106, 893 (1957).

12. WOLFF, P.A., Phys. Rev., 124, 1030 (1961).

13. BLANDIN, A. and FRIEDEL, J., J. Phys. Radium, 20, 160 (1959).

14. KLEIN, A.P. and HEEGER, A.J., Phys. Rev. 144, 458 (1966).

15. YOSIDA, K., OKIJI, A. and CHIKAZUMI, S., Prog. Theor. Phys., 33, 559 (1965).

16. MORIYA, T., Proc. Varenna School 1966 (edited W. Marshall), (New York: Academic Press.

17. BLANDIN, A., Magnetism Vol. V, edited by H. Suhl, (New York: Academic Press) 1973.

18. KONDO, J., Progr. Theor. Phys., 32, 37 (1964).

19. ANDERSON, P.W. and CLOGSTON, A.M., Bull. Am. Phys. Soc. 6, 124 (1961).

20. BLANDIN, A., J. Appl. Phys., 39, 1285 (1968).

21. DAYBELL, M.D., Magnetism, Vol. V (1973), edited by H. Suhl, New York Academic Press.

22. VAN DEN BERG, G.J., Prog. in Low Temp. Phys. Vol. IV, 194, (1964). (North Holland Publ. Co. Amsterdam) Ed. C.J. Gorter.

23. HEDGCOCK, F.T. and MUIR, W.B., J. Phys. Soc. Jap. 16, 2599 (1961).

24. TRIPLETT, B.B. and PHILLIPS, N.E., Proc. Int. Conf. Low Temp. Phys. 12th Kyoto, (1970) (E.Kanda, ed.), 747. Academic Press of Japan, Tokyo, (1971).

25. NAGAOKA, Y., Phys. Rev. A 138, 1112 (1965).

26. NAGAOKA, Y., Progr. Theor. Phys. (Kyoto) 37, 13 (1967).

27. WILSON, K.G., Collective Properties of Physical Systems, Nobel Symposium 24 (London: Academic Press) (1974).

28. NOZIERES, P., J. Low Temp. Phys. 17, 31 (1974).

29. BLOOMFIELD, R., HECHT, R. and SIEVERT, P.R., Phys. Rev. B 2, 3714 (1970).

30. SCHRIEFFER, J.R., J. Appl. Phys. 38, 1143 (1967).

31. CAPLIN, A.D. and RIZZUTO, C., Phys. Rev. Lett. Vol. 21, 11, 746 (1968).

32. RIVIER, N., SUNJIC, M. and ZUCKERMANN, M.J., Phys. Lett. 28A, 492 (1969).

33. RIVIER, N., Thesis, University of Cambridge (1968).

34. SCHRIEFFER, J.R. and WOLFF, P.A., Phys. Rev. 149, 491 (1966).

35. VAN DAM, J.E., GUBBENS, P.C.M. and VAN DEN BERG, G.J., Physica, 62, 389 (1972).

36. BELL, A.E. Thesis, University of London (1973).

37. RIVIER, N., and ZLATIC, V., J. Phys. F: Metal Phys. 2, L87 and L99 (1972).

38. LEDERER, P. and MILLS, D.L., Phys. Rev., 165, 837(1968).

39. KAISER, A.B. and DONIACH, S., Int. J. Magnetism,1, 11 (1971).

40. MILLS, D.L., BEAL-MONOD, M.T. and LEDERER, P., Magnetism Vol.V (1973), edited by H. Suhl (New York: Academic Press).

41. HAMANN, D.R., Phys. Rev., 158, 570 (1967).

42. ZITTARTZ, J. and MULLER-HARTMAN, E., Z. Physik, 212, 380 (1968).

43. RIVIER, N., and ZUCKERMANN, M., Phys. Rev. Lett. 24, 225 (1968).

CHAPTER 2

INTERACTIONS BETWEEN MOMENTS.

The previous chapter essentially dealt with a localized magnetic moment in the single ion impurity limit. In this limit, the impurities are assumed to be sufficiently far apart that interactions amongst them are completely negligible. The present chapter is concerned with the interactions between local moments, the consequences of which are magnetically ordered states.

2.1 The RKKY and other interactions.

This interaction is an indirect coupling of local moments via the conduction electrons, originally developed by Rudermann and Kittel (01) in connection with nuclear magnetic resonance in metals and subsequently adapted by Kasuya (02) and Yosida (03) for local moments in metals.

The interaction with the conduction electrons takes place via an exchange coupling of the type given by equation (1.5), for rare-earth atoms (4f shell) then,

$$H_{sf} = -J_{sf}(\underline{R}_i - \underline{R}_j)\, \underline{S}.\underline{s} \qquad \text{..... 1a}$$

alternatively working in k-space gives,

$$H_{sf} = -\, J_{sf}(q)\, \underline{S}_q.\underline{s}_{-q} \qquad \text{..... 1b}$$

where in equation (1a) $\underline{R}_i$ is the position of the ionic spin $\underline{S}$ and $\underline{R}_j$ is the position of a conduction electron with spin $\underline{s}$. The effect of the ionic spin may be calculated using perturbation theory (04) (05), from which it is found that the spin polarization induced in the conduction electrons is long range and oscillatory in nature. The polarization produced by a spin at site $\underline{r}_i$ will interact with a spin at site $\underline{r}_j$, giving an effective coupling which may be written in the form of an Heisenberg exchange Hamiltonian (see section 2),

$$H_{ex} = -\sum_{i \neq j} j(\underline{r}_{ij})\, \underline{S}_i.\underline{S}_j \qquad \text{..... 2}$$

$$\underline{r}_{ij} = \underline{r}_i - \underline{r}_j .$$

Mapping this into the manifold of states of total angular momentum gives:

$$H_{ex} = -(g-1) \sum_{i \neq j} j(\underline{r}_{ij})\, \underline{J}_i \cdot \underline{J}_j \quad \ldots\ldots\ldots\ldots\ldots\ldots \quad 3$$

The exchange parameter in equations (2) and (3) can be expressed in terms of the generalized susceptibility $\chi(q)$ and the Fourier transform of the s-f exchange constant,

$$j(\underline{r}_{ij}) = \sum_{q} J_{sf}^2(\underline{q})\, \chi(\underline{q})\, e^{i\underline{q}\cdot\underline{r}_{ij}} \quad \ldots\ldots\ldots\ldots\ldots\ldots \quad 4$$

In the RKKY approximation $J_{sf}(\underline{q}) = J_o$ where J_o is a constant. This assumption is clearly a crude approximation and leads to a divergence in the spin density as r tends to zero. Many authors (03) (06) have attempted to overcome this problem with varying degrees of success (see for review Freeman (07)). Using the RKKY approximation it can be shown (04) that

$$j(\underline{r}_{ij}) = \frac{9\pi z^2 J_o^2}{E_f} f(2k_f|\underline{r}_{ij}|) \quad \ldots\ldots\ldots\ldots\ldots\ldots \quad 5$$

where

$$f(x) = (\sin x - x \cos x)/ x^4 .$$

This interaction is of a long range oscillatory type which decreases as $\cos(2k_f r)/r^3$ for large r. Because of this long range oscillatory nature, the coupling is capable of explaining the variety of spin structures found in the heavy rare earth elements (08). The interaction represented by expression 2 is Heisenberg in form, therefore classical molecular field theory (see section 2) may be applied to obtain the paramagnetic Curie temperature Θ_p:

$$k_B \Theta_p = \frac{3\pi z^2}{E_f} G \sum_{i \neq j} f(2k_f r_{ij})$$

where $G = (g_J - 1)^2 J(J+1)$ which is known as the de Gennes factor.

Clearly the paramagnetic Curie temperature should be proportional to the de Gennes factor; this is found to be approximately obeyed (09). The lattice sum $\sum_{j\neq j} f(2k_f r_{ij})$ varies for different crystallographic structures and has been evaluated by several authors (10) (11) (12) to interpret the magnetic properties of certain systems.

The s-f exchange parameter $J_{sf}(q)$ must be positive if only diagonal exchange integrals are considered. From resonance experiments on rare-earth aluminium compounds (13) and PdGd alloys (14) the value of the exchange parameter (for q = 0) obtained from the g-shift was found to be negative. This implies that the conduction electron polarization is antiparallel to that of the local moment. This negative exchange has been attributed to the effect of covalent mixing between the conduction electron and local moment orbitals (15); this is the so-called inter-band mixing effect. It was first recognized by Anderson and Clogston (ch. 1, sect. 2) and discussed in detail by Watson et al (15). Recently there have been a number of different models proposed to explain the effective negative coupling (e.g. ref. 16); these will be discussed in the last chapter in relation to the negative g-shifts found in $LaNi_5$- Gd.

The generalized susceptibility.

The generalized susceptibility $\chi(q)$ in expression (4) is the response of a free electron gas to the application of a magnetic field. In the Hartree-Fock approximation (17), $\chi(q) = \chi_p F(q/2k_f)$ where χ_p is the Pauli susceptibility and

$$F(x) = \frac{1}{2} + \frac{1}{x}(1 - x^2) \log((x + 1) / (x - 1)).$$

If the coulomb correlation U which acts in an atomic cell to separate electrons of opposite spin is taken into account then the susceptibility is enhanced (18). The χ (q = 0) susceptibility is enhanced by a factor $(1 - UN(E_f))^{-1}$. Pure palladium is a typical exchange enhanced metal (19)

with $UN(E_f) \simeq 0.9$. Some compounds such as $LaRu_2$, Ni_3Ga and $LaNi_5$ are also enhanced metals. When $UN(E_f) \geqslant 1$ then band ferromagnetism appears (18); this condition is known as the Stoner criterion.

The Blandin - Caroli interaction.

The RKKY interaction is useful for rare earth alloys where the localized state is either completely empty or completely full. In terms of scattering theory the phase shift δ_1 of the conduction electrons produced by the impurity potential at large distances is either 0 or π. For a 3d transition metal impurity (Mn in Cu) a virtual bound state is produced which gives rise to phase shifts that are not all equal to 0 or π. The coupling between virtual bound states was first considered by Friedel and Blandin (20).

The scattering of an electron by a spin dependent potential implies that electrons of opposite spin will behave differently. Thus the long range perturbation in the electron density is different for the two spin directions. This gives rise to a long range spin polarization and hence a coupling between the spins (21) (22)

$$H \propto \frac{\cos(2k_fR)}{(k_fR)^3} \underline{S}_1 \cdot \underline{S}_2$$

where R is the distance between spin S_1 and spin S_2.

Caroli (23) essentially generalized the above arguements to include the scattering process whereby an electron is first scattered by one impurity and then by another a distance R from the first. Because of the initial scattering by the first impurity, the wave function of the scattered electron is modified. Hence when this electron is scattered by the second impurity the admixture matrix element V_{dk} (which determines the energy position and the width Δ of the impurity state) has to be recalculated using the new electron wave function. This effectively changes the energy and width of the second impurity. Thus in this model

a mechanism for altering the width from that appropriate to the single impurity limit is available.

The spin polarization for the Caroli model can be calculated (23) (24) and leads to an effective coupling between magnetic moments at large R, given by

$$H = - J(R)\underline{S}_1 \cdot \underline{S}_2$$

$$J(R) = \frac{\alpha \cos(2k_f R + \varphi)}{(k_f R)^3}$$

where α and φ are constants depending on the phase shifts. This has the same form as the RKKY interaction (at large R) but the magnitudes are different. For example, Blandin calculated α using both Caroli and RKKY mechanisms for the CuMn system and found that the former was two orders of magnitude greater than the latter (21).

Short range interactions.

There are four main interactions between virtual bound states in metals. The direct exchange interaction, RKKY, indirect exchange via s-d mixing (both considered above) and d-d covalent admixture. The first interaction above is assumed to be relatively small compared with the others and the following two are essentially long range. The only short range interaction is the last, which will now be considered.

For the case of a pair of neighbouring atoms in a metal with non-degenerate localized orbitals the d-d covalent mixing gives rise to two virtual bound states. The coupling is dependent on the relative positions of the two virtual bound states with respect to the Fermi energy. Therefore both ferromagnetic and antiferromagnetic alignments are possible. This may be thought of as the metallic analogue of super and double exchange in insulators (25).

Moriya (26) analysed the more realistic situation of d-d covalent admixture between two adjacent five-fold degenerate impurity orbitals.

He found that the effective exchange varied with the number of localized electrons. For impurity atoms with nearly half filled d-shells the coupling tends to be antiferromagnetic while increasing the number of d-electrons makes ferromagnetic coupling more likely. Moriya used this model to account for the ferromagnetism of Fe, Co and Ni and the antiferromagnetism of the elements Cr and Mn.

Finally the work of Kim (27) on the finite concentration Anderson model will be discussed. He considered how the width of a localized state is altered by the presence of other impurities. The existance of other impurities changes the density of states of the ith impurity at the Fermi surface from $N_i^{\circ}(0)$ to $N_i(0)$. If a single impurity does not have a local moment it may obtain one if it has a given number of impurity neighbours. This can be described by the condition:

$$U_i N_i^{\circ}(0) < 1 \quad \text{and} \quad U_i N_i(0) \geqslant 1 \qquad \ldots\ldots\ldots\ldots\ldots\ldots \quad 6$$

The reverse situation may also occur; CuNi (28) is an example of the former and AuV of the latter (29).

Kim showed how the conditions above, for an impurity level near the Fermi surface, can be written in terms of the change of width of the impurity state from Δ_i° to $\Delta_i = \Delta_i^{\circ} + \delta\Delta_i$. He then analysed $\delta\Delta_i$, this contained three terms, the indirect interaction term Δ_i^{1}, the direct transfer term Δ_i^{2} and a cross term Δ_i^{3}. Usually alloy systems fall into two classes, either $|\delta\Delta_i^{1}| \gg |\delta\Delta_i^{2}|$ or $|\delta\Delta_i^{1}| \ll |\delta\Delta_i^{2}|$ in which case Kim showed that the cross term may be neglected. He used the above model to analyse the experimental properties of the system $Co(Rh_{1-x}Pd_x)$ (30).

2.2 Magnetic Order

Any system which has spontaneous long range ordering of the direction of the magnetic moment it possesses, at a given temperature, is said to have a magnetically ordered phase. The ordering may take one of several forms, for instance, parallel alignment of magnetic moments (ferromagnetism), antiparallel alignment (antiferromagnetism) or complex arrangements depending on the crystal structure (ferri and helimagnetism).

To produce any type of spontaneous ordering interactions between the moments must occur. The interaction most commonly assumed to take place is the Heisenberg exchange, given by the Hamiltonian

$$\hat{H}_{ex} = -\sum_{i>j} J(\underline{R}_i - \underline{R}_j)\, \underline{S}_i \cdot \underline{S}_j \qquad \ldots\ldots\ldots\ldots\ldots\ldots\ldots \quad 7$$

for an atom of spin $\underline{S}_i$ at $\underline{R}_i$ coupling with an atom of spin $\underline{S}_j$ at $\underline{R}_j$. The solution of this Hamiltonian is very difficult (17) and approximations have to be made. The simplest, is to consider one spin only and replace the others by an effective field. This is the classical molecular field theory approximation.

Molecular field theory (MFT) first introduced by Weiss (31) long before the use of the Hamiltonian in expression 7, is a phenomenological theory based on the assumption that the molecular field, H_m, which acts on each atom is just proportional to the magnetization of the whole crystal, hence the total field acting on a given atom is

$$H = H_{ap} + \lambda M \qquad \ldots\ldots\ldots\ldots\ldots\ldots\ldots\ldots\ldots\ldots \quad 8$$

where H_{ap} is the applied magnetic field and λ is the molecular field constant. The link with the Heisenberg Hamiltonian can be made by considering only one spin $\underline{S}_i$ and replacing the remaining spins by an average value $\langle \underline{S}_j \rangle$ whence the Hamiltonian becomes

$$\hat{H}_{ex} = -\sum_{i>j} J(\underline{R}_i - \underline{R}_j) \langle \underline{S}_j \rangle \cdot \underline{S}_i$$

From the MFT assumption we wish to replace the interaction by an effective molecular field, H_m, therefore H_{ex} becomes:

$$H_{ex} = -g\mu_B \underline{S}_i \cdot \underline{H}_m .$$

Using the last two equations it is simple to obtain an expression for the molecular field constant $\lambda = J_o / N\bar{\mu}^2$, where $\bar{\mu}$ is the average molecular moment and $J_o = \sum_{i>j} J(\underline{R}_i - \underline{R}_j)$. If the applied magnetic field is taken along the z-axis then the one atom Hamiltonian is given by $H_{ex} = -g\mu_B S_{iz} H$, the solutions of this are well known (32). By using the methods of statistical mechanics the magnetization, specific heat etc. can easily be found (33) (34).

Molecular field theory predictions for the transition temperature and specific heat are incorrect, The transition temperature being too high and the specific heat showing a finite discontinuity and no high temperature "tail". The reason for this is that short range order which is present above the critical temperature is neglected. Therefore as we approach the critical temperature MFT breaks down. Even so this theory has been successful in describing the overall properties of magnetic systems (Curie-Weiss law, magnetization curves etc.) (33).

Ferromagnetism.

In this type of order the exchange between neighbouring spins is positive, therefore the alignment of the spins is parallel in the ground state. The low lying excitations of the system are not single particle spin flips but collective modes where each spin is at a constant angle compared with that of its neighbour (35). These excitations are called spin waves and can be quantized in a manner similar to that of lattice vibrations, the quantum of spin wave energy being the magnon (36) (37). Spin wave theory has been used to explain various properties of ferromagnetic systems below the transition temperature.

When approaching the critical temperature from the high

temperature side series expansion methods of evaluating the thermodynamic properties have been widely used (38) (39). In this method the partition function,

$$Z = \sum_i \exp(\ -E_i \ / \ k_B T \ )$$

where E_i is the energy of the ith excited state, is expanded into a series of powers of $(1 \ / \ k_B T)$. The coefficients of the first few terms can be obtained using either the Heisenberg or Ising (the Ising model considers only components of the spin operators in some fixed direction, say z and hence $H_{ex} = -J \sum_{i>j} S_{iz} S_{jz}$) Hamiltonian, hence the susceptibility, specific heat and energy of a ferromagnetic crystal at temperatures above the Curie point can be estimated.

In the region around the critical point correlations between spins must be accounted for, as mentioned above, neglecting this leads to the failure of molecular field theory. The appearance of short range spin correlation on the high temperature side of the critical temperature manifests itself in a non-zero value of the static pair correlation function (34)

$$\Gamma_r(T) = \langle S_{oz} S_{rz} \rangle \ / \ \tfrac{1}{3}S(S + 1)$$

$$r = 0,1,2,3,....$$

for a reference spin and its neighbours at varying distances, r. The factor $\frac{1}{3}S(S + 1)$ is a normalization constant. As the temperature approaches the critical temperature (T_c) then the correlation length (the range of the correlation function) increases until at $T \sim T_c$ it becomes very long range (34). The pair correlation function is a convenient measure of the short range order present in a system.

Antiferromagnetic and Helical Ordering.

If the exchange constant in expression (7) between nearest neighbours, is negative then the minimum energy will occur if the spins are aligned antiparallel. This is antiferromagnetic order. Molecular field theory can be applied by assuming two sublattices with nearest and next nearest neighbour interactions (32). This leads to the well known result that the high temperature susceptibility is Curie-Wiess like, with a negative Curie temperature Θ, and

$$\Theta / T_N = -(A' + A) / (A - A')$$

for the ratio of Θ to the critical temperature T_N the Neel temperature, where A and A' are the molecular field constants for the nearest and next nearest neighbours. The inadequacy of MFT applies equally to antiferromagnetism and methods have been devised (similar to those for ferromagnetism mentioned above) to overcome its limitations(40) (33) (39).

The first direct evidence that spin structures of this type existed was obtained by neutron diffraction work on MnO (41). The diffraction patterns above and below the Neel temperature were obtained and the extra peaks associated with the long range antiparallel ordering of spins.

Given the Heisenberg Hamiltonian, to find the spin structure for a given system it is necessary to minimize the energy with respect to the crystal structure. Changing expression (7) to Fourier components gives

$$H_{ex} = -\sum_q J(q)\, \underline{S}_q \cdot \underline{S}_{-q}$$

$$J(\underline{q}) = \sum_n J_n \exp -i\underline{q}\cdot\underline{R}_n \quad .$$

This exchange energy must now be minimized subject to the condition $\sum_q \underline{S}_q \cdot \underline{S}_{-q} = (\text{constant})$. Under this condition the minimum energy is obtained by taking that q for which J(q) has a highest maximum.

Denoting this q by Q the energy is then (33) (42)

$$E = -NS^2J(Q) \quad . \qquad \ldots\ldots\ldots\ldots\ldots\ldots\ldots\ldots\ldots\ldots \quad 10$$

Therefore to find the magnetic structure present J(Q) must be evaluated.

The value of q at which the maximum occurs will essentially define the spin structure, for q = 0, the coupling is positive for all neighbours, hence a ferromagnetic structure. If $q = \frac{\pi}{a}(\underline{x} + \underline{y} + \underline{z})$ for a simple cubic structure of lattice spacing a, then the coupling alternates between positive and negative from one lattice position to the next giving antiferromagnetic order. An interesting situation arises when Q does not fall at one of these values. When this happens a helical arrangement occurs, the period of which is generally incommensurate with that of the lattice (42). Helical structures have been experimentally confirmed by neutron diffraction studies (43) (44).

In the molecular field approximation the critical temperature for a system having complex ordering is given by the following:

$$T_N = \frac{2S(S + 1)}{3k_B} J(Q) \quad .$$

The paramagnetic temperature is

$$\Theta_p = \frac{2S(S + 1)}{3k_B} J(0) \quad .$$

The situation as outlined above is complicated by the fact that magnetostriction and anisotropy effects must be included when minimizing the energy. Magnetostriction and planar anisotropy are generally large at low temperatures and fall off sharply as the temperature increases (44). For hexagonal close packed structures (rare earth elements) the exchange interaction favours helical ordering, while magnetostriction and anisotropy favour ferromagnetic coupling. Therefore as the temperature dependences vary for the different contributions to the free energy there will usually be a phase

transition from helical to ferromagnetism, for example Dy (45) (46) has a Curie temperature of 85K and a Neel temperature of 179K.

2.3 Spin Glasses.

A metal with a moderate concentration of magnetic impurities distributed at random, which interact via a potential that oscillates as a function of the separation of the impurity spin and shows no long range order, but has its spins frozen in random orientations below a certain temperature, is known as a spin glass (47) (48). The meaning of moderate concentration in the above, is that the concentration is such that the impurities have statistically independent positions. The absence of long range order is a consequence of the randomness of the impurity spin position and the oscillatory nature of the potential. In a metallic system the potential is assumed to be of the RKKY type.

Physically the impurity spins when cooled to a low temperature in zero applied field are "frozen" into the local molecular field. These local fields have a distribution of magnitudes and directions such that the average magnetization of a region, comprising of a few tens of impurity atoms, is zero. Even though there is no long range order there will be a critical temperature, T_{sg}, at which the spins begin to lock. At T = 0 and in zero applied field each moment is frozen in the direction of the local field at its particular site. Cooling the spin glass in a large applied field through the critical temperature will give a bias to the molecular field distribution, hence remnant magnetization effects will be observed (48) (49).

The unusual electrical and magnetic properties of CuMn, AgMn and AuFe in the regime 0.5 to 10 atomic percent impurity lead to the concept of a spin glass. These systems being typical spin glasses have been extensively studied and show the following properties:

(a) At low temperatures the resistivity increases monotonically with temperature rising initially as $A(c)T^{3/2}$ with A(c) depending weakly on concentration (50) (51). A smooth maximum occurs in the gradient of the resistivity close to the spin glass temperature.
(b) The zero field magnetic susceptibility has a sharp cusp at T_{sg}. The application of a small magnetic field is sufficient to round off the cusp (52) (53) (54). The high temperature paramagnetic susceptibility obeys the Curie-Weiss law with a positive intercept on the temperature axis. Spin glass alloys also show marked intrinsic thermo-remnant effects.
(c) The specific heat has a broad maximum at the spin glass temperature. The low temperature specific heat being linear in temperature and concentration independent (57).
(d) The magnetization (M/c) and specific heat (C_p/c) can be represented by universal functions of H/c and T/c where c is the concentration and H the applied magnetic field (54).

By using a model in which the local molecular field at a given magnetic impurity is represented by a distribution function P(H), the properties of a spin glass may then be found. Using this idea the initial studies by Marshall (55) and Klein and Brout (56) with the indirect Ising model for the interactions between the magnetic impurities explained reasonably well the observed low temperature specific heat and magnetic susceptibility. At that time the cusp in the zero field magnetic susceptibility had not been observed. Later work using a more realistic Heisenberg exchange produced similar results (58).

The cusp in the susceptibility of AuFe found by Cannella and Mydosh (52) presented difficulties owing to the absence of long range order in a spin glass system. Adkins and Rivier (59) generalized the

local molecular field theories in an attempt to explain this anomaly. They defined a local order parameter which because of the infinite range of the (RKKY) interaction between the spins is a collective feature of the system, long range order being averted by the random position of the spins together with the oscillatory nature of the interaction. The disappearance of the local order is essentially a collective effect, hence there will be a unique transition temperature and a cusp in the susceptibility.

Recently another theory, similar to the above, has been put forward by Edwards and Anderson (60). They showed that by defining a definite ground state in which the spins are aligned in a given direction, although this direction may be random, that a transition to this state is sufficient to cause a cusp in the susceptibility. From their theory it would seem that all random magnetic impurity systems with oscillatory interactions should show spin glass behaviour at some impurity concentration. The order parameter is defined as $q = \langle \underline{S}_i^{\alpha} . \underline{S}_i^{\beta} \rangle$ taken over a long time period where α and β are different time indices. Below T_{sg}, $q \neq 0$ and at $T = 0$ $q = 1$. Local ordering is unecessary in this theory for a spin glass transition to occur.

Rivier and Adkins (50) explained the resistance behaviour of spin glasses in terms of elementary excitations in the system. As a spin glass has no well defined long range order any spin-flip excitation on an impurity can only diffuse away and not propagate as a magnon. Therefore the low temperature elementary excitations are long wavelength spin diffusion modes. Using this model Rivier and Adkins derived the low temperature $T^{3/2}$ resistivity term.

REFERENCES CHAPTER 2

1. RUDERMAN, M.A., and KITTEL, C., Phys. Rev., 96, 99 (1954).

2. KASUYA, T., Prog. Theoret. (Kyoto), 16, 45 (1956).

3. YOSIDA, K., Phys. Rev., 106, 893 (1957).

4. KITTEL, C., Solid State Phys., 22, 1 (1968).

5. WATSON, R.E. and FREEMAN, A.J., Phys. Rev., 152, 566 (1966); Phys. Rev. Letters, 14, 695 (1965); Phys. Rev.,178, 725 (1969).

6. OVERHAUSER, A.W., J. Appl. Phys., 34, 1019 (1963).

7. FREEMAN, A.J., Magnetic properties of Rare Earth Metals, 245, (Plenum Press) Ed. R.J.Elliott (1972).

8. KOEHLER, W.C., Magnetic Properties of Rare Earth Metals, 81, (Plenum Press) Ed. R.J.Elliott (1972).

9. TAYLOR, K.N.R., and DARBY, M.I., Rare Earth Solids, (Chapman and Hall Ltd.) (1972).

10. DARBY, M.I., and TAYLOR, K.N.R., Phys. Lett. 14, 179 (1965)

11. BUSCHOW, K.H.J., FAST, J.F., VAN DIEPEN, A.M. and DE WIJN, H.W., Phys. Stat. Sol., 24, 715 (1967).

12. MATTIS, D.C., Theory of Magnetism (Harper and Row), 201, 275 (1965).

13. SHALTIEL, D., WERNICK, J.H., WILLIAMS, H.J. and PETER, M., Phys. Rev. 135, A1346 (1964).

14. PETER, M., SHALTIEL, D., WERNICK, J.H., WILLIAMS, H.J., MOCK, J.B. and SHERWOOD, R.C., Phys. Rev. 126, 1395 (1962).

15. DE GENNES, P.G., J. Phys. Radium, 23,510 (1962).
WATSON, R.E., KOIDE, S., PETER, M. and FREEMAN, A.J., Phys. Rev. 139A, 167 (1965).

16. COLES, B.R., GRIFFITHS, D., LOWIN, R.J., TAYLOR, R.H., J. Phys. C. (Sol. St. Phys.)L121 (1970).

17. WHITE, R.M., Quantum Theory of Magnetism (McGraw-Hill) (1970)

18. STONER, E.C., Proc. Roy. Soc. (London) A165, 372 (1938).

19. DONAICH,S., and ENGELSBERG, S., Phys. Rev. Lett., 17, 750 (1966).

20. BLANDIN, A. and FRIEDEL, J., J. de Phys., 20, 160 (1959).

21. BLANDIN, A. Proc. Varenna School, (1966), (W. Marshall, ed.), 393. Academic Press, New York (1967).

22. BLANDIN, A., J. Appl. Phys. 38, 1143 (1967).

23. CAROLI, B., Thesis, Univ. of Paris (1966) and J. Phys. Chem. Sol., 28, 1427 (1967).

24. CAROLI, B. and BLANDIN, A., J. Phys. Chem. Solids, 27, 503 (1966).

25. ALEXANDER, S. and ANDERSON, P.W., Phys. Rev., 133, 6A, (1964).

26. MORIYA, T., Prog. Theor. Phys., 33, 157 (1965).

27. KIM, D.J., Phys. Rev., 1, 3724 (1970).

28. PERRIER, J.P., TISSIER, B. and TOURNIER, R., Phys. Rev. Letts., 24, 313 (1970).

29. VAN DAM, J.E., Thesis, University of Leiden, (1972).

30. JACCARINO, V. and WALKER, L.R., Phys. Rev. Letts., 15, 258 (1965).

31. WEISS, P., J. Phys. Rad. (Paris) 6, 667 (1907).

32. MARTIN, D.H., Magnetism in Solids, (Iliffe Books Ltd.) (1967).

33. SMART, J.S., Effective Field Theories of Magnetism, (W.B.Saunders and Co.) (1966).

34. STANLEY, H.E., Introduction to Phase Transitions and Critical Phenomena, (Clarendon Press) (1971).

35. HERRING, C. AND KITTEL, C., Phys. Rev., 81, 869 (1951).
KITTEL, C., Introduction to Solid State Physics, (John Wiley) (1971).

36. HOLSTEIN, T. and PRIMAKOFF, H., Phys. Rev., 58, 1098 (1940).

37. DYSON, F.J., Phys. Rev., 102, 1217 (1956).

38. DOMB, C. and MIEDEMA, A.R., Prog in Low Temp. Phys., ed. C.J. Gonser, North Holland, 4 (1964).

39. DOMB, C., Magnetism, ed. G.T.Rado and M. Suhl, Academic Press Vol. 2A (1964).

40. KASTELEIJN, P. W. and VAN KRANENDONK, J., Physica, 22, 317 (1956)

41. SHULL, C.G., STRAUSER, W.A. and WOLLAN, E.O. Phys. Rev. 83, 333 (1951).

42. NAGAMIYA, T., Sol. St. Phys., Edited F. Seitz, D. Turnbull and H. Ehrenreich, Vol. 20., 306 (1967).

43. CABLE, J.W., WOLLAN, E.O., KOEHLER, W.C. and WILKINSON, M.K., Phys. Rev., 140, 1896 (1965).

44. COOPER, B.R., Sol. St. Phys., Edited F. Seitz, D. Turnbull and H. Ehrenreich, Vol. 21, 393 (1968).

45. BOYS, D.W., and LEGVOLD, S., Phys. Rev., 174, 377 (1968).

46. WILKINSON, M.K., KOEHLER, W.C., WOLLAN, E.O., and CABLE, J.W., J. Appl. Phys. 32, 48S (1961).

47. COLES, B.R., Quoted by P.W.Anderson, Mater. Re Bull. 5, 549 (1970).

48. COLES, B.R., Amorphous Magnetism, (ed. H.O. Hooper and A.M. deGraaf). Plenum Press, 169, (1973).

49. KOUVEL, J.S., J. Phys. Chem. Sol., 24, 795 (1963).

50. RIVIER, N. and ADKINS, K., J. Phys. F: Metal Phys., 5, 1745 (1975).

51. FORD, P.J.and MYDOSH, J.A., J. de Phys., 35, C4-241 (1974).

52. CANNELLA, V. and MYDOSH, J.A., Phys. Rev. B6, 4220 (1972).

53. CANNELLA, V. , Amorphous Magnetism, (ed. H.O. Hooper and A.M. deGraaf) Plenum Press, 195 (1973).

54. THOLENCE, J.L. and TOURNIER, R., J. de Phys., 35, C4-229 (1974)

55. MARSHALL, W., Phys. Rev., 118, 1519 (1960).

56. KLEIN, M.W. and BROUT, R., Phys. Rev., 132, 2412 (1963).

57. ZIMMERMAN, J.E. and HOARE, F.E., J. Phys. chem. Sol., 17, 52, (1960).

58. RIVIER, N. and ADKINS, K., Amorphous Magnetism, (ed. H.O. Hooper and A.M. deGraaf). Plenum Press, 217, (1973).

59. ADKINS, K. and RIVIER, N., J. de Phys., 35, C4-273 (1974).

60. EDWARDS, S.F. and ANDERSON, P.W., J. Phys. F: Metal Phys., 5, 965 (1975).

CHAPTER 3

THE ONSET OF MAGNETIC ORDER.

In this chapter we shall discuss how various magnetic alloys and intermetallic compounds behave near the onset of magnetic order and the way in which magnetic resonance can give valuable information about this behaviour.

3.1 Behaviour near the critical point.

A parameter which is common to all physical systems having phase transitions is the order parameter which is non-zero below the critical temperature and zero above it. In a magnetic system the order parameter is the zero field magnetization M(0), which is a measure of the alignment throughout the crystal of the magnetic moments. The variation of the order parameter with temperature is defined by using critical exponents.

To define a critical exponent consider a function $F(\epsilon)$ where

$$\epsilon = (T - T_c) / T_c$$

is a dimensionless variable. Then the limit

$$\lambda = \lim_{\epsilon \to 0} \ln F(\epsilon) / \ln \epsilon$$

is called the critical exponent associated with $F(\epsilon)$. The expression $F(\epsilon) = A\epsilon^{\lambda}$ does not usually hold and a more general relation including correction terms is often used,

$$F(\epsilon) = A\epsilon^{\lambda}(1 + B\epsilon^{y} + \dots) \quad y > 0.$$

The notation usually employed is $F(\epsilon) \sim \epsilon^{\lambda}$ (01).

Critical exponents may be obtained from experimental data, provided T_c is known, from the slope of log-log plots since from the above $\lambda = d(\ln F(\epsilon))/d(\ln \epsilon)$. For a magnetic system, the magnetization is given by $M(0,T) \sim (-\epsilon)^{\beta}$ or $M(0,T) = B(-\epsilon)^{\beta}(1+\dots)$, $T < T_c$. Similarly for the isothermal susceptibility , the specific heat and the

critical isotherm, critical exponents can be defined;

$$\chi_T = C\epsilon^{-\gamma}(1 + \ldots) \qquad T > T_c$$

$$C_v = A\epsilon^{-\alpha}(1 + \ldots) \qquad T > T_c$$

$$H = D\,|M(H, T=T_c)|^{\delta} \qquad T = T_c$$

where A, B, C and D are constant coefficients. Behaviour of a ferromagnet near the Curie point as predicted by classical molecular field theory is given in terms of the critical exponents in Table 1, together with observed values.

To investigate the properties of a ferromagnet above T_c, using a better approximation than molecular field theory, then series expansion methods are used (see Ch. 2). For temperatures around T_c cluster (constant-coupling) approximations are used which take into account the interactions between magnetic moments (02) (03). In this method the interactions among the spins within a given cluster are treated exactly and the remaining spins averaged. This approach leads to the result that short range order appears at $T > T_c$ and a definition of a short range order parameter $\langle S_i . S_j \rangle$ for nearest neighbours. This varies between 1 and 0 as the crystal passes from a completely ordered to a completely disordered state. The properties of a ferromagnetic system are summarized in Fig. 1. Predictions of the cluster method are quite good; the critical exponent of the magnetization is $\beta = \frac{1}{3}$(04) and the Curie temperature is lower than that predicted by molecular field theory. Unfortunately one of the main features determining critical behaviour, the dimensionality of the lattice, is not taken into account.

Recent treatments of the magnetic phase transition have used the static pair correlation function. Thermodynamic quantities can be

Table 1.

	α	β	γ	δ
MFT	0	0.5	1	3
Observed values	-	0.3-0.4	1.1-1.4	4.2

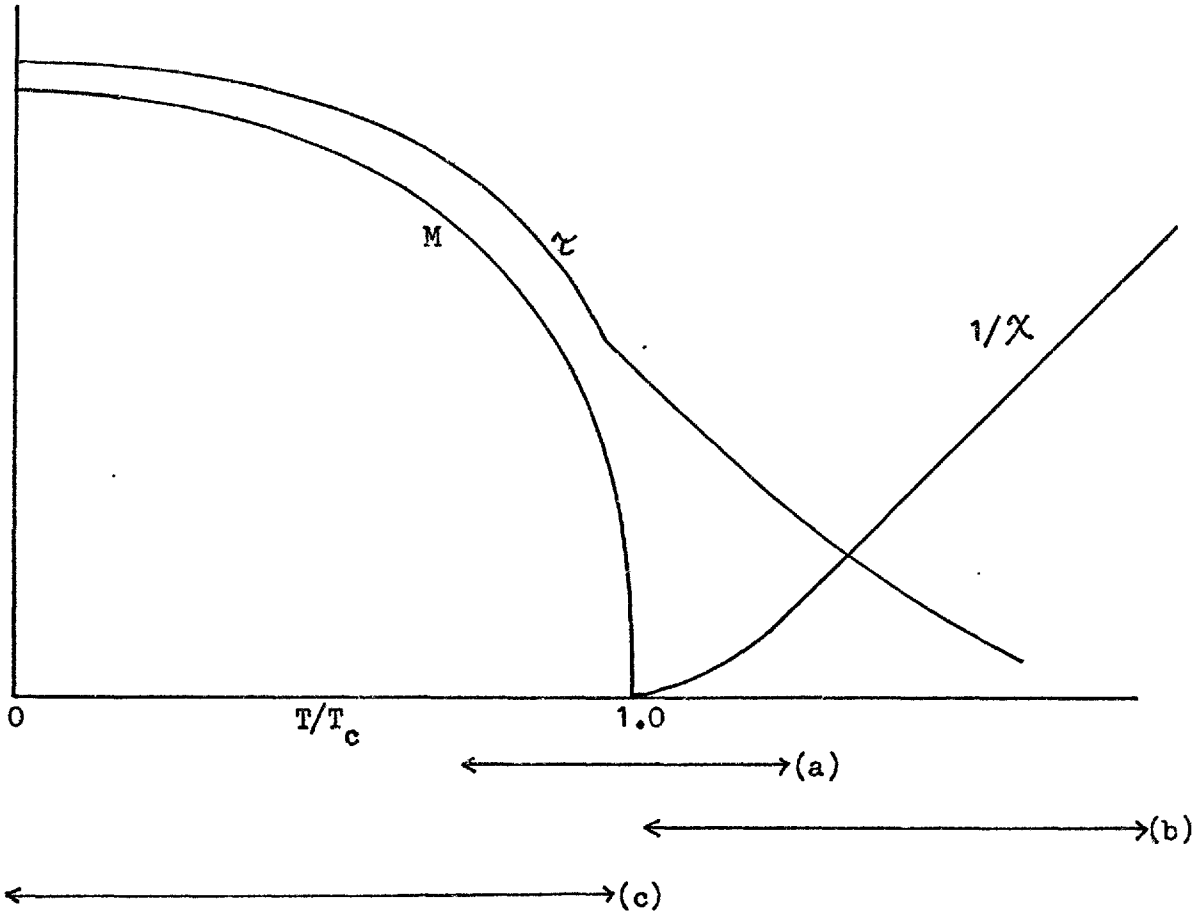

FIG. 1 The thermodynamic properties of a ferromagnetic material. M is the magnetization or long range order parameter, τ is the short range order parameter and χ is the susceptibility. (a) Is the range of validity of the cluster approximation, (b) the series expansion methods and (c) the spin wave model, (after Martin (41)).

$$\Gamma_r(T) = \langle S_{oz} S_{rz} \rangle \; / \; \tfrac{1}{3}S(S+1)$$

related to Γ_r. For example $\Gamma_\infty = \langle S_{oz} S_{z\infty} \rangle$ is proportional to the spontaneous magnetization and may be thought of as a long range order parameter. The susceptibility in terms of the pair correlation function is given by the following:

$$\chi T/C = 1 + \Gamma_r(T) \qquad \ldots\ldots\ldots\ldots\ldots\ldots\ldots\ldots \quad 1$$

where C is the Curie constant. For purely paramagnetic systems $\Gamma_r(T)=0$ for all r, hence expression 1 reduces to the Curie law. The susceptibility and other properties can therefore be determined by analysis of the correlation function (01) (05), although in many cases this is far from straightforward. In fact exact solutions have only been obtained for the two dimensional Ising model.

3.2 Resistivity near T_c.

To investigate the details of the magnetic interaction near the ordering temperature in conducting materials, transport properties are very useful due to their sensitivity to spin interactions. This can be readily seen from the wide variety of resistivity anomalies displayed by the pure rare earth metals (06) and many intermetallic compounds (07).

Two general types of behaviour have been observed in the temperature dependence of the resistance for ferromagnetic materials:

1. A monotonic temperature dependence of the resistivity in the vicinity of T_c, typical examples are nickel (08) and iron (09).
2. A resistivity temperature dependence with a maximum in the neighbourhood of T_c, for example Gd(c-axis) (10) and $GdNi_2$ (11).

These anomalies have been explained in terms of a reduction in the spin disorder scattering of the conduction electrons as the ordering process takes place (12) (13) (14). Spin disorder scattering gives a term in the resistivity proportional to $1 - |\langle \underline{S} \rangle|^2 \; / \; S(S+1)$ which

is essentially just a measure of the spin disorder present at a given temperature. Below T_c the decrease in the resistivity will be proportional to the square of the spontaneous magnetization.

The anomalies in the vicinity of the critical temperature are usually characterized by the temperature derivative of the resistivity $d\rho/dT$ and the data fitted to a power law $d\rho/dT = A\epsilon^{-\lambda}$ where A is a constant. The resistivity due to spin scattering can be obtained from the relaxation time τ associated with the scattering from spin fluctuations,

$$\rho = m / ne^2 \tau$$

where n is the density of conduction electrons and m is the effective mass at the Fermi surface (17). The relaxation time may be analysed in terms of the static spin-spin correlation function $\Gamma_q(T)$, giving (14)

$$\rho = B\int_0^{2k_f} q^3 \Gamma_q(T)\, dq$$

where B is a constant and k_f is the wave vector at the Fermi surface.

De Gennes and Friedel (12) and Kim (15) using essentially the molecular field (Ornstein-Zernike (01)) approximation for $\Gamma_q(T)$ showed that the resistance is given by the following

$$\rho_s = \rho_o \frac{T}{T_c} \gamma \left(1 - \frac{\epsilon\gamma}{2} \ln(1 + 2/\epsilon\gamma)\right) \quad \ldots\ldots\ldots\ldots \quad 2$$

where γ is a temperature independent parameter which depends on the details of the model for Γ_q. Expression 2 is valid for $T > T_c$. In the MFT approximation $\Gamma_q(T) = C/(K^2 + q^2)$ where K is the inverse of the correlation length and C is a normalization constant. From their results they explained the second type of critical behaviour in the region of the ferromagnetic transition. Kawatra et al (19) have fitted expression 2 to their data on $GdNi_2$ with reasonable success. Essentially the de Gennes-Friedel approximation considers only long range critical fluctuations in the spin-spin correlations.

To explain the first type of anomaly Fisher and Langer (14) included in their analysis of $\Gamma_q(T)$ short range spin correlations and deduced that $d\rho/dT \propto \epsilon^{-\alpha}$ just above T_c for sufficiently small ϵ, where α is the specific heat critical exponent. With their theory they were able to explain the anomaly found in Ni. However, this approach is only valid for $k_f > \kappa$. Kasuya and Kondo (18) have linked the two approaches by noting that the de Gennes-Friedel approximation has the qualitatively correct asymptotic behaviour for ϵ greater than a given limit, ϵ'. For relatively small k_f de Gennes-Friedel type anomalies - ρ increasing with decreasing T near T_c - should occur (18). Therefore depending on k_f and ϵ' either type 1 or type 2 behaviour may result.

The above theories are based on the assumption that the moment is well localized and that the conduction electrons are contained in a single band. This is rather unrealistic for metals such as nickel but the qualitative features should be similar. For examples of the collective band model see the review by Mott (16).

Unfortunately the situation near the critical temperature may be complicated by other factors, for example anomalous lattice expansion. This leads to an extra term in the temperature dependence of the resistivity which is proportional to the thermal expansion coefficient (20).

Below the ordering temperature the magnetic scattering is due to spin waves. For simple ferromagnets the spin wave resistivity is proportional to T^2 while for magnetically anisotropic materials there is also an exponential term, $\rho_{sw} = CT^2 e^{-\Delta E/k_B T}$ where ΔE is the spin wave excitation energy (21) (22).

Materials which do not order ferromagnetically show a wide variety of resistivity behaviour. When such a system becomes magnetically

ordered the conduction electrons move in a combined potential of the lattice plus that of the exchange field. If the exchange field has a symmetry different from that of the lattice then new superzone bounderies will appear within the Brillouin zone. The exchange field often has complex symmetry especially in materials which order helically. Cooling through the Néel temperature will produce a reduction in the spin disorder scattering and also a change in the configuration of the electrons due to the superzone bounderies. The change in the electron structure will effectively increase the resistance above the value which would be found in a ferromagnet.

Coles (08) suggested that to a first approximation the resistivity in an antiferromagnet may be written in the form,

$$\rho = (P_a + P_b + P_T)F$$

where P_a, P_b and P_T represent the perturbations due to the disordered spins, atomic disorder and thermal disorder respectively and F is a factor depending on the conduction electron configuration which includes the electrons effective mass and the density of states to which they can make transitions.

Using the same basic idea a number of authors have explained the electrical resistivity anomalies in the heavy rare earth metals (23) (24) (25).

3.3 Magnetic resonance and order.

The theory of paramagnetic resonance will be presented in the next chapter. Here the main points of interest are how the effects of magnetic order influence the observed resonance signal and the type of resonance obtained in an ordered system.

Below the critical temperature in a ferromagnet a resonance is observed (26) but it is shifted from the simple Lamor frequency. Kittel (27) showed that this is due to the resonance frequency

depending on the shape of the sample through the demagnetization corrections. The field inside a ferromagnetic sample is different from the applied field because the magnetization produces a reverse field inside the specimen which is known as the demagnetization field.

The macroscopic demagnetization field H_d is determined by

$$\text{div } \underline{B} = \text{div}(\underline{H}_d + 4\pi \underline{M}) = 0,$$

then it follows from curl $\underline{H}_d = 0$ that

$$\nabla^2 \phi = 4\pi \text{ div } \underline{M} \quad \ldots\ldots\ldots\ldots\ldots\ldots\ldots\ldots \quad 3a$$

and

$$\nabla \phi = -H_d \quad \ldots\ldots\ldots\ldots\ldots\ldots\ldots\ldots \quad 3b$$

Hence by calculating ϕ the demagnetization field may be found. If $\underline{H}'$ is the field inside the specimen and $\underline{H}$ is the applied field then $H_d = \underline{H} - \underline{H}'$ and it is usual to write

$$\underline{H}' = \underline{H} - \underline{N}.\underline{M}$$

where $\underline{N}$ is the demagnetization factor which depends on the shape of the sample through the potential ϕ in equations 3. Clearly for ferromagnetic samples the magnetization and hence the demagnetization fields are large.

The demagnetization factors can only be calculated for a number of simple shapes where the internal field is uniform and parallel to the applied field. For example, an infinite cylinder with the applied field along the axis of the cylinder has $N_x = N_y = \frac{1}{2}, N_z = 0$ (28).

Magnetocrystalline anisotropy occurs in most materials. The anisotropy can be expressed as a direction dependent term in the energy of spontaneous magnetization. For a cubic crystal where α_1, α_2, and α_3 are the direction cosines of the magnetization relative to the principal cubic axis then ,

$$E = K_o + K_1 (\alpha_1^2\alpha_2^2 + \alpha_2^2\alpha_3^2 + \alpha_3^2\alpha_1^2) + \ldots$$

Kittel (27) showed how this term may be included into the resonance Hamiltonian.

The resonant frequency of a ferromagnetic crystal, including the last two effects, is given by the equation (27) (29),

$$\omega_o^2 = \gamma^2(H_o + (N_y - N_z)M + a_1)(H_o + (N_x - N_z)M + a_2) \quad \ldots \quad 4$$

where N_x, N_y and N_z are the demagnetization factors defined by $H_x^i = H_x - N_x M_x$ etc., H_x^i being the internal field in the x-direction and a_1 and a_2 are expressions which take account of the magnetic anisotropy energy. For a sample of simple geometry expression 4 reduces considerably. For example, an infinite disc with the applied field perpendicular to the disc has $N_x = N_y = 0$ and $N_z = 1$ therefore

$$\omega_o = \gamma(H_o - 4\pi M).$$

This assumes that the anisotropy constants are small.

From a microscopic point of view the demagnetization effects arise because of the dipole-dipole interaction between the magnetic moments. This may be included into the Hamiltonian by a dipolar coupling term. Similarly the anisotropy can be treated as a quadrupolar coupling between spins (29).

The linewidth of a ferromagnetic resonance has many contributions and is not clearly understood. The underlying processes for a metallic system include, the coupling to the conduction electrons, scattering by impurities and lattice defects and direct magnon-phonon interactions. Therefore the linewidth is of interest mainly as a guide to the general temperature behaviour of a system. The resonant field and linewidth as a function of temperature are shown in Fig. 2, for a metallic system.

In the paramagnetic region, the width of the resonance from dipolar broadening can be obtained from second moment calculations. This broadening is inhomogeneous in nature, the line consisting of a spectral distribution of individual resonant lines combined into one

overall line. The calculated width is usually far broader than the observed value. Van Vleck (30) showed that this discrepancy was due to exchange narrowing of the line.

The effect of exchange narrowing is to change the line shape from Gaussian to Lorentzian. The total intensity remains constant; therefore the result is a narrowing of the line. In the absence of any exchange, the effective field acting on a particular spin is a combination of the external field and the local dipolar field of the neighbouring spins. Since each spin is in a slightly different environment the distribution of resonant frequencies gives rise to a broadening of the absorption line (dipolar broadening). The effect of the exchange interaction is to make the local dipolar field less effective in broadening the line.

This occurs because of changes in the orientation of the magnetic moment at a rate of J/h, introduced by the exchange interaction, cause the dipolar field to fluctuate at this frequency. Only fields that

Fig. 2 The linewidth and resonant field as a function of temperature for a polycrystalline ferromagnet.

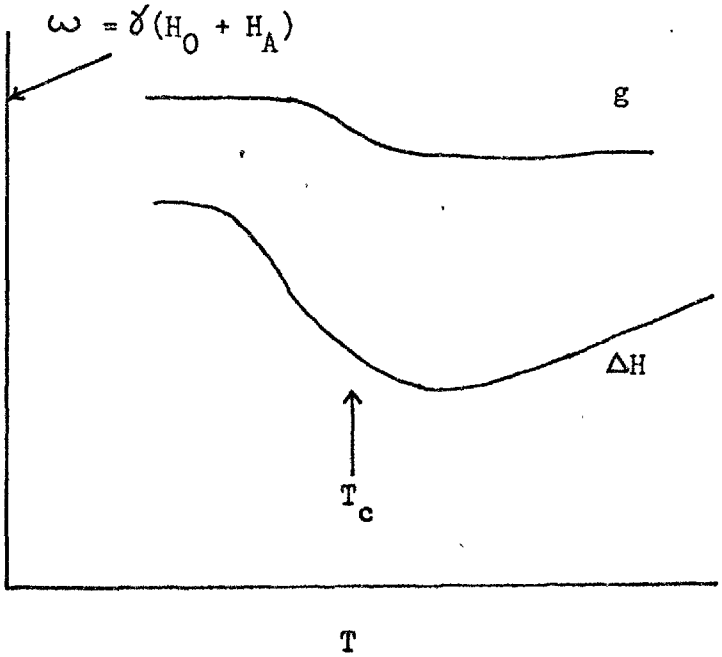

remain constant over a period of time long compared with the relaxation time (T_2) can broaden the line. Therefore provided the fluctuations introduced by the exchange are sufficiently fast, then a narrowing occurs. Exchange narrowing should be even more pronounced in the ferromagnetic region. There are other mechanisms adding to the linewidth in the paramagnetic regime (unresolved fine structure etc.) especially in metals (see ch. 4).

It would be expected that a typical paramagnetic resonance signal would be observed until close to T_c as the temperature is lowered. With a ferromagnetic resonance, obeying equation 4, below the Curie temperature. The shift in the resonant field (g-value) observed just above T_c can be fitted to the form of the magnetization using demagnetization factors appropriate for the system (31). In this work the g-shift in low concentration, less than 10at.%, Gd in $LaNi_5$ is interpreted in this way.

On approaching the Curie temperature in metallic systems the linewidth shows a strong broadening just above the critical temperature. This is due to a number of factors. Most experiments are usually performed on powders where the demagnetization factors are unknown and some average value has to be assumed. The linewidth will therefore be an envelope of shifted lines and broader than expected for a specimen of simple geometry. The presence of short range order above the Curie temperature may be expected to broaden the line, at least for s-state ions. No complete theory has yet been produced which correctly predicts the change in linewidth above T_c.

There will also be an inhomogeneous broadening in polycrystalline samples from magnetocrystalline anisotropy. This gives rise to a width ΔH_a of the form (29)

$$\Delta H_a \propto K_1 / M_s$$

where K_1 is the first order anisotropy constant and M_s is the saturation magnetization. The linewidth in a series of iron alloys has been interpreted in this way by Bagguley (32).

The situation in materials that order antiferromagnetically is rather different. Keffer and Kittel (33) give the condition for resonance in a uniaxial or cubic antiferromagnetic crystal with the static applied field parallel to the axis:

$$\omega_o = \gamma H_o \pm \gamma (H_K (2H_e + H_K))^{\frac{1}{2}}$$

where H_e is the exchange field and H_K is the anisotropy field. Usually $H_e \gg H_K$ therefore,

$$\omega_o = \gamma H_o \pm \gamma (2H_K H_e)^{\frac{1}{2}}.$$

The shift in the resonant field given by $(2H_K H_e)^{\frac{1}{2}}$ is sufficiently large for typical values of H_K and H_e that the resonance is shifted well outside the range of a 3cm paramagnetic resonance spectrometer below the Neel temperature; hence no signal is observed. On approaching T_N the linewidth broadens considerably and generally a minimum occurs at a temperature several times that of T_N. Taylor and Coles (34) have reported a line broadening at more than $10T_N$ for the metallic compounds GdB_6 and Gd_2Zn_{17}. This has been attributed to the effects of short range order in these alloys although there is no fundamental understanding of why this should be so.

Kawasaki (35) attempted to describe the linewidth of an antiferromagnet in the vicinity of the Neel temperature taking into account the short range order. He found

$$\Delta H \propto (T - T_N)^{-p}$$

where $p = 1.66$. Experimentally Maxwell and McGuire (36) and Battles (37) have reported work on the antiferromagnets Cr_2O_3, MnO, MnTe and MnS.

They reported values of p in the range .75 to 1.2. Recently Taylor and Coles (31) found values of p in the range 0.7 to 1.6 for the Gd-B and Gd-Zn systems but due to experimental uncertainties it is doubtful how significant these values are.

Electron paramagnetic resonance in conjunction with magnetization measurements is useful in elucidating the magnetic phase diagram. Bagguley et al (32) have made measurements on a single crystal of Gd-Y and obtained information about the magnetic ordering of the system. They studied six alloys in the range 6% to 64% Gd, measurements being made from 4 to 293 K at both 9.5 GHz and 35 GHz. In the low concentration regime (6 and 28%) resonance in the spiral phase with $g = 2.02 \pm 0.02$ was observed. The g-value in the paramagnetic region for these alloys was $g = 1.95 \pm 0.02$ suggesting that the anisotropy is virtually zero. For the 64% alloy which has no spiral phase a ferromagnetic resonance was observed below 210 K. From this they deduced the ferromagnetic anisotropy constants. The intermediate concentration regime, between 30 and 60%, gave complex behaviour due to metamagnetic transitions.

As can be seen from the examples above epr is sensitive to the local spin environment. This is particularly striking in the work on spin glasses, for example CuMn. This system is a spin glass which eventually becomes a defective antiferromagnet (38) at high Mn concentrations. The system was first investigated by Owen et al (39) who observed resonance in a range of alloys from 0.07% to 11.1% Mn at a few fixed temperatures (2, 4.2, 77 and 295K). They noticed that the resonant field shifted to low field below the ordering temperature and that the line at 4.2K was greatly altered if the sample had been cooled in an applied field.

Later Griffiths (40) investigated these effects fully. He examined two alloys, the 4 and 15 atomic percent Mn through the

temperature range 2 to 295 K. In these two alloys the transition temperature is believed to be (from a maximum in the initial susceptibility (40)) 20 and 55K respectively. In the 4% alloy cooled in zero field a maximum in the plot of signal amplitude (A + B) against temperature was observed at approximately 43K. Slightly higher at 50K the linewidth showed a weak minimum and the resonant field began to shift (Griffiths' Fig. 1). Similarly the 15% alloy had a peak in (A + B) at 115K and a minimum in the linewidth at 135K. Field cooling the samples changed the subsequent character of the resonance behaviour. CuMn is a spin glass system and as such field cooling effects would be expected, although a detailed explanation of Griffiths' results has not yet been given.

From the above remarks it is clear that magnetic resonance is very sensitive to the effects of spin correlations above the ordering temperature. This is also demonstrated in this work, where the effect of the onset of magnetic order is observed in a number of compounds. The epr linewidth in a metallic system shows the effects of short range order but due to the lack of a proper theoretical desciption of the processes involved no quantitative information can be obtained. Experimental work on single crystals of simple geometry would remove uncertainties about demagnetization factors and anisotropy effects.

REFERENCES CHAPTER 3

1. STANLEY, H.E., Introduction to Phase Transitions and Critical Phenomena, (Clarendon Press) (1971).

2. SMART, J.S., Effective Field Theories of Magnetism, (W.B.Saunders and Co.) (1966).

3. KASTELEIJN, P.W. and VAN KRANENDONK, J., Physica,22, 317 and 367 (1956).

4. CALLEN, E. and CALLEN, H.B., J. Appl. Phys., 36, 1140 (1965).

5. FISHER, M.E., In Lectures in theoretical Physics, Vol. 7C. University of Colorado Press, Boulder, Colorado (1965).

6. LEGVOLD, S., Magnetic Properties or Rare Earth Metals, Ed. R.J. Elliott, (Plenum Press, London and New York) (1972).

7. VAN DAAL and BUSCHOW, K.H.J., Solid State Commun. 7, 217 (1969). MYDOSH, J.A., KAWATRA, M.P., and BUDNICK, J.I., Phys. Lett. 24A, 421 (1967).

8. COLES, B.R., Advance. Phys., 7, 40 (1958).

9. WALLACE, D.C., SIDLES, P.H., and DANIELSON, G.C., J. Appl. Phys. 31, 168 (1960).

10. NIGH, H.E., LEGVOLD, S. and SPEDDING, F.H., Phys. Rev., 132, 1092 (1963).

11. KAWATRA, M.P., MYDOSH, J.A. and BUDNICK, J.I., Phys. Rev., B2, 665 (1970).

12. DE GENNES, P.G. and FRIEDEL, J., J. Phys. Chem. Solids, 4, 71, (1958).

13. KASUYA, T., Progr. theor. Phys., Japan 16, 58 (1956).

14. FISHER, M.E. and LANGER, J.S., Phys. Rev. Lett., 20, 665, (1968).

15. KIM, D.J., Progr. Theoret. Phys., 31, 921 (1964).

16. MOTT, N.F., Advance. Phys., 13, 325 (1964).

17. MOTT, N.F. and JONES, H., The Theory of the Properties of Metals and Alloys. (Clarendon Press, Oxford) (1936).

18. KASUYA, T. and KONDO, A., Sol. Stat. Comm. 14, 249 and 253 (1974).

19. KAWATRA, M.P., SKALSKI, S., MYDOSH, J.A. and BUDNICK, J.I., Phys. Rev. LETT., 23, 83 (1969).

20. ZUMSTEG, F.C., CADIEU, F.J., MARCELJA, S. and PARKS, R.D., Phys. Rev. Lett., 25, 1204 (1970).

21. MACKINTOSH, A.R., Phys. Letts., 4, 140 (1963).

22. MANNARI, I., Progr. Theor. Phys. (Kyoto) 22, 335 (1959).

23. ELLIOTT, R.J. and WEDGWOOD, F.A., Proc. Phys. Soc., 84, 63 (1964).

24. MIWA, H., Prog. Theor. Phys., 28, 208 (1962).

25. EDWARDS, L.R. and LEGVOLD, S., Phys. Rev., 176, 753 (1968).

26. BLOEMBERGEN, N., Phys. Rev., 70, 572 (1950).

27. KITTEL, C., Phys. Rev., 71, 270 (1947); 73, 155 (1948).

28. MORRISH, A.H., The Physical Principles of Magnetism. John Wiley and Sons, (1965).

29. VAN VLECK, J.H., Phys. Rev., 78, 266 (1950).

30. VAN VLECK, J.H., Phys. Rev., 74, 1168 (1948).

31. TAYLOR, R.H. and COLES, B.R., J. Phys. F. (Metal Physics) 5, 121 (1975).

32. BAGGULEY, D.M.S., Proc. Roy. Soc. A, 228, 549 (1955).

33. KEFFER, F. and KITTEL, C., Phys. Rev., 85, 329 (1952).

34. TAYLOR, R.H. and COLES, B.R., Proceedings of the Haute-Nendaz Conference, P. 99,Ed.G. Cohen and B. Giovannini, (1973).

35. KAWASAKI, K., Prog. Theor. Phys., 39, 285 (1968).

36. MAXWELL, L.R., and MCGUIRE, T.R., Rev. Mod. Phys., 25, 279 (1953).

37. BATTLES, J.W., J. Appl. Phys., 42, 1286 (1971).

38. KOUVEL, J.S., J. Phys. Chem. Sol., 21, 57 (1961).

39. OWEN, J., BROWNE, M.E., ARP, V. and KIP, A.F., J. Phys. Chem. Sol. 2, 85 (1957).

40. GRIFFITHS, D., Proc. Phys. Soc., 90, 707 (1967).

41. MARTIN, D.H., Magnetism in Solids., Iliffe Books (1967).

CHAPTER 4

THE THEORY OF MAGNETIC RESONANCE

When an atom of total angular momentum $\underline{J}$ is placed in an external magnetic field the $2\underline{J} + 1$ energy levels are split by the Zeeman interaction (01). Magnetic resonance is the phenomenon of inducing transitions among the $2\underline{J} + 1$ levels, an outline of which will be given in this chapter. The first sections deal with the quantum mechanics of a particle with spin in a magnetic field which forms a basis for the description of resonance effects in insulators. The last sections consider the resonance of magnetic impurities in metals.

4.1 Fundamental Theory.

Consider a particle having spin $\underline{S}$, then we can define a vector $\underline{\sigma}$ such that $\underline{S} = \frac{\hbar}{2}\underline{\sigma}$ where $\underline{\sigma} = (\sigma_x, \sigma_y, \sigma_z)$ are the Pauli spin matrices. Assuming the particle has a magnetic moment operator given by

$$\underline{\mu} = \gamma \underline{S} \qquad \ldots\ldots\ldots\ldots\ldots\ldots\ldots\ldots \quad 1$$

where γ is the gyromagnetic ratio, then the application of a magnetic field $\underline{H}$ will give rise to the interaction Hamiltonian

$$\mathcal{H} = -\underline{\mu}.\underline{H}$$

If $\underline{H}$ is a static field parallel to the z-axis then the Hamiltonian is

$$\mathcal{H} = -\gamma \hbar H S_z \qquad \ldots\ldots\ldots\ldots\ldots\ldots\ldots \quad 2$$

and the energy of a stationary state is

$$E_m = -\gamma \hbar H m, \quad m = S, S-1, \ldots, -S. \qquad \ldots\ldots \quad 3$$

To induce transitions between the $2S + 1$ levels an oscillatory magnetic field is needed in a plane normal to $\underline{H}$. There will be an additional perturbation due to the oscillating field described by the Hamiltonian,

$$\mathcal{H}' = -(H_x \mu_x + H_y \mu_y)$$

assuming that $\underline{H}$ is in the z-direction. Changing to an exponential

notation and using the relation $\mu_{\pm} = \mu_x \pm i\mu_y$ gives

$$\mathcal{H}' = -\frac{H_1}{2}(\mu_+ e^{-i\omega t} + \mu_- e^{i\omega t}). \quad \ldots\ldots\ldots \quad 4$$

It is a well known result from time dependent perturbation theory that if $H_{kn} = \langle k|\mathcal{H}'|n\rangle \neq 0$ and $\omega_{kn} = (E_k - E_n)/\hbar$ then a transition between the k and n states takes place (04). This phenomenon of absorption is known as magnetic resonance. The only matrix elements of H_{kn} which are non zero are $\langle m\pm1|\mu_{\pm}|m\rangle$, hence the selection rules $\Delta m = \pm 1$. The energy of a transition is therefore

$$\hbar\omega = E_m - E_{m-1} = \gamma\hbar H = g\mu_B H \quad \ldots\ldots\ldots\ldots \quad 5$$

where μ_B is the Bohr magneton and g is the spectroscopic splitting factor.

The equation of motion for a particle with spin $\underline{S}$ is

$$\frac{d}{dt}\underline{S} = \frac{i}{\hbar}[\mathcal{H}, \underline{S}] \quad \ldots\ldots\ldots\ldots\ldots\ldots\ldots \quad 6$$

The commutation relation for the components of angular momentum is

$$[S_x, S_y] = i S_z. \quad \ldots\ldots\ldots\ldots\ldots\ldots\ldots \quad 7$$

Therefore using equation 2 and the last two expressions

$$\frac{d}{dt}S_x = \gamma H S_y, \quad \text{etc.}$$

which are components of the vector equation

$$\frac{d}{dt}\underline{S} = \underline{S} \times \gamma \underline{H}. \quad \ldots\ldots\ldots\ldots\ldots\ldots\ldots \quad 8$$

If the average magnetic moment is substituted for the spin in equation 8 then this is equivalent to the classical equation for the precession of a moment in a magnetic field (02) (03).

The oscillatory magnetic field, which is in the radiofrequency region of the electromagnetic spectrum, stimulates with equal probability both "upward" and "downward" transitions between the magnetic sublevels. Absorption on energy occurs only if the populations of the sublevels differ, as they do at thermal equilibrium in a magnetic field. The difference in

populations between the spin levels is therefore decreased by the application of a radiofrequency field. This equalisation is opposed by relaxation mechanisms which tend to restore thermal equilibrium.

Consider a system with two energy levels $+\frac{1}{2}$ and $-\frac{1}{2}$ with populations N_+ and N_- respectively, see Fig. 1. The application of an oscillatory field will induce transitions between the $+\frac{1}{2}$ and $-\frac{1}{2}$ levels, thereby altering the relative populations. The total population will remain constant.

Fig. 1 Energy levels for $s = \frac{1}{2}$

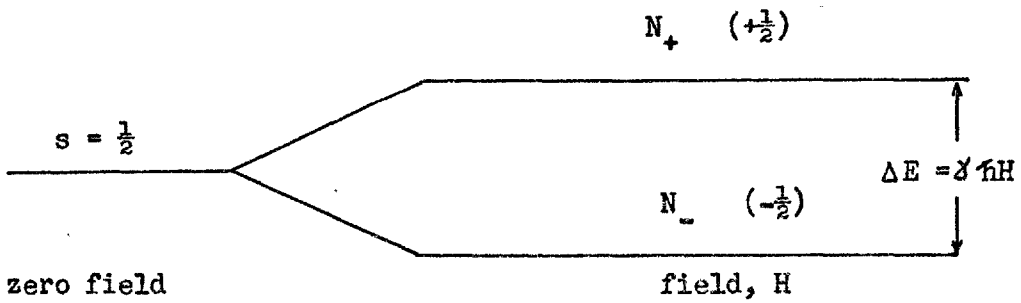

If the probability per unit time of inducing a transition in either direction is w then it follows that (01)

$$\frac{dn}{dt} = -2nw, \qquad n = N_+ - N_- \text{ and } N = N_+ + N_- .$$

There is an exponential solution to this equation and this effectively means that the populations will equalize under the action of the induced transitions. At a finite temperature T however, the populations will equilibriate at a level corresponding to that temperature,

$$N_-^e / N_+^e = e^{-\Delta E/k_B T}.$$

Therefore there must be a mechanism for coupling the energy to another system. In a crystal the other system is usually the lattice, the energy being exchanged by the emission and absorption of phonons.

Without specifying the relaxation process in detail, assume the transition probability per unit time for a spin in the $+\frac{1}{2}$ state to relax to the lattice is w_+ and that the probability for absorption of energy from the lattice is w_- . Then the rate equation for this process will be

$$\frac{dn}{dt} = \frac{n_o - n}{T_1}$$

where $n_o = N(w_- - w_+) / (w_- + w_+)$ and $1 / T_1 = (w_- + w_+)$. A solution of the above equation is given by $n = n_o + Ae^{-t/T_1}$, n_o is the equilibrium population difference and T_1 is the characteristic time (the spin lattice relaxation time) associated with the onset of equilibrium. Combining the two rate equations gives,

$$\frac{dn}{dt} = \frac{n_o - n}{T_1} - 2wn,$$

a steady state solution of which is

$$n = n_o /(1 + 2wT_1).$$

The power absorbed is given by

$$\frac{dE}{dt} = n\hbar\omega w = n_o\hbar\omega \frac{w}{1 + 2wT_1} .$$

If $2wT_1 \ll 1$ then the power absorbed can be increased simply by increasing the transition probability which is proportional to the squared amplitude of the modulation field (01)

$$w = \tfrac{1}{4}\gamma^2 H_1^2 F(\nu)$$

where $F(\nu)$ is the shape function. When w reaches a certain value, $1 / 2T_1$, the power absorbed begins to decrease and the system is said to have saturated. It is possible to measure T_1 by this effect. Lloyd and Pake (06) have given the theory of saturation effects in multi-level systems. Experiments performed on zinc sulphide phosphors, using saturation techniques, found a value of $T_1 = 10^{-6}$ s (07) (08).

4.2 Relaxation Effects.

The classical equation of motion for a particle with angular momentum J and magnetic moment $m = \gamma J$ in a magnetic field $\underline{H}$ is

$$\frac{d}{dt}\underline{J} = \underline{m} \times \underline{H} = \gamma \underline{J} \times \underline{H} \quad \ldots\ldots\ldots\ldots\ldots\ldots \quad 9$$

The solution of this equation is one in which $\underline{J}$ and $\underline{m}$ precess about $\underline{H}$ with angular frequency $\omega_L = -\gamma \underline{H}$. Equation (9) can be transformed to a rotating frame, the axis of rotation being along the $\underline{H}$ field (01) (02). Transformed in this way, the motion relative to the rotating system will be a precession with angular velocity $\omega' = \omega_L - \omega$, which is equivalent to an effective field $H_{eff} = H_o - \omega/\gamma$.

For a system of particles which have identical values of γ then (compare with 8)

$$\frac{d}{dt}\underline{M} = \gamma \underline{M} \times \underline{H} \quad \ldots\ldots\ldots\ldots\ldots\ldots\ldots \quad 10$$

where $\underline{M}$ is the magnetization. This equation describes the undamped motion of the magnetization vector (03). Relaxation effects must be included to give a realistic description of the spin system in a solid. They are included by a damping term $\underline{R}(\underline{M}, \underline{H})$, on the right hand side of equation 10. There are several types of phenomenological damping terms in common use, the two most important being the Landau and Lifshitz (09) and Bloch (10) forms.

(a) Landau and Lifshitz.

Landau and Lifshitz in 1935 proposed the following damping term

$$\underline{R}(\underline{M}, \underline{H},) = \frac{1}{2T} \frac{\underline{M} \times (\underline{M} \times \underline{H})}{|M|^2} \quad \ldots\ldots\ldots\ldots\ldots \quad 11$$

where 1/T is a relaxation rate. This damping term describes the relaxation of $\underline{M}$ towards $\underline{H}$; the magnitude of the magnetization is unchanged because

($\underline{M} \times \underline{H}$) is perpendicular to $\underline{M}$ so that $\underline{M} \times (\underline{M} \times \underline{H})$ represents a time rate of change at constant $\underline{M}$.

(b) The Bloch Equations.

Bloch (10) proposed a set of phenomenological equations to describe the dynamic behaviour of interacting nuclear moments in the presence of a magnetic field. These equations apply equally to the case of electron spin resonance. The Bloch equations are

$$\frac{d}{dt} M_{x,y} = \gamma (\underline{H} \times \underline{M})_{x,y} - M_{x,y} / T_2 \quad \ldots\ldots\ldots\ldots\ldots \quad 12$$

$$\frac{d}{dt} M_z = \gamma (\underline{H} \times \underline{M})_z + (M_o - M_z) / T_1 \quad \ldots\ldots\ldots\ldots \quad 13$$

To understand the meaning of the damping terms, consider the effect of firstly removing the radiofrequency field then the static $\underline{H}$ field. The relaxation can be viewed as a two stage process. Firstly, the z-component of the magnetization remains constant and the magnetic moment spirals towards the z-axis; since the energy of the system in a static field is $\underline{M}.\underline{H}$ the state of minimum energy is parallel to $\underline{H}$ (assumed to be applied in the z-direction). The time constant for this process is T_2, the transverse relaxation time.

The second process is the relaxation of the magnitude of the magnetic moment back to its equilibrium value, $M_z = \chi_o H_z$. The relaxation time of this is T_1, longitudinal time constant. Physically the interactions which give rise to these relaxation times occur together; therefore the two steps actually occur simultaneously.

The solution to Blochs equations can be obtained by transforming from the laboratory frame to a rotating frame of reference, rotating at a frequency ω of the radiofrequency field. Solutions have been obtained in this way by many authors (01) (05) and are given in terms of the complex susceptibility, $\chi = \chi' - i\chi''$

$$\chi' = \frac{\chi_0}{2} \frac{\omega_0 T_2 (\omega_0 - \omega) T_2}{1 + (\omega - \omega_0)^2 T_2^2} \quad \ldots\ldots\ldots\ldots \quad 14(a)$$

$$\chi'' = \frac{\chi_0 \omega_0 T_2}{2} \frac{1}{1 + (\omega - \omega_0)^2 T_2^2} \quad \ldots\ldots\ldots\ldots \quad 14(b)$$

The magnetic susceptibility is essentially the response of the system to the magnetic field and as such is an important quantity. It can be directly associated with the average power absorbed per unit volume of a paramagnetic sample.

$$P_{av} = \frac{1}{2} \omega H_1^2 \chi'' \quad \ldots\ldots\ldots\ldots\ldots\ldots\ldots\ldots \quad 15$$

This relation is not dependent on the form of the Bloch equations and can be obtained from quite general consideration (Slichter (05)).

The above solutions give a characteristic Lorentzian line shape, shown in fig. 2 .

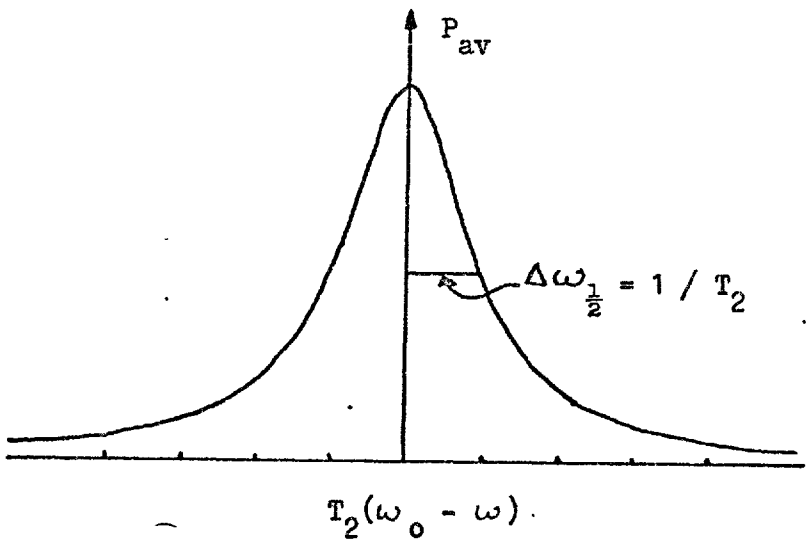

Fig. 2 Absorption versus frequency as obtained from a solution of the Bloch equations.

4.3 Ions in Crystals.

The most important interaction of an ion in a crystal is given by the Coulomb term, which is spin independent and of order 10^5 cm^{-1}. The next two terms in the Hamiltonian, the spin-orbit coupling and the crystal field interaction, vary in magnitude according to the ions involved. A summary of the energies is given in table 1.

Table 1

	Crystal Field Energy	Spin-Orbit Energy
Fe-group ions	$10 - 20 \times 10^3$ cm^{-1}	$100 - 800$ cm^{-1}
Pd-group ions	$20 - 40 \times 10^3$ cm^{-1}	$400 - 2000$ cm^{-1}
Rare-earth ions	200 cm^{-1}	$600 - 3000$ cm^{-1}

An ion usually has both orbital and spin momentum, the value of g depending on the coupling between them. This interaction is known as the spin-orbit coupling and can be written as $\lambda \underline{L}.\underline{S}$. The ground state before a magnetic field is applied usually has at least spin degeneracy therefore direct products of the orbital wavefunctions with the spin wavefunctions α and β must be formed in order to treat the spin-orbit coupling. This will give ground state wavefunctions in an applied field which are not pure "spin up" or "spin down" states. Nevertheless it is convenient to assign an effective spin S to the system, where 2S + 1 is the number of levels into which a magnetic field splits the ground state arising under crystal field and spin-orbit effects. Hence an effective spin Hamiltonian can be defined $\hat{H} = \mu_B \, g\underline{H}.\underline{S}$. This assumes that the energy depends only on the angle between the effective spin and the magnetic field. Generally this is not so, as the interaction also depends on the angle the field makes with certain crystallographic axes. Hence,

$$\hat{H} = \mu_B \, \underline{H}.\underline{g}.\underline{S} \qquad \ldots\ldots\ldots\ldots\ldots\ldots\ldots\ldots\ldots\ldots \quad 16$$

For example, axial symmetry gives $g_x = g_y = g_\perp$ and $g_z = g_\parallel$ thus

$$H = (g_\perp (S_x H_x + S_y H_y) + g_\parallel H_z)$$

As can be seen from table 1 the magnitude of the crystal field varies from the first transition series to the rare-earths. In the first transition series the large crystal fields must be considered before the spin-orbit coupling; this leads to the orbital angular momentum being quenched (03) and magnetic properties due almost entirely to spin. In the rare-earth series the crystal field can be treated after the spin-orbit term, hence $\underline{J}$ is a good quantum number.

Crystal field theory assumes that the paramagnetic ion is situated in a crystalline electric potential whose sources are point charges lying wholly outside the ion. Then as the electric field has a certain symmetry, due to the crystallographic structure of the solid, group theoretical arguments can be applied to obtain the Stark splittings (04). Group theory will only give the number of levels into which a given energy state is split and not the ground state or order of the various levels. For example, consider a rare-earth ion where the crystal field is a weak perturbation and the total angular momentum $\underline{J}$ is a good quantum number. For such an ion, with integral $\underline{J}$, in a cubic field there are five energy levels into which the ions original state may be split; they are Γ_1 to Γ_5. An ion with half integral $\underline{J}$ (which obeys Kramers theorem) can be split by a cubic field into three levels Γ_6 to Γ_8. Table 2 gives the degeneracy of the various crystal field levels.

	Γ_1	Γ_2	Γ_3	Γ_4	Γ_5	Γ_6	Γ_7	Γ_8
Degeneracy	1	1	2	3	3	2	2	4

Table 2

Γ_1 and Γ_2 being singlets are of no interest in electron spin resonance experiments, Γ_3 is a non-magnetic doublet and has no Zeeman splitting while Γ_4 to Γ_8 should all produce a resonance (11). For

the magnitudes and order of the energy levels the crystal field Hamiltonian has to be solved; it is given by the following eqation,

$$H_{cf} = \sum_{k,q} B_k^q \, O_k^q \qquad \begin{matrix} k \leqslant 2j \\ q \leqslant (m_j - m_j') \end{matrix}$$

where O_k^q are the spin operators (12) and B_k^q are the crystal field coefficients.

When the effective spin is one or more, there may be a number of lines in the epr spectrum due to the crystal field splitting. This is known as fine structure (01) (13).

There are other interactions which influence the epr of an ion in a crystal. The dipole-dipole interaction is due to the magnetic moments of the ions. It depends on the angle between the moments and on the angle between the spin and the vector to the other ion. As the local dipolar field depends on the distribution and orientation of the near neighbour moments it will vary from ion to ion. This therefore gives rise to a broadening of the resonance line. If exchange terms are included then the line is narrowed, as discussed in ch.3, section 3.

If a nucleus of a paramagnetic ion possesses an angular momentum and hence a nuclear moment then hyperfine structure is observed in the resonance spectrum. A nucleus with spin $\underline{I}$ will interact with a magnetic moment $\underline{S}$ via the contact Hamiltonian (01),

$$H_N = A \, \underline{I}.\underline{S}$$

where A is a coupling constant. This gives rise to a splitting of the paramagnetic line into $2I + 1$ equally spaced lines.

There is also an electrostatic interaction with the nucleus via the quadrupole moment of the nucleus. This is usually of the order 10^{-3} cm^{-1}, and therefore considerably smaller than most of the other interactions.

4.4 Electron Spin Resonance in Metals.

The resonance of magnetic impurities in metal hosts is fundamentally different from that in insulators. The reason for this is that the magnetic impurities cannot be considered as independent ions weakly perturbed by the conduction electrons. They must be considered as strongly linked to the conduction electrons via the local moment conduction electron exchange interaction given by

$$H_{ex} = -J \sum_i S(\underline{R}_i).s(\underline{r})\,\delta(\underline{R}_i - \underline{r}) \quad \ldots\ldots\ldots\ldots \quad 17$$

where J is the exchange integral, $S(\underline{R}_i)$ is the ion spin at the position R_i and $s(\underline{r})$ is the conduction electron spin at the position $\underline{r}$. Hasegawa (14) in 1959, was the first to present a full treatment of the linked conduction electron-local moment system.

The exchange interaction, in the molecular field approximation, should produce an additional internal field on the magnetic ion, resulting in a shift of the resonance proportional to the magnetic field. For the static susceptibility then

$$M_i^z = \chi_i (H^z + \lambda_{ie} M_e^z) \quad \ldots\ldots\ldots \quad 18$$

$$M_e^z = \chi_e (H^z + \lambda_{ie} M_i^z) \quad \ldots\ldots\ldots \quad 19$$

where M_i^z, M_e^z are the z components of the magnetization of the ions and electrons respectively, H^z is the external field, λ_{ie} the molecular field constants and $\chi_{i,e}$ are the respective magnetic susceptibilities. The effective field acting on the ions is given by

$$H_{eff} = H^z (1 + \lambda_{ie}\chi_e + \lambda_{ie}\chi_e\chi_i)$$

derived from equations (18) and (19). This effective field gives rise to a shift in the resonance position, known as the Knight shift (15) in nuclear magnetic resonance. For ions in exchange enhanced metals, the g-shift induced by H_{eff} is, to the first order (14) (16),

$$\Delta_g = J(0)\, N(E_f) / (1 - \alpha) \quad \ldots\ldots\ldots\ldots \quad 20$$

where $N(E_f)$ is the density of states at the Fermi surface and $J(0)$ is the local moment conduction electron exchange integral for $q = 0$ which is given by $J(0) = \lambda \chi_e / N(E_f)$. $J(0)$ has a number of contributions and its interpretation is not straightforward (see ch. 6, sect.1). There will also be a broadening of the resonance line due to the exchange:

$$\Delta H = \frac{\pi}{2\mu_B} (\Delta_g)^2 k_B T\, K(\alpha) \quad \ldots\ldots\ldots\ldots\ldots \quad 21$$

this relation was first deduced by Korringa (17) for nuclear relaxation in metals. In the above, α is the exchange enhancement factor for the static longitudinal susceptibility (18) and $K(\alpha)$ is a function given by Narath and Weaver (19). For metals which are not exchange enhanced then $\alpha = 0$ and $K(\alpha) = 1$.

The various relaxation paths for the local moment conduction electron system are shown in Fig. 3, where T_{iL}, T_{ie}, T_{ei} and T_{eL} are the relaxation times of the ions to the lattice, of the ions to the electrons, of the electrons to the ions and of the electrons to the lattice respectively (corresponding to the relaxation rates $\delta_{iL} = 1 / T_{iL}$, etc.). The magnetic resonance of the coupled local moment conduction electron system can be described by the equations (Giovannini (23)) -

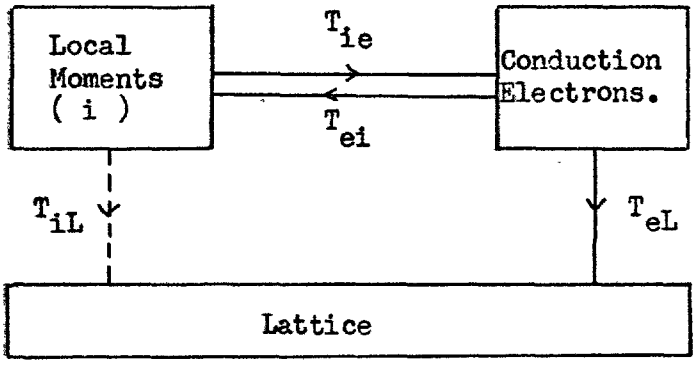

Fig. 3 A schematic diagram of the relaxation paths for a local moment in a metal.

$$\frac{d}{dt}\underline{M}_i = g_i\mu_B\left(\underline{M}_i \times \left(\underline{H} + \lambda_{ie}\underline{M}_e\right)\right) + \underline{R}_i \quad \ldots\ldots \quad 22(a)$$

$$\frac{d}{dt}\underline{M}_e = g_e\mu_B\left(\underline{M}_e \times \left(\underline{H} + \lambda_{ie}\underline{M}_i\right)\right) + \underline{R}_e \quad \ldots\ldots \quad 22(b)$$

where $\underline{R}_i$, $\underline{R}_e$ are the relaxation terms which they must obey the following criteria;

(a) They must be functions of T_{ie}, T_{ei}, T_{eL} and T_{iL}.

(b) Kittel and Mitchell (21) showed that when the gyromagnetic factors are equal, the exchange interaction alone cannot alter the resonance line shape ($\underline{S}.\underline{s}$ commutes with the total spin of the system), therefore when $1 / T_{iL} = 1 / T_{eL} = 0$, then $\underline{R}_i + \underline{R}_e = 0$.

(c) The energy absorption must be positive, this implies the detailed balance condition $\chi_i / T_{ie} = \chi_e / T_{ei}$.

Hasagawa examined equations (22) with the following relaxation terms

$$\underline{R}_i = -\underline{M}_i / T_{ie} + \underline{M}_e / T_{ei}$$

$$\underline{R}_e = -\underline{M}_e / T_{ei} + \underline{M}_i / T_{ie} - \left(\underline{M}_e - \chi_e\left(\underline{H} + \lambda_{ie}\underline{M}_i\right)\right) / T_{eL}$$

He analysed two limits, "case A" with the relaxation towards the equilibrium external field direction and "case B" with the relaxation towards the instantaneous external and internal fields. Cottet et al (20) showed that the Hasagawa equations did not fulfil condition (c) above and proposed the following relaxation terms which satisfy conditions(a), (b) and (c):

$$\begin{aligned}\underline{R}_i = &-\delta'_{ie}\underline{M}_i \times \left(\underline{M}_i \times \left(\underline{H} + \lambda_{ie}\underline{M}_e\right)\right) \\ &+\delta'_{ei}\underline{M}_e \times \left(\underline{M}_e \times \left(\underline{H} + \lambda_{ie}\underline{M}_i\right)\right) \quad \ldots\ldots\ldots \quad 23 \\ &-\delta'_{iL}\underline{M}_i \times \left(\underline{M}_i \times \left(\underline{H} + \lambda_{ie}\underline{M}_e\right)\right)\end{aligned}$$

similarly for $\underline{R}_e$. The relaxation rates are primed because they are defined by $M_e^z\left(H^z + \lambda_{ie}M_e^z\right)\delta'_{eL} = \delta_{eL}$, etc.

These are Landau-Lifshitz type relaxation terms as previously described in section 4.2(a). The small transverse magnetization limit of expression 23

reduces to Hasegawa's case B. From the above equations the following expressions for the g-shift and linewidth, as a function of the relaxation rates may be obtained(14) (22)

$$\Delta g = \Delta g_o \frac{\delta_{eL}^2}{d^2 + (\delta_{eL} + \delta_{ei})^2} \quad \ldots\ldots\ldots\ldots\ldots\ldots \quad 24$$

$$\Delta H = \Delta H_o \frac{(\delta_{ei}^2 + d^2)\,\delta_{eL} / \delta_{ei} + \delta_{eL}^2}{d^2 + (\delta_{eL} + \delta_{ei})^2} \quad \ldots\ldots\ldots\ldots\ldots \quad 25$$

where $d = \lambda \gamma \chi_i H$, in this expression γ is the gyromagnetic ratio, λ is the molecular field constant and χ_i is the static susceptibility of the impurity ion. Δg_o and ΔH_o are given by equations (20) and (21).

The magnetic ions relax to the conduction electrons at the Korringa (17) rate

$$\delta_{ie} = \frac{\pi}{\hbar} \left(J(0)\, N(E_f) \right)^2 k_B T \quad \ldots\ldots\ldots\ldots\ldots\ldots \quad 26$$

This relation is only approximate even allowing for the exchange enhancement factor $K(\alpha)$. For example, in Pd-Gd (31) there is still a large difference between experiment and theory. It has been suggested (28) that this discrepancy arises from the fact that only J(0) is included in δ_{ie}, a consequence of the delta function range of the exchange. The simple Korringa relation should therefore be modified by the inclusion of

$$J^2(q) = (J^{(o)})^2 + 3\,(J^{(1)})^2 + 5(J^{(2)})^2 + \ldots$$

The conduction electrons relax to the ions at the Overhauser (29) rate. This has been specifically adapted for the esr of ions in metals by Hasegawa (14),

$$\delta_{ei} = \frac{2\pi}{3\hbar} J^2\, N(E_f)\, S(S+1)\, c \quad \ldots\ldots\ldots\ldots \quad 27$$

where c is the concentration of magnetic impurities of spin S. The direct lattice relaxation rate, δ_{iL}, is assumed to be negligible compared with the other rates (24).

There are two extreme limits of the above expressions (24) and (25):

(1) When $\delta_{eL} \gg \delta_{ei}$ the full g-shift is observed and is equal to Δg_o. In this limit, the conduction electron spins relax so rapidly to the lattice that the controlling rate is that of the local-moment to the conduction electrons, δ_{ie}, and therefore the Korringa line width ΔH_o is observed. This limit applies to many systems especially when the host is strongly d-like (Gd in $LaNi_5$ (22), Mn in Pd (25)).

(2) When $\delta_{eL} \ll \delta_{ei}$, the g-shift tends to zero and the linewidth is given by

$$\gamma \Delta H = \frac{\delta_{ie}}{\delta_{ei}} \cdot \delta_{eL} = \frac{3}{2} \frac{N(E_f)\, k_B T}{S(S+1)\, c} \cdot \delta_{eL} \quad \ldots\ldots\ldots\ldots \quad 28$$

using equations (25), (26) and (27). In this limit the magnetic impurities and conduction electron spins are strongly coupled and cannot exert a torque on one another. This is essentially the adiabatic limit, as the energy in the spin system is "locked in" and unable to relax faster than δ_{eL}. This is the so called bottlenecked limit. Here we observe a g-value and linewidth which are susceptibility weighted averages of the ion and conduction electron values.

It is possible to open the bottleneck by either decreasing δ_{ei} or increasing δ_{eL}. δ_{ei} is proportional to the concentration of the magnetic impurity, equation (27), and therefore can be decreased simply by altering the concentration. δ_{eL}, which is the conduction electron lattice relaxation rate, can be increased by adding impurities with large spinflip cross sections. These tend to be heavy atoms with significant spin-orbit coupling (24) (26).

Gossard et al (27) carried out one of the first studies of a bottleneck system. They observed the resonance of Mn in Cu and found relaxation rates which were about a factor of 10^{-4} smaller than the Korringa rate and that a broadening of the resonance line was produced when non-magnetic impurities were added.

A bottlenecked system may be identified from the following characteristics:

(a) The g-value for an s-state ion will be close to two and J(0) calculated from the g-value will be an underestimate.

(b) The slope of the linewidth against temperature will be much lower than that predicted by the Korringa relation.

(c) Equation (28) should hold after subtracting any residual linewidth (see ch. 5, sect. 1 for definition of residual linewidth).

(d) Addition of impurities, which open the bottleneck, should increase the slope of the linewidth in the paramagnetic region. The opening of the bottleneck will always be observed in the linewidth before the g-value since the former varies as $\delta_{eL} / \delta_{ei}$ whilst the latter as the square of that ratio.

In equations (24) and (25) the term $(\lambda\gamma \chi_i H)$ in the denominator gives rise to the so called "dynamic effects" (22). If the temperature is sufficiently reduced then this term may become comparable in magnitude to $(\delta_{ei} + \delta_{eL})^2$. This leads to a strong field and concentration dependence of the g-shift. A number of authors (22) (30) have claimed that they have observed dynamic effects. These claims will be discussed in ch.6 together with contrary evidence from this work on $LaNi_5$- Gd.

4.5 Fine and Hyperfine structure.

Fine structure splittings for 4f s-state ions in metals have only been seen recently, firstly as line shape anomalies and shifts (29) (30) and then as fully resolved fine structure (31) (32). This fine structure is highly exchanged narrowed (35) (36) (37) for bottlenecked systems but only mildly narrowed for unbottlenecked systems. The narrowing can be thought of as a hopping between fine structure levels caused by the cross relaxation between impurities via the conduction electrons.

This effectively leads to a wiping out of fine structure for most systems except at low temperatures and very low concentrations.

For example, consider the bottlenecked system MgGd, studied by Tao et al (30), who observed a single line where seven should have been found. Even so, unresolved fine structure was implicated as the mechanism for the temperature and angular shifts of the resonance field. Resolved fine structure has been observed in the unbottlenecked PdGd (31) and $BaAl_4$ (Eu^{2+}) (32) systems. For 3d impurities where the interactions are much stronger it will be very difficult to resolve fine structure and as yet none has been seen.

Hyperfine structure due to the interaction of the impurity spin with the nuclear spin has also been observed (33). Barnes et al (38) analysed the hyperfine problem by adding an effective field term, due to the impurities' own nuclear spin, to equations (22). They concluded that in the unbottlenecked limit hyperfine splittings should be observed. In the bottlenecked limit, with δ_{ie} greater than the hyperfine splitting there will be no structure observed but with δ_{ie} less than the splitting then hyperfine structure should be present, although each hyperfine component will be reduced from the non-metallic case by $2I / (2I + 1)$ where I is the spin of the nucleus. For more details of fine and hyperfine structure see the review by Taylor (34).

REFERENCES CHAPTER 4

1. PAKE, G.E., Paramagnetic Resonance, New York: W.A. Benjamin, 1962.

2. RABI, I.I., RAMSEY, N.F., and SCHWINGER, J., Revs. mod. Phys. 26, 167 (1954).

3. KITTEL, C., Introduction to Solid State Physics, John Wiley and Son, New York (1971).

4. SCHIFF, L.I., Quantum Mechanics, McGraw-Hill, (1968).

5. SLICHTER, C.P., Principles of Magnetic Resonance, Harper and Row (1964).

6. LLOYD, J.P., and PAKE, G.E., Phys. Rev., 94, 579 (1957).

7. SCHNEIDER, C.P. and ENGLAND, J.S., Physica, 17, 221 (1951).

8. ESCHENFELDER, A.H. and WEIDNER, R.T., Phys. Rev., 92, 869 (1953).

9. LANDAU, L. and LIFSHITZ, E., Physik. Z. Sovjetunion, 8, 153 (1935).

10. BLOCH, F., Phys. Rev., 70, 460 (1946).

11. LOW, W., Sol. Stat. Phys., Ed. F. Seitz and D. Turnbull, Sup.2 (1960).

12. STEVENS, K.W.H., Proc. Phys. Soc., A65, 209 (1952).

13. ABRAGAM, A. and BLEANEY, B. Electron Paramagnetic Resonance of Trans. Ions., Clarendon Press, Oxford (1970).

14. HASEGAWA, H., Progr. Theo. Phys., (Kyoto) 21, 483 (1959).

15. KNIGHT, W.D., Sol. St. Phys., Ed. F. Seitz and D. Turnbull, Vol. 2, 93 (1956).

16. NARATH, A., Hyperfine Interactions, Ed. A.J. Freeman and R.B. Frankel, Academic Press, 344 (1967).

17. KORRINGA, J., Physica, 16, 601 (1950).

18. WHITE, R.M., Quantum Theory of Magnetism, McGraw-Hill, (1970).

19. NARATH, A. and WEAVER, H.R., Phys. Rev., 175, 373 (1968).

20. COTTET, H., DONZE, P., DUPRAZ, J., GIOVANNINI, B. and PETER, M., Z. Angew, Phys., 24, 249 (1968).

21. KITTEL, C. and MITCHELL, A.H., Phys. Rev., 101, 1611 (1956).

22. DAVIDOV, D. and SHALTIEL, D., Phys. Rev. Lett., 21, 1752 (1968).

23. GIOVANNINI, B., Phys. Letts., 26A, 80 (1967).

24. ORBACH, R., PETER, M. and SHALTIEL, D., Proc. of Conf. on EPR of magnetic ions in metals, Haute-Nendaz, 9, (1973).

25. TAYLOR, R.H., , Thesis, Univ. of London, 1972.

26. YAFET, Y., J. Phys. Chem. Sol. 30, 1957, (1969).

27. GOSSARD, A.C., HEEGER, A.J. and WERNICK, J.H., J. Appl. Phys., 38, 1251 (1967).

28. DAVIDOV, D. MAKI, K., ORBACH, R., RETTORI, C. and CHOCK, E.P., Sol. Stat. Comm. 12, 621 (1973).

29. ELSCHNER, B. and WEIMANN, G., Solid State Comms., 9, 1935 (1971).

30. TAO, L.J., DAVIDOV, D., ORBACH, R., SHALTIEL, D. and BURR, C.R., Phys. Rev. Letts. 26, 1438 (1971).

31. DEVINE, R.A.B., SHALTIEL, D., MORET, J.M., ORTELLI, J., ZINGG, W. and PETER, M., Solid State Comms., 11, 525 (1972).

32. ELSCHNER, B., LUFT, H., SCHAFER, W. and SCHON, G., Proc. Conf. on ESR of ions in metals, Haute-Nendaz, 105, (1973).

33. CHUI, R., ORBACH, R. and GEHMAN, B.L., Phys. Rev., B2, 2298 (1970).

34. TAYLOR, R.H., Adv. Phys. 1975 (to be published).

CHAPTER 5

EXPERIMENTAL METHODS AND APPARATUS.

All the paramagnetic resonance measurements reported in this work were made using a spectrometer originally built by Dr.D.Griffiths. The measurements of magnetic susceptibility were made on a newly built Faraday microbalance which is described in the second section of this chapter. The resistance results were obtained on a standard four terminal DC resistance rig originally designed by Dr.A.D.Caplin and later modified by Dr.A.J.Barber (01).

5.1 Electron Paramagnetic resonance (EPR) spectrometer.

The spectrometer is a conventional homodyne x-band reflection spectrometer, a block diagram of which is shown in Fig.1. A detailed description of this apparatus has been given by Taylor (02).

The microwave power is supplied by conventional klystron which feeds one arm of a four armed wave guide system. This supply arm joins a hybrid tee at which the power is split between the "bucking" and the cavity arms. The frequency of the klystron is locked to that of the cavity by an automatic frequency control (AFC) loop. The purpose of the bucking arm is to feed an additional signal to the detector so that the absorption and dispersion signals may be separated. The required amount of suppression of the undesired signal is achieved by an attenuator and phase shifter in the bucking arm. The reflected signal from the bucking and the cavity arm recombine in the hybrid tee and then pass down a fourth arm via a directional coupler to a crystal diode detector.

The signal from the diode then passes through a series of variable gain wide band amplifiers to a 4.7KHz tuned stage and phase

Fig.(1) E.S.R. Spectrometer.

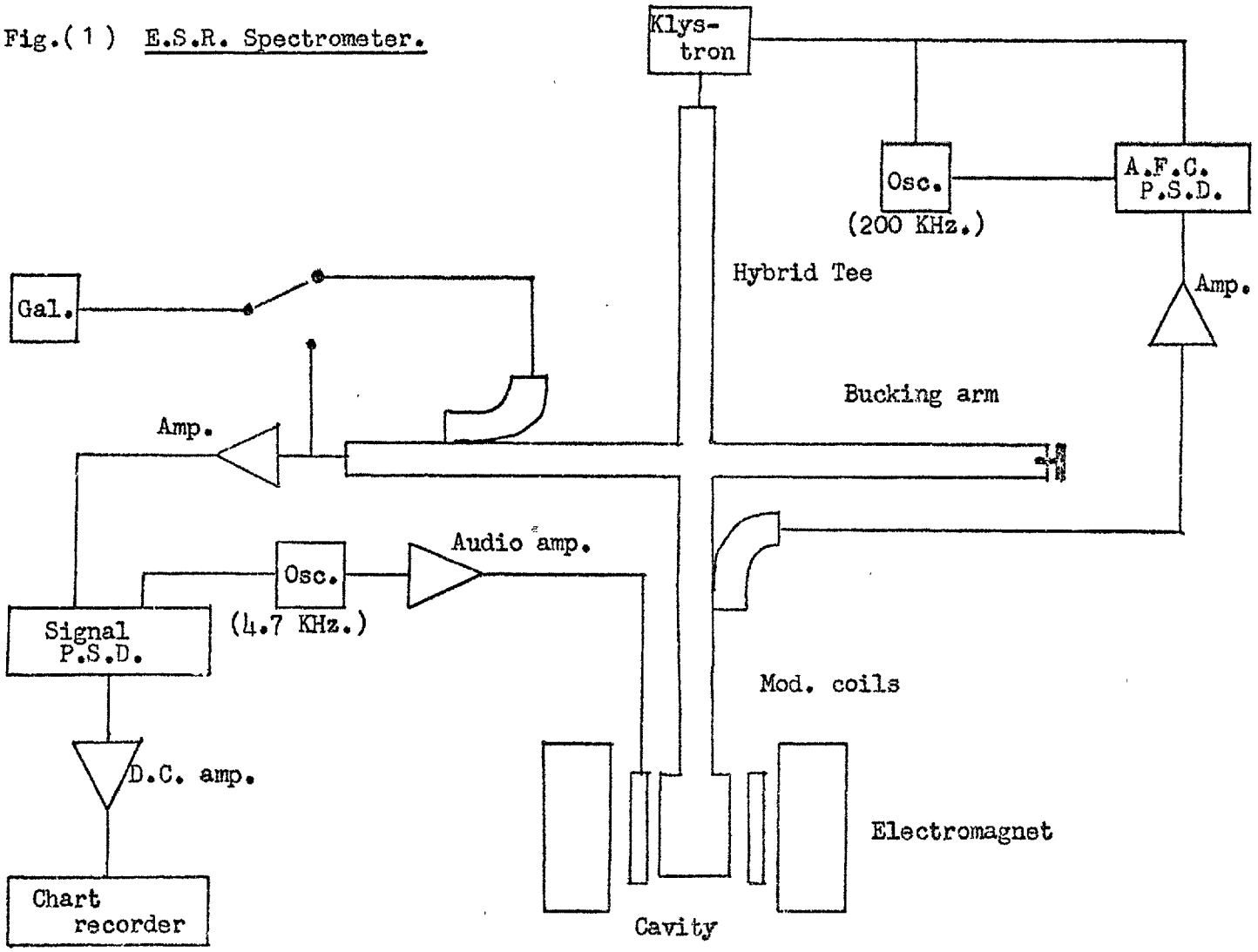

sensitive detector (PSD). The signal from the PSD then passes into a DC amplifier, the output of which is connected to a chart recorder.

The method of obtaining a signal used in this instrument requires the magnetic field to be modulated. This is provided by coils in the pole gap of the electromagnet, which are driven by a 4.7KHz signal. This produces an oscillating magnetic field with a maximum amplitude of 15 Gauss. This amplitude is small compared with the typical width of a spectral line (150 Gauss upwards); therefore the chart recorder traces out a derivative curve (03).

The static magnetic field is supplied by an electromagnet with a pole gap of 6.5cm. Fields up to approximately 8KG may be obtained, with a homogeneity of better than 1 part in 10^3 across the pole faces. The field is swept electronically by a unit that has sweep times of $\frac{1}{2}$ minute to 16 minutes for zero to full field. It is measured using a Bell 620 Gaussmeter via a Hall probe which is mounted in the pole gap as close as possible to the dewars. The output of the Gaussmeter is monitered on a digital voltmeter. Field calibration marks are obtained by a chart marking facility (04) which causes a "blip" to appear on the pen recorder chart when the first counter of the DVM is at the beginning of its display period. These marks are then calibrated in terms of the magnetic field using a nuclear magnetic resonance probe.

The resonant cavity.

A resonant cavity can maintain standing wave configurations at a given frequency. For a particular size and shape a number of configurations may be sustained; these are called modes. The cavity in this spectrometer has a cylindrical TE_{112} mode. It was originally designed and constructed by Lowin (05) but unfortunately the original

Fig. 2 Spectrometer Cavity.

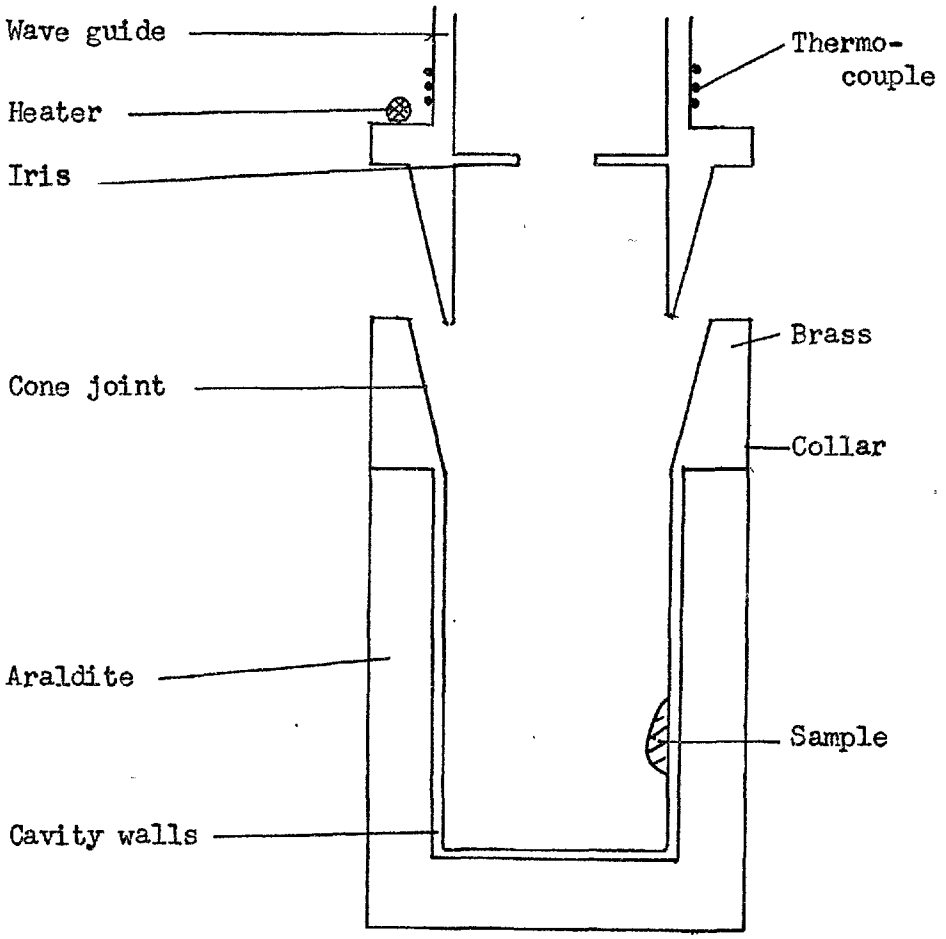

cavity cracked and therefore a new one had to be made.

The new cavity, which was the same design as the original, was constructed from Naval brass (Cu 62%: Zn 37%: Sn 1%) which is relatively free from magnetic and superconducting impurities. The brass was machined to the correct shape (see Fig.2) with the walls at this stage being approximately 10 thou thick. The walls must be of such a thickness that they allow the modulation field into the cavity but prevent the microwaves from escaping; this means a thickness of the order 6 to 8 thou. After machining, the brass is thoroughly cleaned to remove any grease and fitted with a cylindrical mould made from aluminium which is a "push fit" around the collar.

The body of the cavity is made of Araldite which gives thermal mass and mechanical strength. The resin used consisted of Araldite MY 750, hardener HY 906 and accelerator DY 063 in the proportion by volume of 100:80:3. This was mixed with a mineral filler (Millikarb) in order to minimize shrinkage and decrease the coefficient of expansion, thus making the Araldite less likely to crack under repeated thermal cycling. The ratio of filler to resin was 1:1. The mixing and pouring of the Araldite into the mould should be carried out under vacuum to minimize the formation of voids but unfortunately this was not possible. In order to release as much air as possible the mould, after filling, was placed in a vacuum chamber. The epoxy resin was cured in two stages. Firstly, the mould was placed in an oven at 100 C for two hours to gel the resin and secondly, it was left overnight (approximately 12 hours) at a temperature of 160 C.

The mould was carefully machined away and any rough edges on the cavity were trimmed. Finally the walls were etched to the correct thickness. The modulation field was measured inside and outside of the cavity

with a small search coil to make sure that the difference was less than 5%. It was then cleaned and polished. The unloaded Q factor for the cavity is approximately 6000.

Cryogenics.

The temperature may be varied from 1.8K to room temperature by means of a conventional double dewar technique. This consists of an inner (helium) dewar with its interspace connected to a diffusion pump and an outer (nitrogen) dewar. The interspace of the helium dewar is pumped to a pressure of 10^{-2} torr before filling the outer dewar with liquid nitrogen. This ensures that the cool down rate is sufficiently slow to prevent the Araldite of the cavity from cracking. When the temperature of the cavity has reached about 77K liquid helium may be transferred into the inner dewar.

Temperatures below 4.2K are obtained by pumping on the liquid helium and measured by recording the vapour pressure with a mercury manometer. The pressure is held steady by a manostat. Above 4.2K the thermal mass of the cavity is relied on to stabilize the temperature, measurements of which are made by a Au 0.03% Fe -chromel thermocouple (annealed) referenced to room temperature. Calibration below liquid nitrogen temperatures is from the work of Rosenbaum (06) and above from that of Berman (07). During a warm up to 77K the average temperature drift in the course of a sweep is less than $\frac{1}{2}$K.

If it is necessary to take measurements above liquid nitrogen temperatures, adjustment of the helium dewar interspace pressure allows the cooling rate from room temperature to be made slow enough to take sweeps in this region. For temperatures in the range 55 - 77K liquid nitrogen may be put into the inner dewar and pumped on, the pressure being stabilized by a manostat.

Experimental Procedure.

The skin depth of a metal at microwave frequencies is of the order 10^{-4} to 10^{-5}cm, therefore samples are made into powders to give the maximum surface area and hence maximize the number of spins the microwaves can "see".

To obtain specimens in the form of powders one of two methods is used, either grinding in a mortar and pestle or filing. The preparation of intermetallic compounds is straightforward because they are generally very brittle. About half of a gram is placed under acetone in a glass mortar and crushed into a fine powder. The size of the particles produced in this way was in the region of 10μm. The powder and acetone are transferred to a glass tube and the acetone pumped off. The powder is then tipped into vacuum grease. The majority of work in this thesis is on intermetallic compounds but some dilute alloy work has been done. Dilute alloys have to be filed to obtain powders and care must be taken not to contaminate the sample. The details of this procedure can be found in Taylor (02). Particle sizes from filing are in the range 50-100 μm.

Some crystals of DPPH (diphenyl picryl hydrazyl) are added to the sample as a g-value marker (g_{DPPH} = 2.0036 (08)). The specimen is then attached to the cavity wall, approximately $\lambda/4$ from the bottom. The amount of sample used, about $\frac{1}{4}$ cm^3, is adjusted so that the cavity is slightly under matched thus allowing correct matching to occur at low temperatures.

The cavity cone joint is greased with low temperature vacuum grease and then attached to the waveguide which is then evacuated. The dewars are put into position and the specimen cooled down to helium temperatures. At 4.2K the klystron is tuned to the resonant frequency of the cavity and the matching checked. The resonant

frequency is then measured by a wavemeter. The automatic frequency control output is monitered and the klystron electrically fine tuned until the frequency is precisely adjusted to that of the cavity. The AFC loop is then closed, locking the klystron to the cavity frequency. Finally, the bucking signal is adjusted to give only the absorption signal whilst maintaining the signal crystal current at its optimum value (i.e. the value which gives the best signal to noise ratio).

The pen recorder may now be zeroed after which the appropriate amplifier gain and time constant are set. The magnetic field is then swept to a high value and the magnet rotated to minimize any offset due to "wall-breathing". This effect is the mechanical vibration of the cavity walls caused by the interaction of induced currents in the walls with the static magnetic field. These currents are induced by the 4.7KHz modulation field. An extra signal is produced at the modulation frequency due to wall breathing which passes through the tuned amplifier and the PSD. This gives an offset on the chart recorder which increases with field and causes a baseline drift (02) (09). After this final adjustment the spectrometer is ready to run, a typical trace is shown in Fig.3.

Line shapes and corrections.

At microwave frequencies skin effects in metals must be accounted for when analysing the epr line shape. Dyson (10) studied the problem theoretically and showed that the line shape depends on the time that it takes an electron to diffuse through the skin depth T_d, the time T_T it takes for an electron to transverse the sample, the electron spin-lattice relaxation time T_1 and the spin-spin relaxation time T_2($T_1 = T_2$ for metals). The skin depth δ is the distance in which the amplitude of an electromagnetic wave falls to e^{-1} of its initial value when entering a metal. Experimental confirmation of

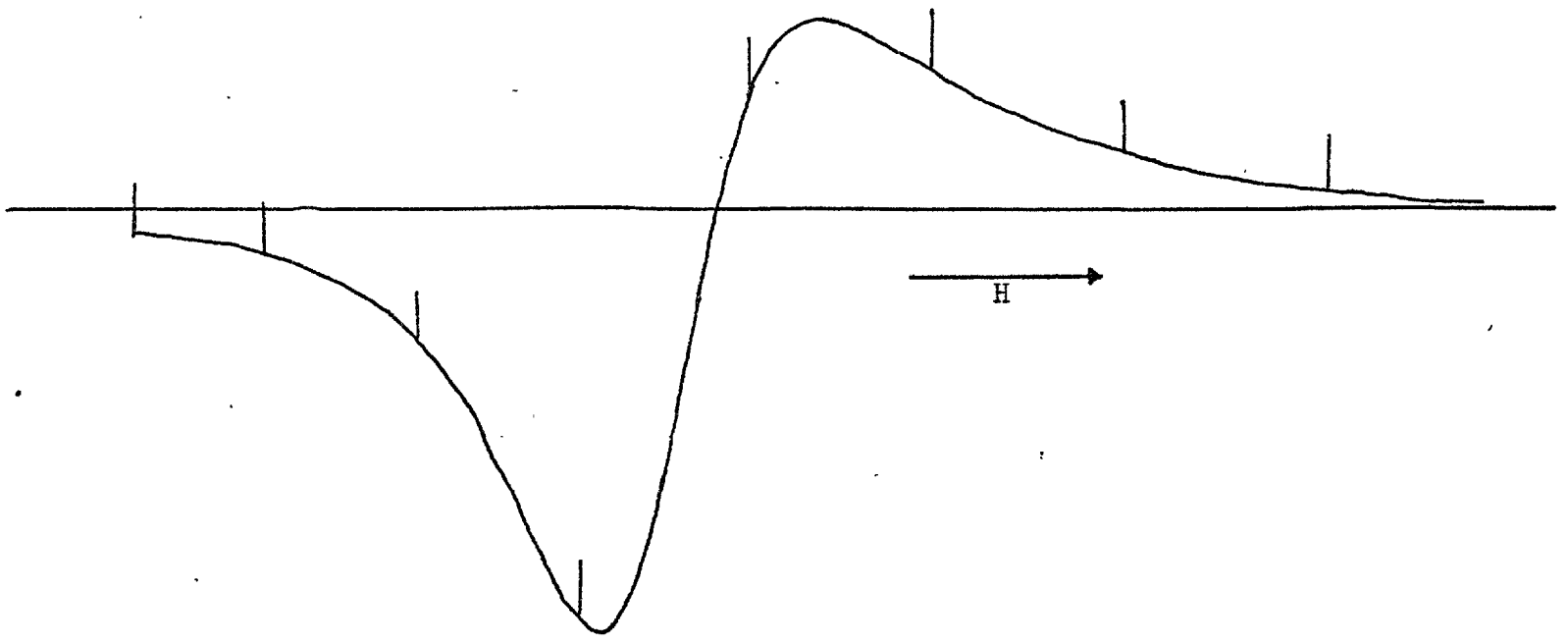

FIG.3 A typical epr derivative trace from a metallic system. The "blips" are magnetic field calibration marks.

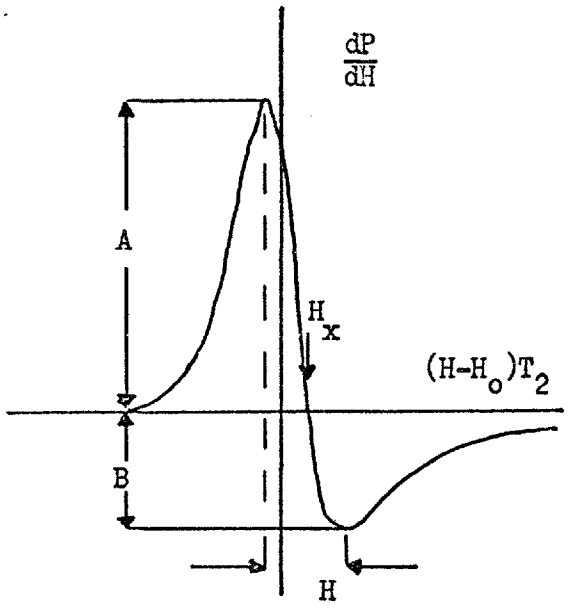

(a)

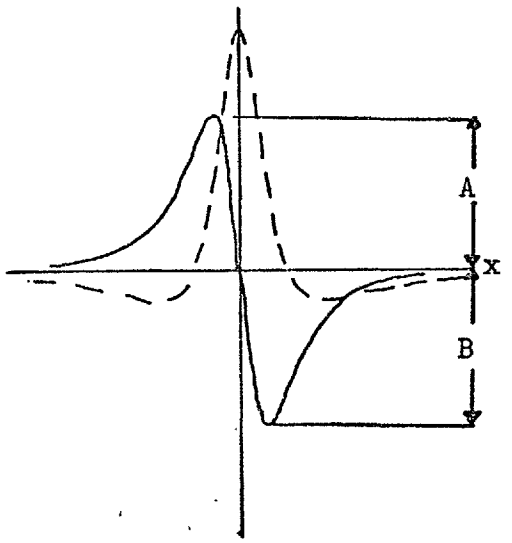

(b)

FIG.4 a. epr absorption curve for a metal (after ref.11)

b. A comparison of the dispersion ($d\chi'/dx$ – –) and absorption ($d\chi''/dx$ ——) for a Lorentzian line (after ref.13)
$x = (H - H_o)T_2$.

Dyson's theory was given by Feher and Kip (11).

If the dimensions of a particle are small compared with the skin depth, the results are independent of diffusion through the skin depth and a symmetrical Lorentzian line shape is obtained, Fig.4b. The ratio of the maximum to minimum of the derivative absorption line versus field, A / B,is1.

The case which is relevent to this work is the one in which

$$T_T \gg T_d \gg T_2.$$

In this limit the skin depth is small compared with the particle size and the magnetic moments are diffusing very slowly. This is appropriate to the case of paramagnetic impurities distributed throughout the volume of a metal. Dyson showed that the observed signal contains a certain amount β of the dispersive component, therefore the susceptibility may be represented by

$$\chi = \beta\chi' + i\chi''.$$

In the above limit $\beta = 1$ and A / B = 2.55 (Owen et al (12)).

For this value of A / B the centre of the true resonance, $H_{x,true}$, is given by approximately (12) (15),

$$H_{x,true} = H_{x,obs} - H_{obs}/3$$

and the peak to peak linewidth by

$$\Delta H_{true} = 0.9\Delta H_{obs}.$$

The above equations all refer to the derivative of the absorption signal, shown in Fig.4a.

If the observed line shape ratio is different from 2.55, the correction factors of $\frac{1}{3}$ and 0.9 will also change. Dr.D.Griffiths has calculated the correction factors for varying A / B ratios (14). Therefore simply by measuring A / B from the observed line the corrections may be read from a graph.

The final correction to the line shape is for the time constant

of the last amplifier stage. This is determined by displaying a signal at a set value of the field and then rapidly turning off the modulation. The time taken for the signal to decay by e^{-1} is then measured and the true cross over found from

$$H_x = H_{xc} \pm \tau R \qquad \tau R \ll \Delta H$$

where τ is the time constant, R the chart speed and H_{xc} is $H_{x,true}$ above.

The linewidth can usually be fitted to a linear function of the temperature;

$$\Delta H = A + BT$$

where A is a constant known as the residual linewidth and B is the Korringa slope. The linewidth is obtained by judging the position of the maximum and minimum in the derivative signal and then measuring their separation. The position of a point on the trace may be obtained to $\pm$ 5 G, therefore if an average line is 300 G broad the minimum error is $\pm$ 3%. This assumes that the minimum and maximum are located exactly; however, as they are estimated by eye this will not be so, especially for broad lines of small intensity. The total error in the linewidth is likely to be between $\pm$ 3-10% depending on the quality of the signal.

The measurement error in the g-value is approximately $\pm$ 0.3% but due to the corrections, distorted line shapes and base line drift (the major contribution) a more realistic figure is $\pm$ 0.5%.

5.2 The Faraday Susceptibility Balance.

The construction of a Faraday magnetic susceptibility balance is described in this section. This instrument allows measurement of susceptibility to be made in the range 1.8K to room temperature. The balance was designed around an electromagnet which has a pole gap of 3 cm and a maximum field of 10 KG. The apparatus is shown in Figs. 5 to 7.

The Faraday method.

This method of measuring magnetic susceptibility is essentially a measurement of the force exerted on a small sample placed in a inhomogeneous magnetic field. The force on a magnetic moment $\underline{\mu}$ in such a field is

$$\underline{F} = \underline{\mu} \cdot \nabla \underline{H} \quad \ldots\ldots\ldots\ldots\ldots\ldots \quad 1$$

If the magnetic field is such that the field gradient is only in one direction, say the z-direction then the force in this direction is given by the following (16)

$$F_z = v\,(\chi_v - \chi_o)\,H_y \frac{dH}{dz}y \quad \ldots\ldots\ldots\ldots\ldots \quad 2$$

where F_z is the force in the z-direction, χ_v is the susceptibility of the sample per unit volume, χ_o is the susceptibility of the surrounding medium, v is the volume of the sample and H_y is the magnetic field in the y-direction (Fig.5). χ_o can be neglected as all measurements were performed in 1 - 3 torr of helium, the susceptibility of which at 20 C and 760 torr is -8.4×10^{-12} emu cm^{-3}. Changing to the susceptibility per gram gives

$$F_z = m\chi_m H_y \frac{dH}{dz}y \quad \ldots\ldots\ldots\ldots\ldots\ldots \quad 3$$

$$F_z = m\chi_m K$$

where m is the mass of the sample and K ($=H_y\, dH_y/dz$) is the field gradient at the sample position. Hence, the susceptibility can be found if the force F_z on the sample and the constant K are known.

Experimentally the field gradient is supplied by an electromagnet and the constant K obtained by using a sample of known susceptibility to calibrate the magnetic field. The force is measured by a commercial chemical microbalance, $F_z = Wg$ where W is the apparent increase in mass due to the magnetic field and g is the acceleration due to gravity.

For a sample where the demagnetization fields cannot be ignored then the magnetization is given by

$$\mu_y = m \chi_m \frac{H_y}{1 + 4\pi D \chi_m}$$

where D is the demagnetization factor.

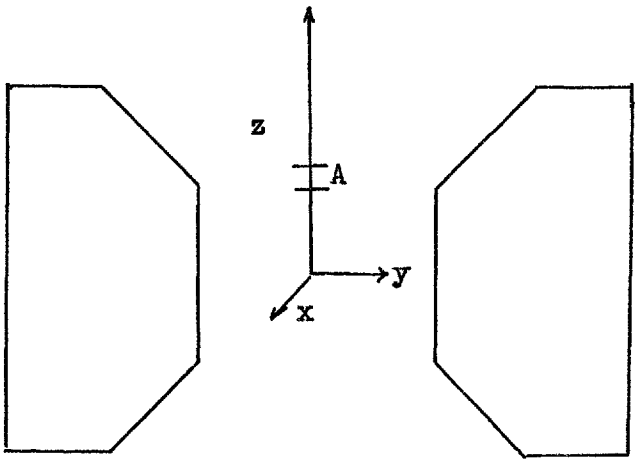

Fig. 5 Magnetic pole pieces and coordinate system, A is the approximate sample position.

Cryogenics.

The cryostat consists of two tailed dewars, an outer nitrogen dewar and an inner helium dewar. As the gap between the magnetic pole pieces is only 3 cm it was impossible to make both dewars of glass and still have sufficient space for the suspension tube. Therefore the outer dewar was made from non-magnetic stainless steel, the tail of which (o.d. 3.175 cm) had a section machined down to fit between the poles. A valve was fitted to the body of the dewar so that it could be pumped out periodically. The dewar body was lined with super-insulation. The whole unit was made by Vaughan and Cameron Ltd..

The inner dewar was constructed from glass and is connected to the balance head assembly by a rubber seal. This is an 8 cm band of rubber which fits around the dewar cap at point A, see Fig. 7,and over the side of the top few centimeters of the dewar. This method of sealing the inner dewar has the advantage that precise location is unnecessary to make a good seal. The tail of the dewar is 42 cm long and this enables a substantial volume of helium to be kept under the sample chamber, allowing stable temperatures (in the range 4.2 to 77K) to be obtained by balancing the heat input with the boil off rate of the helium.

To accommodate the long tails of the dewars the original electromagnet had to be turned through 90° and placed on a steel frame. This gave a clearance under the magnetic pole pieces of approximately 60 cm.

The helium level in the inner dewar is detected by a bridge circuit (17) based on a 741 operational amplifier. The circuit diagram for the detector is shown in Fig.6. The detecting probe consists of three Allen-Bradley 1/8 watt carbon resistors (22Ω, 47Ω and 100Ω) for the dewar body and one,hundred ohm for the tail. The body resistors were connected in series and glued with GE 7031 varnish to a rod of

PTFE (diameter $\frac{1}{4}$"), at least 30 cm of wire was used to connect each resistor with its neighbour in order to prevent thermal contact becoming too large. The resistors were spaced at approximately 15 cm intervals.

As each resistor enters the helium its resistance changes by approximately a factor of five. This unbalances the bridge and hence produces a voltage at AB which is amplified and monitered on a meter. The meter changes in equal steps (because of the value of the resistors) until full scale deflection occurs when all the resistors are emersed. The tail detector is the same in principle and indicates when the helium level is below the end cap of the suspension tube.

The nitrogen level detector is a simplified version of the above and uses light emitting diodes to indicate high and low levels of the liquid.

FIG. 6 The helium detector circuit diagram; TP = tail probe and BP = body probe.

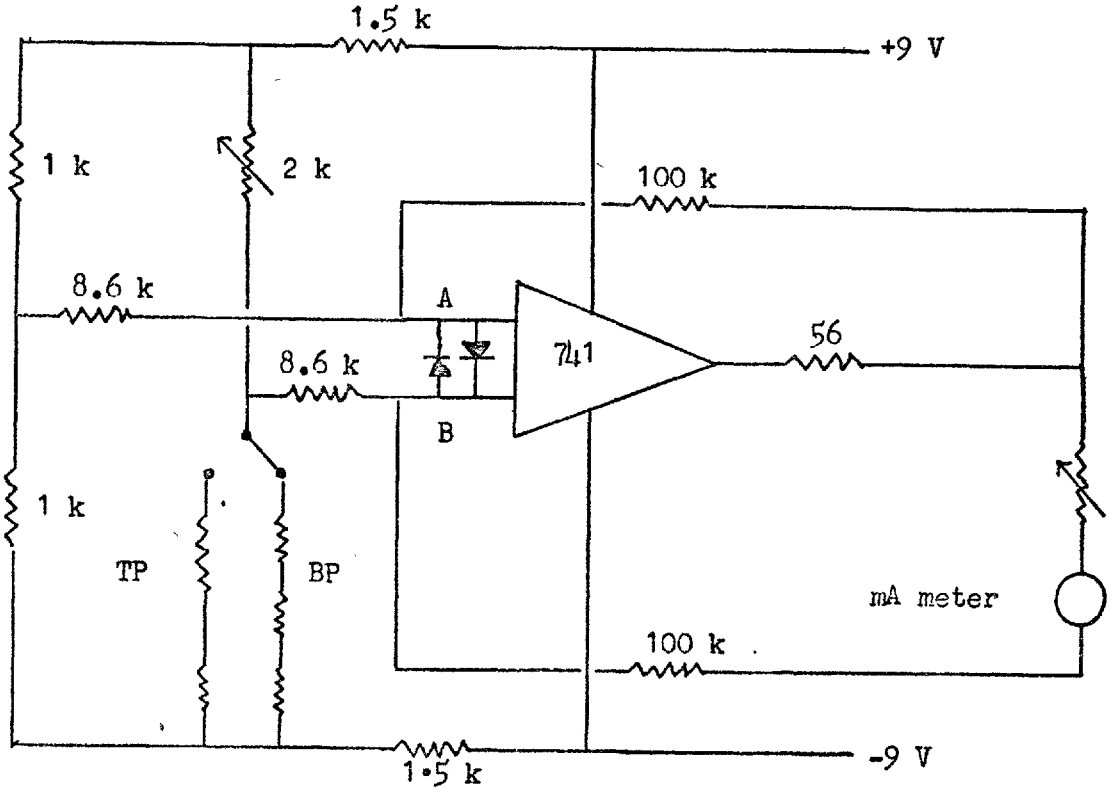

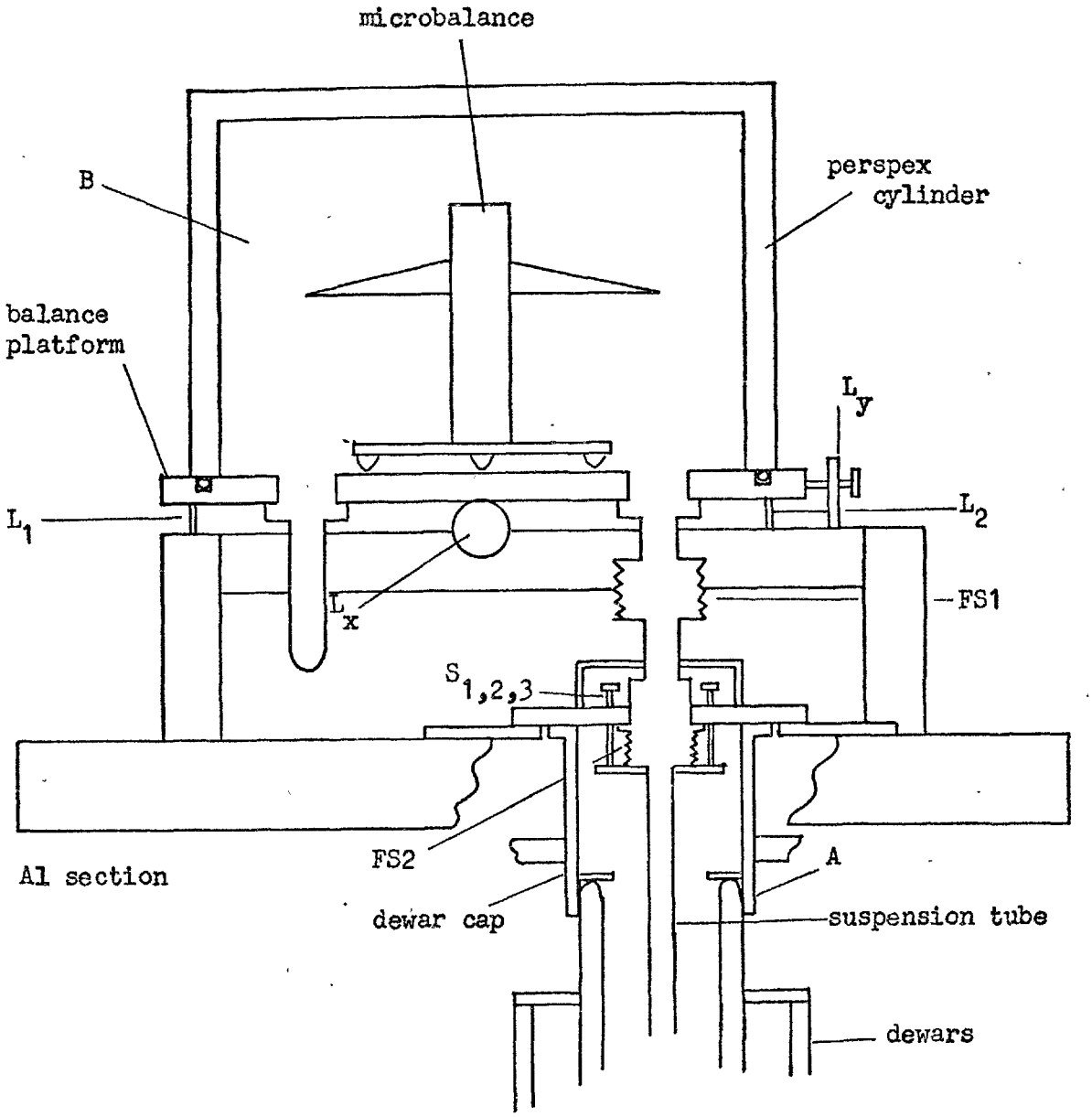

FIG. 7 The microbalance assembly.

The microbalance.

The apparent mass change is measured on a commercially available microbalance manufactured by Beckmann-Ricc (No. LM600).

The balance works on the following principle. Any movement of the balance beam is detected by means of a pair of photocells connected in opposition. These pick up light reflected from a mirror fixed to the balance beam. Attached to this beam are restoring coils which are supported by a torsion ribbon so that they may rotate freely between the poles of a permenant magnet. Movement of the beam gives a net output from the photocells which is automatically amplified and adjusted to give the correct restoring current through the coils to bring the balance beam back to its initial position.

The restoring current passes through a pre-set resistor, the voltage across which is measured by either the internal potentiometer or an external digital voltmeter. On all ranges of the balance full scale output is 100 mV. Using a digital panel meter (Analogic model AN 2544) with a resolution of 100 μV then on the 1mg range 1 μg can be resolved. The balance has an over range capability of 3 V, therefore 30 mg may be measured on the 1mg range. The maximum pan difference measurable is 600 mg although the balance can support up to 2.5gm on each pan.

The reproducibility of the balance is 0.05% of the weight range but under experimental conditions this is likely to be higher depending on the apparent weight change.

The microbalance assembly.

The microbalance has three adjustable rubber legs which are positioned in depressions made in the balance platform (Fig. 7). This platform is the base for a perspex cylinder, closed at one end, which is sealed to it by an o-ring thus forming the balance vacuum

chamber, B. There are three outlets from the platform, the suspension tube, the electronic connector for the microbalance controller and a pumping line to allow the balance chamber and suspension tube to be evacuated. The balance chamber must be able to sustain a good vacuum, as any leaks may allow air into the system. Oxygen and water vapour may then condense on the sample giving spurious results.

The suspension tube is connected to the platform by means of two flexible vacuum joints FS1 and FS2. This enables the balance to be adjusted independently of the down tube. Adjustment in the xy-plane is by the screws L_y and L_x and in the z-direction by the adjustable legs $L_{1,2,3}$. The lower part of the suspension tube, from FS2 to the end cap, is made from stainless steel tubing (o.d. = 1 cm, i.d. = 0.975 cm) which has mechanical strength as well as low thermal conductivity. This section can be aligned independently of the top section by adjusting $S_{1,2,3}$.

The complete balance platform is supported on two inch square section aluminium (16s.w.g.) which is bolted to the laboratory wall. Vibrations were found not to be a problem due to the type of support and the nature of the microbalance.

A brass dewar cap (DC) permits the dewars to be positioned around the down tube. It also provides outlets for the electrical connectors, the transfer syphon, the helium return line and the pumping line for reducing the helium vapour pressure. Liquid helium is transferred by a detachable syphon. Unfortunately the space between the end cap and the inner wall of the helium dewar was insufficient to allow liquid helium to pass easily into the tail. This problem was overcome by a flattened stainless steel tube, one end of which was attached to the transfer syphon and the other located in the dewar tail. Thus liquid helium passes directly into the tail.

The suspension assembly.

The suspension is housed in a stainless steel down tube joined to the balance platform. The bottom 7 cm of the down tube is made of naval brass to form an isothermal end cap (fig. 8a), on which the thermometers and sample heater are attached. To allow the sample to be easily changed the end cap has a removable lower section (LS) sealed by a cone joint. This seal must be kept scrupulously clean and given a fresh coat of low temperature vacuum grease before every run, otherwise it will not seal effectively at helium temperatures.

The suspension itself is made of a quartz fibre 120 cm in length and approximately 0.2 mm in diameter (fig. 8b). Quartz has the advantage of low thermal conductivity, small coefficient of linear expansion and high tensile strength. The top end of the quartz fibre was glued (GE 7031) to a hook made from constantan (32s.w.g.). Another hook was attached to the middle of the right hand weighing pan by a small amount of solder. The suspension could therefore be simply unhooked from the weighing pan and lowered to change the specimen.

The last 10 cm of the suspension hangs in the magnetic field; therefore this section was made from high purity aluminium wire to avoid problems with magnetic impurities in the quartz. The aluminium link had a small hook made in one end for the sample bucket. The other end was glued to the quartz fibre.

Two heat shields approximately 10 cm apart were attached just above the aluminium link. These were made from aluminium foil (Baco foil) and prevented room temperature radiation from falling onto the sample. A counter weight of gold (1 gm) was placed between the two heat shields. This helps to stabilize the suspension against both lateral forces on the specimen and electrostatic attraction to the down tube walls.

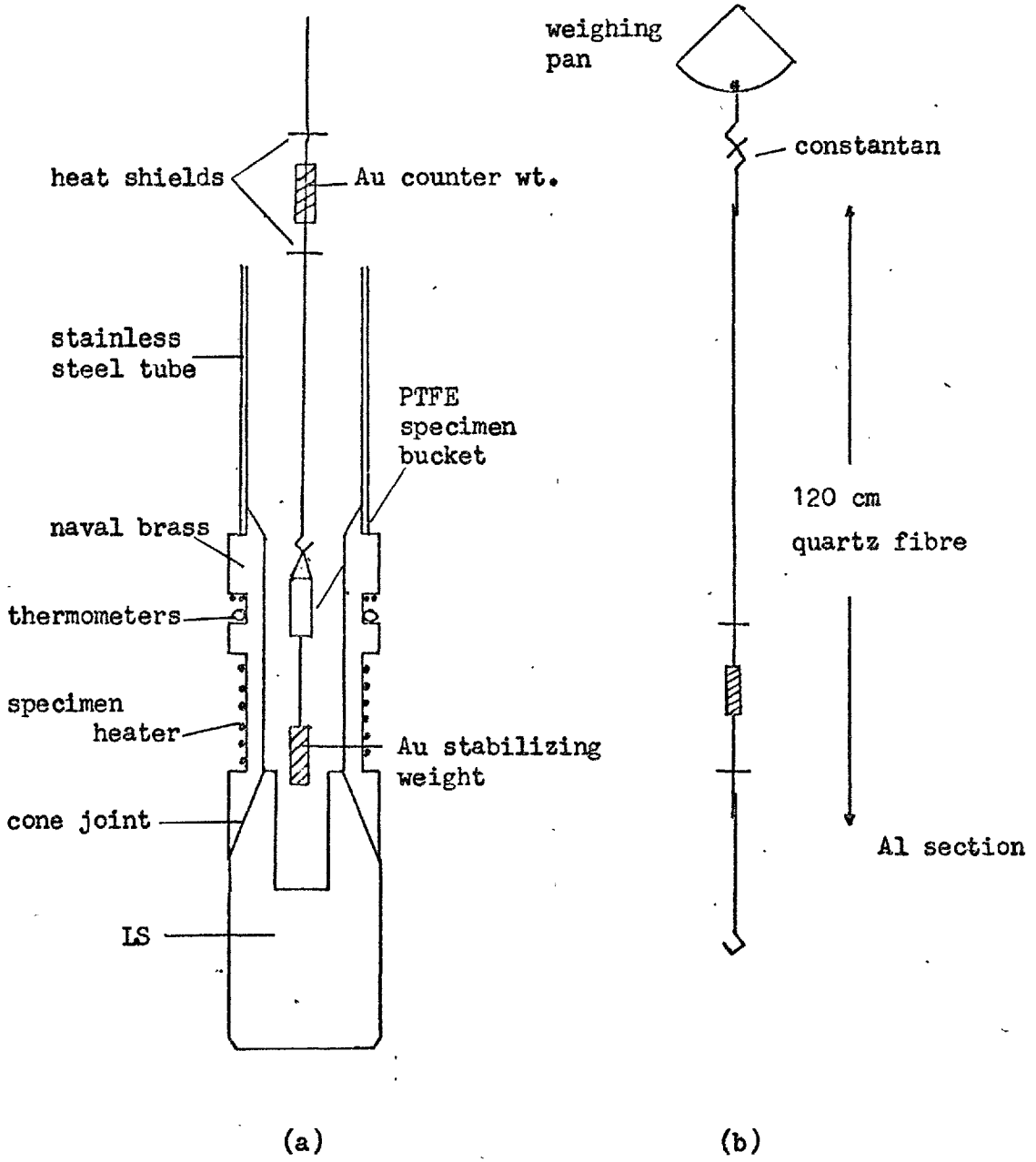

FIG. 8 (a) Suspension tube end cap.
(b) Quartz fibre suspension.

The sample container is a small bucket (5x2 mm) made from PTFE rod. This has the advantage of having a small susceptibility which is virtually temperature independent (18). Movement of the specimen in the xy plane must be avoided as it may touch the side walls of the down tube. There are many reasons for lateral movements (see Stewart (19)) and various methods have been used to reduce them (20) (21). The electromagnet used in this apparatus has conical pole caps (Fig. 5) which give a very small field gradient at the centre of the pole and a region of high H_y dH_y/dz at approximately the radius of the truncated pole tips. This fact was taken advantage of by placing a stabilizing weight under the sample holder in the position of zero field gradient, thus effectively "pinning" the specimen and reducing the tendency for lateral movement. The weight was made from 1 gm of gold.

The Gouy force on the aluminium link and the negative residual force on the gold results in a total apparent weight of the suspension of $\sim 50 \mu g$ for full field(8.5 KG).

Thermometry.

The main thermometers are a carbon resistor for 1.8 to 14K, a platinum for 14 to 77K and a copper-constantan thermocouple for 77 to room temperature. All the thermometers were attached to the end cap as near as possible to the position of the sample.

The carbon thermometer is a 47 Ω 1/8 watt Allen-Bradley resistor. This type of thermometer is excellent for 1.8 to approximately 14 K as in this range the change of resistance with temperature is rapid (22). The carbon resistor's plastic case was gently scraped away to allow good thermal contact with the end cap to which it was glued with GE varnish. The resistance was measured by comparing the voltage drop across a standard resistor, connected in series, with that of the

thermometer. The current supply is stabilized electronically to better than 1 in 10^3.

The thermometer was calibrated against helium vapour pressure below 4.2K and at the nitrogen boiling point, then the data fitted graphically to the empirical expression

$$\log R + A / \log R = B / T + C$$

where A, B and C are constants and R is the resistance at temperature T. The constant A was first assumed (about 2) and $\log R + A (\log R)^{-1}$ plotted against T^{-1}, for the measured values between 1.8 and 4.2K, to find B and C. The calculated and observed resistance values at 77K were then compared, A was then adjusted and the process repeated until the resistance values at 77K agreed.

The platinum resistance thermometer was made from approximately 5 cm of 0.1 mm diameter high purity wire (*). The wire was annealed for about six hours by passing sufficient current through to maintain a dull red glow. Not only does this anneal the wire, but also any iron impurities will tend to diffuse to the surface and oxydize. The resistance ratio $R_{273} / R_{4.2}$ after the heat treatment was 520. The platinum wire was then wound on an insulated copper former 7 by 1 mm. This inevitably decreased the resistance ratio, the final value of which was approximately 450. Contact leads were spark welded to the platinum and the complete thermometer glued into place. The resistance was measured by the same method used for the carbon thermometer.

The thermometer was calibrated using the z-function technique (22) (23).

$$Z(T) = \frac{R_T - R_{4.2}}{R_{273} - R_{4.2}}$$

The resistivity below 77K for different samples of high purity platinum shows little variation. Therefore Pt resistance thermometers

* Supplied by Mr. J. A. Khan.

may be calibrated by measuring the resistance at 273, 4.2K and intermediate points and then comparing with the standard tabulated Z(T) function (23).

A resistance ratio of at least 1000 is required to achieve accuracy to better than ± 0.05K in the range 12 to 77K using the z-function calibration (23). This accuracy is unecessary in this apparatus due to the uncertainty of the actual temperature of the specimen. This is because the suspension must be free of constraints to ensure accurate apparent weight measurements. All thermometers are therefore located in a groove in the brass end cap, the thermal link between them and the sample being helium exchange gas. Resistance ratios above 300 are sufficient to give a calibration accuracy of 1%.

Temperatures from 77K to room temperature were measured using a copper-constantan thermocouple reference to liquid nitrogen and calibrated from the data of Powell et al (24).

Both the platinum and the carbon resistance thermometers have small magneto-resistances in fields up to 8.5 KG and therefore errors due to this source should be small, probably less than 0.2% (22). The effect of a magnetic field on a copper constantan thermocouple has been investigated by Schlosser and Munnings (25). They found an increase in the measured temperature of approximately 1% at nitrogen temperatures for a thermocouple referenced to 273 K and in a field of 30 KG. In fields up to the maximum of 8.5 KG no significant difference was noticed with the thermocouple used in this apparatus.

To find if there was any temperature difference between the thermometers on the end cap and the sample, the initial susceptibility of Au-0.1at.%Gd was measured at various temperatures from 1.8K to 77K. This alloy obeys the Curie-Weiss law with a θ in the range ±0.05K (26). A plot of $1 / (\chi_{alloy} - \chi_{Au})$ against temperature of

the end cap gave an intercept of approximately -0.75K. Therefore there is a temperature difference between the specimen and the end cap of 0.75K. This sample also provided a check of the calibration of the carbon and Pt thermometers as $1/\chi$ is a linear function of temperature.

The Magnetic Field.

The magnetic field was provided by a Newport type A electromagnet with truncated conical pole tips, driven by an Irvin C212 1KW power supply. An energizing current of 7.5 A gives a field of 8.5 KOe at the sample position (Fig. 5).

Control of the power supply is by a digital control unit designed by Dr.D.Griffiths (27). The purpose of this unit is to prevent the output current from being rapidly reduced, thus causing a sharp rise in the voltage across the output transistors because of the inductive nature of the load. This high voltage occurs at a time of large current loading thereby taking the transistors out of their safe operating area. By changing a series of fixed resistors, the current output is altered accordingly. To prevent a sharp reduction in the output current by quickly changing the fixed resistors,the controller input resistors are selected by a counter in a binary sequence giving values between 0-1500Ω in 100 steps. 100Ω is equivalent to a magnet current of $\frac{1}{2}$A. The rate at which the steps can be made is regulated by an internal clock giving delays of about 1s per step. The unit can be stepped manually or automatically.

The magnetic field as a function of current was determined by a Hall probe Gaussmeter. The field was evaluated for several values of z, the centre of the flat pole faces being taken as z = 0. The region of constant and maximum $H_y(dH_y/dz)$ was found to be 2mm above the truncated pole caps. This position was chosen as the sample

position (Fig. 5). At this point the force on the sample is maximal and the variation of $H_y(dH_y/dz)$ is minimal thereby reducing to a minimum errors introduced by the finite size of the specimen. A plot of H_y^2 vs. z is shown in Fig. 9 and as can be seen the position of greatest $H_y(dH_y/dz)$ does not change very much with magnet current although for high currents it does become more sharply defined.

The calibration values of $Hy(dH_y/dz)$ for varying magnet currents were not obtained by the above method for two reasons; firstly, the determination of the gradient is basically not very accurate and secondly, the Hall probe cannot be used when the stainless steel dewar is in position (it is necessary to calibrate the field with this dewar in place as it will alter the field gradient).

The apparatus was therefore calibrated by measuring the force on a sample of known susceptibility. The measurements were made using high purity (4N) tantalum from the Koch-light Co. and assuming a value of $\chi_m(Ta) = +0.8490 \times 10^{-6}$ (28) (29). Calibration points were taken at current values from .5 to 7.5A in 0.5A intervals, at the maximum current $H_y(dH_y/dz)$ had a value of 14.24×10^6 Oe^2cm^{-1}. As a check, the susceptibility of pure platinum was determined at room temperature and compared with values obtained by other authors. The agreement is reasonable.

$\chi_m(Pt)$ (10^{-6}emu gm^{-1})	Ref.
0.985	30
1.013	31
0.979	32
1.010	This work.

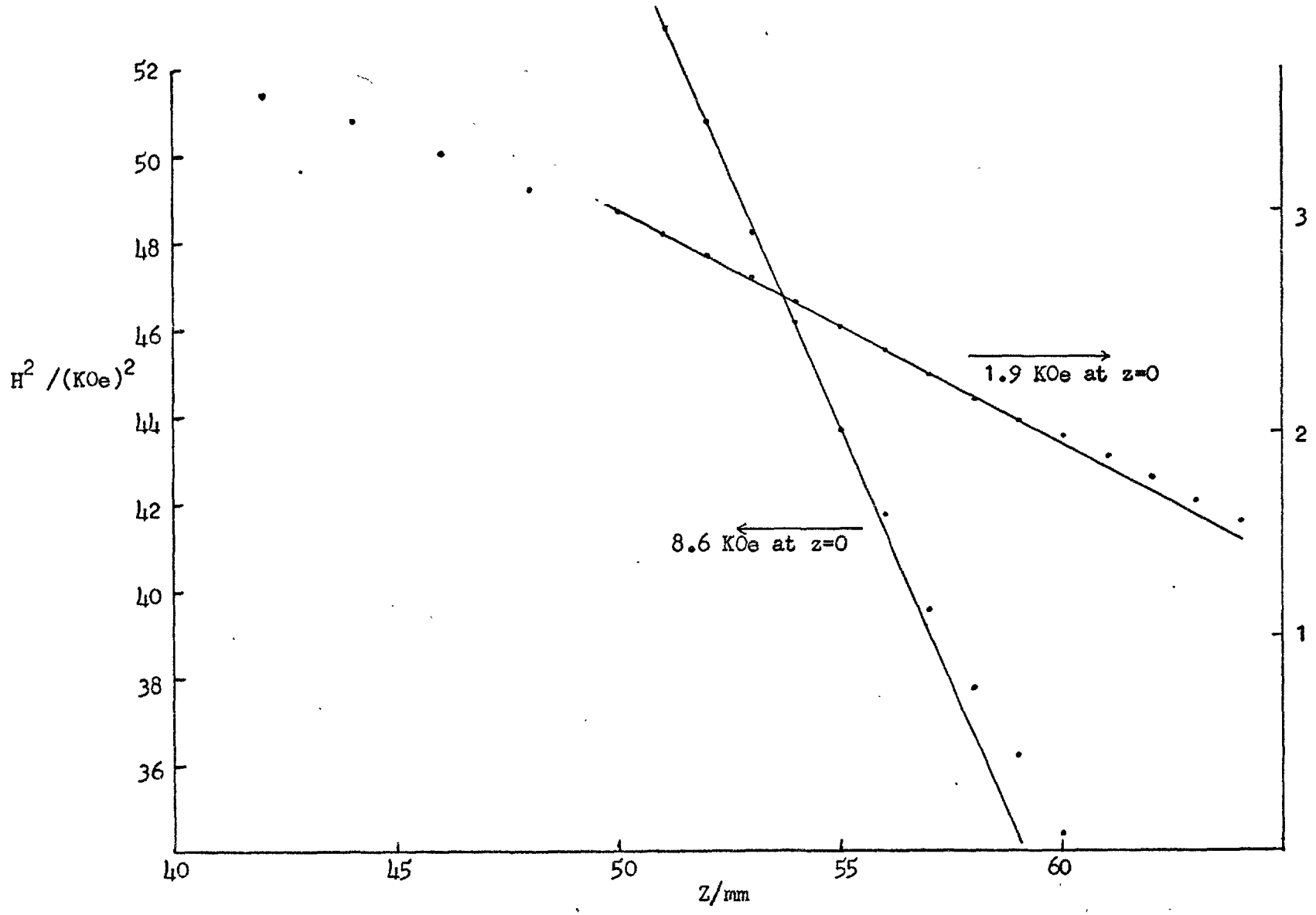

Fig. 9 H^2 against the distance from the middle of the magnet pole gap, z=0.

The calibration was carried out at room temperature and at liquid nitrogen temperature to take account of the contraction of the suspension.

Experimental Procedure.

The lower section of the end cap is removed and the suspension lowered, the sample bucket is then unhooked and a specimen (maximum dimensions 1.5 x 4 mm cylinder) inserted into it. The bucket and sample are replaced and a counter weight put into the opposite weighing pan. The suspension is then reattached to the microbalance and the balance platform adjusted in the xy-plane to bring the sample to the middle of the down tube. As the suspension is not changed from run to run the position of the specimen in the z-direction is assumed to be the same as in the calibration run. The adjustment of the suspension in the xy-plane (by L_x and L_y) allows the sample to be positioned in the centre of the down tube to ± 0.25 mm.

After cleaning and regreasing the cone joint the end cap is replaced. The balance chamber and suspension tube are then flushed with nitrogen (at least three times) and evacuated to about 10^{-3}torr. The dewars are attached and the magnet manoeuvred until its position coinsides with that of the initial calibration run. The overall position accuracy is ± 0.5 mm, which is adequate as $H_y(dH_y/dz)$ is constant to 1% over approximately 5 mm^3 at the sample position.

The inner dewar is flushed and pumped to a pressure of 1 torr. The apparatus is then cooled to 77K at which temperature liquid helium is transferred. At 4.2K one torr of helium exchange gas is allowed into the balance chamber and suspension tube. The value of 1 torr was chosen to minimize changes in force on the suspension due to thermomolecular flow of the exchange gas (33). There will always be some thermomolecular pressure difference along the suspension tube giving

a flow of gas down the centre of the tube which exerts a viscous drag on the suspension. As the thermal gradients, which are responsible for the pressure differences, are changing continuously, the viscous drag also alters thereby causing a drift in the zero position of the balance. This drift may be as much as 10μg during the course of a measurement. Depending on the apparent weight being measured this may be one of the largest sources of error.

As the magnetic field is not directly measured during a run (the field is calibrated in terms of the current through the coils), the magnet is cycled two or three times before beginning the measurement. The value of the field and the field gradient are obtained from the magnitude of the current through the electromagnet.

The microbalance is nulled in zero field after which a given value of the magnetic field is selected and the apparent weight measured. Another field value is then selected and the weighing repeated. Therefore M-H plots and hence the magnetic susceptibility at various temperatures may be found.

5.3 Electrical Resistivity Measurements.

The electrical resistivity measurements were made on a standard four terminal D.C. rig, details of which can be found in Barber (01). The specimen is housed in a copper chamber and is connected in series with an external 0.01 Ω manganin standard resistor, maintained at 25 C in a water bath. The current is supplied by a Tinsley regulated power supply type 5733 which has a stability of better than 1 in 10^5. The resistance is obtained by comparing the potential drop across the specimen with that across the standard. The voltages are measured on a Tinsley Stabaumatic potentiometer type 5545 in conjunction with a galvanometer amplifier, giving a total resolution of 2×10^{-9} V.

Joule heating of the specimen must be avoided, therefore the current used is determined by the resistance of the specimen. An order of magnitude resistivity for the compounds measured in this work, $LaNi_5$- $GdNi_5$ system, is 50 μV cm. It was found that a current in the range 150-200 mA produced negligable internal temperature changes. Typically,samples were in the form of cylindrical rods with dimensions 3cm by 1.4mm.

Precise location of the voltage leads was not possible because the usual method of spot-welding platinum leads could not be used,as the samples shattered during this process. The shattering was caused by the extreme brittleness of the samples. To make a connection,a length of platinum wire was wound around a small section of the specimen as tightly as possible. Heat shrinkable sleeving was then placed over the contact area and warmed with a hot air blower. The sleeving contracts to hold the platinum wire firmly against the specimen. This procedure was repeated for both current and voltage leads. The potential leads were located 5 mm from each end of the sample rod. The current leads were positioned outside these and as near to the end as possible.

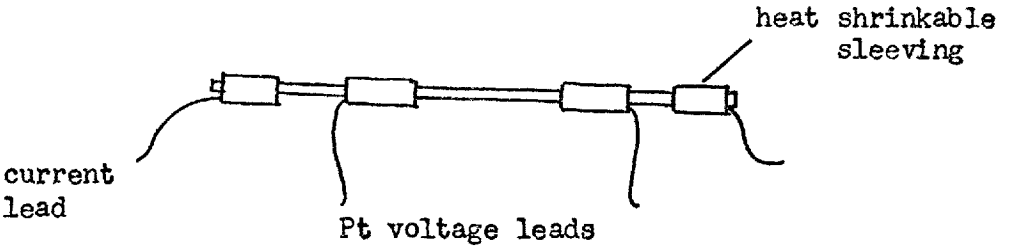

A resistivity sample.

Unfortunately it is impossible to measure the precise distance between the voltage leads with this method of attachment. Therefore absolute resistivities could not be obtained.

The rig is capable of measurements from 1.6K to room temperature by using the double dewar technique. A AuFe vs. chromel thermocouple, referenced to 4.2K, is used for measuring temperatures above 4.2K. Below this temperature standard helium vapour pressure tables are used.

5.4 Metallurgy and Sample Preparation.

Rare-earth metals only form compounds with the 3d transition metals to the right of chromium in the periodic table, i.e. Mn, Fe, Co and Ni. The rare-earth nickel systems form similar intermetallic compounds throughout the 4f series (34).

The phase diagram for the La-Ni system (35) is shown in Fig. 10. There are six compounds in the range 50-100at.% Ni; LaNi, $LaNi_{1.4}$, $LaNi_2$, $LaNi_3$, La_2Ni_7 and $LaNi_5$. The compound of interest in this work is $LaNi_5$. This melts congruently at 1350 C and shows a large region of homogeneity ranging from $LaNi_{4.85}$ to $LaNi_{5.40}$ (36). The structure of $LaNi_5$ and other rare-earth-Ni_5 compounds is hexagonal $CaCu_5$ type with two inequivalent nickel positions (37) (38); it is sketched in Fig. 11. The phase diagram of Gd-Ni (35) is very similar and also has a congruently melting intermetallic compound with the $CaCu_5$ structure, $GdNi_5$. Therefore the pseudobinary $GdNi_5$- $LaNi_5$ can be made. Investigations of a number of $LaNi_5$- Gd alloys across the whole concentration range by electron probe and microscopic examination showed single phase specimens. These alloys are very brittle and were not usually annealed before subsequent measurements.

The systems Gd-Al has been investigated by Buschow and Van Vacht (39) and the phase diagram from their work is sketched in Fig.12. Three intermetallic compounds are formed on the aluminium rich side; GdAl, $GdAl_2$ and $GdAl_3$. The compound of interest here is $GdAl_2$ which has a cubic Laves phase structure, $MgCu_2$. Again with $LaAl_2$ the pseudobinary $LaAl_2$- $GdAl_2$ can be formed. All other alloys examined were solid solutions of the elements concerned.

The specimens were all prepared from the pure metals listed in table 1. To make the alloys the constituents were melted in an Argon arc furnace. This consists of a copper hearth and tungsten elect-

Table 1.

Metal	Supplier and Purity
La	Koch-Light 3N ingot.
Ni	Koch-Light 4N7 sheet.
Gd	Rare-earth Products 3N sublimed.
La	Rare-earth Products 3N ingot.
Sc	Rare-earth Products 3N ingot.
Y	Rare-earth Products 3N ingot.
Al	Johnson Mathey Specpure rod.

rode both of which are water cooled. The furnace is flushed three times with clean argon gas and then filled to a pressure of two thirds of an atmosphere. A current of approximately 100A is used to heat a titanium getter for a few minutes. This removes the last traces of impurity in the furnace atmosphere. To melt the alloy, currents between 70-80A were used; the alloy being turned and remelted three times to ensure homogeneity. It is possible to cast the alloys into rods or sticks while they are in the arc furnace by means of a suction device (40). This process was used to form the brittle intermetallic compounds into cylindrical rods.

The composition and homogeneity of the alloys were checked using microscopic examination, electron microprobe analysis and in some cases x-ray analysis.

(a)

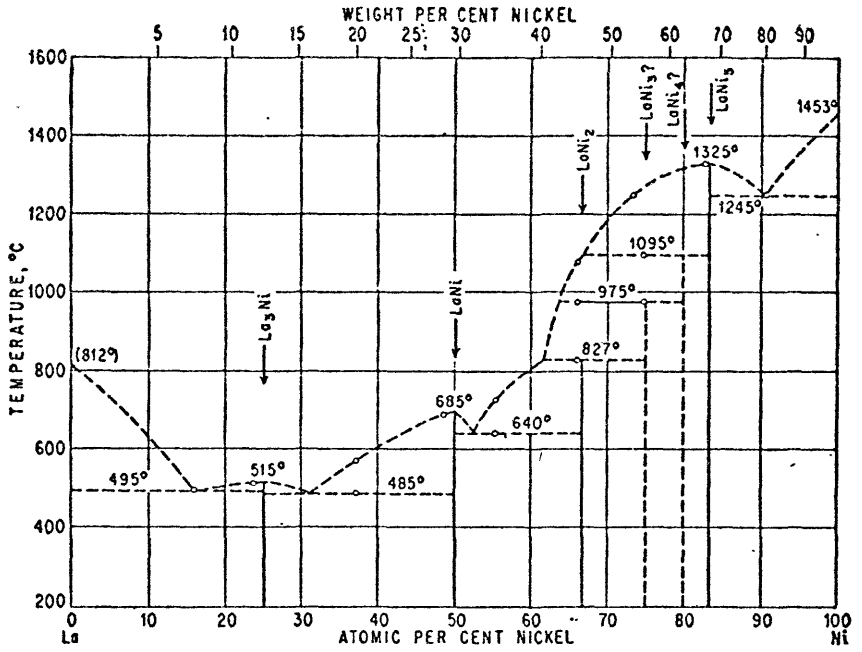

(b)

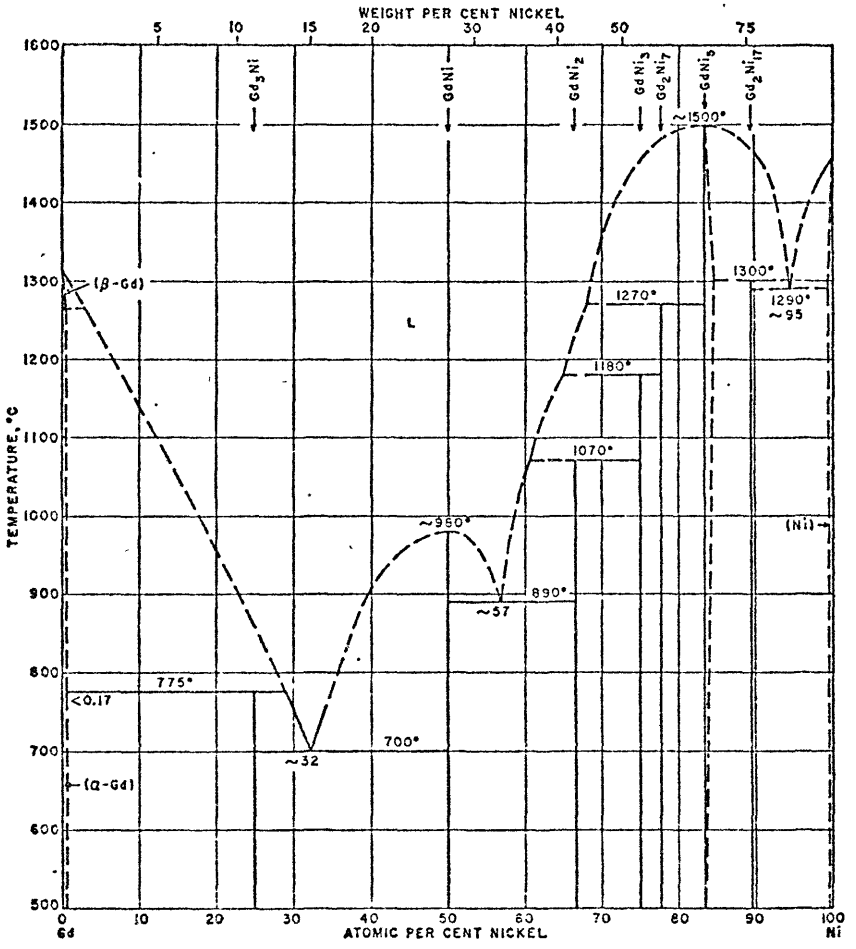

Fig. 10 Phase diagrams for (a) La-Ni and (b) Gd-Ni (after ref. 35).

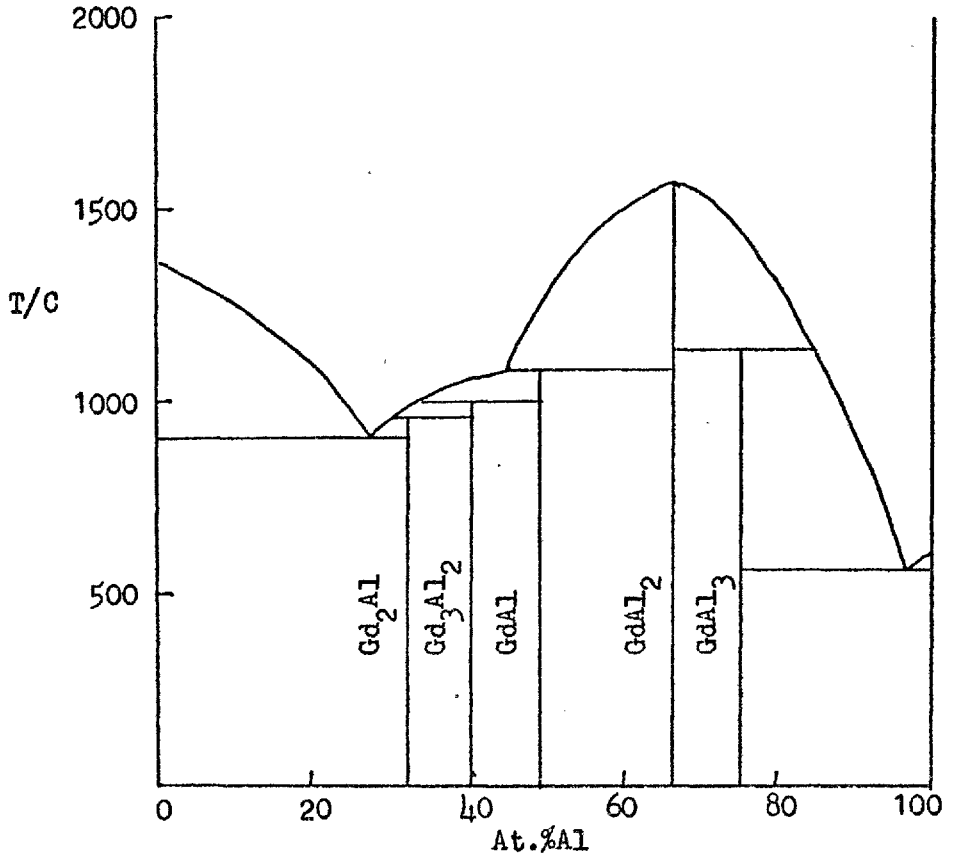

FIG.12 The Gd-Al Phase Diagram (after ref. 39)

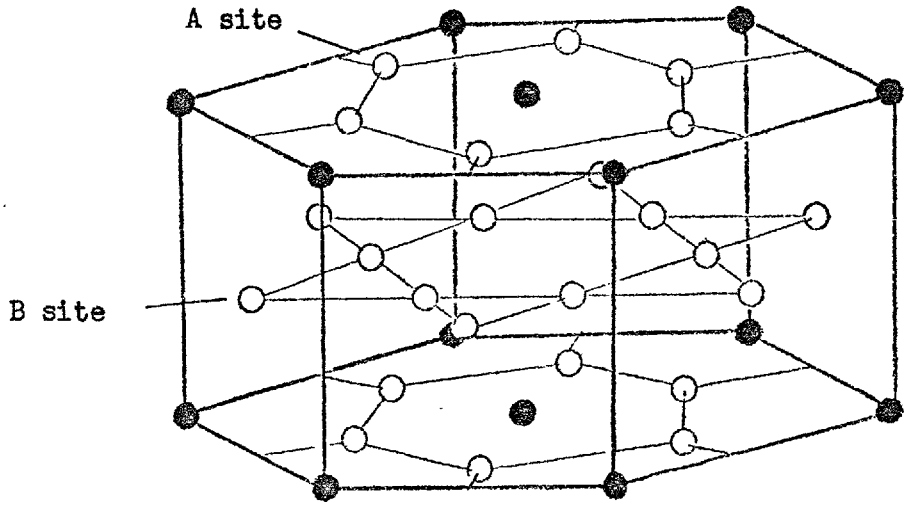

FIG. 11 The structure of $LaNi_5$. ○ Ni, ● La.

REFERENCES CHAPTER 5

1. BARBER, A.J., Thesis, University of London (1973).

2. TAYLOR, R.H., Thesis, University of London (1972).

3. WILMSHURST, T.H., Electron Spin Resonance Spectrometers, Adam Hilger Ltd., (1967).

4. GRIFFITHS, D., J. Sci. Inst. 2(2), 1124, (1962).

5. LOWIN, R.J., Thesis, University of London, (1970).

6. ROSENBAUM, R., Rev. Sci. Inst., 39, 890 (1968).

7. BERMAN, R., Int. Adv. in Cryogenics, Plenum Press,(1965).

8. CAPLIN, A.D., Thesis, University of Cambridge

9. FEHER, G., Bell. Syst. Techn. J., 36, 449, (1957).

10. DYSON, F., Phys. Rev., 98, 349, (1955).

11. FEHER, G. and KIP, A.F., Phys. Rev., 98, 337, (1955).

12. OWEN, J., BROWNE, M.E., ARP, V. and KIP,A.F., J. Phys. chem. Solids, 2, 85, (1957).

13. PAKE, G.E. and PURCELL, E.M., Phys. Rev., 74, 1184, (1948); 75, 534, (1949).

14. SEE APPENDIX 2.

15. PETER, M., SHALTIEL, D., WERNICK, J.H., WILLIAMS, H.J., MOCK, J.B. and SHERWOOD, R.C., Phys. Rev., 126, 1395 (1962).

16. BATES, L.F., Modern Magnetism, Cambridge at the University Press (1939).

17. TALEB, A.M. and MUNRO, I.H., J. Phys. E.; Sci. Inst., 5, 629, (1972).

18. COMMANDER, R.J. and FINN, C.B.P., J. Phys. E.; Sci. Inst., 3, 78, (1970).
SALINGER, G.L. and WHEATLEY, J.C., Rev. Sci. Inst., 32, 872, (1961).

19. STEWART, A.M., J. Phys. E.; Sci. Inst., 2, 851 (1969)

20. SUCKSMITH, W. and PEARCE, R.R., Proc. R. Soc., A 167, 189 (1938).

21. GRIFFITHS, D., Thesis, University of London, (1961).

22. WHITE, G.K., Experimental Techniques in Low Temperature Physics, Oxford Clarendon Press, (1968).

23. CHAN YET-CHONG and FORREST, A.M., J. Sci. Inst. (J. Phys. E), 1, 839 (1968).

24. POWELL, R.L., BUNCH, M.D. and CORRUCCINI, R.J., Cryogenics, 150, (1961).

25. SCHLOSSER, W.F. and MUNNINGS, R.H., Cryogenics, 12, 302, (1972).

26. BELL, A.E., Thesis, University of London, (1973).

27. GRIFFITHS, D., To be Published and see Appendix 1.

28. HOARE, F.E. and WALLING, J.C., Proc. Phys. Soc., B64, 337 (1951).

29. HOARE, F.E., KOUVELITES, J.S., MATTHEWS, J.C. and PRESTON, J., Proc. Phys. Soc., B67, 728 (1954).

30. WEISS, W.D. and KOHLHAAS, R., Z. angew. Phys.23, 175 (1967).

31. FONER, S., DOCLO, R. and MCNIFF JR., E.J., J. Appl. Phys., 39, 551 (1968).

32. BUDWORTH, D.W., HOARE, F.E. and PRESTON, J., Proc. Roy. Soc. A257, 250 (1960).

33. GERRITSEN, A.N. and DAMON,D.H., Rev. Sci. Inst., 33, 301 (1962).

34. TAYLOR, K.N.R., Adv. in Phys., 20, 551 (1971)

35. ELLIOTT, R.P., Const. Binary Alloys, 1st Sup., McGraw-Hill (1962).

36. BUSCHOW, K.H.J. and VAN MAL, H.H., J. Less Common Metals, 29, 203 (1972).

37. WERNICK, J.H. and GELLER, S., Acta. Cryst., 12, 662 (1959).

38. HASZKO, S.E., Trans. Am. Inst. Mining, Met., Petrol. Engrs., 218, 763 (1960).

39. BUSCHOW, K.H.J. and VAN VUCHT, J.H.N., Phillips Research Rep., 22, 233 (1967).

40. STONE, H.E.N., J. Phys. E., 4, 1058 (1971).

CHAPTER 6

RESULTS AND DISCUSSION.

Introduction.

The results of paramagnetic resonance measurements on Gd^{3+} ion in various hosts, $LaNi_5$, $LaAl_2$ and rare-earth metals are presented in this chapter. In all these compounds the Gd ions are in the $^8S_{7/2}$ electronic state. In the last section the epr of the Mn ion in some alloys and compounds is reported.

The epr behaviour of $LaNi_5$- Gd has been studied by many authors mainly from the point of view of the dynamics of the localized moments (01) (02) (03). In this system the Gd moment is well localized (4f shell) and the $LaNi_5$ matrix is an exchange enhanced host similar to Pd. Gadolinium also forms a nickel-five compound; therefore solubility of Gd in $LaNi_5$ is not a problem. Measurements of the epr, resistivity and magnetic susceptibility were performed across the entire range from $LaNi_5$ to $GdNi_5$ in an effort to understand the nature of the magnetic ordering in this system. The epr results are interpreted by taking into account the onset of magnetic order.

The systems $LaAl_2$- Gd, Y-Gd and Sc-Gd were investigated for Gd concentrations which give spin glass like behaviour in the resistivity and susceptibility.

6.1 $LaNi_5$- Gd: Low concentrations of Gd.

There exists a considerable range of composition over which the $LaNi_5$ phase forms (see ch. 5); therefore the linewidth and g-value of $\frac{1}{2}$at. %Gd in three compounds nominally $LaNi_{4.9}$, $LaNi_{5.2}$ and $LaNi_{5.36}$ were obtained in order to check that the change in lattice structure across the phase field would not significantly alter the epr behaviour.

The measurements were performed from 1.8K to a temperature at which the signal intensity was too small to be measurable. The results are shown in Fig.1. The g-value for all the compounds is very similar and so is the slope of the linewidth. To check the structure of $LaNi_5$ and to ascertain the correct stoichiometry of the samples, an x-ray analysis was undertaken (*). The crystallographic structure was confirmed as $CaCu_5$, space group C6/mmm. Comparing the lattice constants with those from Buschow and Van Mal (04) the compositions were found to be the following:

Nominal	Observed
$LaNi_{5.36}$	$LaNi_{5.22}$
$LaNi_{5.20}$	$LaNi_{5.06}$
$LaNi_{4.90}$	$LaNi_{4.90}$

From the epr results there is little indication that structural variations across the homogeniety range have a significant effect on the resonance properties of the substituted Gd (for low concentrations of Gd).

The epr results presented in the remainder of this section refer to $(La_{1-x}Gd_x)Ni_5$ with x less than 0.1. The temperature dependence of the linewidth and g-value is shown in Figs.2-9, the curves through the points are only guides to the eye, unless otherwise stated. A summary of the paramagnetic g-value (g_o), slope of the linewidth, temperature of the minimum in the linewidth (T_{Hm}) and the temperature at which the g-value begins to deviate from g_o (T_g) is given in Table 1. All linewidths and g-values have been corrected by the procedure described in ch.5. The error in the g-value is mainly due to distorted line shapes.

For concentrations of less than 1at.% Gd the g-value is flat and the linewidth is linear with temperature. As the concentration is

* I would like to thank Dr. I.R. Harris for these measurements.

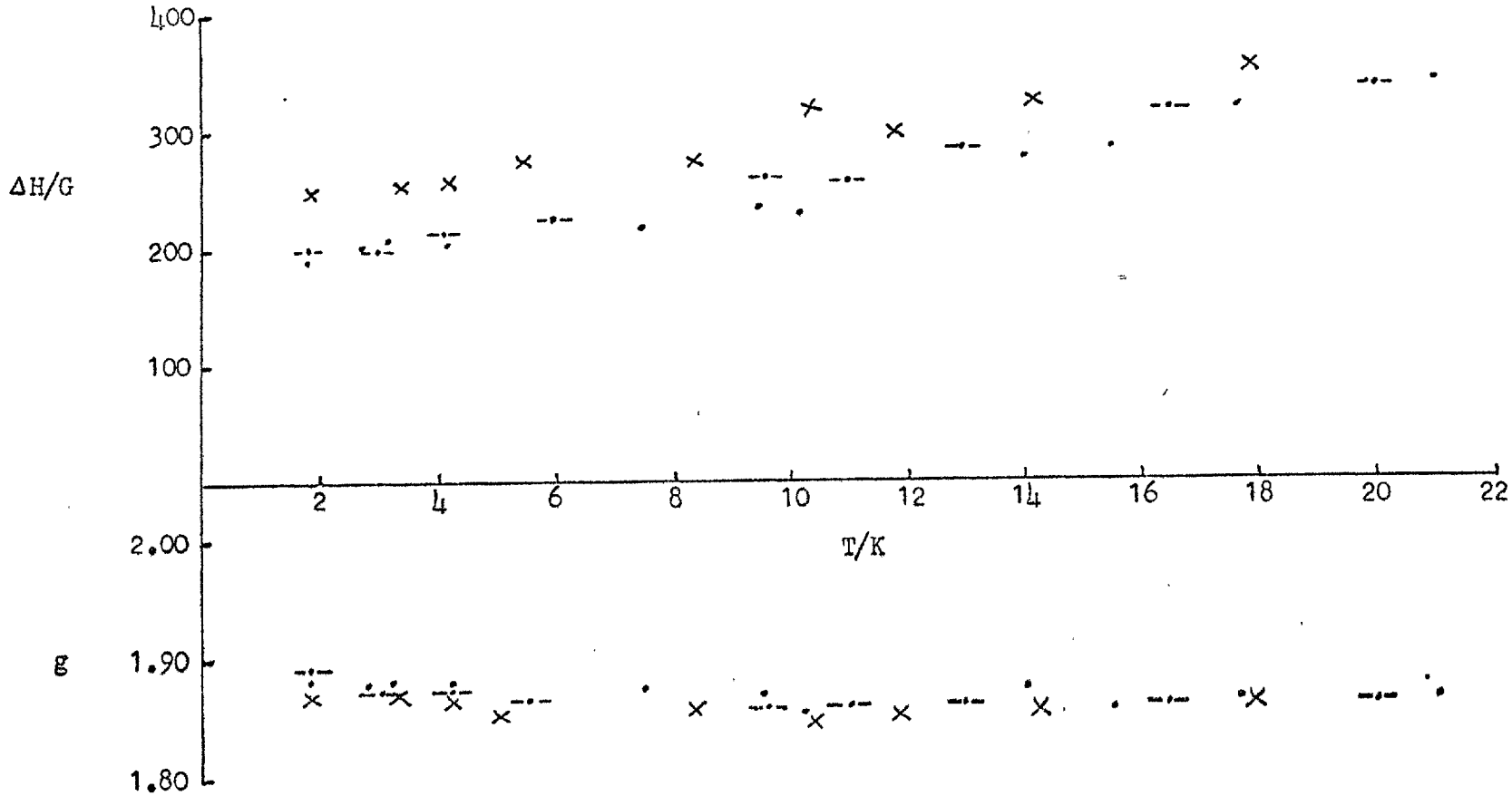

FIG.1 $(La_{0.995}Gd_{0.005})Ni_x$

x	
4.90	•
5.06	-·-
5.22	×

x	g_o	$\frac{d\Delta H}{dT}$ / GK^{-1}	T_{Hm} / K	T_g / K
0.003	1.86(5) ± 0.01	-	-	-
0.006	1.87(2) ± 0.01	10 ± 0.5	-	-
0.025	1.88(3) ± 0.01	9.3 ± 0.5	6	4
0.045	1.88(8) ± 0.01	9.6 ± 0.5	8	5
0.060	1.89(0) ± 0.01	9.2 ± 0.5	8	10
0.075	1.89(6) ± 0.01	9.5 ± 0.5	10	10
0.080	1.89(5) ± 0.01	9.5 ± 0.5	12	15
0.095	1.93(0) ± 0.01	9.0 ± 0.5	12	20

Table 1 EPR data for ($La_{1-x}Gd_x$)Ni_5.

increased so a minimum in the linewidth and an upturn in the g-value begin to appear. By 6at.% Gd there is a relatively deep minimum in the linewidth and a large increase in the g-value at low temperatures from that in the paramagnetic (Korringa) regime. In the 9.5at.% Gd alloy the g-value has increased to such an extent that the g-shift changes sign, Fig.12. The results for concentrations below 5at.% Gd are in agreement with previous work on the system (01) (02).

The main points of the results are the following:

1. Large negative g-shifts in the Korringa region are observed.
2. The concentration dependence of the linewidth and g-shift at low temperatures.
3. For Gd concentrations above 1at.% the g-shift varies appreciably with temperature, changing sign for concentrations above 9.5at.%. Below 1at.% the g-shift is independent of temperature.

The negative sign of the high temperature g-shift is common to Gd dissolved in hosts which have strong d-character (05). The g-shift is linked to the exchange coefficient, J(0), through equation 4.20. Therefore a negative g-shift implies an antiferromagnetic coupling between the local moments and the conduction electrons. The experimentally measured exchange constant J_{eff}, however, needs careful interpretation as there are many contributions which may give an overall negative coupling. The admixture term in the Anderson Hamiltonian is one contribution and has been discussed in detail by Watson et al (07). This is the one atom equivalent of interband mixing (see ch.2).

Interband mixing effects may be important in some systems which give negative g-shifts, however, Coles et al (06) have given an alternative explanation for Gd in d-like hosts. They argued that because Gd $4f^7$ electronic configuration is very stable, the interband

mixing effects will be small and that the d-s hybridization of the host will be the major contribution. The d-s hybridization leads to a polarization of the s-band antiparallel to the magnetization of the d-band. The exchange between the s-band and the 4f electrons is positive, therefore the g-shift is negative. Another mechanism has been put forward by Davidov et al (08). They suggested that the negative g-shift comes from an antiferromagnetic direct exchange between the Gd and the tight binding d-shell of the neighbouring host atoms. To support their view, they used the fact that hyperfine field shifts are positive for rare-earth ions in Pt and Rh but this is not necessarily inconsistent with the previous model (10).

Campbell (09) proposed a mechanism whereby the f-electron spin of the rare-earth creates a positive local d-moment through the usual f-d exchange interaction and that these d-moments then interact via direct d-d interactions. Treating the rare-earths as transition elements, this mechanism produces antiferromagnetic coupling when the rare-earth is dissolved in a metal in the other half of the transition series (eg. PdGd).

Which of the above mechanisms is correct or the relative contributions of each to the negative g-shift is not clear; further experimental work, especially with polarized neutrons, is needed to provide the answer.

An explanation for the behaviour of $LaNi_5$- Gd was put forward by Davidov and Shaltiel (02). They looked at compounds with Gd concentrations up to 5at.% , in a Q-band (14 KG) spectrometer. They interpreted the results in terms of dynamic effects in the epr bottleneck and fitted their g-shift data to expression 4.24. The linewidth data was not plotted explicitly against temperature but at 4.2 K it was

given as a function of Gd concentration. The linewidth was found to increase with increasing concentration. This was explained, not by dynamic effects, but by assuming an inhomogeneous distribution of Gd ions giving clusters which have effectively different g-shifts and hence could lead to a broadening.

This interpretation in terms of dynamic effects raises the problem of consistency with other strongly d-like hosts; $LaNi_5$ is an exchange enhanced d-like metal, (see below). Usually the d-band is sufficiently narrow that the relaxation rate of the conduction electrons due to phonons etc. is large enough to break the bottleneck. For example, PdGd is not bottlenecked at any temperature or concentration (10). The conduction electron relaxation rate to the lattice is high for d-like metals because, as Yafet (11) showed, δ_{eL} is proportional to the host density of states squared. The other major difficulty, in the dynamic effects explanation, is that the onset of magnetic ordering is not explicitly included.

The measurements in this work were taken at x-band and hence in a field of approximately 3.2 KG. Using the numerical values from the work of Davidov and Shaltiel for the various relaxation rates etc., which should not be frequency or field dependent, it was attempted to fit the g-value data to expression 4.24. Unfortunately this was not successful, especially for the higher concentration alloys (> 7at.%Gd) where the g-shift becomes positive at low temperatures. Clearly this is inadmissable from equation 4.24. To overcome these difficulties the results were analysed taking into account the magnetic ordering in the system.

Magnetic ordering has profound effects on the resonance behaviour of a system (see ch. 3) and must be included in any analysis. Taylor and Coles (10) showed that the temperature dependence of the g-value in PdGd alloys (0.4at.% Gd and 6.0at.% Gd) could be explained by magnetic

order and fitted their data using experimental magnetization curves. Similar results have also been obtained with $GdAl_2$(12). The epr data can only be fitted by assuming a demagnetization factor D, because all measurements are carried out on powders and therefore exact demagnetizations calculations are impossible.

The magnetization in 3.2 KG for $LaNi_5$-8at.% Gd is shown in Fig.8 * and the resonance results for the same sample are given in Fig.7. The curve through the g-value is obtained from the magnetization data using an assumed demagnetization factor of 2.8. The value of this factor is reasonable compared with other work on powders (12). As can be seen the g-value follows the general form of the magnetization in 3.2 KG.

The line width passes through a minimum as a function of temperature for concentrations greater than 1at.% Gd. The temperature at which the minimum occurs corresponds roughly to the temperature at which the g-shift begins to fall. The temperature of the minimum increases with increasing concentration. These effects may be understood in terms of the onset of magnetic order. Inhomogeneous broadening of the line will occur at temperatures above the ordering temperature as a result of the distribution of demagnetization factors among the sample particles (the specimen is in the form of a powder).

Ferromagnetic anisotropy will also contribute to the linebroadening process. This broadening will occur because the anisotropy energy depends on the crystal direction, therefore as powder specimens are composed of randomly orientated crystallites the observed resonance line will be a superposition of a large number of single crystal lines. Van Vleck (13) showed that this gives rise to a broadening of the form

$$\Delta H \propto K_1 / M_s$$

* Dr. J.B. Dunlop of the University of Sheffield kindly performed this measurement.

where K_1 is the first order anisotropy constant.

As Gd is in an S-state, ferromagnetic anisotropy constants derived from a single ion crystal field model are expected to be small. However, Bagguley et al (14) found for Y- Gd constants an order of magnitude larger than expected. They proposed multiple spin interactions as the cause.

The addition of non-magnetic impurities to a bottlenecked system will break the bottleneck and reduce the linewidth at a given temperature. Fig.10 shows the g-shift and linewidth for $(La_{0.95}Gd_{0.05})Ni_5$ and $(La_{0.92}Gd_{0.05}Th_{0.03})Ni_5$. The addition of 3at.% Th does not significantly increase the g-shift or the slope of the linewidth. Whereas the addition of 0.1at.% Pt to a bottlenecked Cu 1at.% Mn alloy increases the value of the slope of the linewidth by factor of 4 (15).

On the evidence presented it seems reasonable to conclude that the epr results on low concentration Gd in $LaNi_5$ may be satisfactorily explained by the effects of the onset of magnetic order, thus making $LaNi_5$ consistent with other d-like metals which do not give a bottleneck on the addition of s-state impurities, typically Pd-Gd. Interestingly the temperature at which the g-shift begins to decrease from the work of Davidov and Shaltiel is noticably higher for a given concentration than in this work. This can be reconciled by realizing that their measurements were performed in fields of 14 KG; therefore it is reasonable to expect demagnetization effects to set in at higher temperatures. It is not possible to state categorically that dynamic effects do not occur in $LaNi_5$- Gd but if they are present then they are second order effects compared to the magnetic ordering process.

Dynamic effects have been reported in $LaRu_2$- Gd (16) and Yb-Eu (17). It seems possible from the data on the $LaRu_2$- Gd system that magnetic ordering effects may be present. The work of Schmidt et al (17) on

0.5at% Eu in Yb showed that the g-shift is almost totally suppressed at low temperatures. On adding non-magnetic impurities (2at.% Ca) they found that the g-shift increased, indicating the breaking of the bottleneck. Their linewidth and g-value data fitted expressions 4.24 and 4.25 for both 9.6 and 35 GHz measurements. If ordering effects were involved in this system they would tend to increase the g-shift whereas only a decrease was observed. This combined with the frequency dependence is excellent evidence for dynamic effects in the bottleneck. Rettori et al (18) have recently reported dynamic effects in the $LaAl_2$ and YAl_2- Gd systems at pumped ^3He temperatures.

The increase in the high temperature g-value (g_o) with increasing concentration is due to saturation effects in the $LaNi_5$ d-band (Fig.11). In exchange enhanced hosts magnetic impurity atoms often have giant moments. For example, Pd 0.15at.% Fe the effective moment per iron atom in the paramagnetic regime is $9.5\,\mu_B$(19). Diffuse neutron scattering experiments on Pd with Fe and Co (20) and Ni_3Al-Fe (21) have shown that large magnetic moments induced by the impurities were distributed over hundreds of host atoms nearest to each impurity. The long range induced moments are due to susceptibility enhancement by the exchange interaction in the host d-band (20). The polarization clouds for a given impurity will have a certain range, as the concentration is increased sothe average separation of the impurities is reduced and overlap of polarization clouds will occur. The polarization clouds do not superimpose as the host can only maintain a certain degree of polarization. Therefore as the concentration is still further increased the response saturates.

The difference between $LaNi_5$- Gd and the above mentioned compounds is that the polarization clouds induced by the Gd moment are antiparallel to the moment. This is evident from the negative paramagnetic g-shifts.

FIG.2 $(La_{0.994}Gd_{0.006})Ni_5$

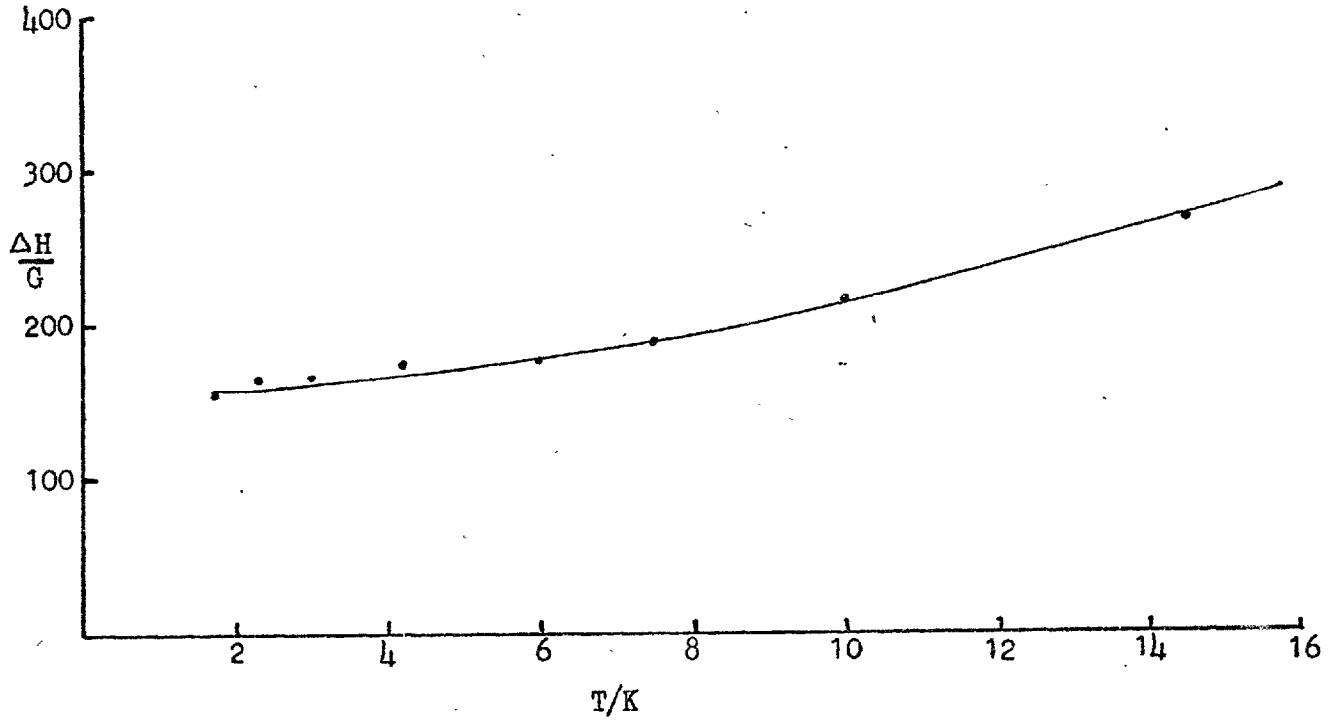

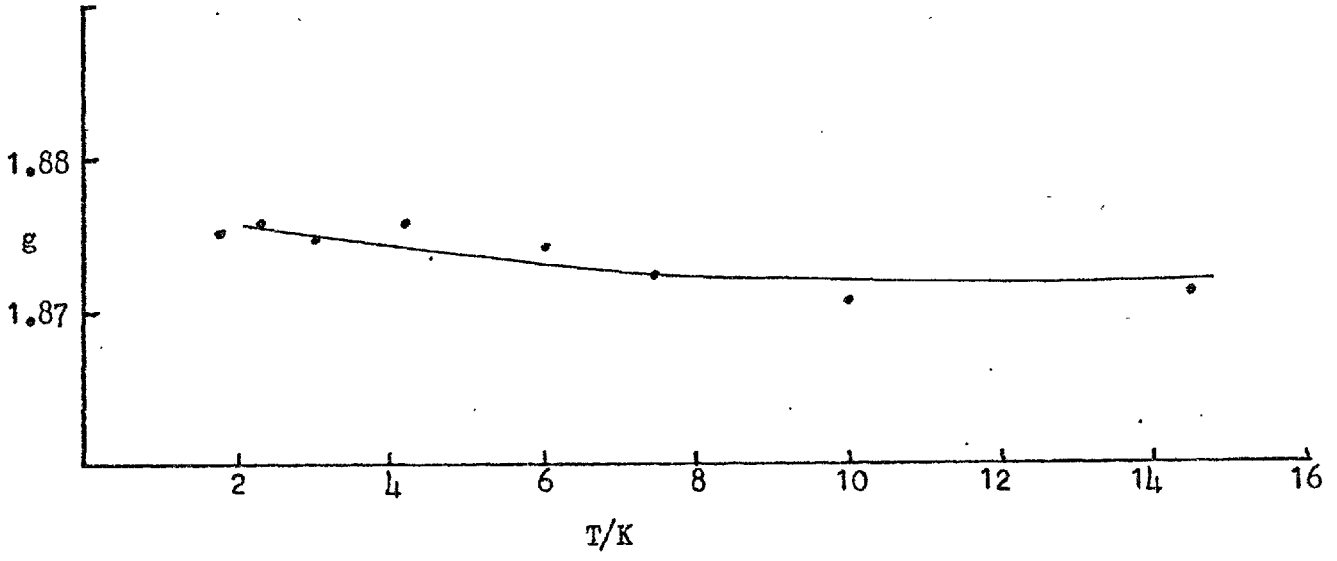

FIG.3 $(La_{0.975}Gd_{0.025})Ni_5$

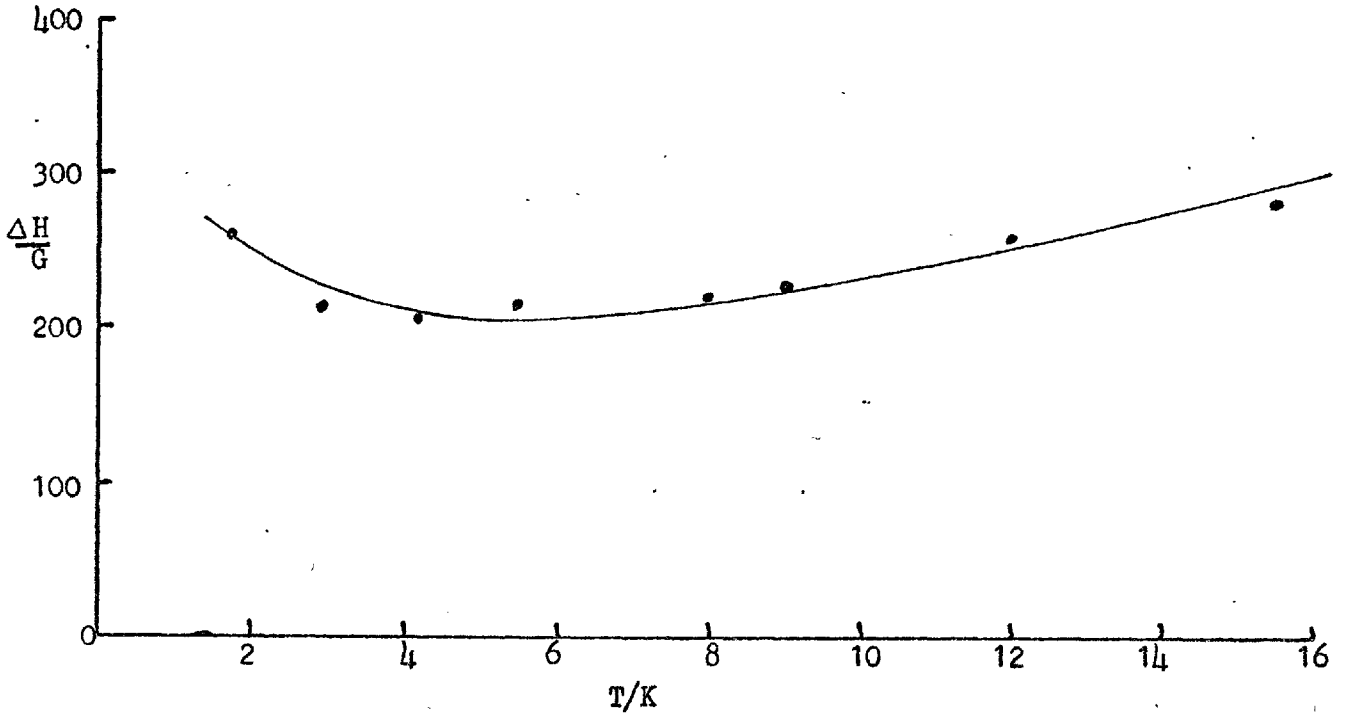

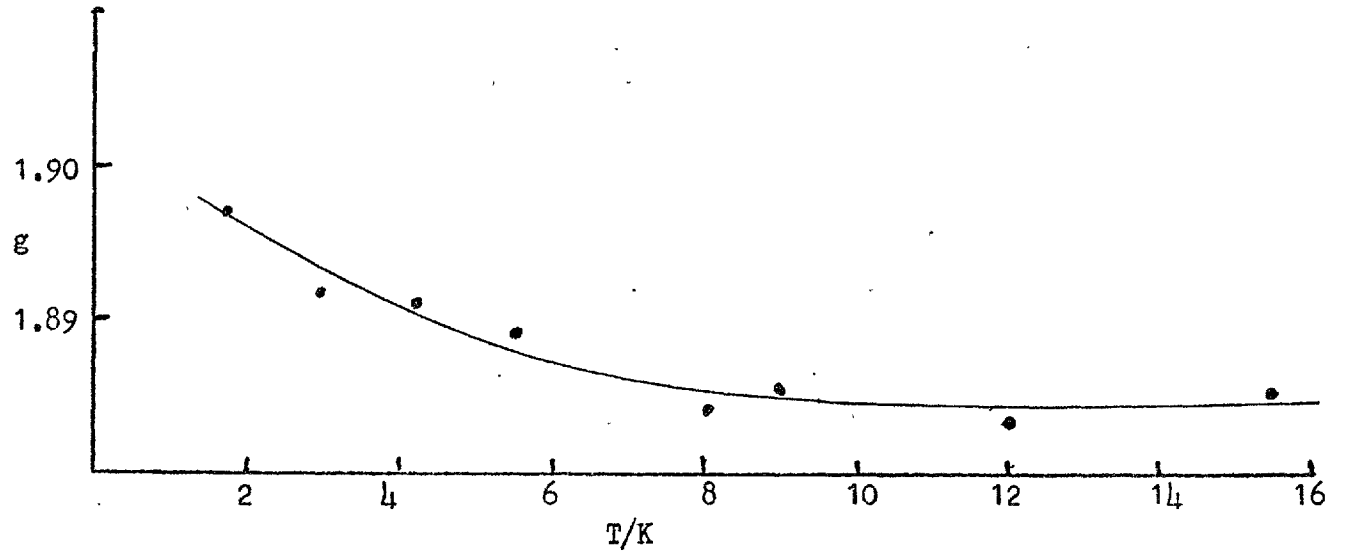

FIG.4 $(La_{0.955}Gd_{0.045})Ni_5$

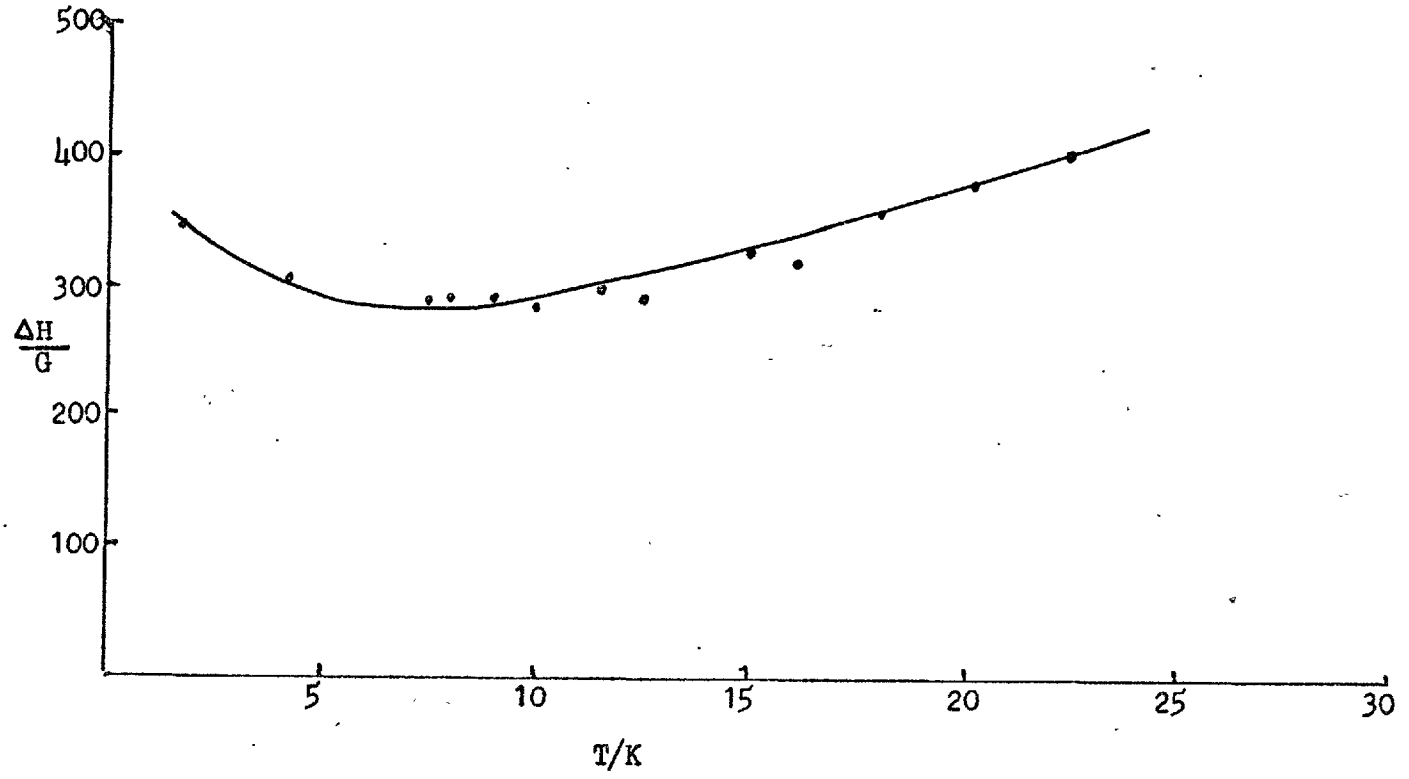

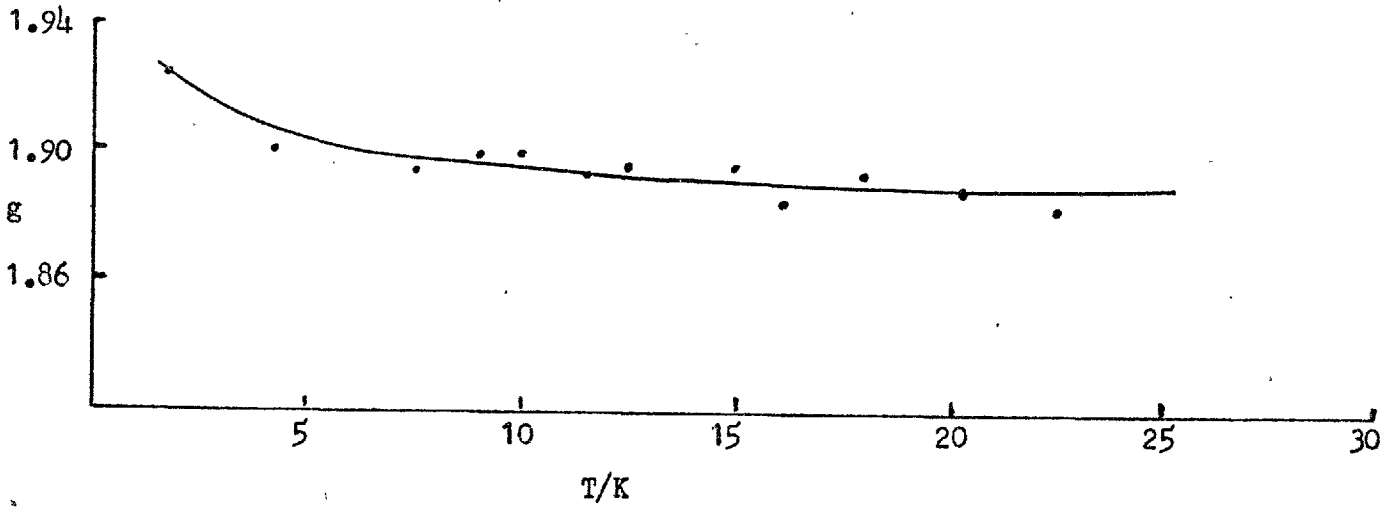

FIG.5 $(La_{0.94}Gd_{0.06})Ni_5$

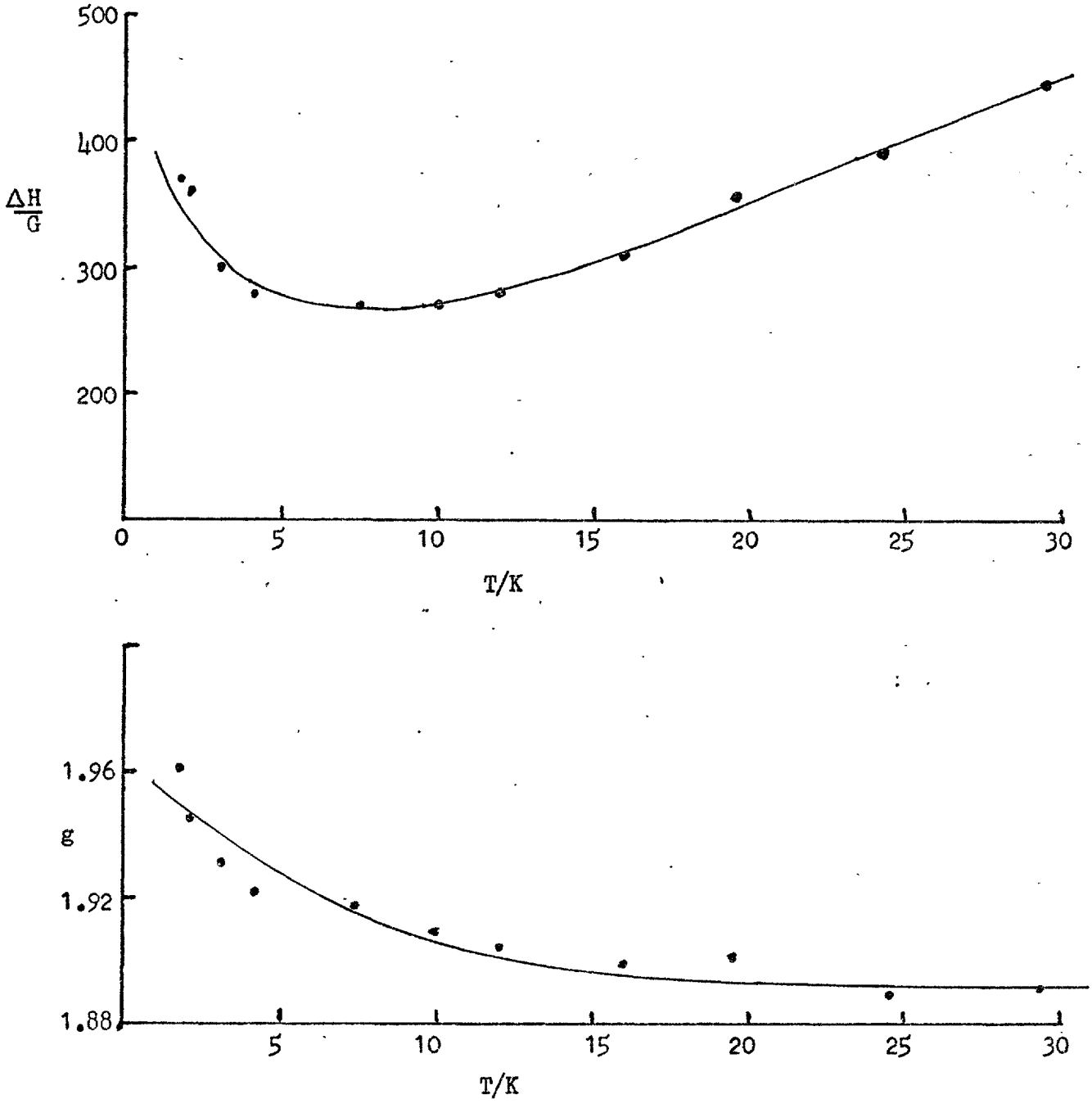

FIG.6 $(La_{0.925}Gd_{0.075})Ni_5$

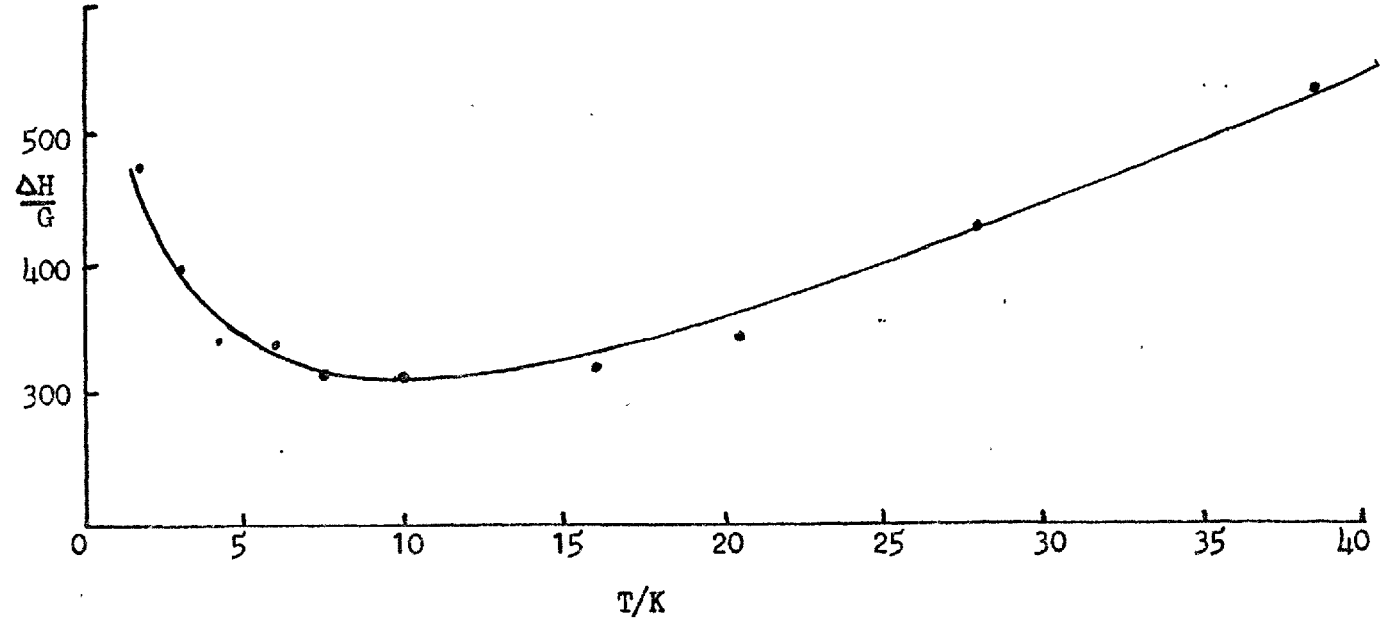

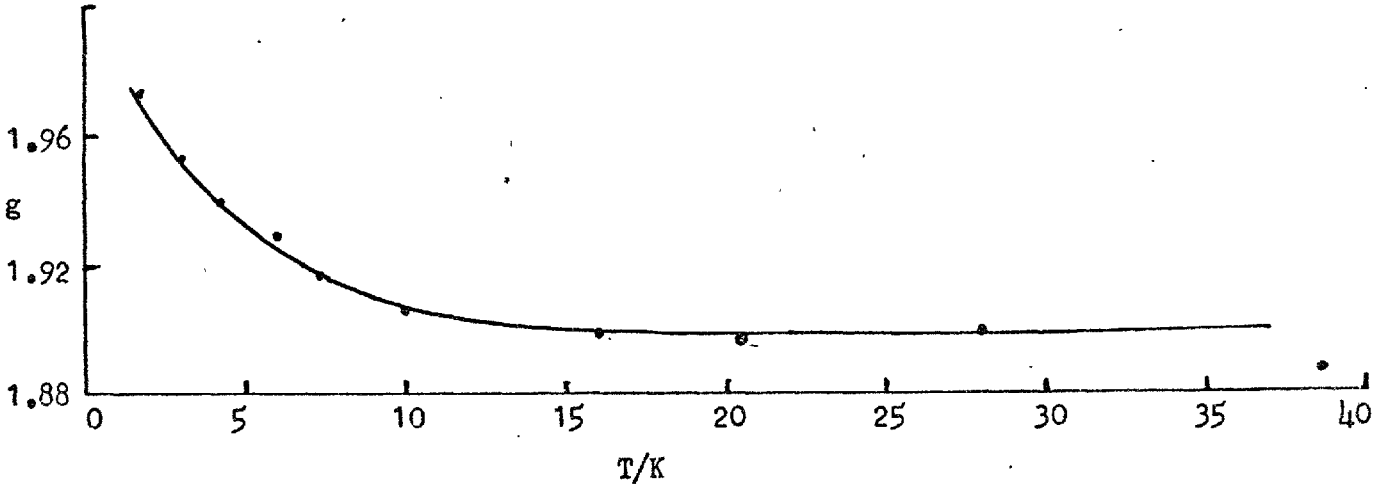

FIG.7 $(La_{0.92}Gd_{0.08})Ni_5$

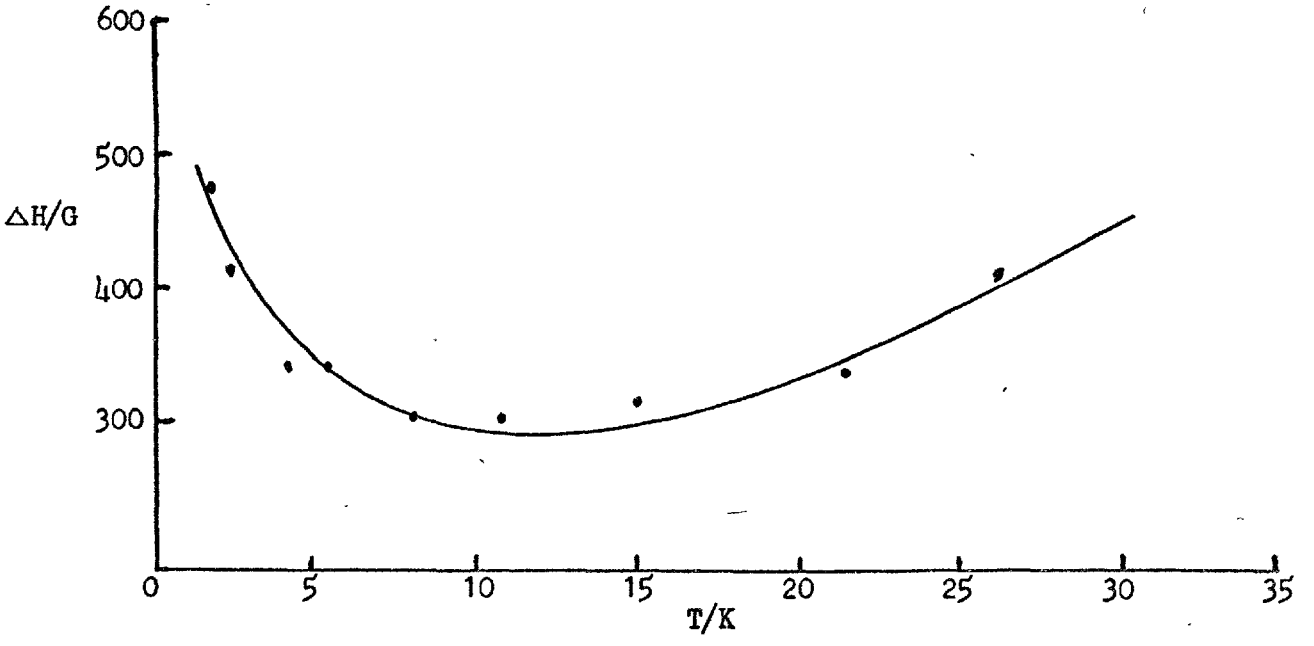

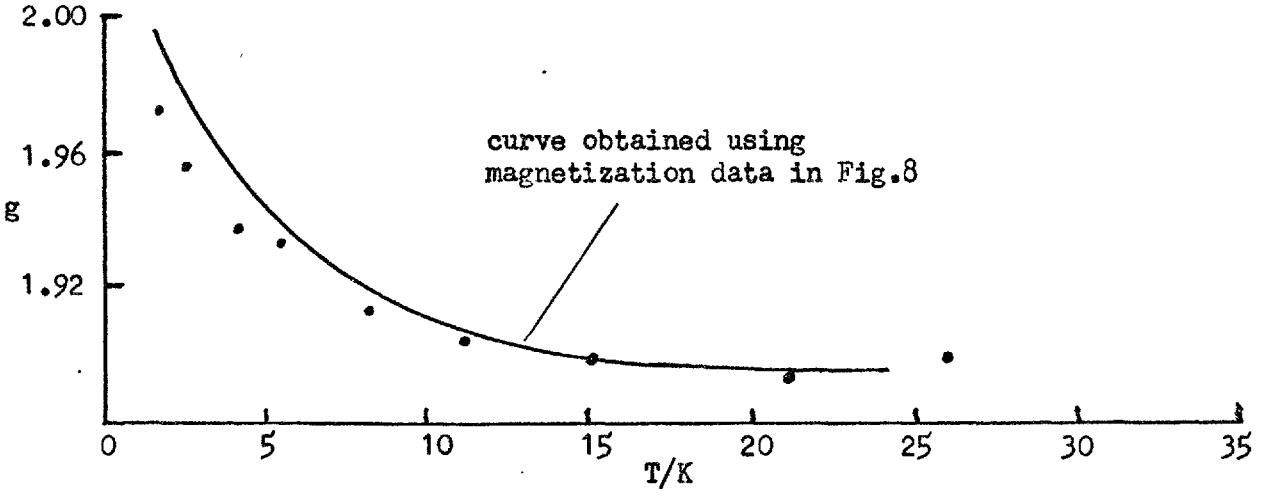

FIG. 8 Magnetization in 3.4 KG for $(La_{0.92}Gd_{0.08})Ni_5$

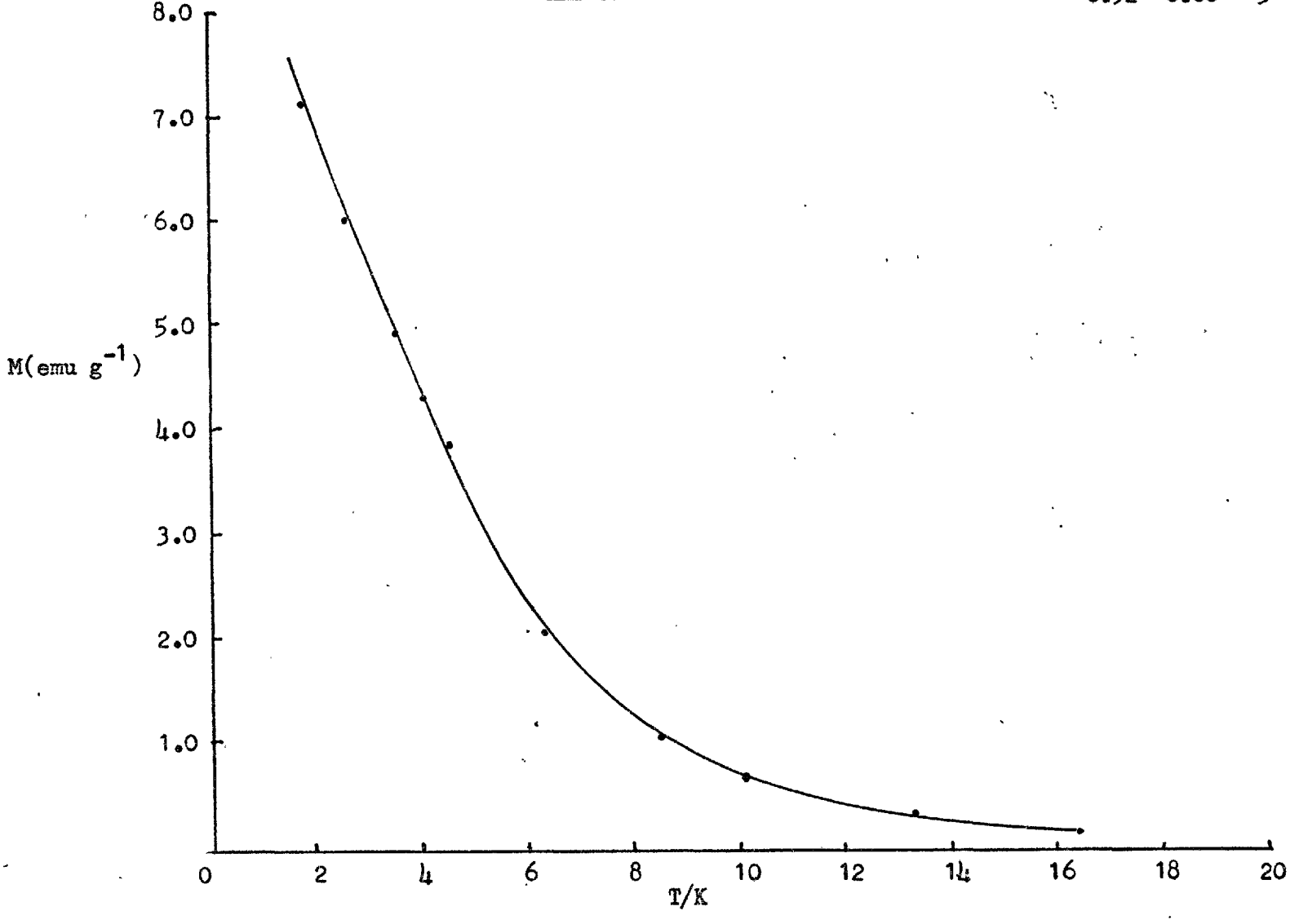

FIG.9 $(La_{0.905}Gd_{0.095})Ni_5$

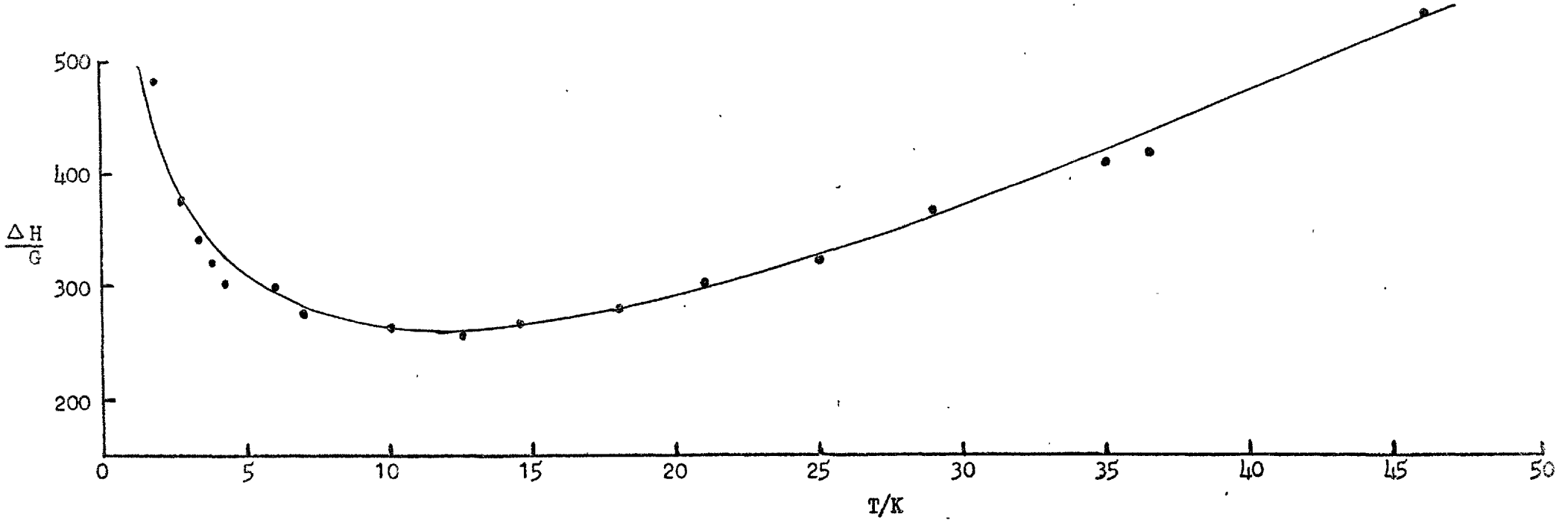

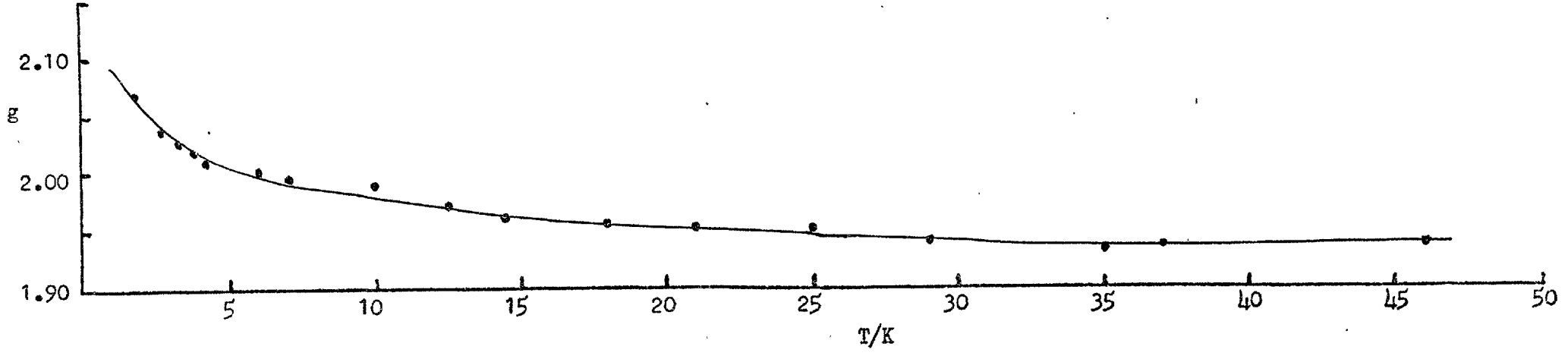

FIG.10. $(La_{0.92}Gd_{0.05}Th_{0.03})Ni_5$ •

$(La_{0.95}Gd_{0.05})Ni_5$ ⊙

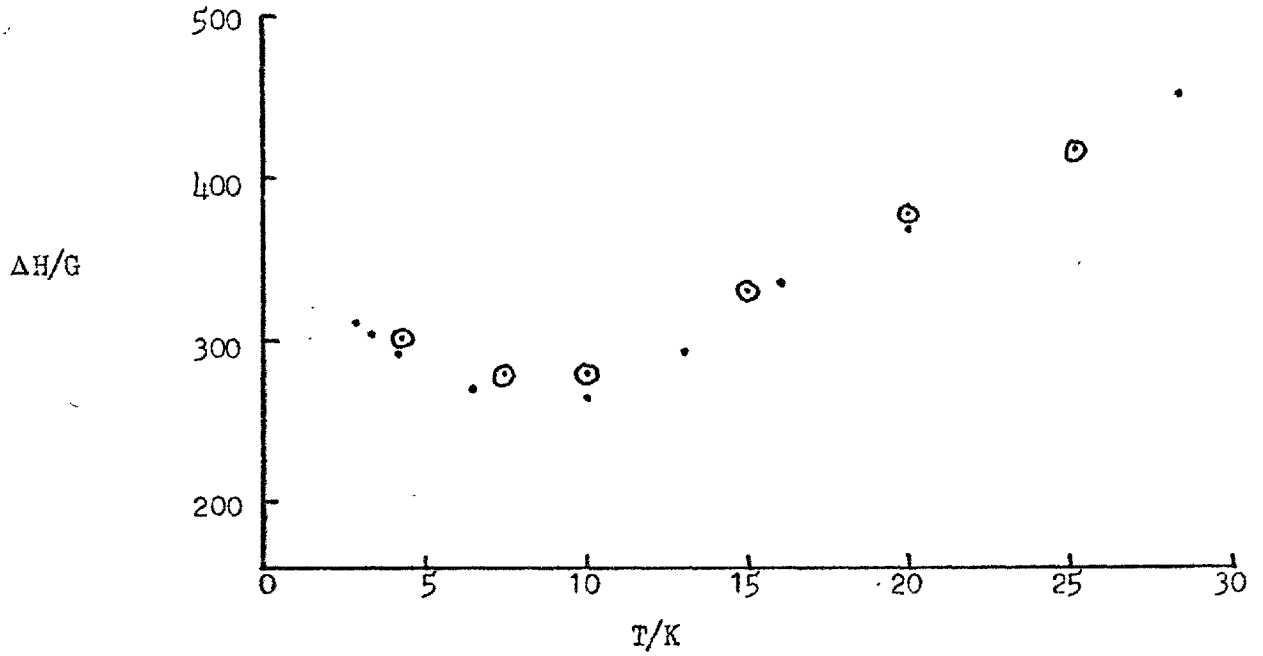

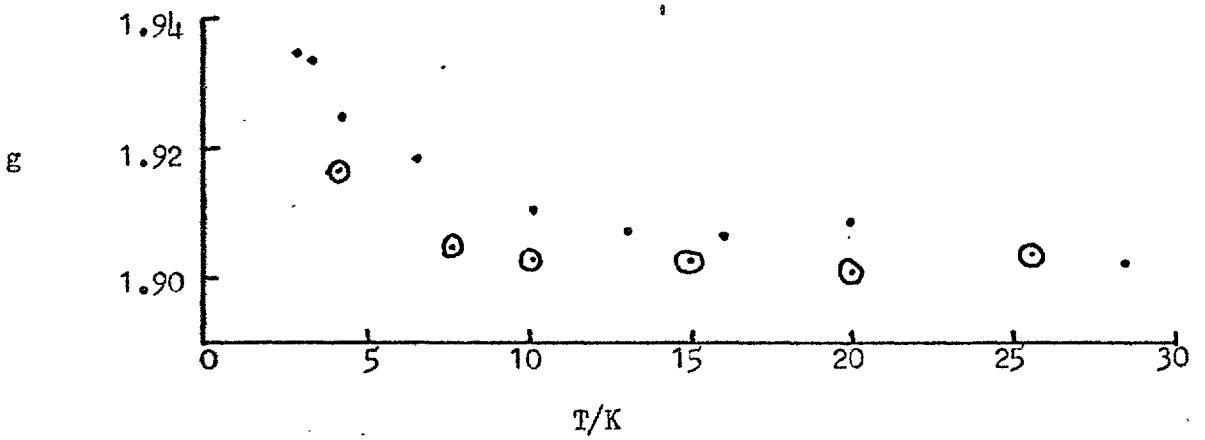

FIG. 11 High temperature g-value and $d\Delta H/dT$ for $(La_{1-x}Gd_x)Ni_5$.

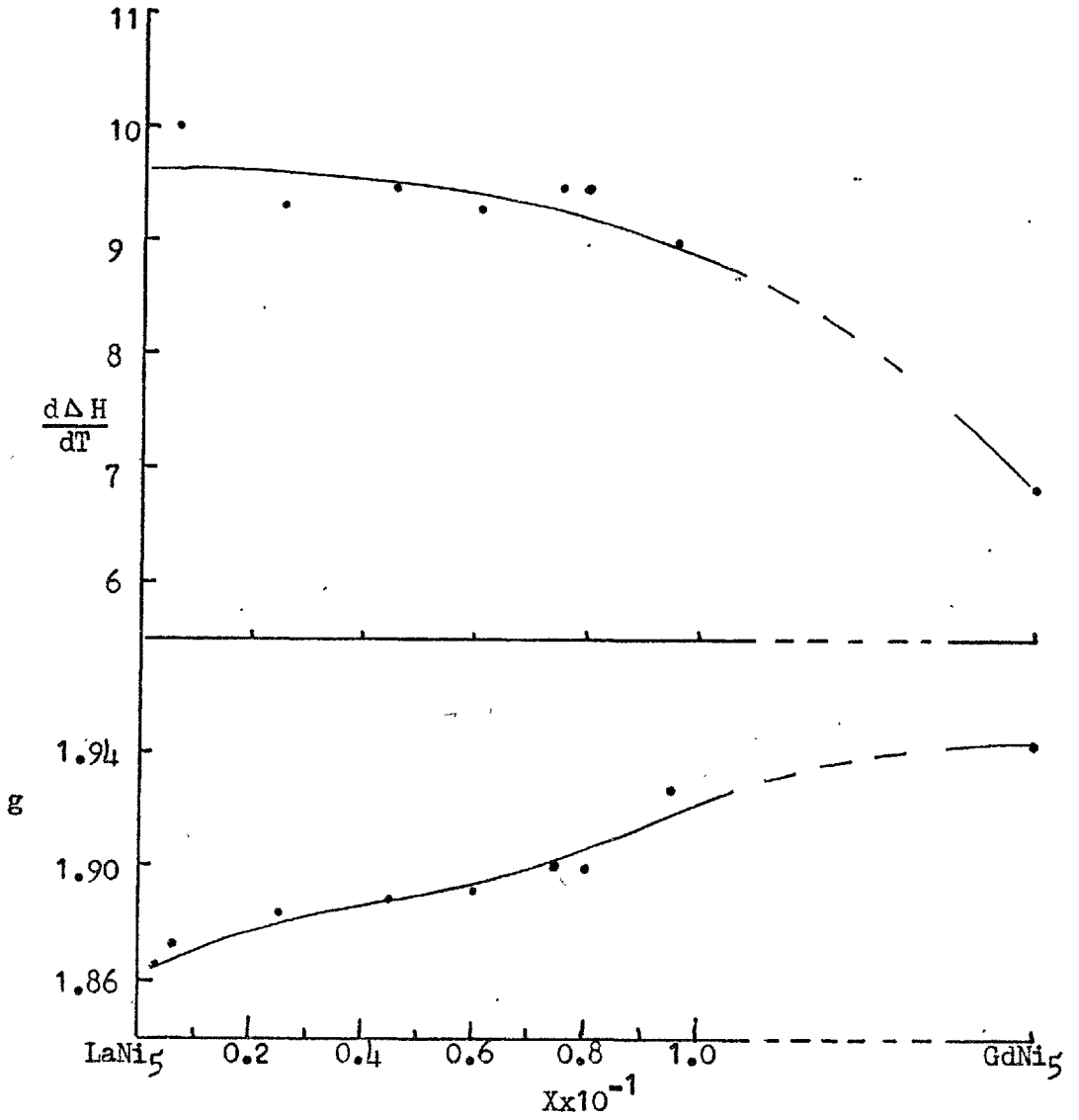

FIG. 12. g-shift for $(La_{1-x}Gd_x)Ni_5$

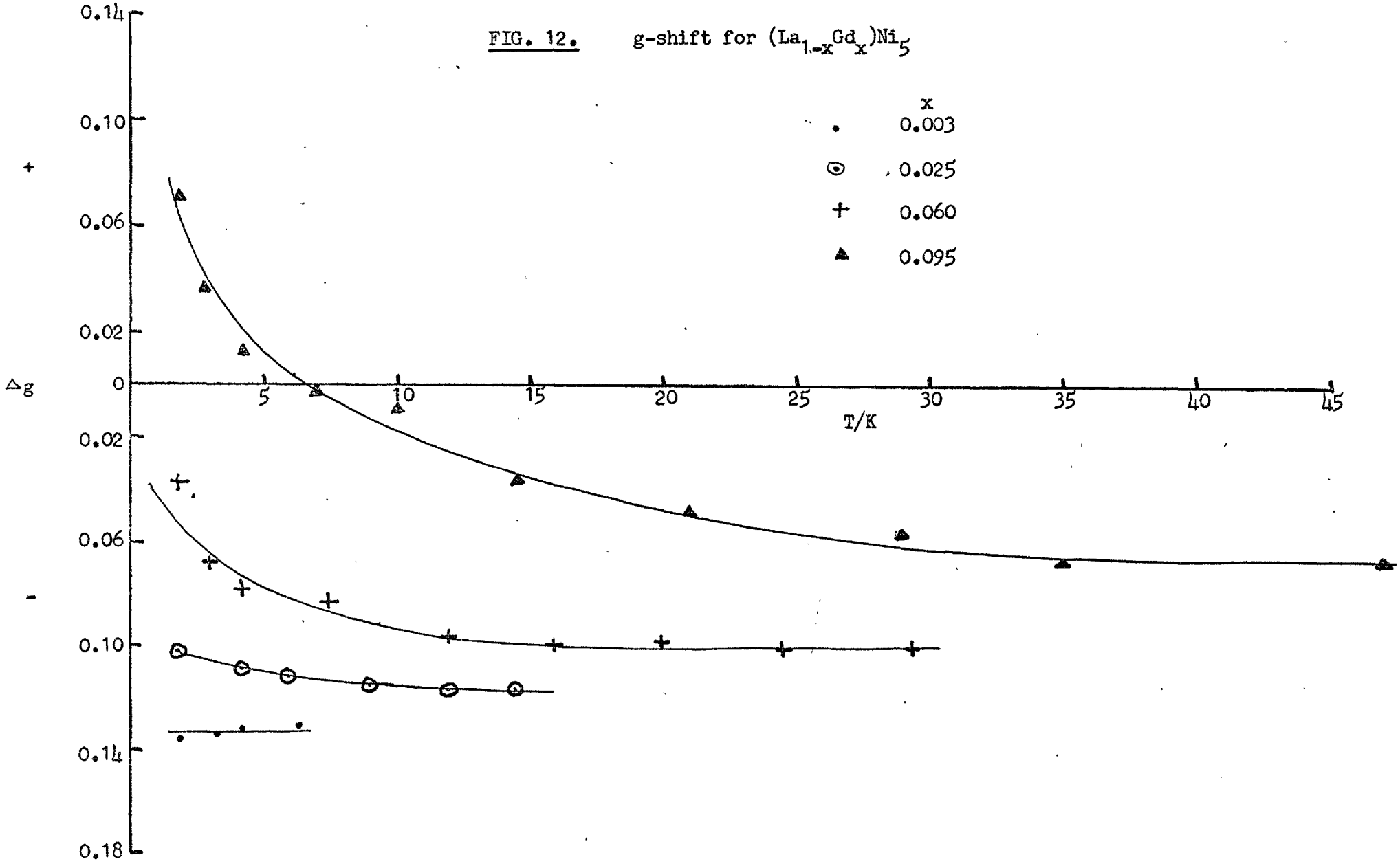

6.2 $LaNi_5$- Gd: High concentration epr results.

The paramagnetic resonance results of $LaNi_5$- Gd for concentrations of Gd above 20at.% are presented in Figs.15 to19 and summarized in Table 2. The 20at.% Gd alloy shows a minimum in the linewidth at approximately 15K well above the ordering temperature (see below); deviations from the paramagnetic g-value (g_o) also set in at approximately this temperature. The shape of the g-value vs. temperature curve is typical of a system undergoing a ferromagnetic transition. The flattening out at low temperatures is due to the effects of saturation of the magnetization in a field of 3.2 KG. The 30at.% sample has similar characteristics but with the linewidth minimum at higher temperatures. As the concentration of Gd is increased so the temperature of the linewidth minimum and the deviation of the g-value also increase . The minimum in the linewidth is due to the spread of demagnetization factors in the powdered samples and ordering effects which become increasingly important as the magnetization in 3.2 KG grows with decreasing temperature. These effects cause the line to broaden at low temperatures thereby giving a minimum as a function of temperature.

The minimum occurs at approximately 2.0-2.5T_c for a given alloy which is higher than that reported by Taylor and Coles (12),for other ferromagnetic compounds, of 1.2-1.5T_c. This is probably due to an extended regime of short range order in these compounds. The linewidth minimum is not really the correct parameter to compare as it occurs due to the different temperature variations of a number of terms. Deviations from the Korringa slope would be a more realistic parameter for ascertaining when ordering effects are becoming important. Unfortunately the data in the high temperature regime are usually not reliable enough to do this successfully.

The high temperature g-value in $LaNi_5$- Gd has practically reached the $GdNi_5$ value by 20at.% Gd. This effect is due to the exhaustion of the response of the host d-band (see above). The slope of the linewidth and the paramagnetic g-value for $GdNi_5$ agree with those of Ursu and Burzo (22) who found values of $g_o = 1.944 \pm 0.006$ and $d\Delta H/dT = 6.4 GK^{-1}$.

The observed resonance line had a differential line shape with a ratio of low field to high field peak heights (A/B) close to the theoretical value of 2.55 in the high temperature (Korringa) region. The line shape became more symmetric, with $A/B \sim 1$ as the temperature passed through the critical point.

An interesting phenomenon, in compounds with Gd concentrations greater than 50at.%, occurred at certain temperatures. As the temperature was reduced so the line broadened but at a given temperature for a particular alloy a double resonance signal appeared (see Fig.13). The line shape altered as the temperature was lowered still further, eventually the double resonance disappeared and a line with approximately a 1:1 shape remained. This process is illustrated in Figs.14 a and b for $LaNi_5$- 75at.% Gd. Fig.14b is the actual differential signal obtained for a number of temperatures. Fig.14a shows schematically the integrated intensity for the same temperatures, because of offsets at high and low fields the integration cannot be performed precisely.

It is difficult to understand what mechanism gives rise to these effects and no explanation has yet been obtained. Metallographic examination of the samples showed only one mechanical phase to be present. Even if small amounts of another phase were present it is hard to understand why a double resonance should only appear at low temperatures (around the ordering temperature) as both the neighbouring phases have high transition temperatures (Gd_2Ni_7 $T_c = 119$ K (23)

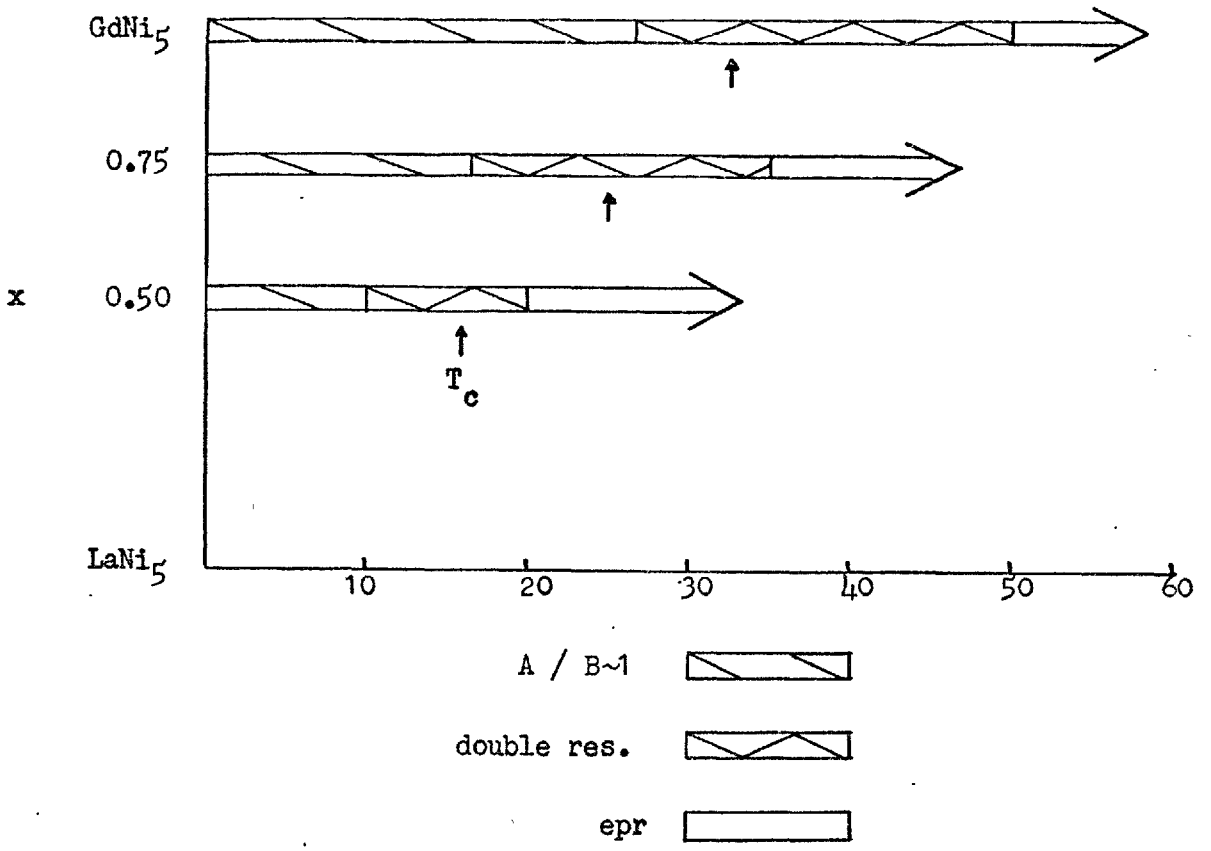

FIG. 13 Temperature dependence for the various types of resonance behaviour. T_c is from the maximum in the resistivity.

x	g_o	$d\Delta H / dT$ (GK^{-1})
0.20	1.91(5)±0.01	11
0.30	1.94(5)±0.01	-
0.50	1.94(5)±0.01	8.8
0.75	1.94(8)±0.01	7.3
$GdNi_5$	1.94(9)±0.01	6.0

TABLE 2 Epr data for $(La_{1-x}Gd_x)Ni_5$ with $x > 0.20$.

and Gd_2Ni_{17} T_c = 205 K (23)).

The magnetic susceptibility measurements on $GdNi_5$ (34) show that the moment per Gd ion is approximately the free ion value thereby indicating that the nickel atoms carry no moment. Therefore it is unlikely that the second resonance comes from the nickel. All the samples which were measured contained a very small amount of free nickel (see the susceptibility measurements on $LaNi_5$), but any resonance from this would be present at all temperatures and in all concentrations.

The effect may be due to the spurious behaviour of the spectrometer but this seems unlikely as these effects have not been observed for any other system.

An indication that the double resonance is a genuine effect is the observation in other measurements of anomalous behaviour around the critical temperature for $GdNi_5$. For example, the heat capacity measurements of Marzouk et al (26) showed two λ-type anomalies peaking at 29.8 and 30.6 K superimposed on a broad thermal anomaly. They suggested that the double anomaly was an intrinsic property of the system and possibly evidence for a magnetic phase existing over a very narrow range of temperatures, as in Lu_2Fe_{17} (27). The excess entropy above the critical temperature was associated with the persistence of short range order well above T_c.

Reidi (28) has also found anomalous behaviour in the AC susceptibility as a function of temperature, in the same temperature range as the heat capacity. He found a broad maximum with increasing temperature followed by a minimum and then a sharp maximum in the region of the ordering temperature. A normal ferromagnet gives a maximum at T_c with a sharp fall on the high temperature side. These results have yet to be explained.

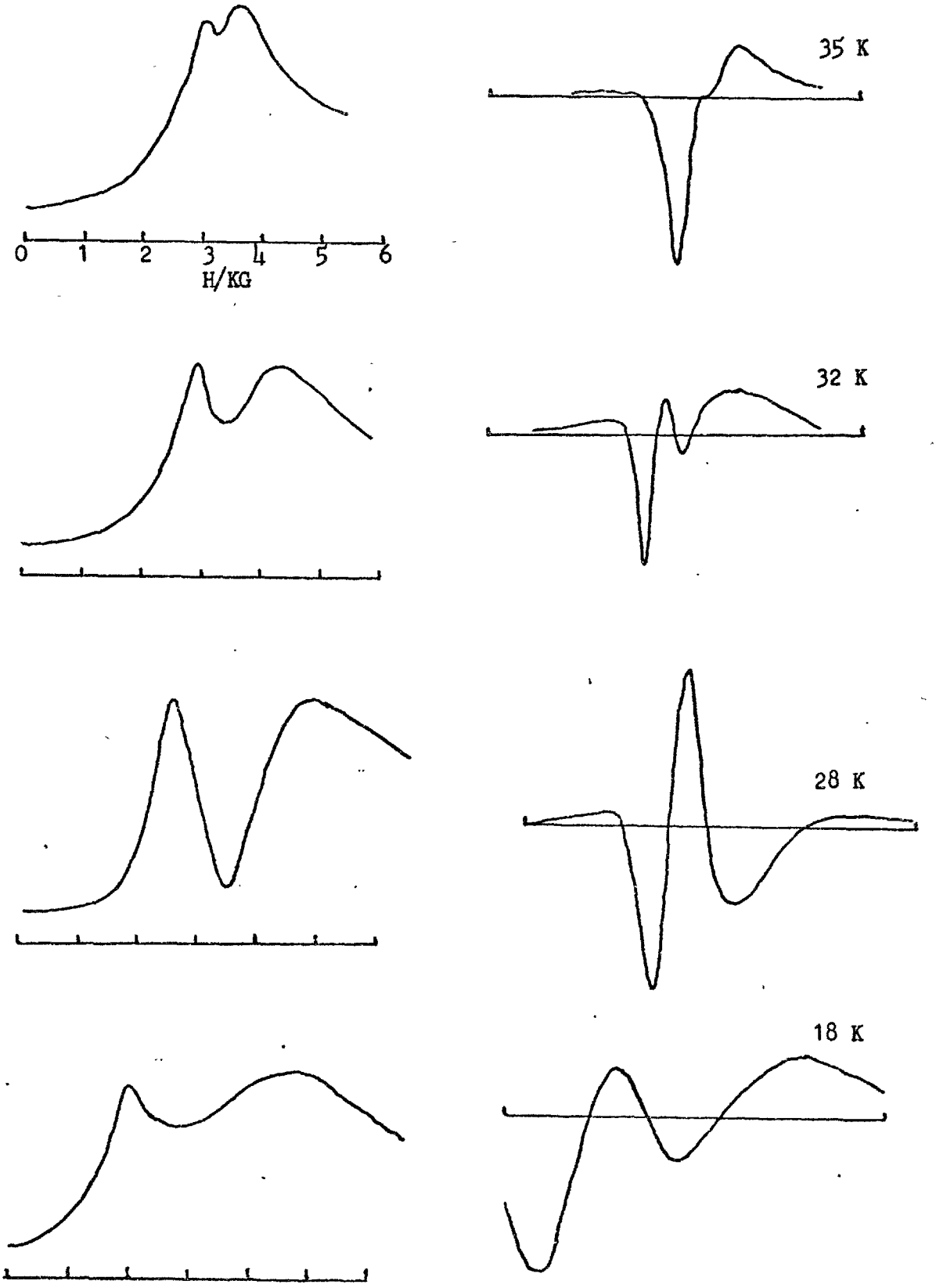

FIG.14 The double resonance signal from $LaNi_5$ - 75at.%Gd.
(a) Relative intensity against field (see text).
(b) Observed differential signal.

FIG. 15 $(La_{0.80}Gd_{0.20})Ni_5$

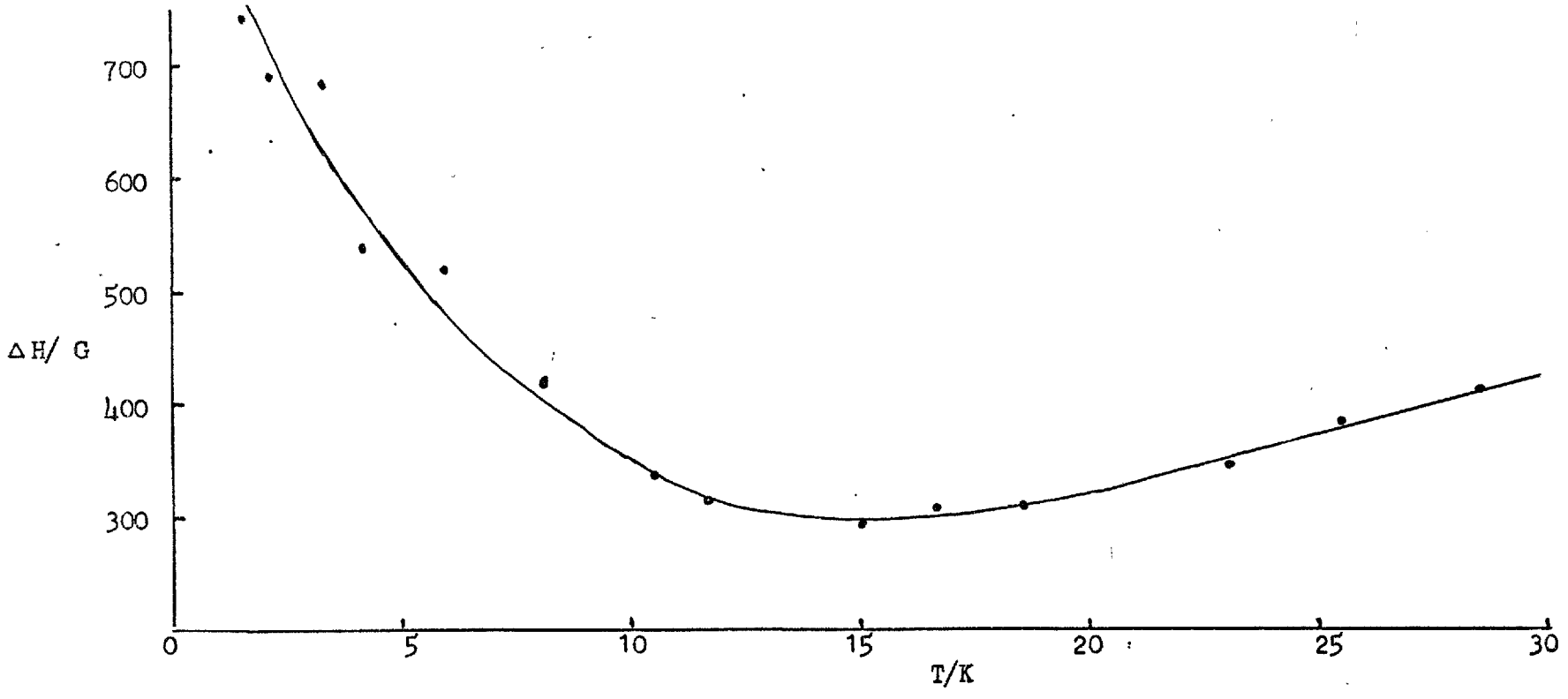

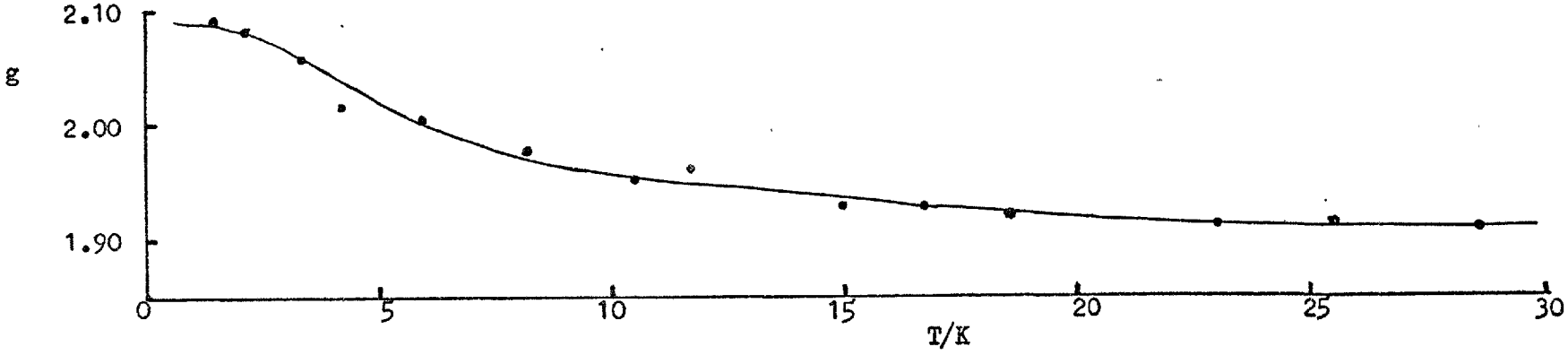

FIG. 16 $(La_{0.70}Gd_{0.30})Ni_5$

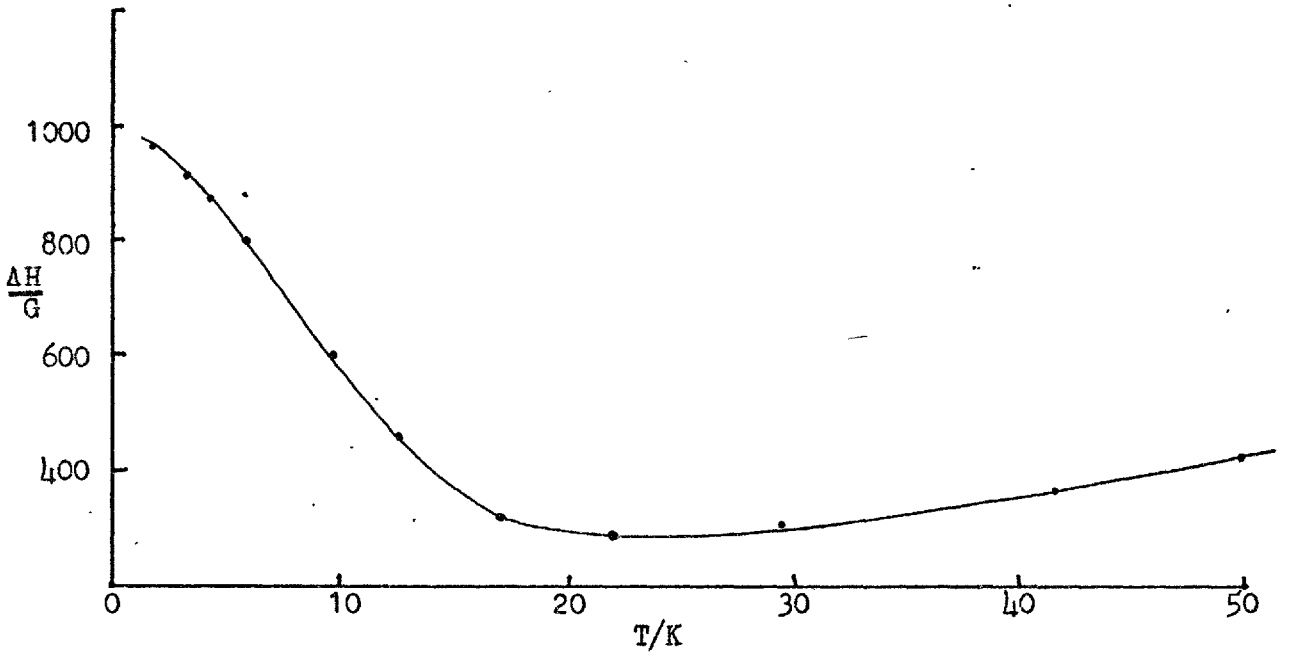

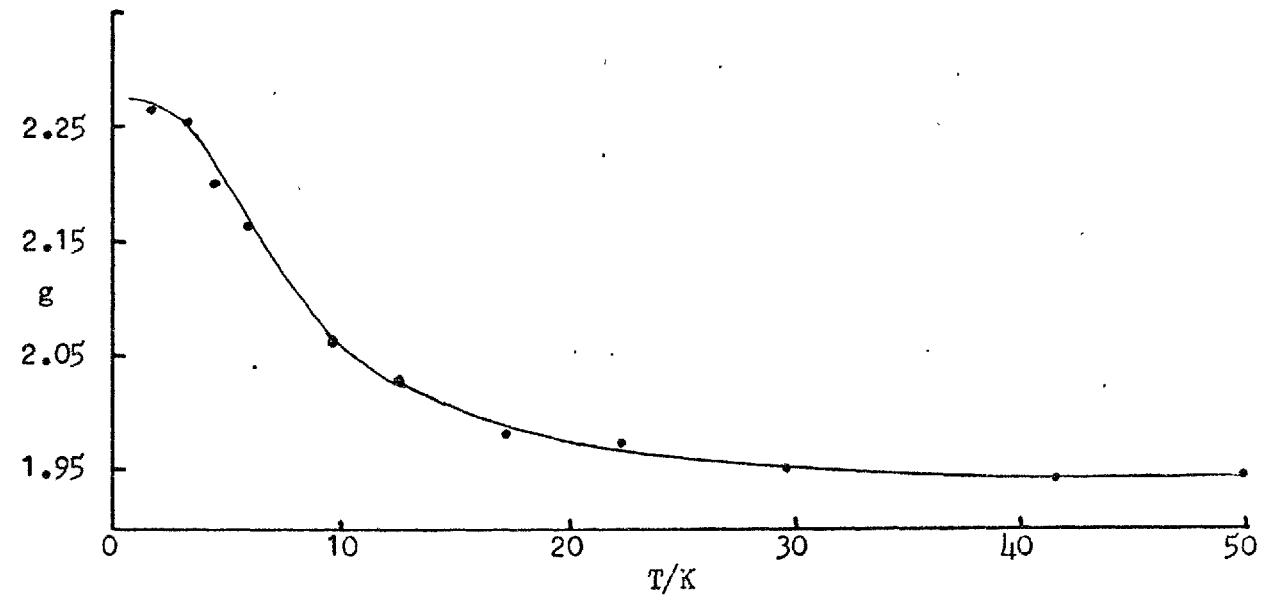

FIG.17 $(La_{0.50}Gd_{0.50})Ni_5$

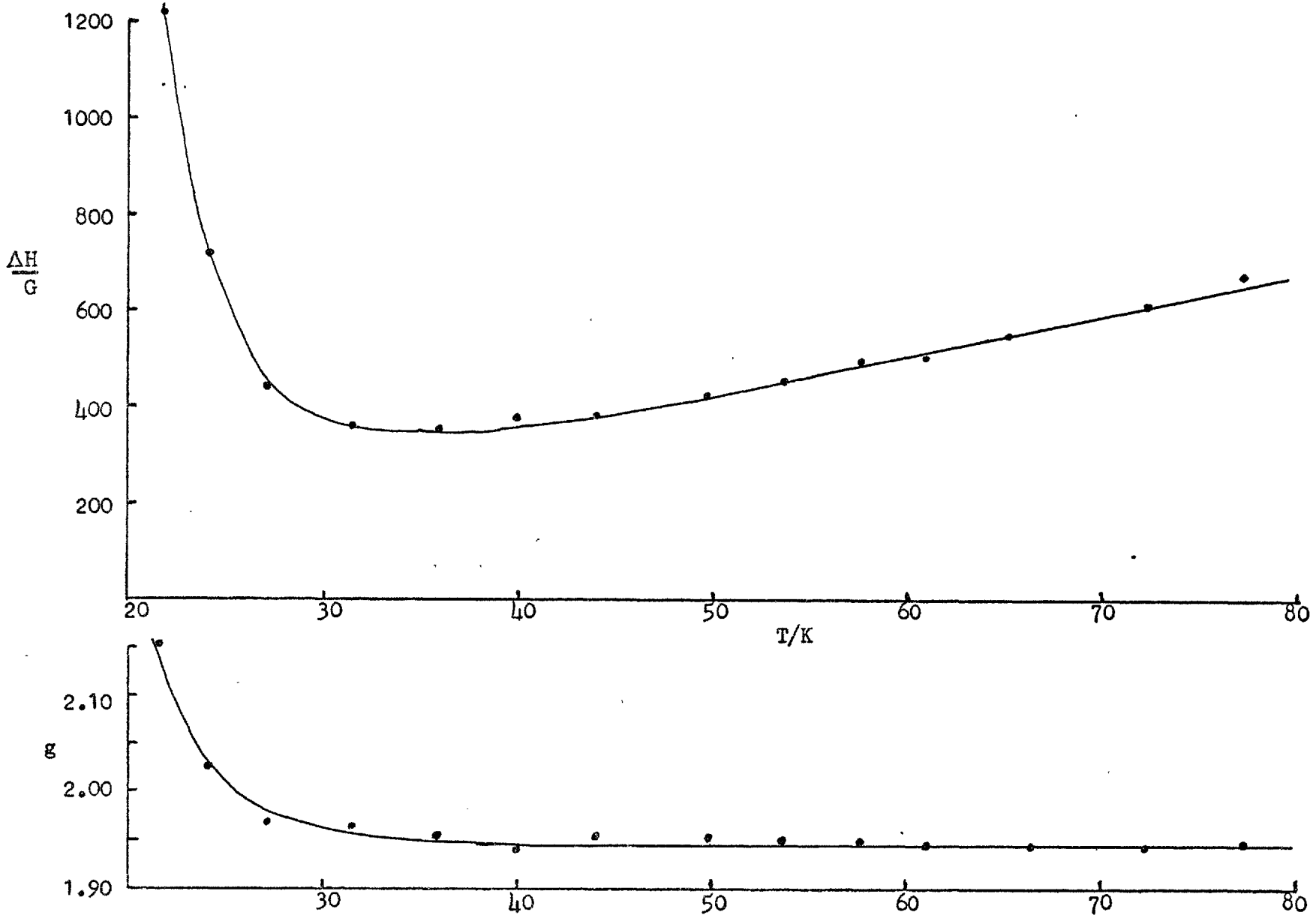

FIG.18 $(La_{0.25}Gd_{0.75})Ni_5$, X represents the linewidth and resonant field in the ferromagnetic region (uncorrected).

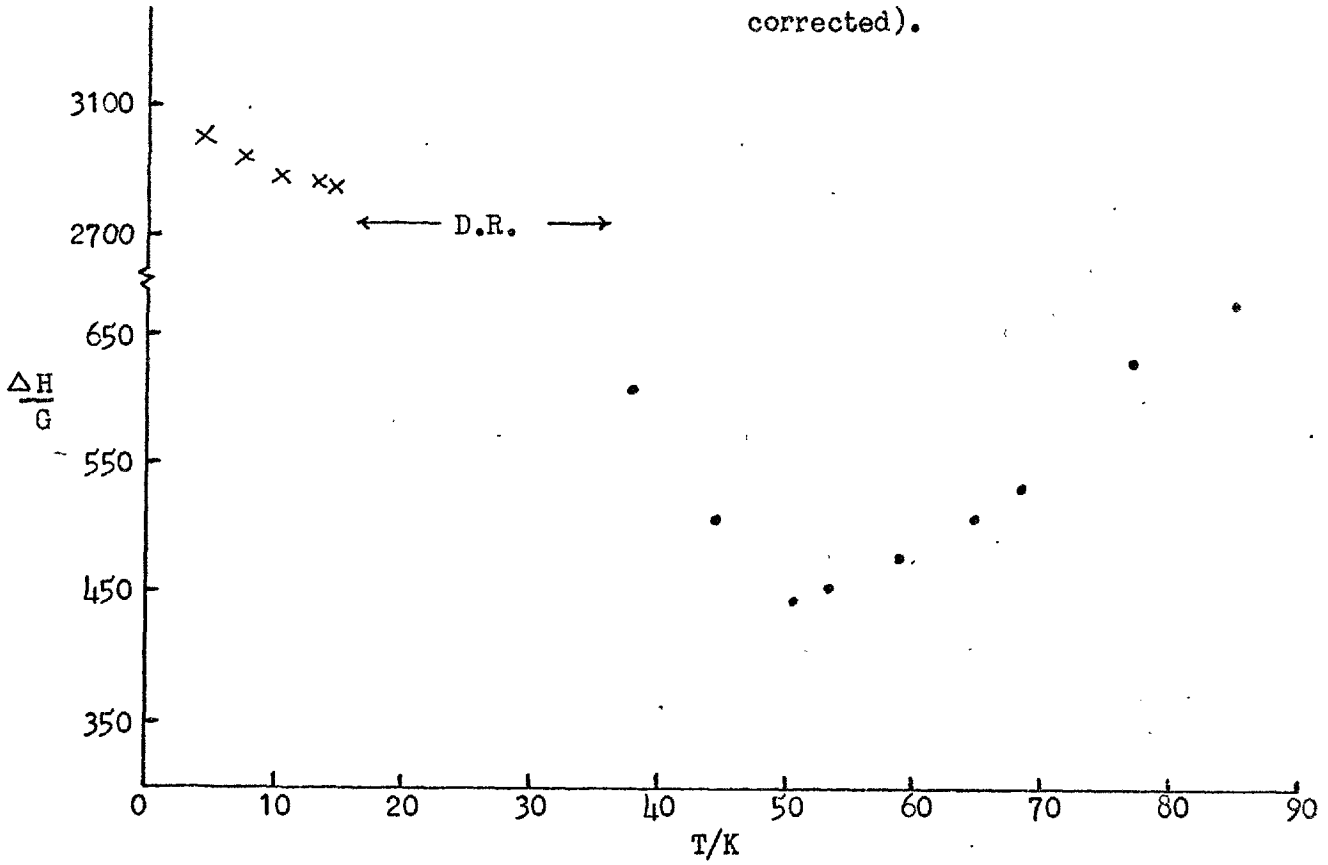

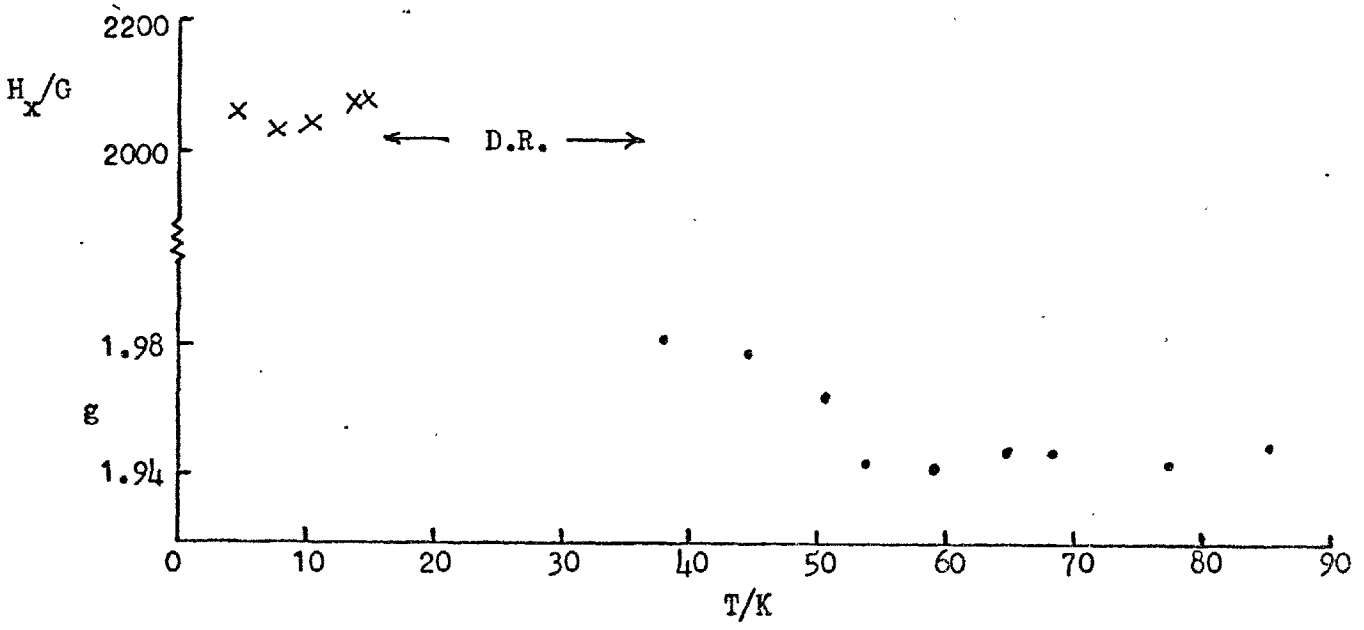

FIG. 19 $GdNi_5$

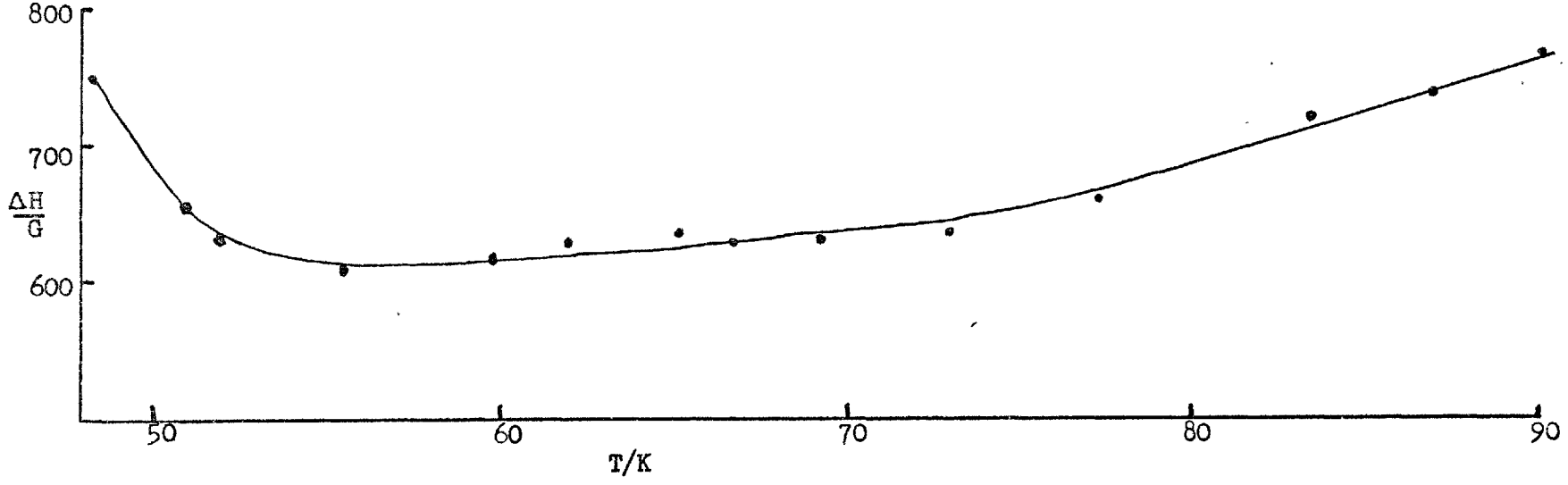

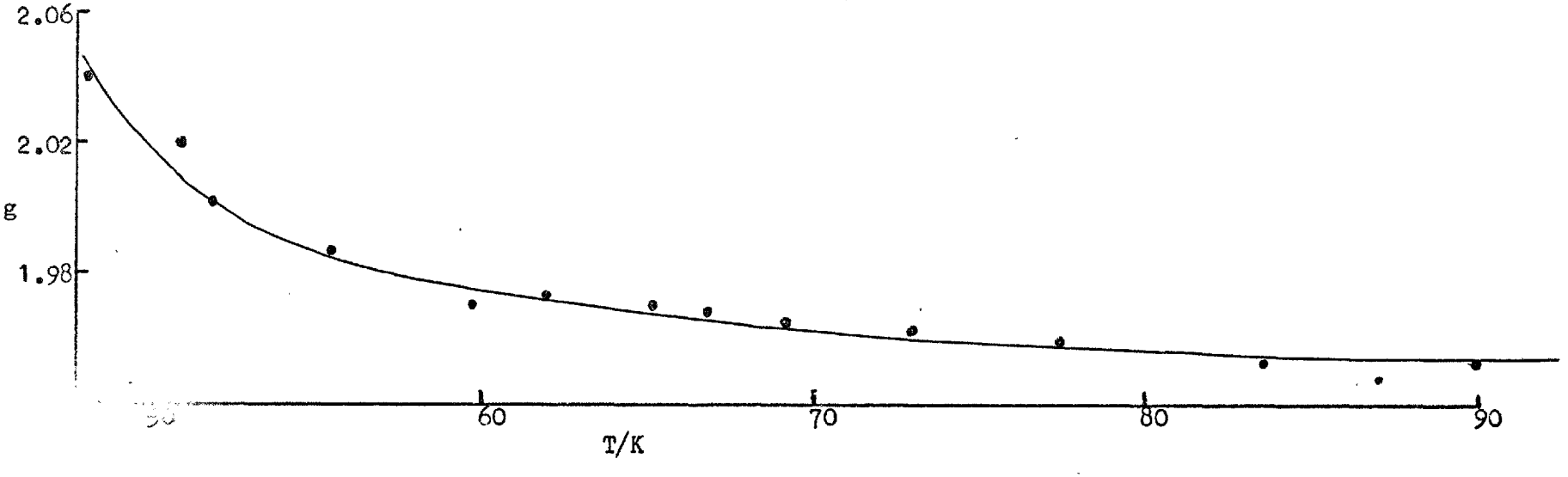

6.3 $LaNi_5$ - Gd: Resistivity and susceptibility.

To investigate the magnetic ordering in the $LaNi_5$ - Gd system in more detail resistance measurements were made on a number of samples from 9.5 at.% Gd to $GdNi_5$. The results are shown in Figs. 20 to 28. The absolute resistivity could not be measured (see ch. 5), therefore the resistivity scale is in arbitary units.

The low temperature resistance of $LaNi_5$ is shown in Fig.20. The curve through the points is a fit to the expression,

$$\rho = \rho_o + AT^2 + BT^5$$

where ρ_o is the residual resistance and A and B are constants having the values 1.63×10^{-1} and 5.96×10^{-6} respectively. The low temperature resistance of exchange enhanced metals has a term proportional to T^2 in addition to the usual electron-phonon scattering term ($\propto T^5$). The first observation of this type of behaviour was made by Schindler and Rice (29) who investigated the resistivity of Pd and a series of Pd-Ni alloys. The T^2 term has been attributed to the scattering of conduction electrons from spin density fluctuations (s-electron paramagnon scattering) (29) (30). The strong T^2 dependence observed in $LaNi_5$, together with the magnetic data to be presented below, suggests that this compound is exchange enhanced and similar in character to Pd.

The low concentration alloys, less than 15at.% Gd, show a minimum in the resistance at low temperatures. As the concentration increases a sharp maximum appears, the resistivity falling steeply away on the low temperature side. At the highest concentrations the maximum is still present and even persists in $GdNi_5$. In the 50, 75at.% alloys and $GdNi_5$ there is evidence for another anomaly at lower temperatures, approximately at 10, 16 and 27K respectively.

$GdNi_5$ has been shown to order ferromagnetically (24) (34). In

a localized ferromagnet, above the ordering temperature, there will be a spin disorder term in the resistance. Cooling through T_c will produce a reduction in the spin disorder scattering and hence a sharp change in gradient of the resistivity at T_c. This change of slope is characteristic of a ferromagnetic transition. From the data it can be seen that this type of anomaly does not occur.

Two mechanisms which can give an increase in the scattering of conduction electrons and hence a maximum in the resistance, on passing through a magnetic phase transition, are superzone boundary effects and critical scattering.

Superzone boundary effects are introduced when the exchange field below the ordering temperature has a symmetry different from that of the crystal lattice (see ch. 3). This only occurs in antiferromagnetic and helical ordered materials. The $LaNi_5$- Gd series of compounds order ferromagnetically, as will be shown later, therefore superzones cannot be formed.

A maximum can also occur in the resistance of a ferromagnet due to critical fluctuations in the magnetic order around T_c (see ch.3). This mechanism is essentially localized in a region around T_c and does not extend to temperatures much above $1.2T_c$. If the temperature of the resistance maximum is taken as T_c, then deviations from the anticipated behaviour in the high concentration alloys ($\geq$ 50at.% Gd) comes within the $1.2T_c$ limit. However, in the lower concentration compounds the minimum occurs at temperatures up to $3T_{max}$ and therefore it seems unreasonable to interpret the increase in the resistivity solely to critical scattering.

An explanation which is consistant with the susceptibility and epr data is that the increase in the resistance is due to the effects of short range magnetic order occuring at temperatures well above T_c.

At temperatures $T > T_c$ the short range order of the spins will strongly perturb the conduction electron scattering leading to an increase in the resistivity. This combined with the sharp decrease in the spin disorder scattering at T_c, due to the ferromagnetic transition, will lead to the observed anomaly.

Short range order (SRO) is common to many Gd compounds (12) (31) and a possible reason for this is the following. The Gd ions couple via the RKKY interaction (long range and oscillatory) hence the sign of the coupling between given ions depends upon their relative positions. It is therefore reasonable to expect that the ferromagnetic coupling of the nearest neighbours relative to a given spin direction at the origin may not be repeated over long distances, as it may conflict with the lattice periodicity. The free energy may therefore be minimized over an extended temperature range by the presence of SRO. This type of competing interaction mechanism for SRO was first proposed by Fisk et al (32) to explain their epr data on the Gd-B system. An example of a system with competing interactions where it is known that SRO exists well above the ordering temperature is MnO (12). In MnO the interactions present try to make all nearest neighbour couplings antiferromagnetic but this conflicts with the lattice periodicity. Neutron studies have shown that SRO is present at room temperature even though T_N = 116 K(33).

The above explanation in terms of SRO is consistent with the susceptibility results which show deviations from Curie-Weiss behaviour at temperatures well above T_c. The temperature of the resistance minimum is taken as a rough measure of the onset of SRO in the system. The results are summarized in table 3.

The ordering temperature obtained for $GdNi_5$ by resistance measurements is higher than previously reported. Nesbitt et al (24) and Burzo and Ursu (34) found T_c = 28 K and θ = 31 K from bulk magnetization

TABLE 3 The temperature of the maximum and minimum in the resistivity of $(La_{1-x}Gd_x)Ni_5$.

X	Temperature (K)	
	max.	min.
0.12	--	9
0.16	3	9
0.20	5.5	10.5
0.30	9.5	14.5
0.50	16.0	20.5
0.75	25.0	28.0
$GdNi_5$	32.0	34.0

measurements. Heat capacity work previously mentioned (26) gave two λ-type thermal anomalies at 29.8 and 30.6 K.

The magnetic susceptibility and magnetization of $GdNi_5$ has been measured by a number of authors (24) (34), who showed that this compound orders ferromagnetically. The latest work, by Burzo and Ursu (34), gave an effective magneton number for Gd of $7.94\mu_B$. To ascertain whether the compounds $(La_{1-x}Gd_x)Ni_5$ also order ferromagnetically, the susceptibility was measured for various samples across the composition range. The results are shown in Figs. 29 to 35.

The Curie-Weiss plots for all the compounds have a positive θ and show no signs of a minima, indicating the ordered phase is ferromagnetic. The spontaneous magnetization $\sigma_T(0)/\sigma_o(0)$ for $LaNi_5$ - 20at.% Gd at various temperatures was estimated by plotting the magnetization against field at a given temperature and extrapolating the linear region to the magnetization in zero field. The result is shown in Fig. 32. Graphs of σ^2 vs. H/σ (35), at various temperatures, for

the same alloy are given in Fig. 33. From the σ^2 intercepts of $H/\sigma = 0$ vs. temperature, the transition temperature was found to be 5.5 K, (T_c is the temperature at which $\sigma^2 = 0$ in Fig. 31). Both the spontaneous magnetization and the σ^2 vs. H/σ plots confirm that this alloy is a ferromagnet. The transition temperature from Fig. 33 coincides with the maximum in the resistance thereby justifying the earlier assumption that the resistance maximum was located at T_c.

The plots of $1/\chi$ vs. T show Curie-Weiss behaviour at high temperatures for all the alloys. The lines drawn through the high temperature point are such that they intersect the $1/\chi_{77}$ point. The susceptibility was measured in a field of 0.8 KG. The values of Θ are substantially higher than T_c obtained from the resistance maximum suggesting the presence of short range order. An indication of the extended range of the SRO is given by the deviation from the Curie-Weiss behaviour.

These deviations correlate quite well with the temperature at which the minimum in the epr linewidth occurs. This is to be expected as the linewidth minimum is caused by the increasing magnetization of the sample. The linewidth minimum should be slightly higher in temperature as the measurements are carried out in fields of approximately 3 KG.

$LaNi_5$ shows a small ferromagnetic moment even at room temperature. This is attributed to small aggregates of free nickel atoms. Therefore to obtain a value for the true susceptibility of $LaNi_5$ a Honda-Owen correlation was performed (36). This correlation assumes that the apparent susceptibility χ_H is connected to the true susceptibility χ in an extremely high field by the equation

$$\chi = \chi_H - M_s/H$$

where M_s is the saturation magnetization of the ferromagnetic impurity. From a plot of χ against 1/H the value of χ_{LaNi_5} was deduced at room

temperature. The value obtained is $\chi = 5.00 \pm 0.03 \times 10^{-6}$ emu gm^{-1}. This value is slightly lower than that of Pd at room temperature which equals 5.26×10^{-6} emu gm^{-1} (37). Thus it is reasonable to expect that, to a first approximation, the exchange enhancement factor α should be similar in the two materials. Recent work by Weisman et al (53) on the NMR properties of $LaNi_{5-x}Pt_x$ also confirms that $LaNi_5$ is an exchange enhanced metal.

From the slope of $1 / (\chi_{alloy} - \chi_{LaNi_5})$ as a function of temperature for a given alloy, the effective moment (p_{eff}) per Gd ion in the paramagnetic region can be obtained. The effective moment is shown as a function of concentration in Fig.36. The magnetic moment for Gd in $GdNi_5$ is $7.94\mu_B$. This value is reached by approximately 20at.% Gd in $LaNi_5$. Below this concentration the effective moment is less than $7.94\mu_B$ indicating a polarization of the host d-band antiparallel to that of the Gd moment. The negative g-shifts obtained in the epr measurements also lead to this conclusion.

The increase of the moment per Gd ion with increasing concentration can be explained as follows. The reverse polarization induced around each Gd atom in the matrix has a certain range. As the concentration is increased overlap of the polarization clouds occurs but the polarization does not superimpose, thus the effective moment per ion increases. This behaviour of the effective moment is just that which would be expected from the high temperature g-value data (g_o vs. T, Fig.11).

6.4 Conclusion

On the basis of the work presented the $LaNi_5$- Gd system may be summarized by a magnetic phase diagram, as sketched in Fig.37. This system has a ferromagnetic phase for concentrations of Gd greater than 15at.%; below this concentration no long range order has been detected

at any temperature (down to 1.8K), but short range order (SRO) was found to be present. SRO also occurs in the compounds with a ferromagnetic phase. If the minimum in the epr linewidth is taken as an indication of the onset of short range order then there exists an extended temperature regime of SRO above the ferromagnetic phase for all concentrations including $GdNi_5$. Compounds forming with Gd ions (or generally s-state ions) seem particularly prone to develop short range order (12). This point will be expanded in the summary of the next section on spin glasses.

Below 15at.% Gd the system may condense into a spin glass ground state at low enough temperatures. To see if this is the case an 11at% Gd sample was cooled in a field of 8.5KG and the magnetization vs. field obtained at 2K. If the system has a spin glass phase then this alloy should show an isothermal remanent magnetization (39). No such effect was observed. This was not wholly unexpected as the isothermal remanent is only observed if the sample is field cooled to a temperature below the spin glass temperature. In this particular case T_{sg}, if it exists,would probably be about 4K or lower.

$LaNi_5$ has been shown to be an exchange enhanced metal with properties very similar to that of Pd. Consequently, $LaNi_5$- Gd (or Mn) may be directly compared with Pd-Gd (or Mn).

The epr properties of the two systems are similar in many ways. Pd-Gd in the dilute limit has a paramagnetic g-value of 1.77 ± 0.01 (10) therefore the g-shift is large and negative as it is in $LaNi_5$. The negative g-shift in both compounds is probably due to the d-s hybridization mechanism put forward by Coles et al (06) and described in section 6.1. Neither system is bottlenecked at any concentration due to the high density of d-states at the Fermi surface and both show the effects of magnetic ordering in the linewidth and g-value.

The paramagnetic g-value increases in Pd-Gd as a function of concentration from the dilute limit value to approximately 1.95 at 6at.% Gd (Taylor (10) fig. 7). This effect was interpreted as a consequence of the reduction in the d-band susceptibility of Pd as Gd was added, due to the filling of the Pd d-band. For $LaNi_5$- Gd, which shows the same type of g-value shift with concentration (fig. 11), band filling effects would not be expected as both La and Gd supply the same number of electrons to the Ni d-band. The explanation for $LaNi_5$ was given in terms of the d-band response saturating with increasing Gd concentration. This effect must also be present in Pd-Gd and therefore it is likely that the Pd-Gd g-shift is a combination of the two effects.

Pd-Mn and $LaNi_5$-Mn have very different epr properties. Pd-Mn is a well known system, on which epr measurements have been made by a number of authors (25) (38) (41). The system is ferromagnetic below concentrations of approximately 5at.%; above this the spin glass ordering sets in. In the paramagnetic phase the g-value is 2.15 for all concentrations studied (41). The g-shift is therefore positive and the net polarization of the Pd d-band must be parallel to that of the 3d momemt on Mn. $LaNi_5$- Mn shows no magnetic resonance absorption up to Mn concentrations of 5at.% even though resistance measurements indicate Mn bears a moment (see below). The probable reasons for the non-appearance of an epr signal will be discussed in section 6. But with regard to the comparison with Pd, in this respect $LaNi_5$ behaves more like Pt.

The similarity of $LaNi_5$ to Pd derives from the basic properties of nickel. Both Ni and Pd are in the same column of the periodic table and therefore have properties which are alike. The difference in the magnetic properties of nickel and palladium is that the former is ferromagnetic while the latter is an exchange enhanced paramagnet. There are several reasons for this difference.

Nickel has a free atom ground state configuration of (Ar) $3d^8\ 4s^2$ which contrasts with the palladium configuration of (Kr) $4d^{10}$ (the state (Kr) $4d^9\ 5s^1$ is very close to the ground state). In the metallic phase both the 4s state of Ni and the 5s state of Pd are lowered in energy relative to the d-states and the broad conduction band arising from the s-states overlaps the narrow d-band. This gives rise to 0.55 holes in the nickel d-band and 0.36 holes in the palladium d-band. The width of the palladium d-band is also greater than that of the nickel. Clearly these factors will be important in determining the magnetic state of both materials.

A major factor in deciding whether a material shows band ferromagnetism is correlations within the d-band. The susceptibility $\chi(q)$ will be greatly enhanced when correlations are present and if they are sufficiently strong, $\chi(q)$ will diverge which is indicative of ferromagnetism (see ch. 2, section 1). The correlations within the d-band are far greater in nickel than in palladium.

The addition to nickel of an element with a greater electron to atom ratio of the conduction electrons has the effect of reducing the moment per atom. This has been interpreted by the rigid band model as d-band filling by the "excess" number of s-electrons supplied by the solute (58). The classic example of this is the CuNi system. However, band filling models take little account of the reduction in correlations due to the addition of impurity atoms.

Lanthanum has an electronic structure of (Xe) $5d^1\ 6s^2$. Therefore the addition of La to Ni is likely to fill some of d-holes but exactly how many is difficult to say. It will also reduce the correlations within the d-band, so that ferromagnetism is no longer favourable and thus produce a metal which is exchange enhanced and similar to palladium.

FIG.20 $LaNi_5$

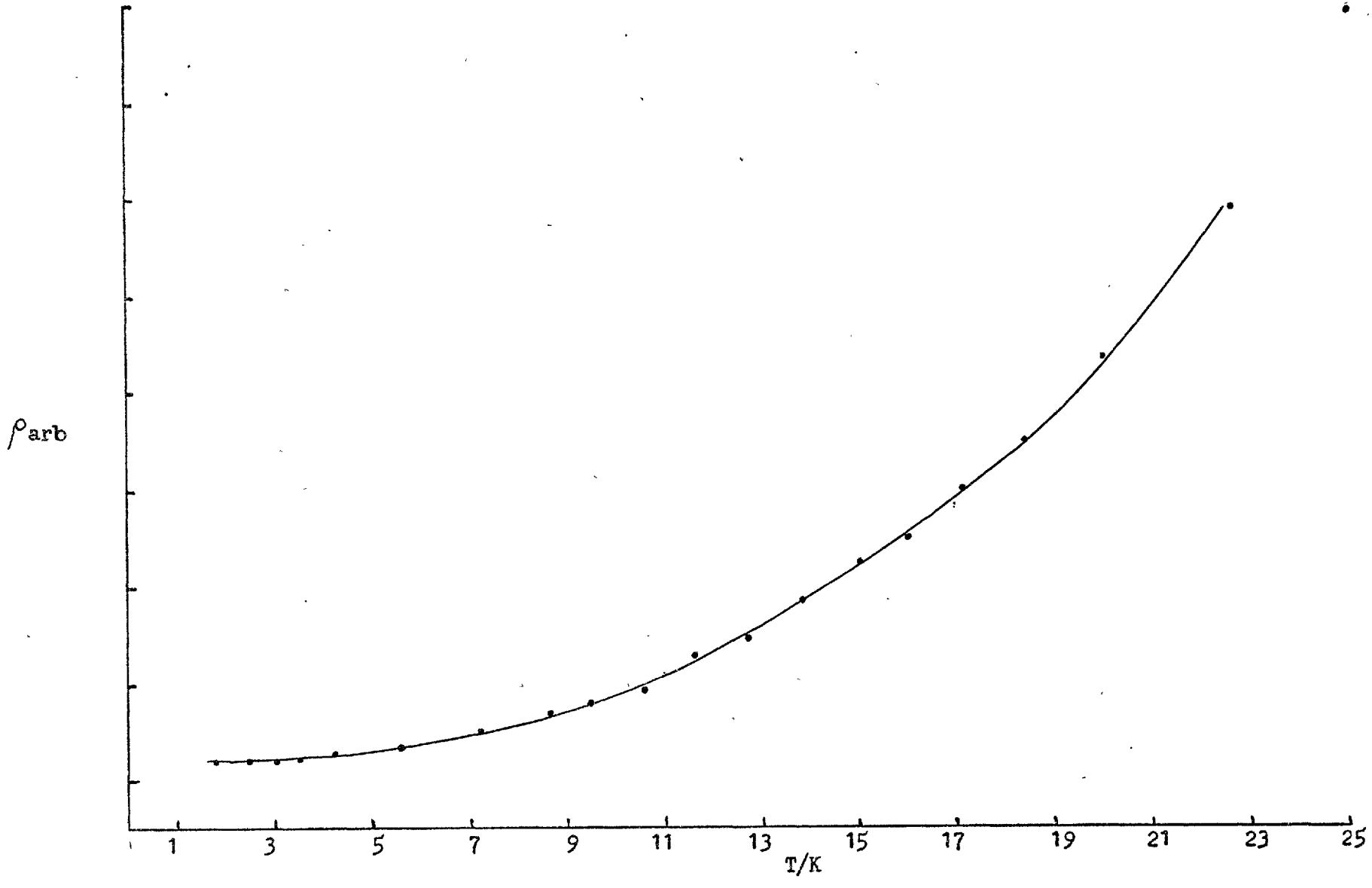

FIG. 21 $(La_{0.905}Gd_{0.095})Ni_5$

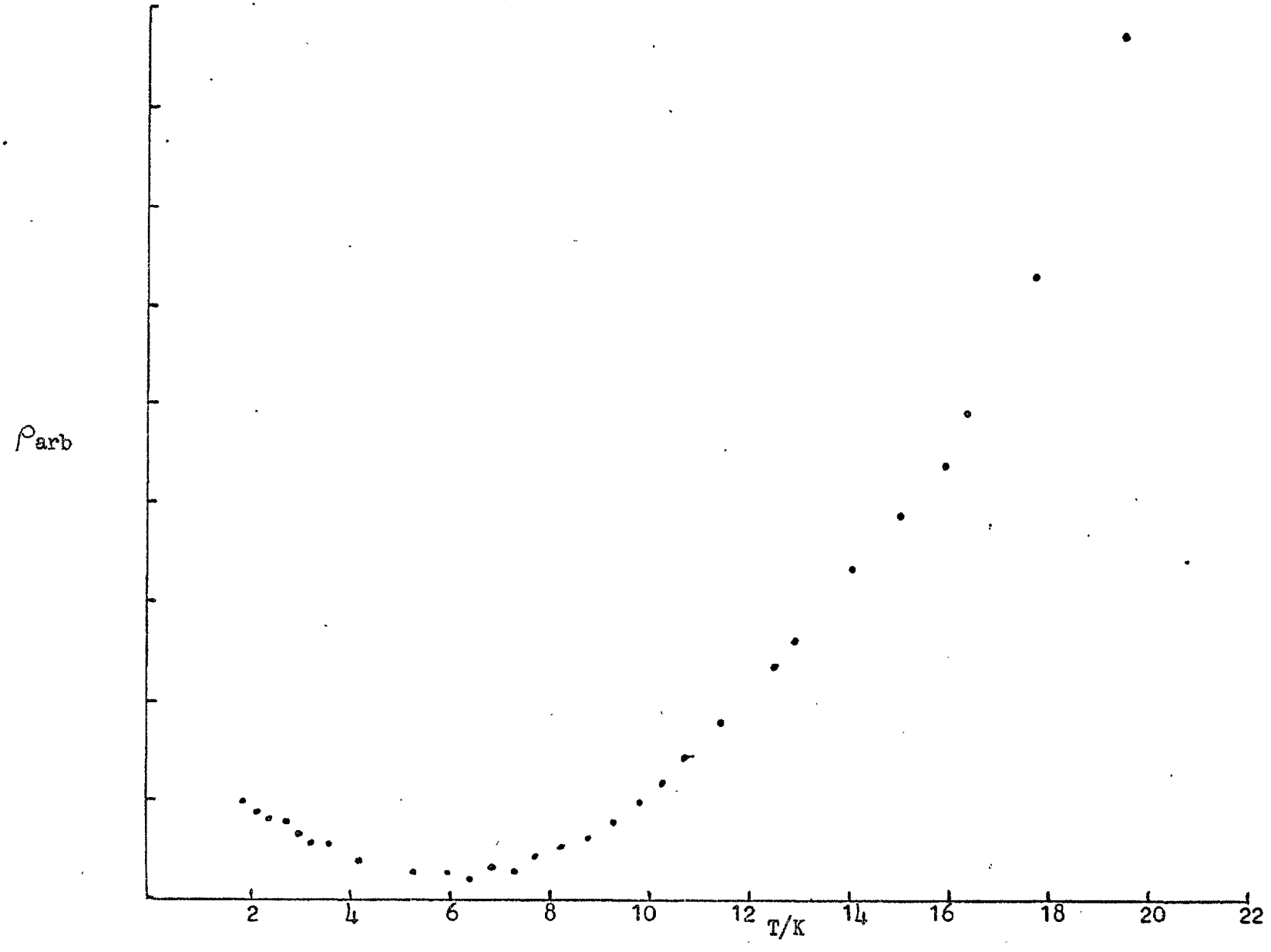

FIG.22 $(La_{0.88}Gd_{0.12})Ni_5$

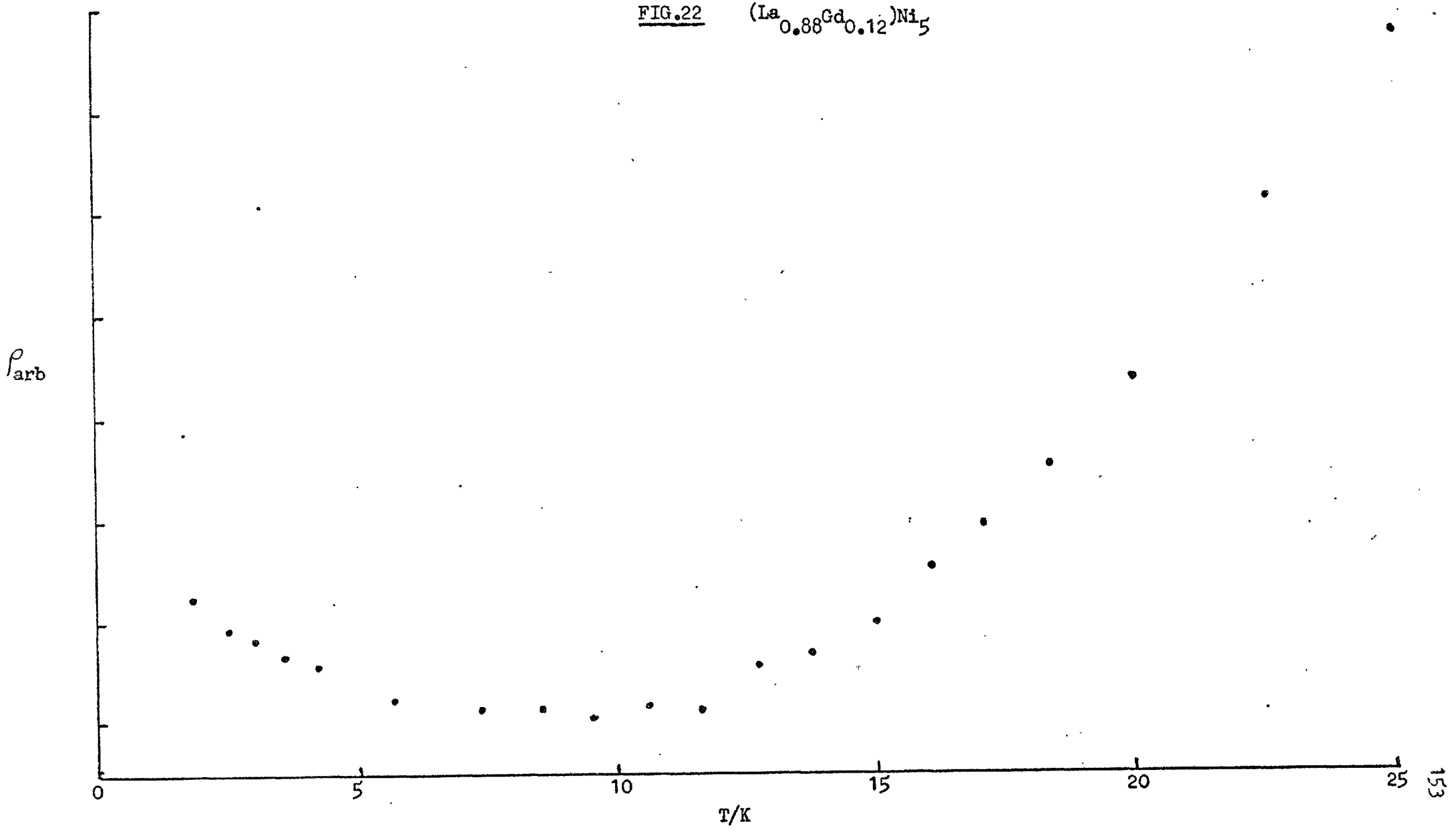

FIG.23 $(La_{0.84}Gd_{0.16})Ni_5$

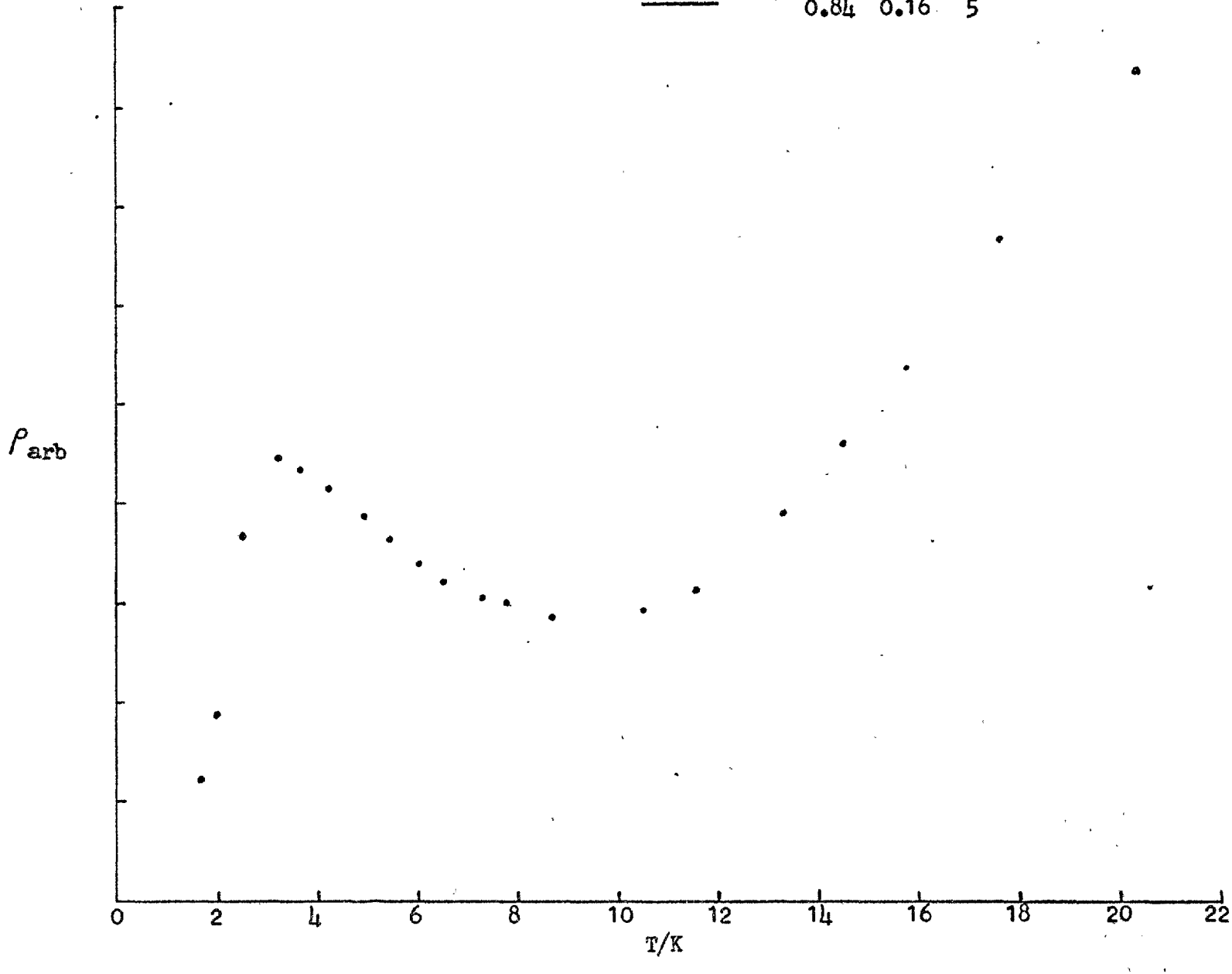

FIG.24 $(La_{0.80}Gd_{0.20})Ni_5$

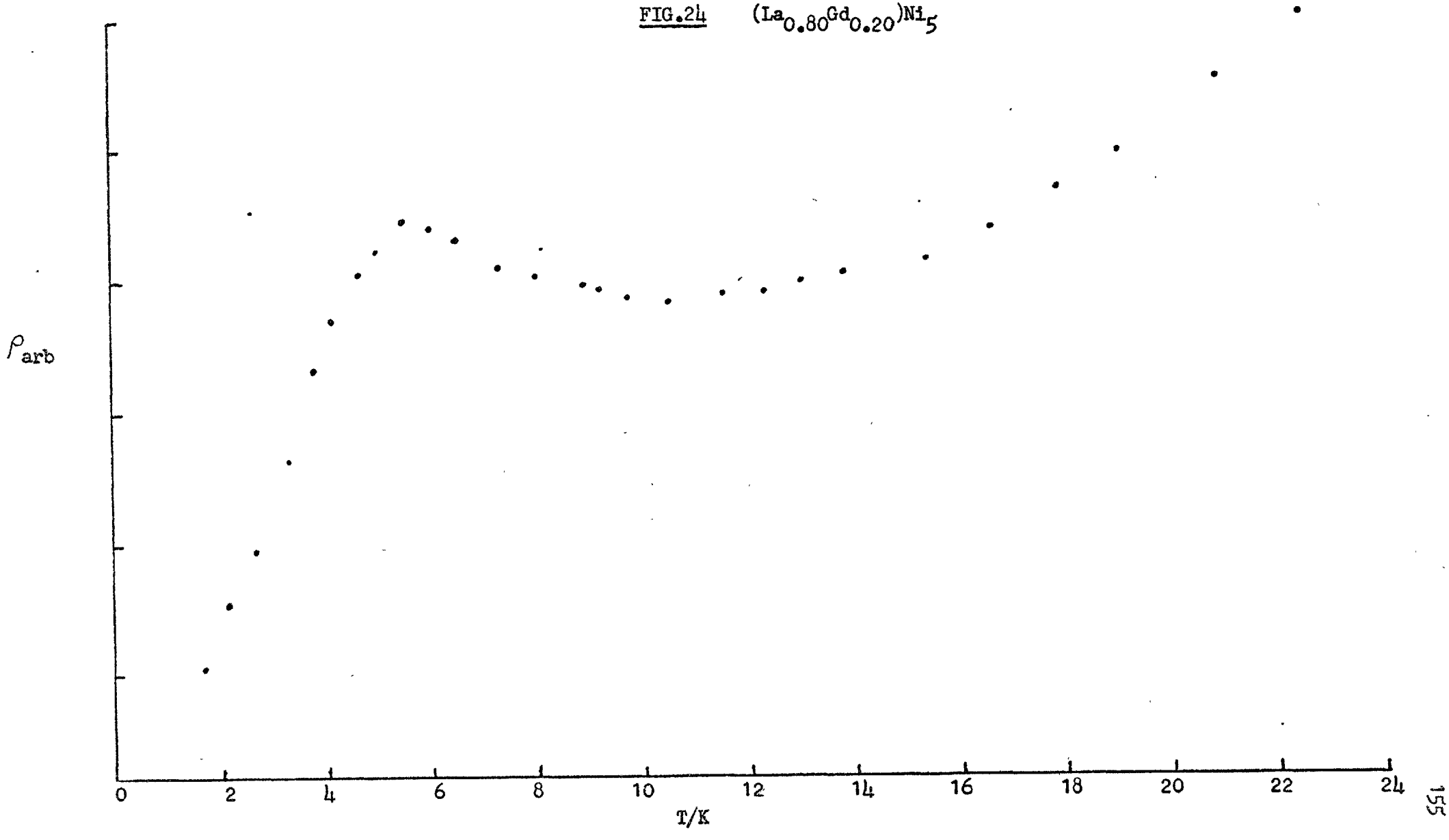

FIG.25 $(La_{0.70}Gd_{0.30})Ni_5$

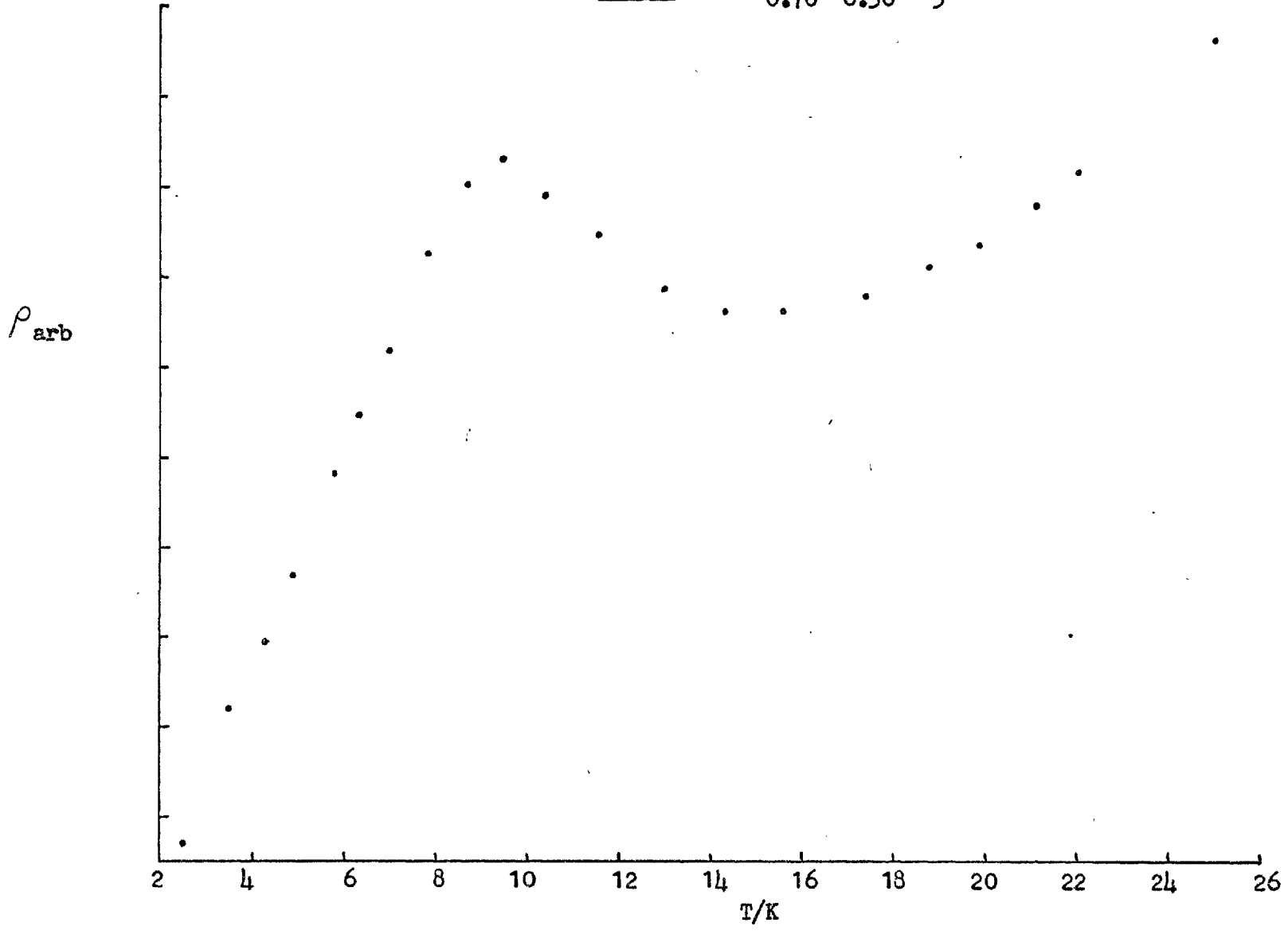

FIG.26 $(La_{0.50}Gd_{0.50})Ni_5$

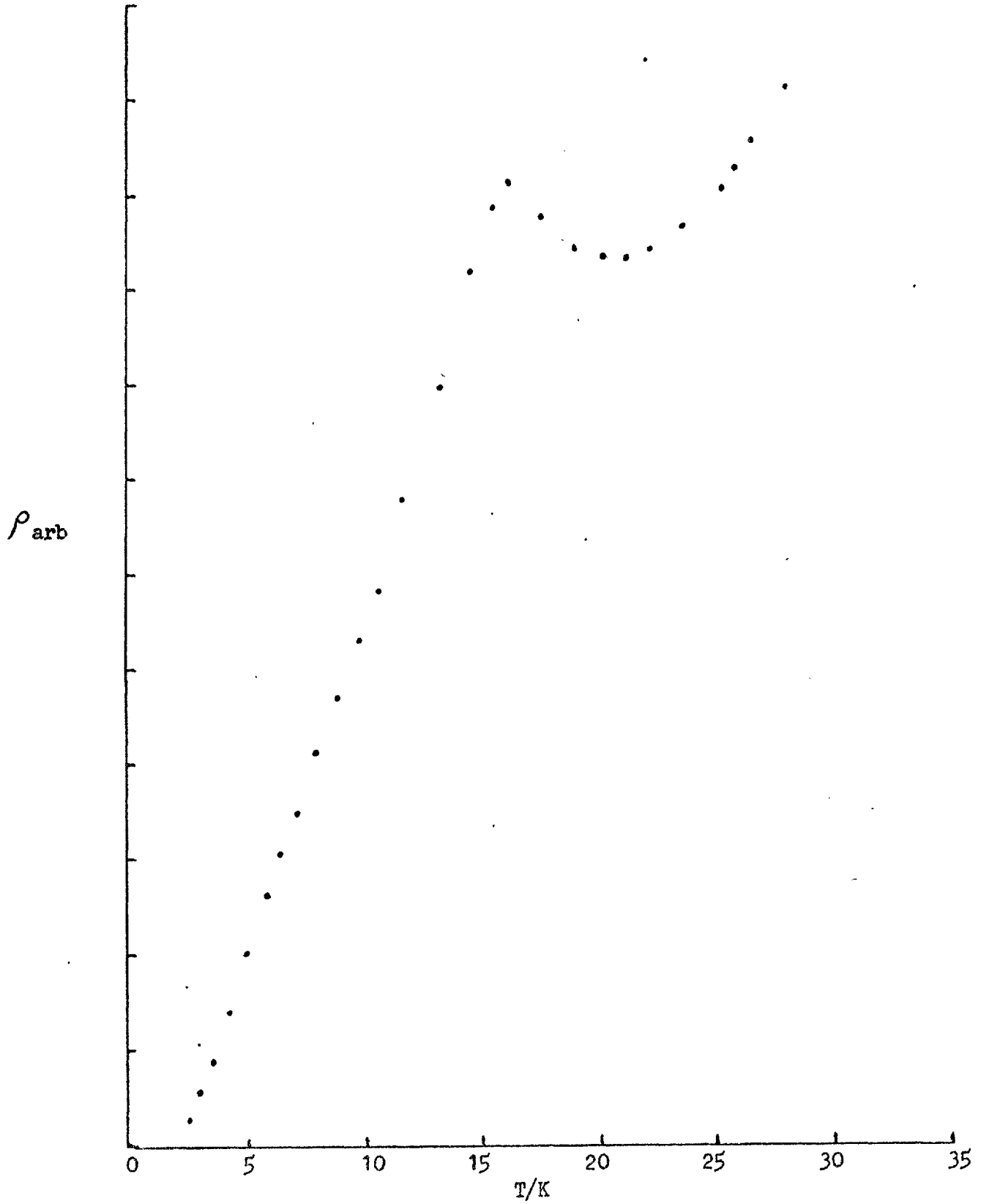

FIG.27 $(La_{0.25}Gd_{0.75})Ni_5$

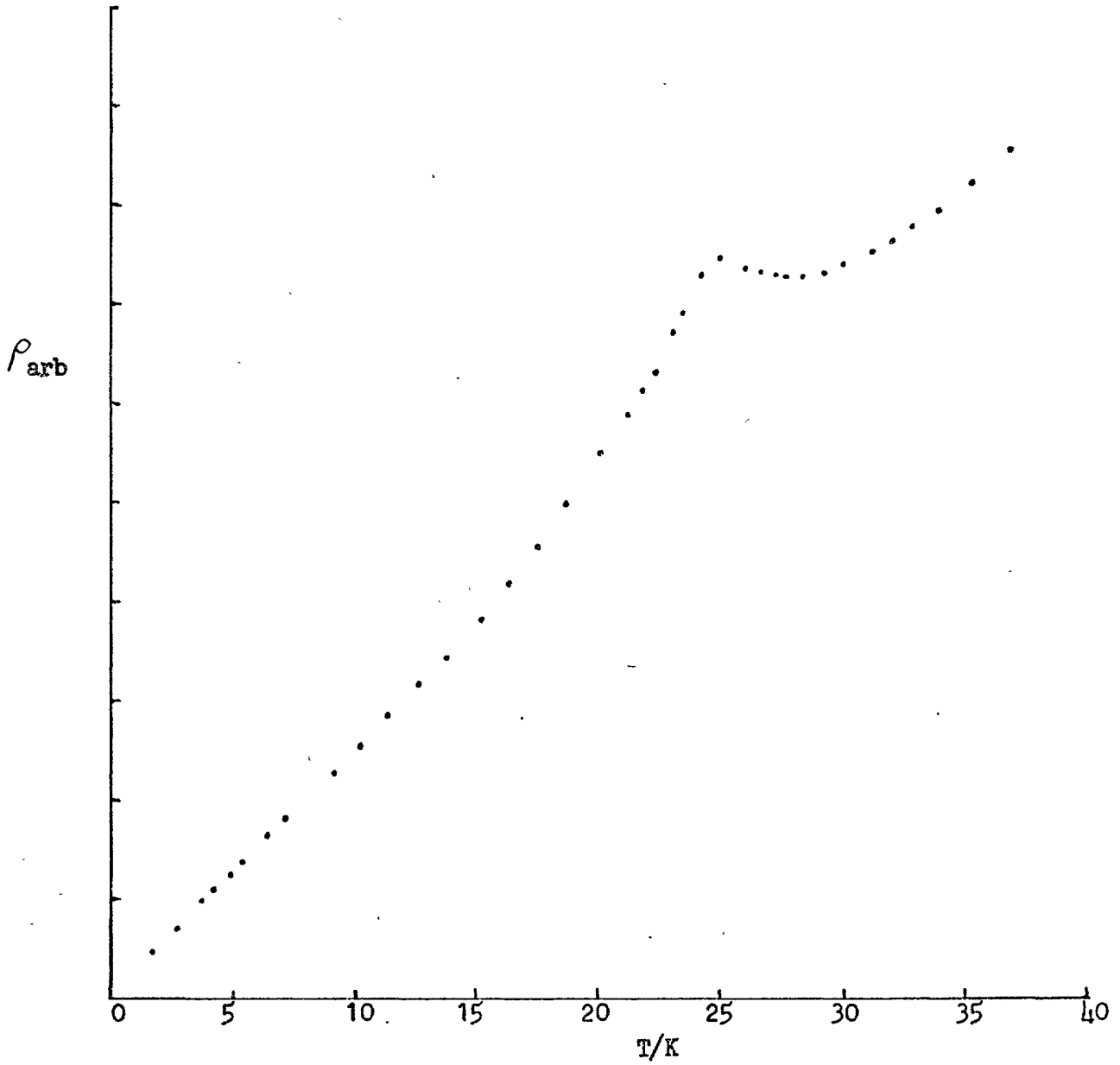

FIG.28 $GdNi_5$

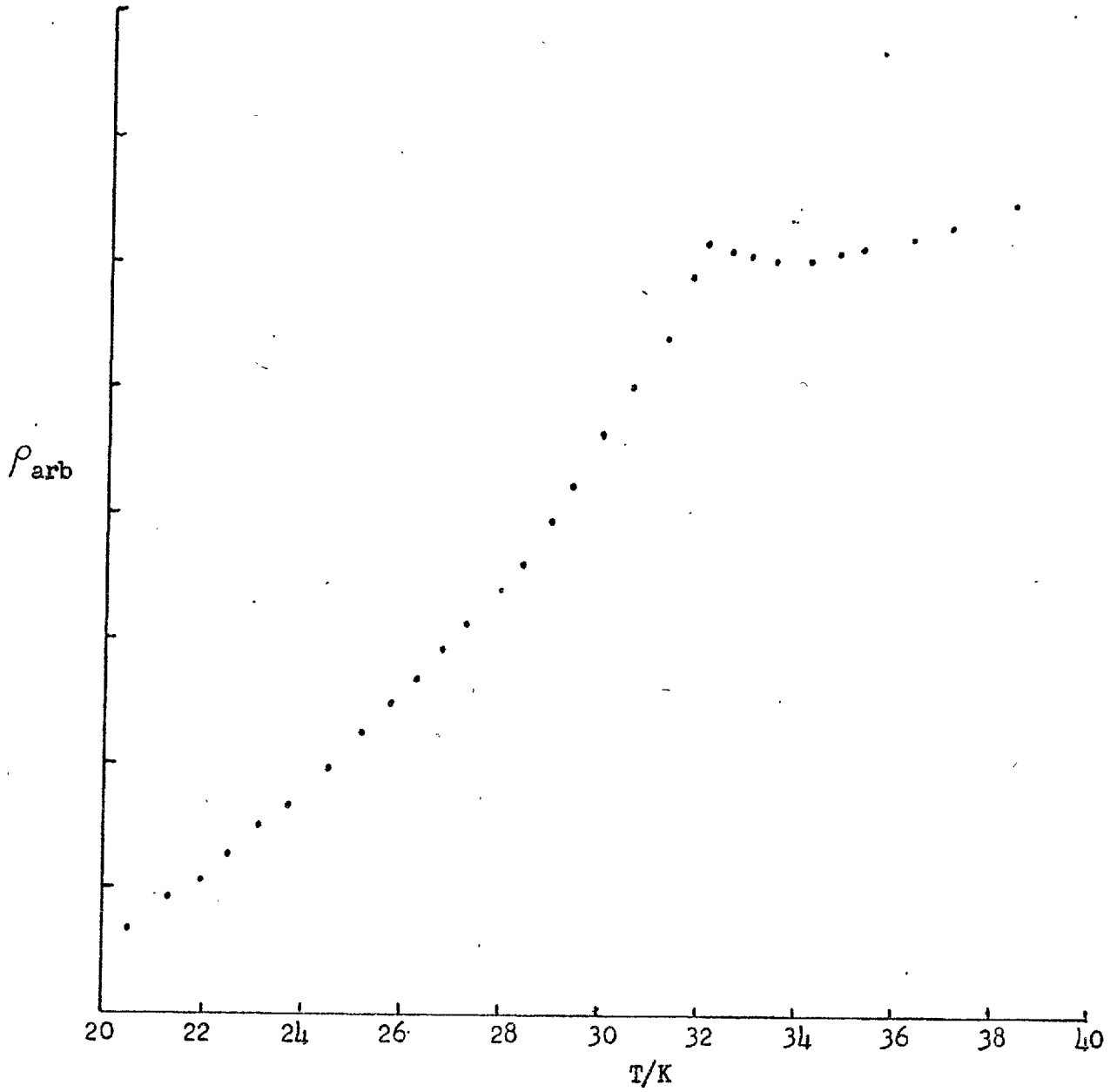

FIG. 29 $(La_{0.89}Gd_{0.11})Ni_5$

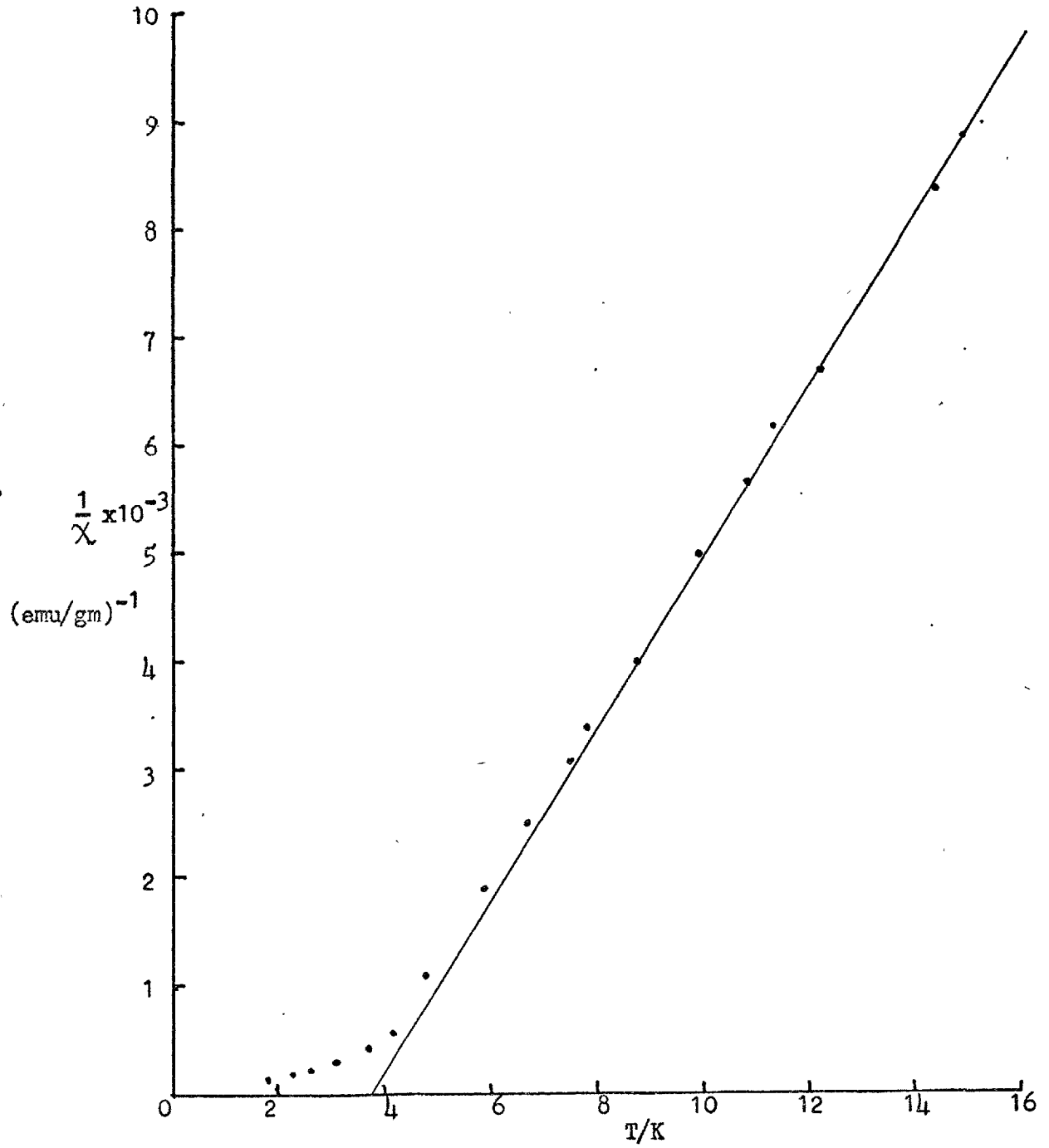

FIG. 30 $(La_{0.80}Gd_{0.20})Ni_5$

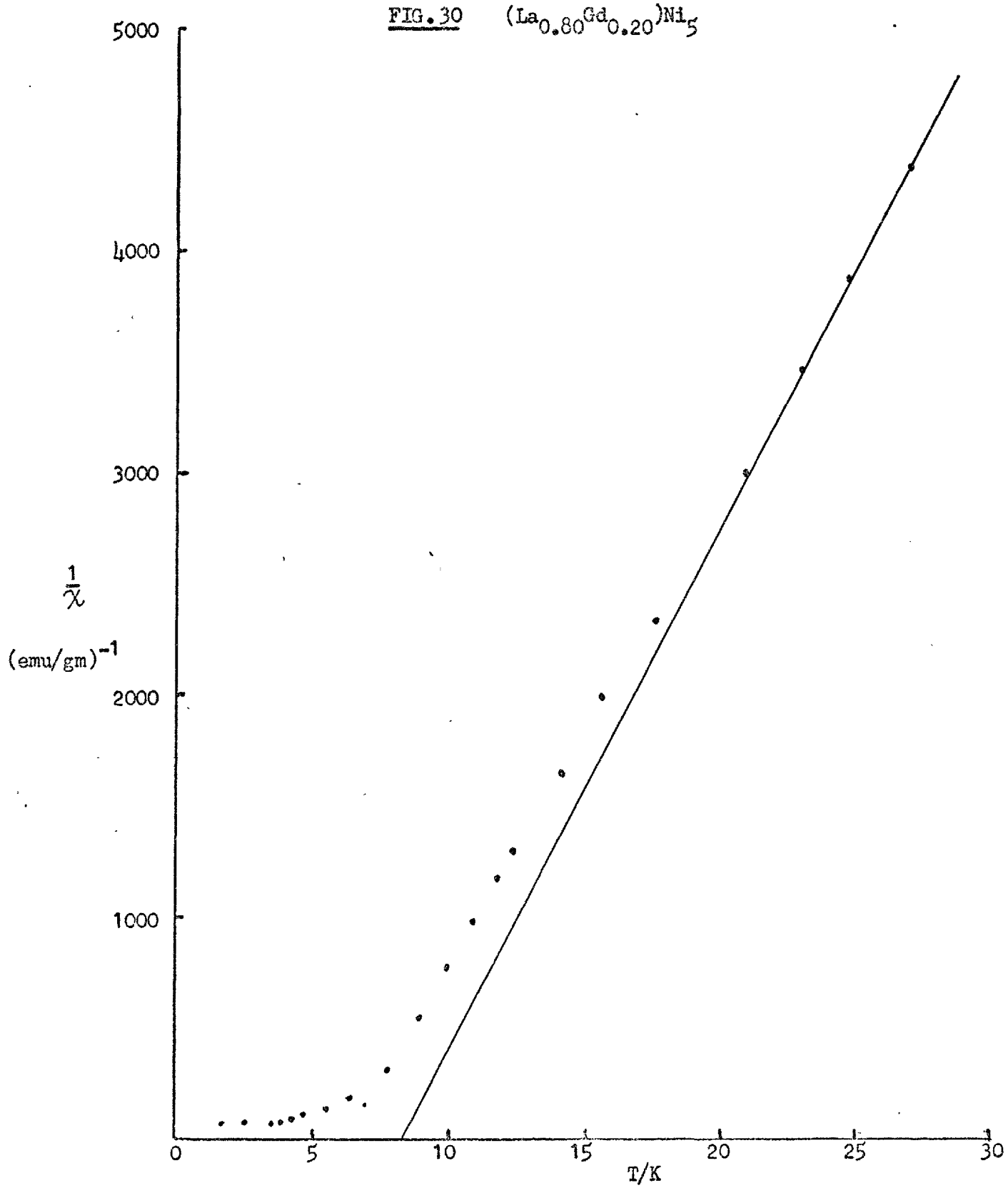

FIG. 31 $(La_{0.80}Gd_{0.20})Ni_5$

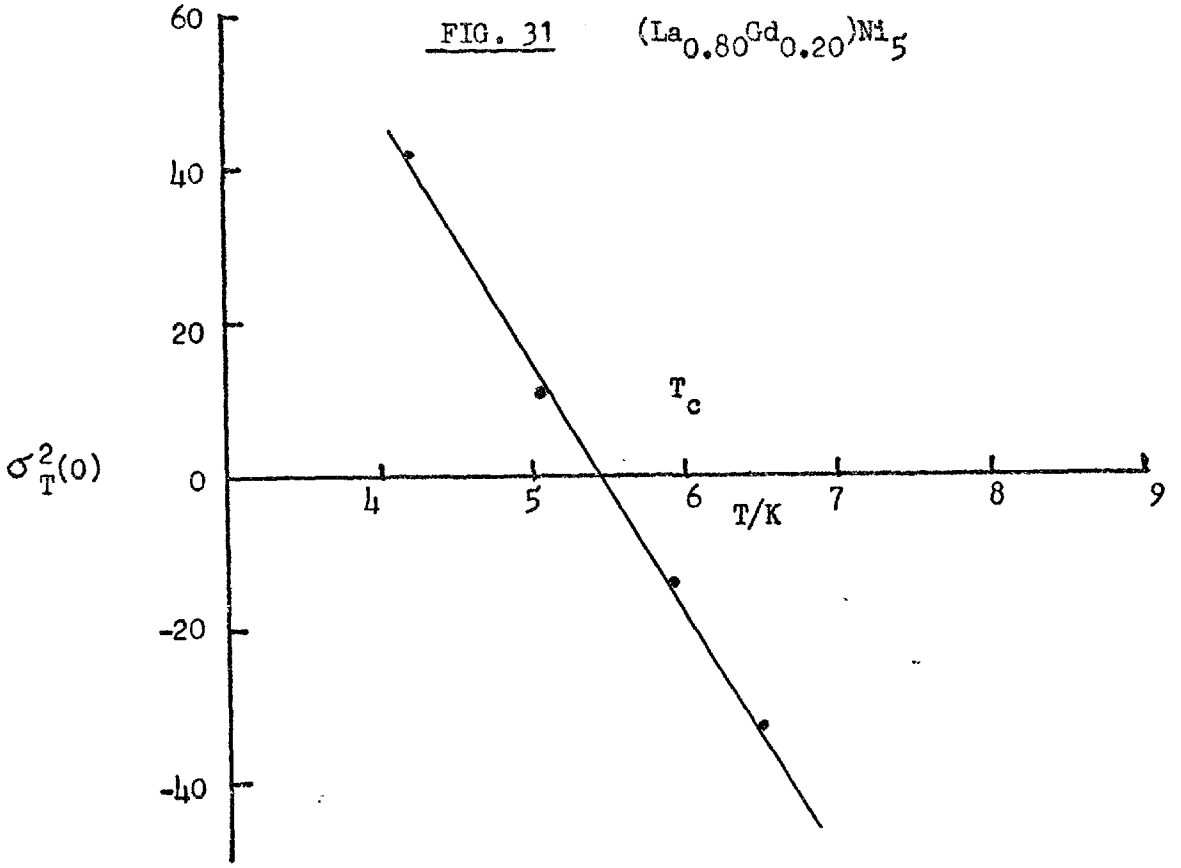

FIG. 32 Zero field magnetization for $(La_{0.80}Gd_{0.20})Ni_5$

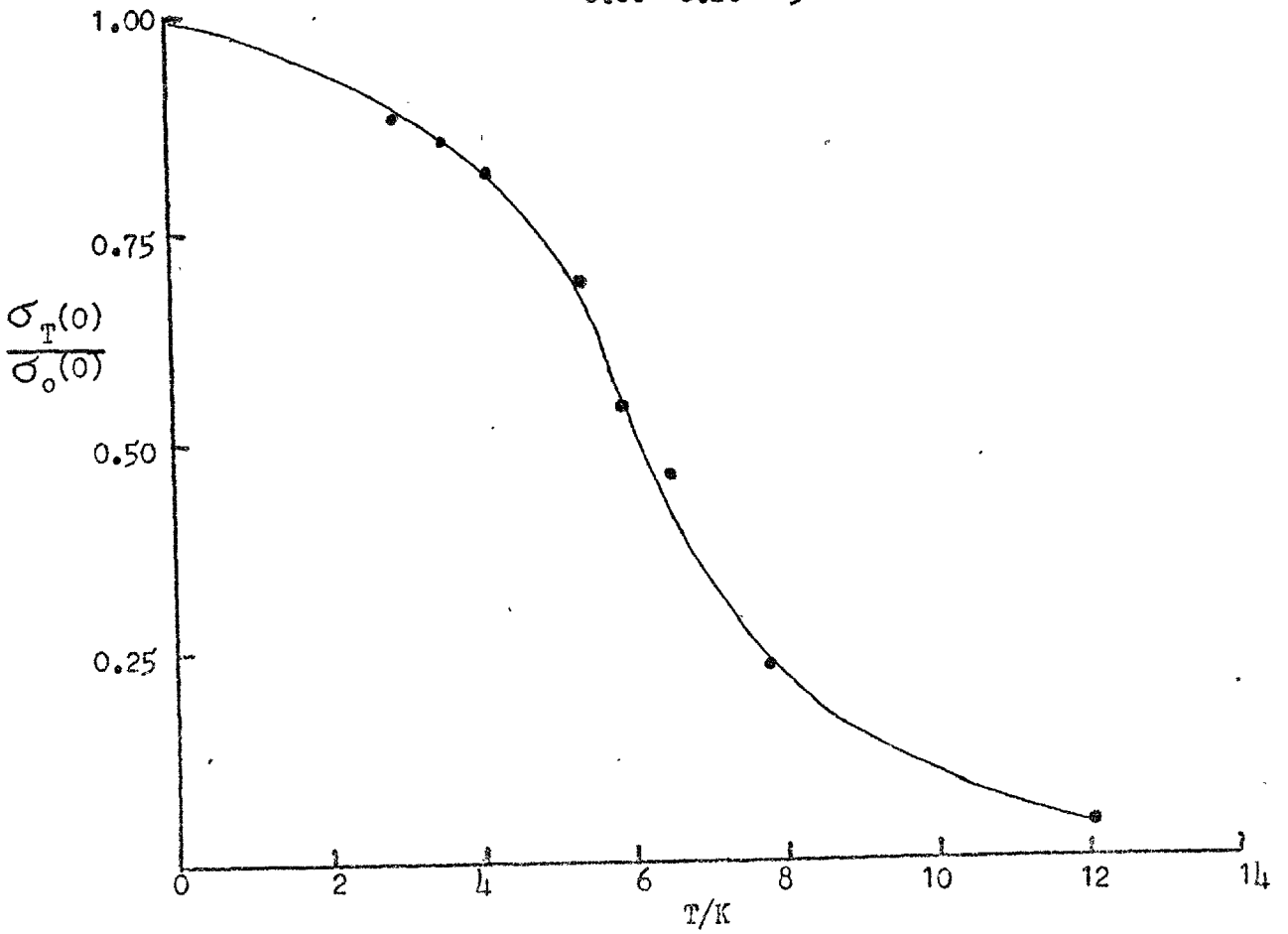

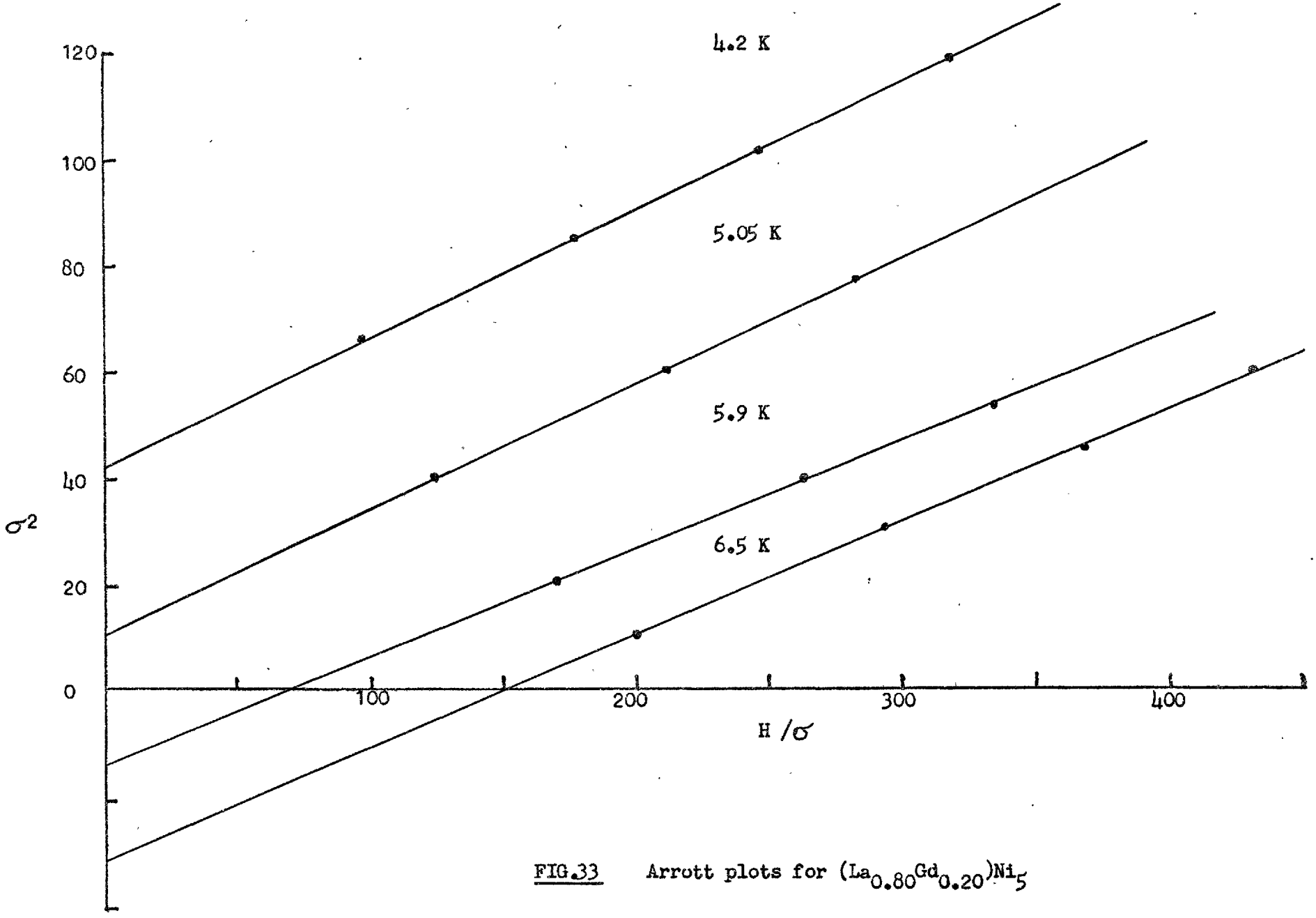

FIG.33 Arrott plots for $(La_{0.80}Gd_{0.20})Ni_5$

FIG.34 $(La_{0.70}Gd_{0.30})Ni_5$

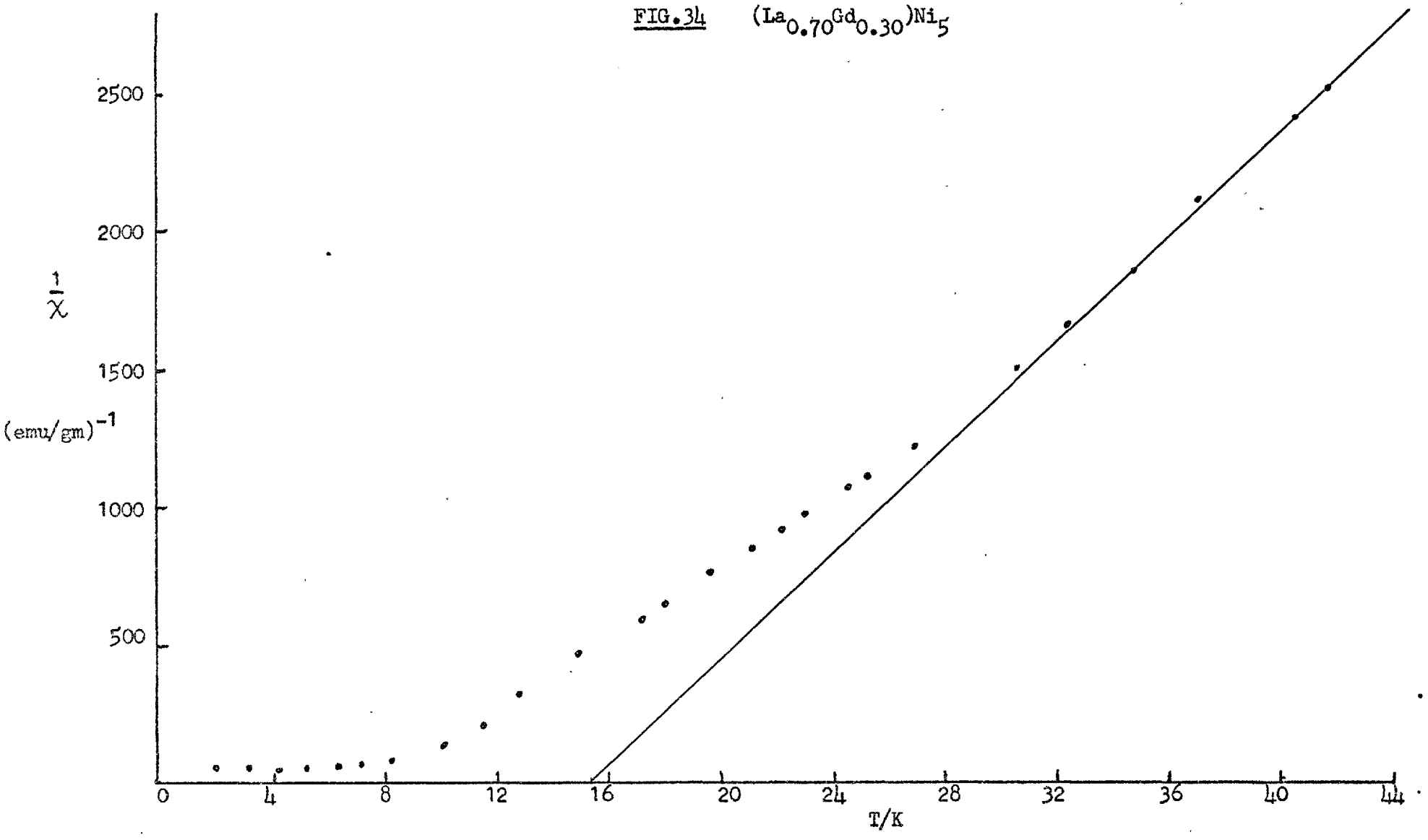

FIG.35 $(La_{0.25}Gd_{0.75})Ni_5$

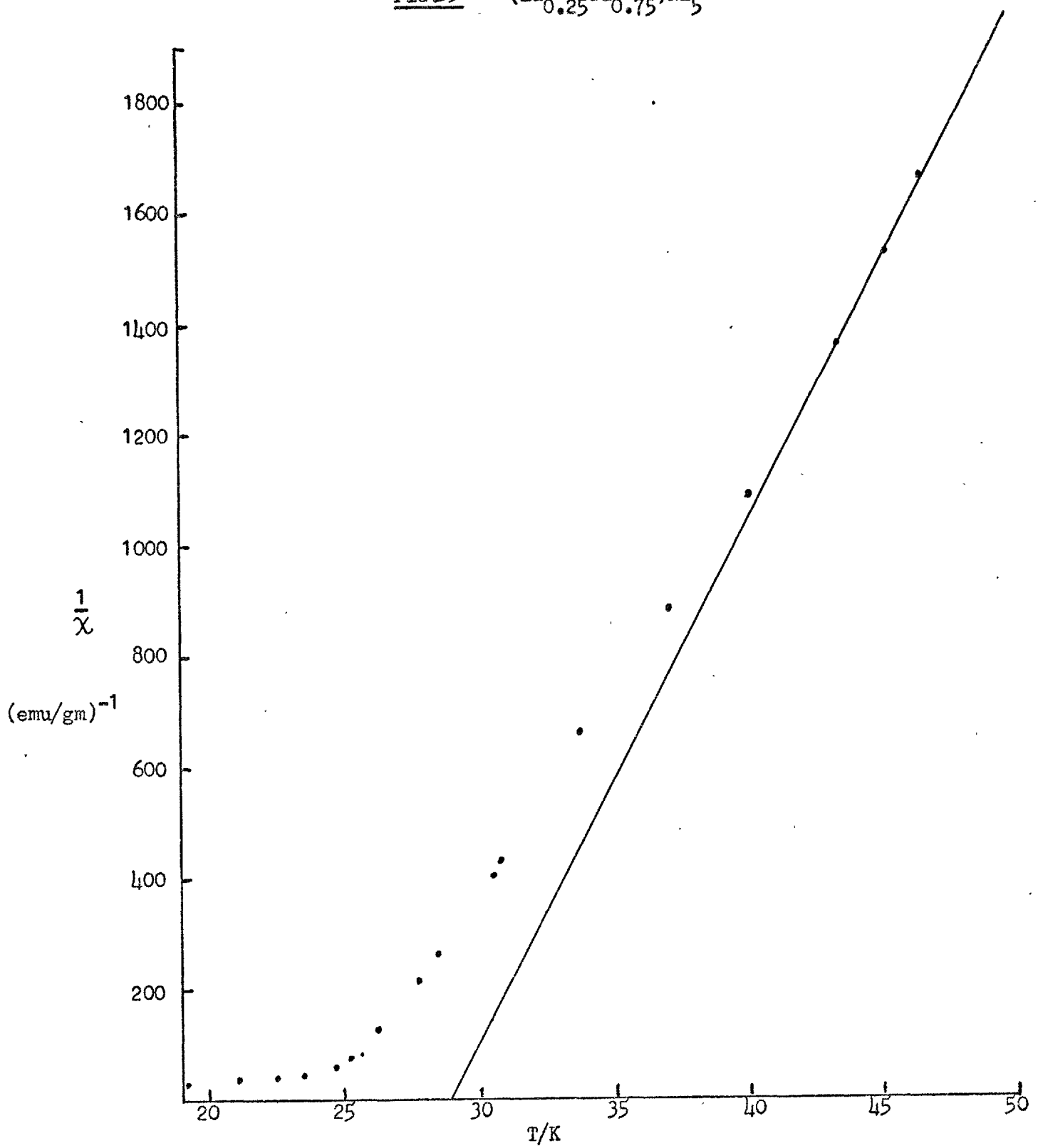

FIG. 36 The effective moment per Gd ion in $(La_{1-x}Gd_x)Ni_5$

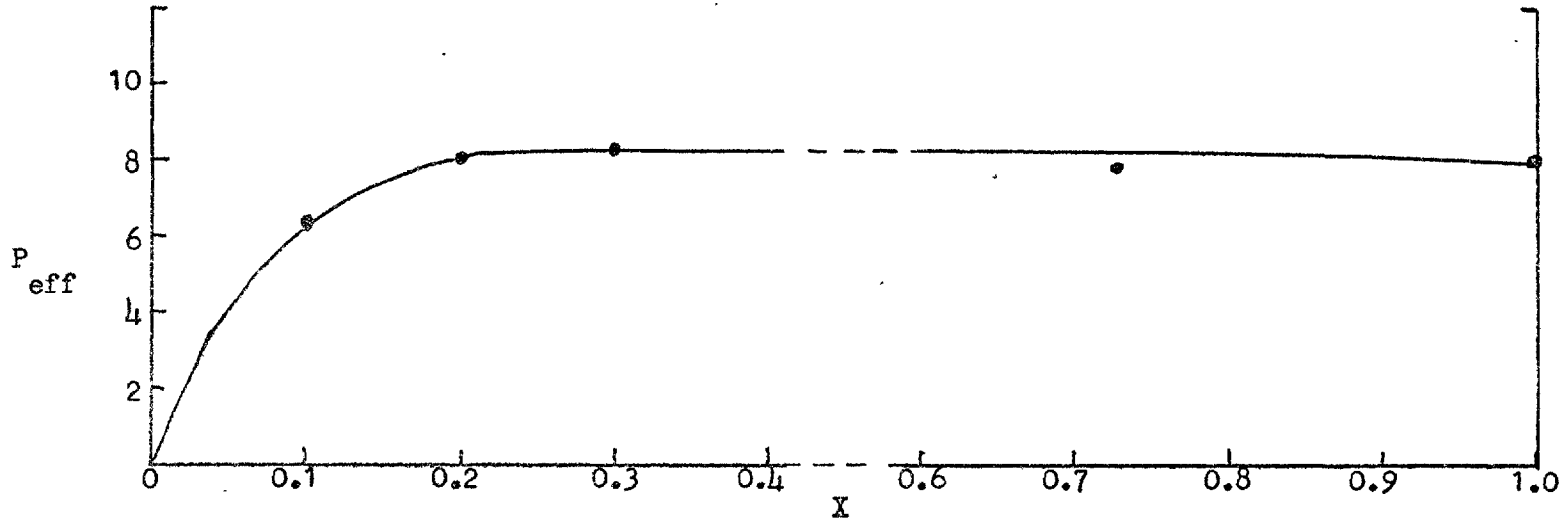

FIG. 37 Magnetic phase diagram for $(La_{1-x}Gd_x)Ni_5$

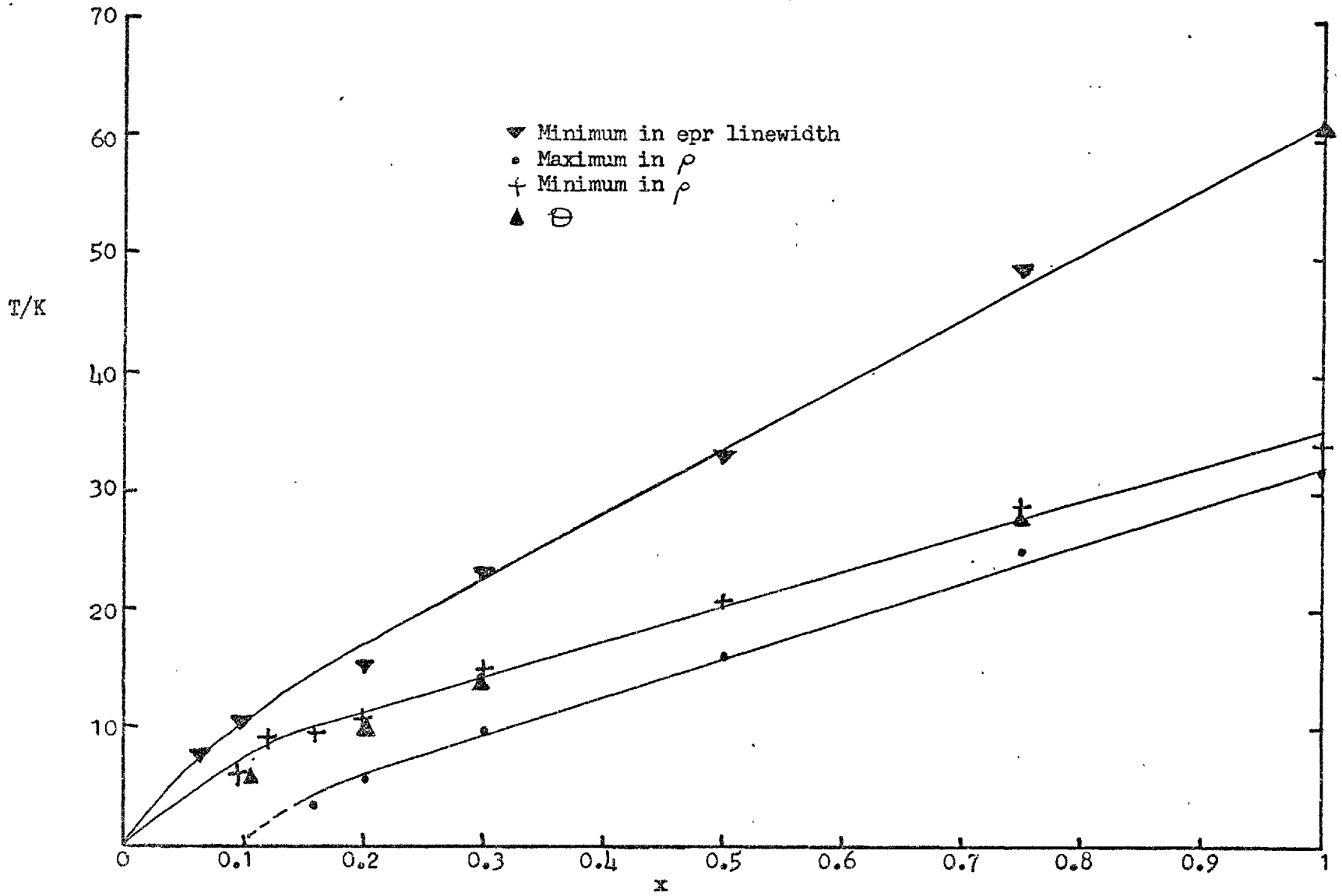

6.5 EPR in spin glasses.

(a) Y-Gd and Sc-Gd.

Recent work by B.V.B.Sarkissian (42) on the electrical resistivity and magnetic susceptibility of Y-Gd and Sc-Gd has shown that both these systems have spin glass phases. The magnetic phase diagrams from Sarkissian's work are shown in Fig.38. Above 3at.%Gd in Y and 20at.%Gd in Sc helical ordering takes place. Susceptibility investigation of alloys within the spin glass regime (Y-2%Gd and Sc-15%Gd) showed that deviations from Curie-Weiss behaviour set in at temperatures far above the ordering temperature. This was interpreted as due to the effects of short range magnetic order. Magnetic resonance experiments have been performed on the same alloys to confirm this explanation and to see if their epr behaviour is similar to other spin glass systems. The results are shown in Figs.39 and 40.

The epr line for the Y-2%Gd specimen begins to broaden and shift to lower fields on cooling at temperatures well above that of the susceptibility maximum (4.7K). The signal intensity (A + B) shows a maximum at approximately the spin glass ordering temperature. The Sc-15%Gd alloy has the same general type of behaviour but due to the extreme width of the line (1500 G) the data is not as good. In both cases these alloys resemble the 4 and 15% Cu-Mn alloys examined by Griffiths (43) and thus show typical spin glass behaviour. Field cooling experiments were not performed because of the relatively low spin glass temperature of these alloys.

The minimum in the linewidth occurs for both alloys at approximately the temperature at which helical ordering would occur if that was, in fact, the ground state. Around this temperature there are strong exchange interactions between the Gd ion which leads to a short range antiferromagnetic ordering of the spins. This short range

order produces a line broadening in the epr signal (12).

(b) $LaAl_2$- Gd.

$LaAl_2$ and $GdAl_2$ are both cubic Laves phase compounds and therefore can form a pseudobinary $(La_{1-x}Gd_x)\,Al_2$ where Gd is substituted on the La sites. A number of authors have studied the epr bottlenecking process in this intermetallic compound and in the dialuminides in general (YAl_2, $LuAl_2$ with Gd and Eu) (40) (44) (46). This system is particularly useful as the intrinsic g-shift, for the lower concentration compounds, is positive. Dynamic effects would tend to reduce the g-shift whereas ordering effects will have the opposite effect, therefore it should be possible to distinguish between the two processes.

Taylor (44) has shown that the system becomes bottlenecked as the concentration of Gd is increased. He also found no sign of dynamic effects. At the lowest concentration ($x \sim 0.0025$) a large positive g-shift was observed, $\Delta g = 0.063 \pm 0.01$, the system becoming bottlenecked as the concentration was increased. This occurs because the condition for a bottleneck is given by the inequality $\delta_{eL} \ll \delta_{ei}$, therefore it is possible to open a bottleneck by reducing δ_{ei} which is proportional to the concentration (see equation 4.27). Davidov et al (54) tried to find evidence for the existance of dynamic effects but were unable to do so.

To observe the effects of magnetic order in this system, two compounds, $LaAl_2$- 5at.% Gd and $LaAl_2$- 12at.% Gd were measured. The results are shown in Figs. 42 and 43. The g-value in the paramagnetic regime for the 5at.% sample is $1.99(4) \pm 0.01$ and for the 12at.% alloy is $1.99(0) \pm 0.01$, and the slope of the linewidths are 12.5 and $12GK^{-1}$ respectively. The g-value result for the 5at.% Gd agrees with the

previous work by Shaltiel (55). The g-value for the fully substituted $GdAl_2$ in the paramagnetic region is 1.989 ± 0.005 (45) (47); therefore the above two compounds are in the bottlenecked region. The linewidth for both the compounds has a minimum as a function of temperature and at approximately the same temperature, the g-value begins to increase.

$GdAl_2$ is a ferromagnet with a transition temperature of 170K (48) (49). To explain their epr measurements on this compound Taylor and Coles (12) used the magnetization data taken in 3KG of Hacker et al (45) to fit their g-shift results, using a demagnetization factor of approximately 2.7. Reasonable agreement with experimental points was obtained. They observed a minimum in the linewidth at approximately $1.2T_c$ and explained the subsequent broadening on the basis of a spread of demagnetization factors.

Maple (50) investigated the system using bulk magnetization measurements and found that below about 12at.% Gd the ordering temperature no longer decreased linearly with decreasing concentration. Above 12at.% Gd ferromagnetic order was observed. The magnetic phase diagram from Maples work is shown in Fig.41. The region below approximately 12at.% Gd (ABC) is probably a spin glass phase. Recent work by Bennett (51) on the electrical resistivity and low field susceptibility has confirmed that this is so. The spin glass transition temperature for an 8at.% Gd alloy was found to be approximately 2.5K.

The epr line for the 5at.% Gd specimen begins to broaden and shift at temperatures far above that of the ordering temperature from Maples work, $4T_c$. This behaviour is similar to that of other spin glass systems (see previous section). The broadening is probably due to a regime of short range order above the spin glass temperature. This seems to be a common feature of most Gd spin glass systems.

The 12at.% compound has a linewidth minimum at approximately $2T_c$. From this and the magnetization measurements this concentration seems to be on the edge of the spin glass phase field.

The negative high temperature g-shifts for both compounds indicate that the $LaAl_2$ is becoming more d-like with the addition of Gd.

The broadening of the linewidth above the spin glass temperature, observed in Y, Sc, and $LaAl_2$- Gd, is probably due to the effects of short range order. Gadolinium compounds and in general s-state ions show the effects of short range order to a greater extent than non-s-state ions. This can be seen in the resistivity and susceptibility measurements of Tb in Sc and Y where the deviations above the ordering temperature are much less than in the comparable Gd compounds (42). The mechanism described in section 3, where the couplings of the nearest neighbours cannot be repeated over long distances as this conflicts with the lattice periodicity, thereby producing conditions favourable for short range order, is consistant with the above behaviour. In materials containing non-s-state ions such effects will be reduced because of the crystal field.

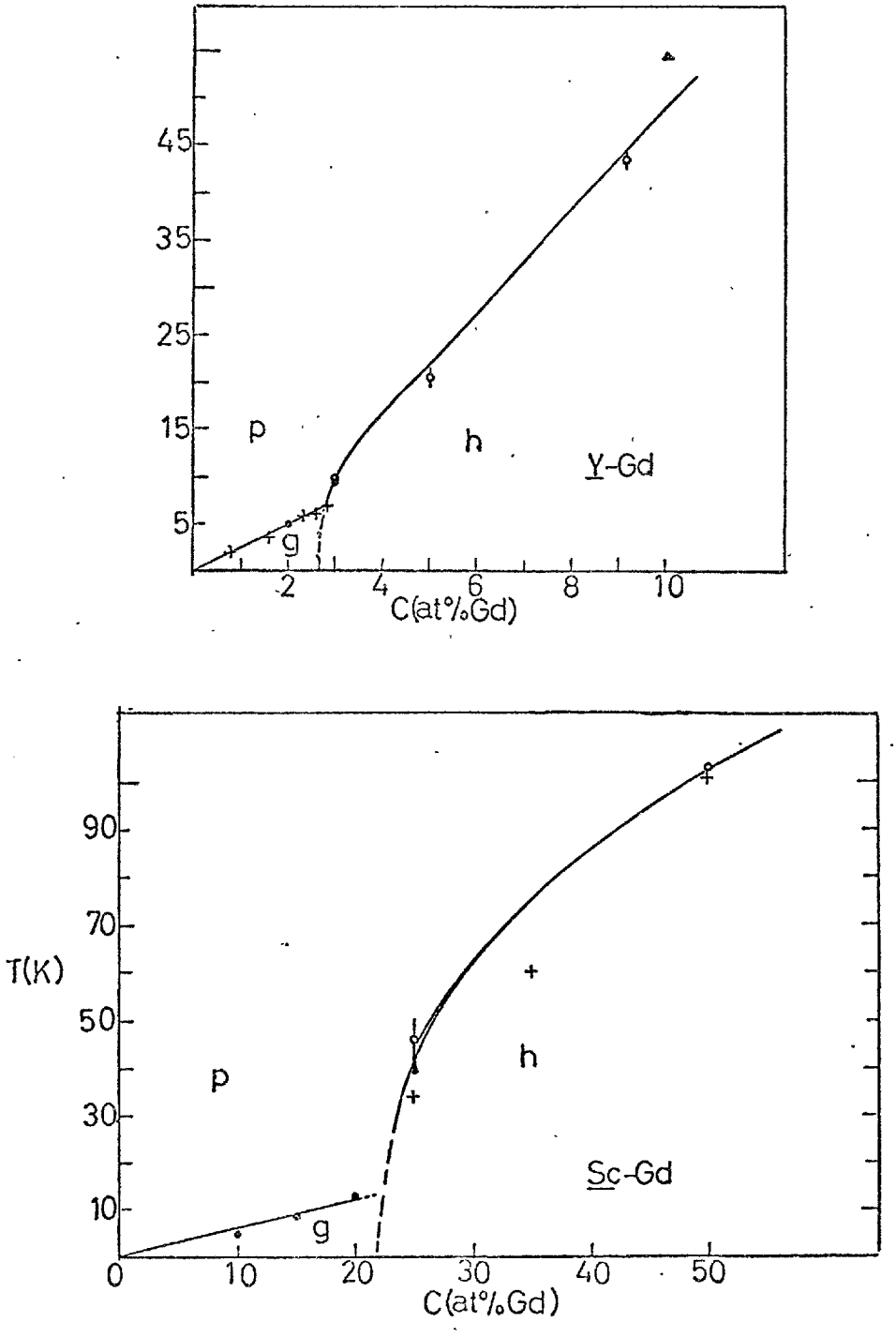

FIG. 38 Phase diagrams for Y-Gd and Sc-Gd.

FIG.39 Y-2%Gd, (A + B) is the intensity in arbitary units (+).

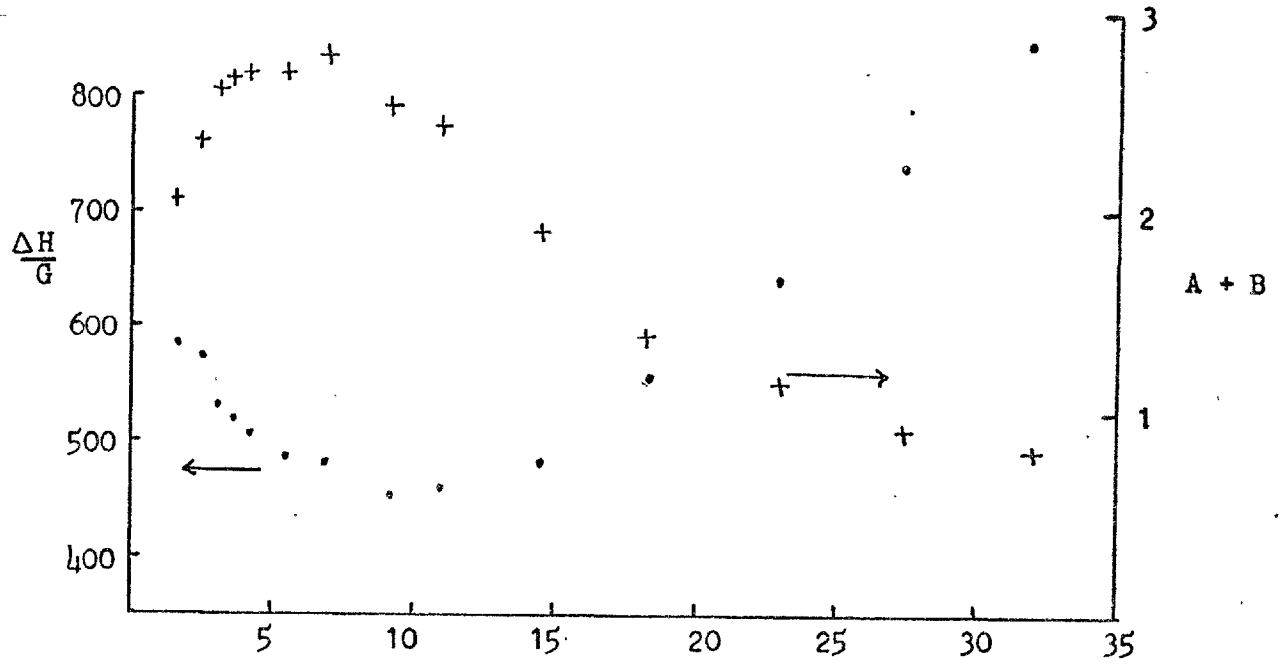

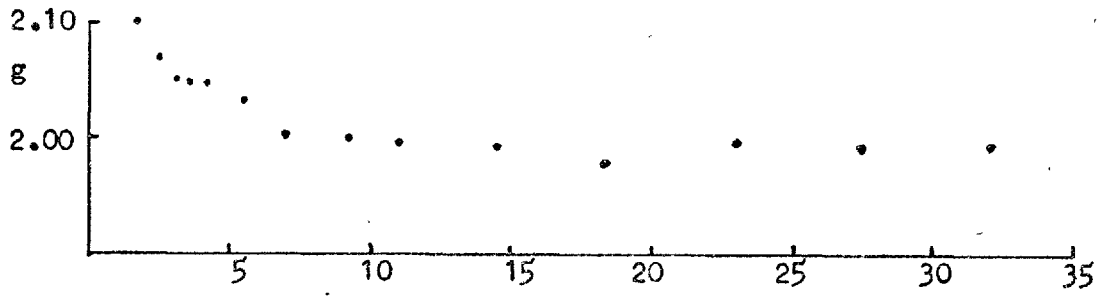

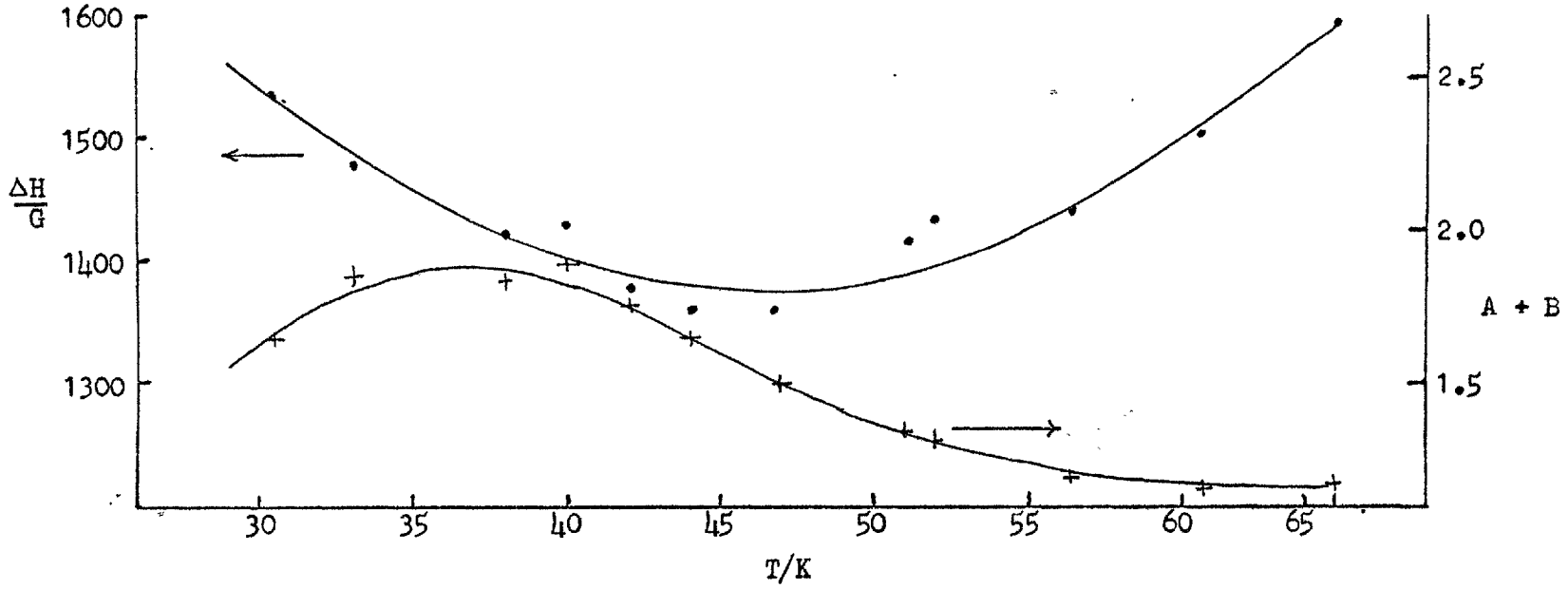

FIG.40 Sc-15%Gd, (A + B) is the intensity in arbitary units (+).

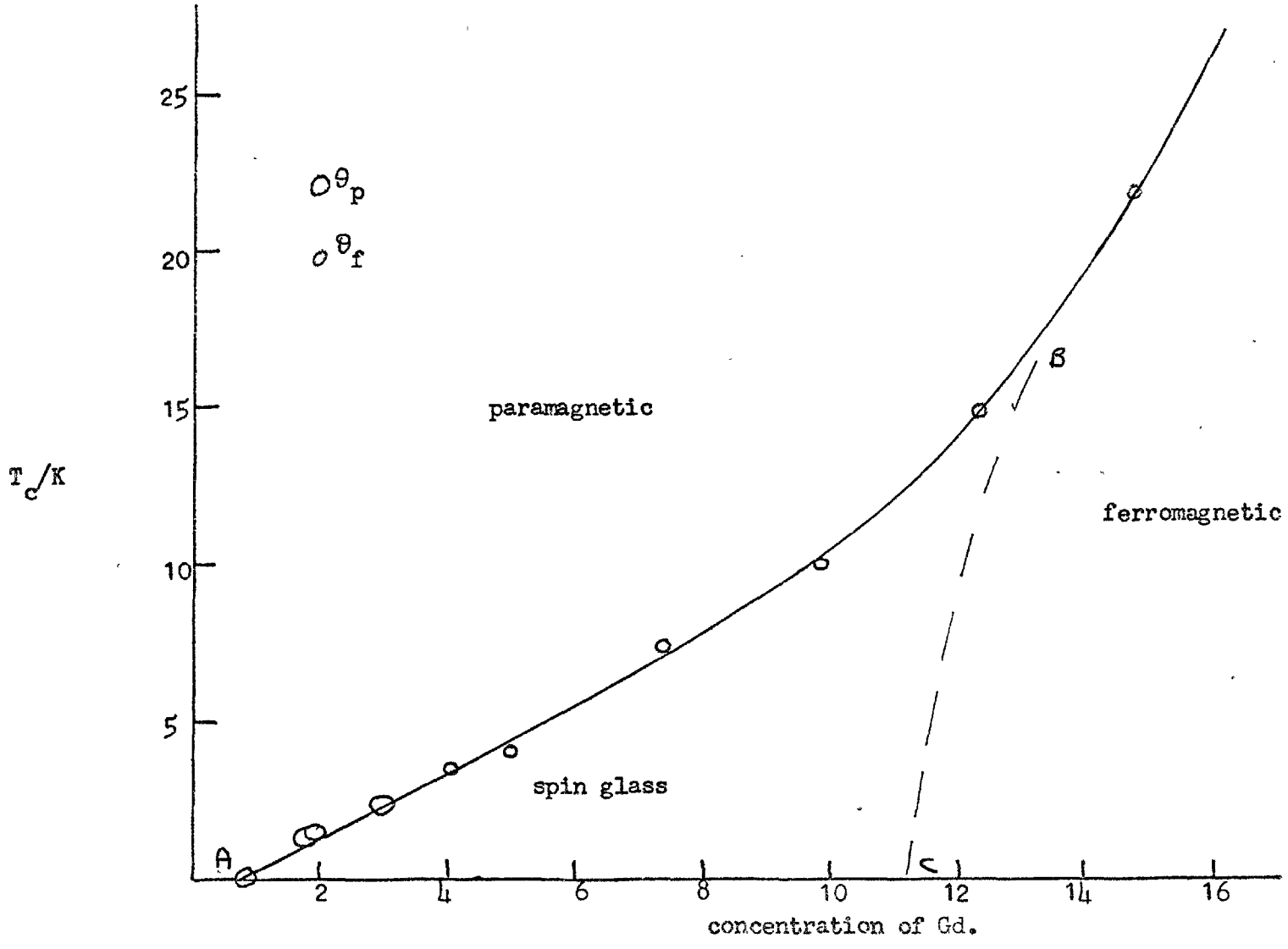

FIG. 41 The magnetic phase diagram for $LaAl_2$- Gd (after ref. 50)

FIG. 42 $LaAl_2$ - 5%Gd

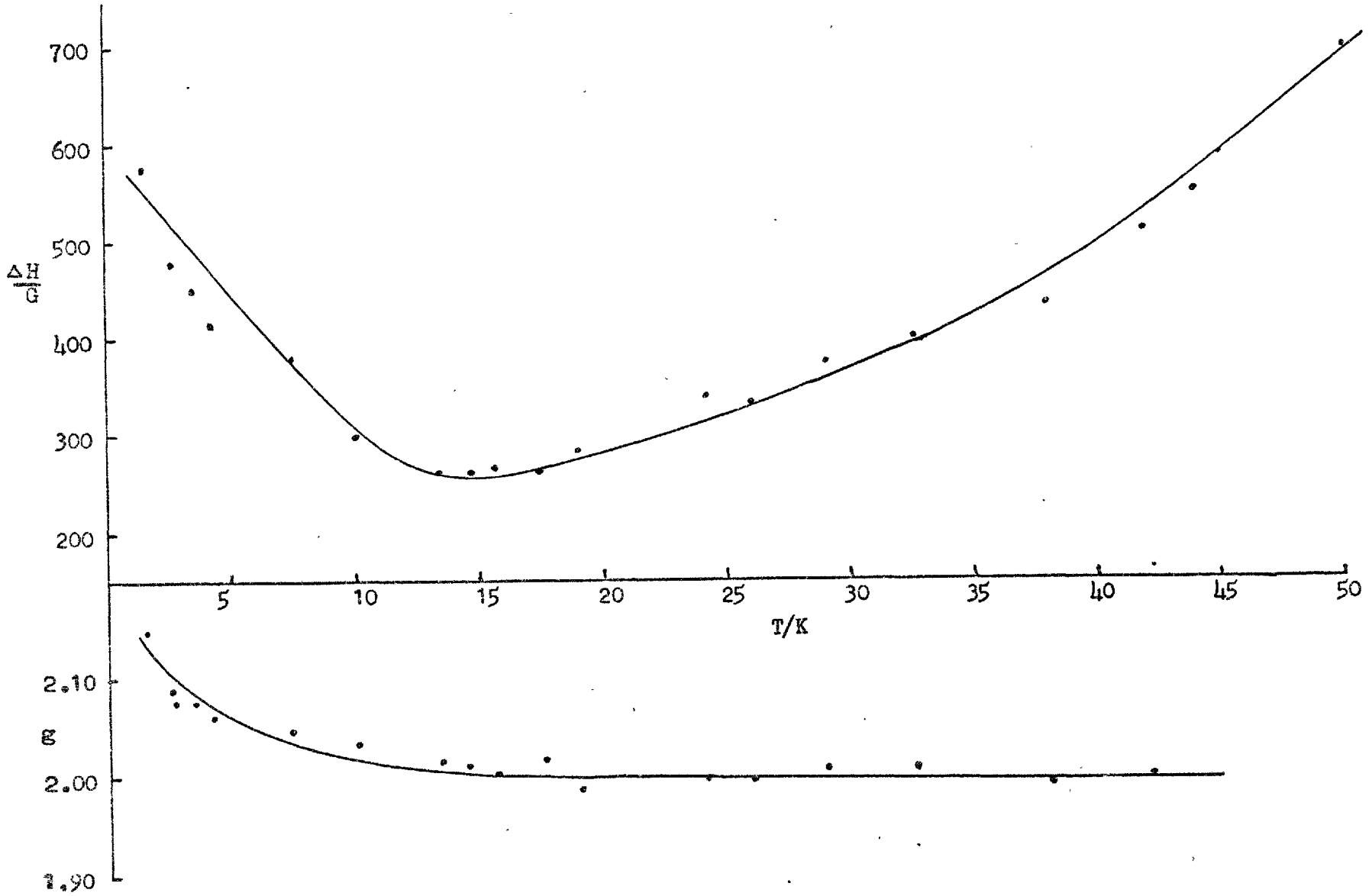

FIG.43 $LaAl_2$- 12%Gd

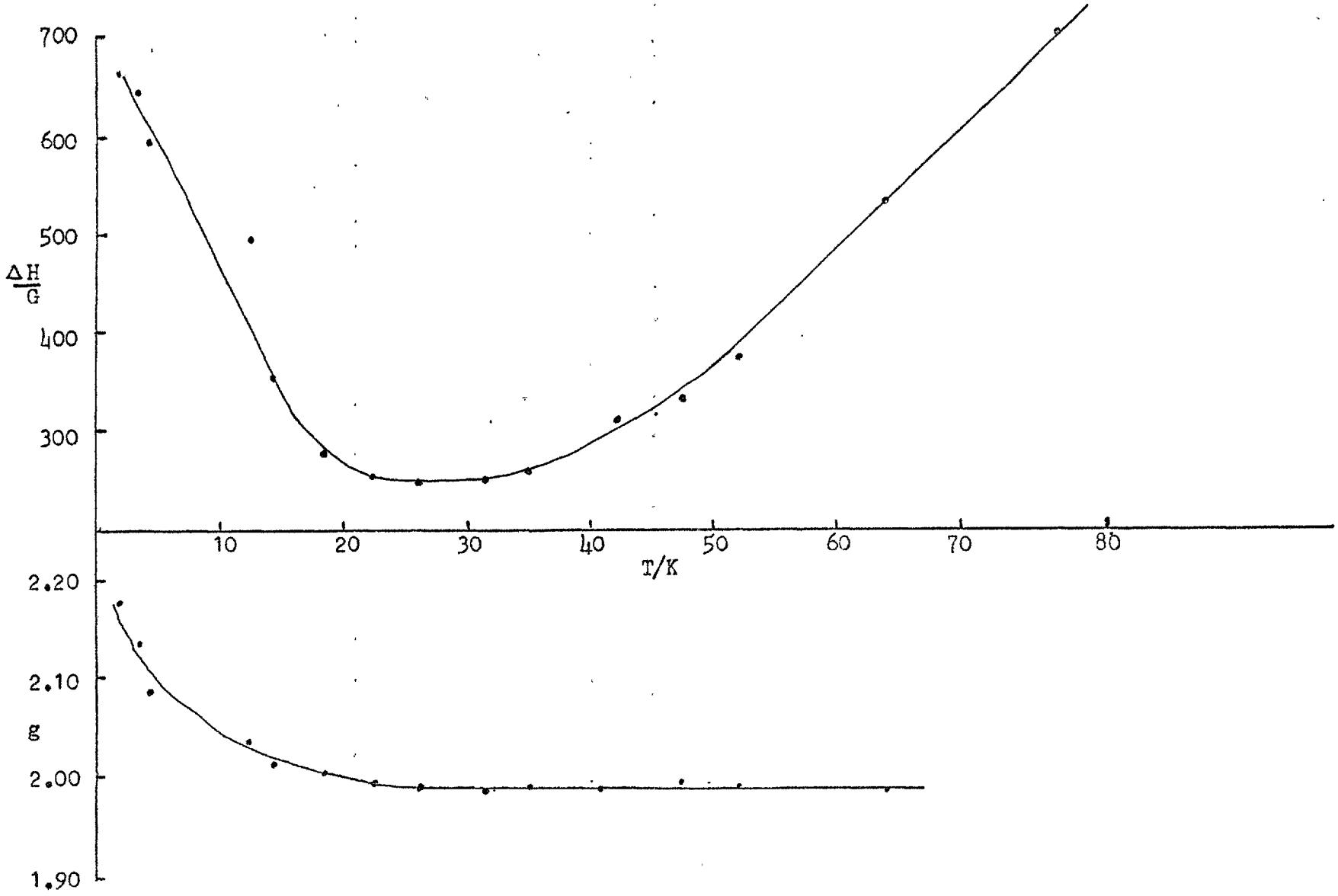

6.6 Compounds and Alloys with Mn.

The stoichiometry RB_5 where R is a rare earth element and B is a 3d transition metal occurs for Ni and Co in the 3d series (23). Mn and Fe form many compounds with the rare earths, RB_2, R_6B_{23} being common to both elements, but not RB_5. Therefore it is uncertain how much Fe or Mn may be substituted into $LaNi_5$ before precipitation of another phase occurs.

Samples were made of $LaNi_5$ with 5at.% Mn and 0.5 and 5at.% Fe. Examination of these compounds under the microscope and by microprobe analysis revealed that only one phase was present. Unfortunately no magnetic resonance was observed in these compounds. The $LaNi_5$- Mn sample showed a ferromagnetic transition in the electrical resistivity at 3.4K, the data is shown in Fig.44. Therefore Mn possesses a moment in these compounds.

The non-observation of a resonance in the alloys containing iron is not unduly surprising as the resonance of Fe has not yet been observed in any metallic system. Hirst (52) has attempted to explain this and the negative epr results in general for the 3d transition metals apart from Mn.

He showed that the orbital degrees of freedom are crucially important in epr and included them in a general form of the s-d interaction. This was based on a Hunds-rule L-S ground state within the configuration $3d^n$ appropriate to the ion under consideration, he then projected L onto the orbital ground state in the crystal field. When the crystal field orbital ground state is degenerate then the impurity has an effective orbital degree of freedom. As only spin magnetization of the conduction electrons can participate in the bottlenecking process, relaxation between the conduction electrons orbital angular momentum and the impurity cannot be short circuited

and hence a strong broadening of the line occurs. From Hirst's results a resonance of the single ion type would not be expected from Fe in a metallic host.

The Mn resonance has been observed in a number of hosts, Cu-Mn (43), Pd-Mn (38) but not in other alloys,where from other measurements the Mn ion clearly has a moment. For example, Taylor (38) has failed to observe a resonance in either Pt or Rh for concentrations at which a moment is known to exist from resistivity and magnetic susceptibility measurements.

To observe a resonance at reasonable temperatures (above 2K) either the thermal broadening of the line must not be excessive or the resonance bottleneck must be sufficiently strong to reduce the thermal linewidth. The latter effect is responsible for the presence of a resonance in CuMn.

Pd is a d-like host; therefore Pd-Mn shows no bottleneck (for the reasons mentioned in section 1) and the probable reason for observing a resonance line is that the thermal broadening is reduced by exchange enhancement effects (see equation 21, ch.4). Both Rh and Pt are exchange enhanced but not to the extent of Pd and perhaps this is one reason for the non-observation of a resonance in these alloys.

However, the data presented in Figs.45 and 46 tends to indicate another mechanism. The epr of two samples of PdPt-Mn was observed from 1.8K to a temperature at which the signal intensity was too weak to be useful. The slope of the linewidth for both $(Pd_{0.95}Pt_{0.05})$ 2%Mn and $(Pd_{0.99}Pt_{0.01})$ 2%Mn is 54 GK^{-1}. This is more or less the same value that was reported by Coles et al (41) for the Pd 2.3%Mn alloy, they gave a value of $d\Delta H/dT = 55\ GK^{-1}$.

It would be expected that if a large thermal broadening was responsible for the non-observation of the epr in PtMn then increasing

the Pt concentration in PdPt-Mn would increase the Korringa slope but this does not seem to happen. The residual linewidth at T = OK is defined as the linewidth extrapolated from the Korringa slope. This increases as the amount of Pt is increased, $\Delta H_{res} \sim$ 180G for the 1at.% Pt alloy and $\Delta H_{res} \sim$ 680G for the 5at.% Pt alloy. No resonance was observed for the 10at.% Pt alloy. Clearly if the residual linewidth of any system is large enough the observation of an epr line is not going to be possible.

To give significance to residual linewidths is hazardous as no theoretical framework exists. Some authors (56) (57) have measured the residual linewidths and referred to them as measures of δ_{iL}, the direct relaxation rate of the localized spins to the lattice, but it is by no means obvious that this is so. The widths are probably due to a combination of effects, for example, unresolved hyperfine and fine structure and inhomogeneous broadening due to interactions.

Fig.44 $LaNi_5$- 5at.% Mn.

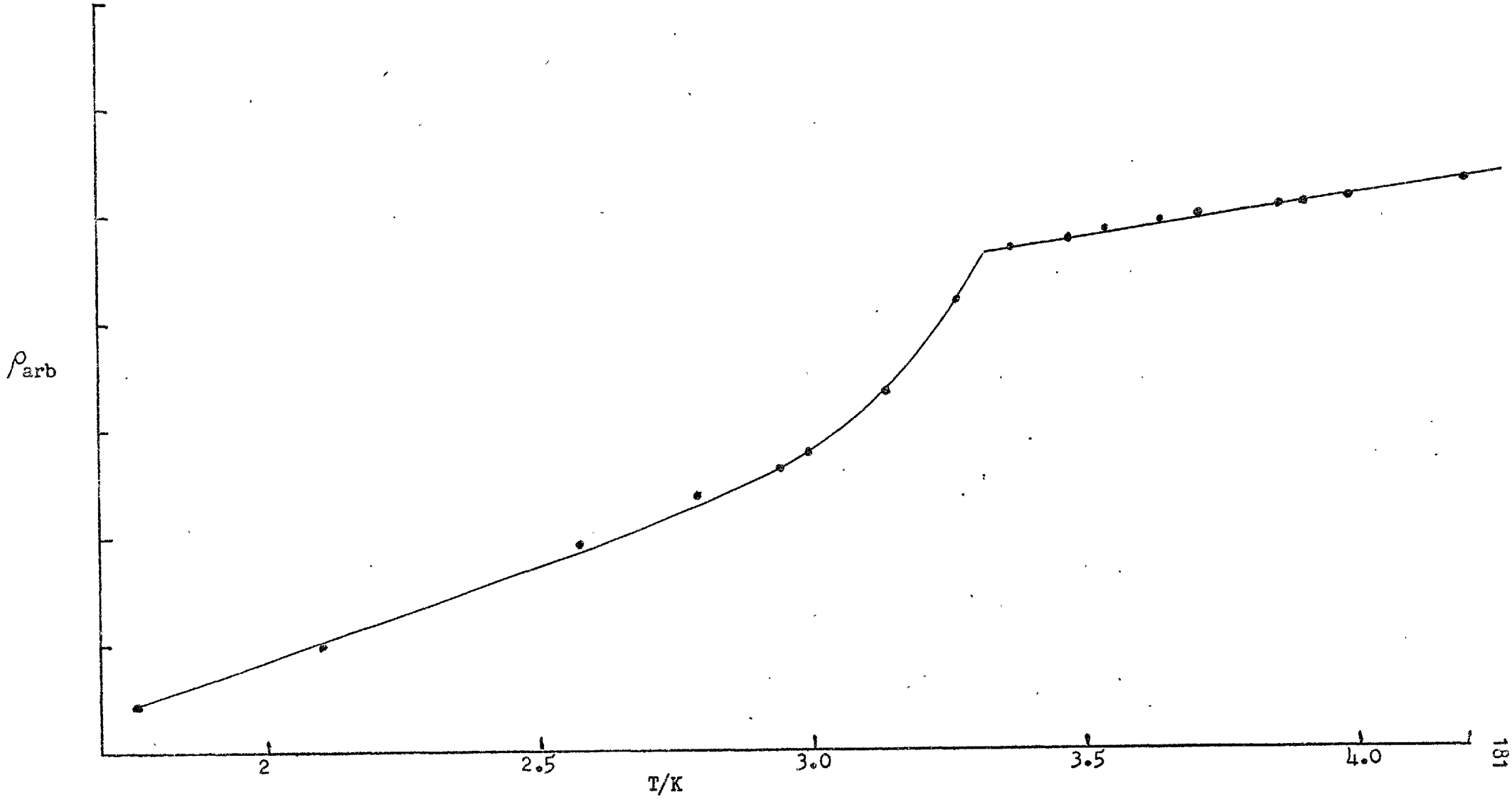

FIG.45 $(Pd_{0.95}Pt_{0.05})$2at.% Mn

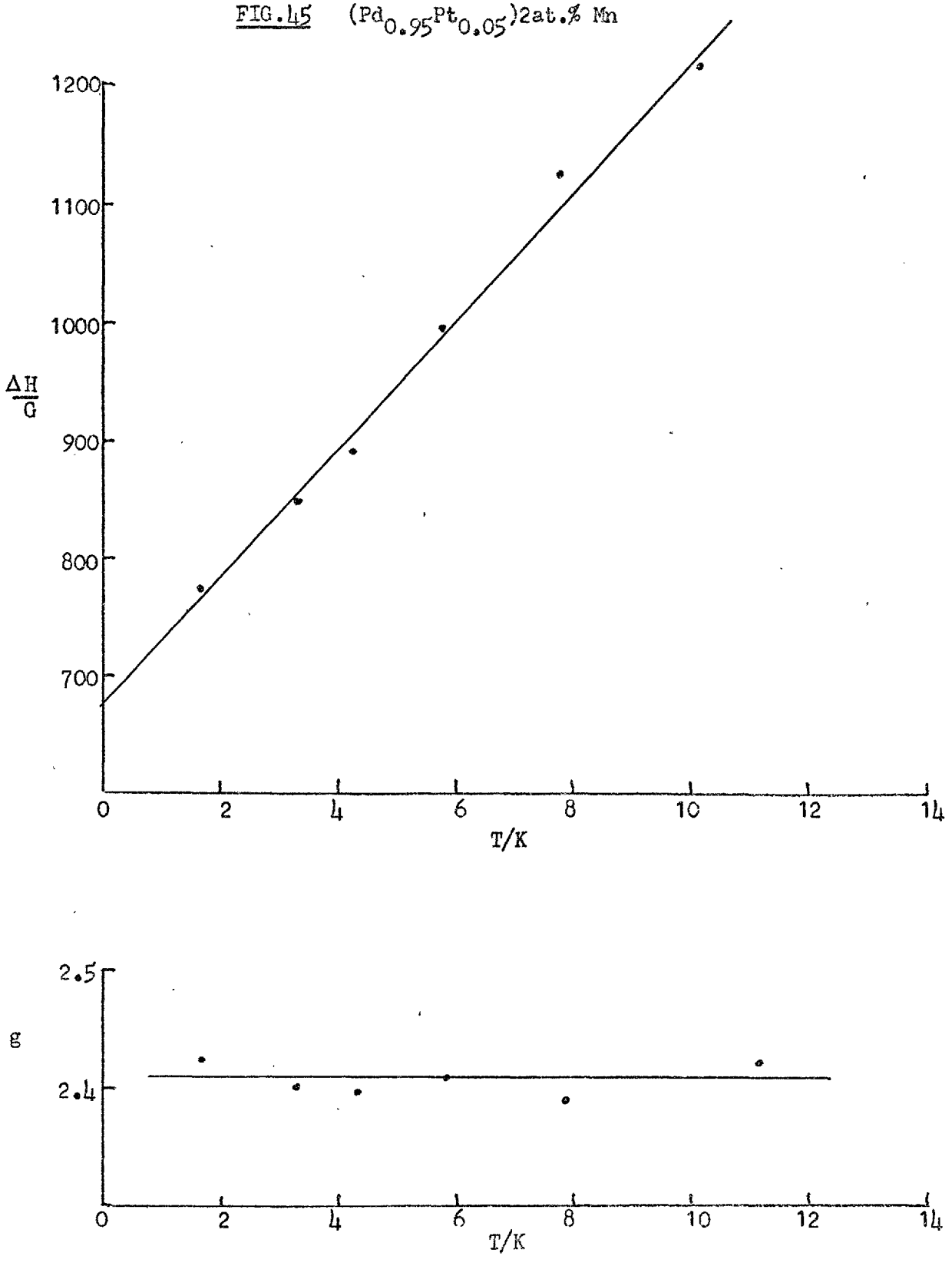

FIG. 46 $(Pd_{0.99}Pt_{0.01})$2at.% Mn

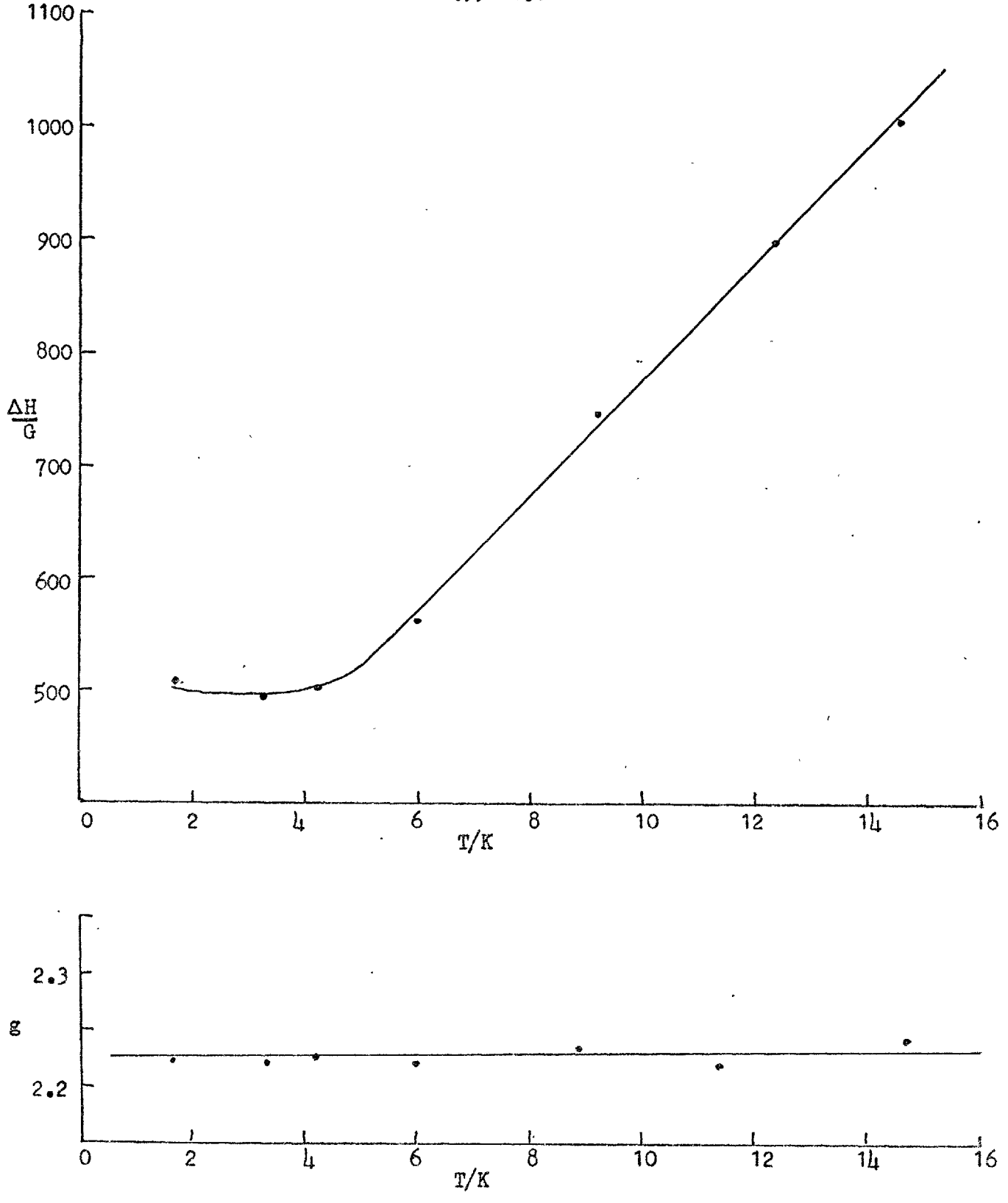

REFERENCES CHAPTER 6

1. SHALTIEL, D., WERNICK, J.H., WILLIAMS, H.J. and PETER, M., Phys. Rev. 135, A1346 (1964).

2. DAVIDOV, D. and SHALTIEL, D., Phys. Rev. Lett., 21, 1752 (1968).

3. MALE, S.E. and TAYLOR, R.H., J. Phys. F: Metal Phys., 5, L26 (1975).

4. BUSCHOW, K.H.J. and VAN MAL, H.H., J. Less. Comm. Met., 29, 203 (1972).

5. TAYLOR, R.H., Adv. in Phys. (to be published).

6. COLES, B.R., GRIFFITHS, D., LOWIN, R.J., and TAYLOR, R.H., J. Phys. C, 3, L121. (1970).

7. WATSON, R.E., KOIDE, S., PETER, M. and FREEMAN, A.J., Phys. Rev. A, 167, 139 (1965).

8. DAVIDOV, D., ORBACH, R., RETTORI, C., SHALTIEL, D., TAO, L.J. and RICKS, B., Solid St. Comm., 10, 451 (1972).

9. CAMPBELL, I.A., J. Phys. F, 2, 147 (1972).

10. TAYLOR, R.H. and COLES, B.R., J. Phys. F: Metal Phys. 4, 303 (1974).

11. YAFET, Y., J. Appl. Phys., 39, 853 (1968).

12. TAYLOR, R.H. and COLES, B.R., J. Phys. F: Metal Phys. 5, 121 (1975).

13. VAN VLECK, J.H., Phys. Rev., 78, 266 (1950).

14. BAGGULEY, D.M.S., LIESEGANG, J. and ROBINSON, K., J. Phys. F: Metal Phys., 4, 594 (1974).

15. COTTET, H., Thesis, University of Geneva (1971).

16. DAVIDOV, D., LOTEM, H. and SHALTIEL, D., Phys. Lett., 28A, 672 (1969).

17. SCHMIDT, H.K., SCHAFER, W., KELLER, G. and ELSCHNER, B., Phys. Lett, 38A, 201 (1972).

18. RETTORI, C., KIM, H.M., CHOCK, E.P. and DAVIDOV, D., Phys. Rev. B10, 1826 (1974).

19. CRANGLE, J. and SCOTT, W.R., J. of Appl. Phys. Vol. 36, No. 3 921, (1965).

20. HICKS, T.J., HOLDEN, T.M. and LOW, G. G., J. Phys. C, 1, 538 (1968).

21. LING, P.C. and HICKS, T.J., J. Phys. F: Metal Phys., 3, 697 (1973).

22. URSU, T. and BURZO, E., J. Mag. Res., 8, 274 (1972).

23. TAYLOR, K.N.R., Adv. in Phys. 20, 551 (1971).

24. NESBITT, E.A., WILLIAMS, H.J., WERNICK, J.H. and SHERWOOD, R.C., J. Appl. Phys. 33, 1674 (1962).

25. SHALTIEL, D. and WERNICK, J.H., Phys. Rev. A245, 136 (1964).

26. MARZOUK, N., CRAIG, R.S., and WALLACE, W.E., J. Phys. Chem. Sol. 34, 15 (1973).

27. GIVORD, G. and GIVORD, F. and LAMAIRE, R., J. de Phys. 32, C1-668 (1971).

28. REIDI, P.C., Private Communication.

29. SCHINDLER, A.I. and RICE, M.J., Phys. Rev. 164, 759 (1967).

30. LEDERER, R. and MILLS, D.L., Phys. Rev., 165, 837 (1968).

31. STEWART, A.M. and COLES, B.R., J. Phys. F: Metal Phys. 4, 458 (1974).

32. FISK, Z., TAYLOR, R.H., AND COLES, B.R., J. Phys. C,4,L292 (1971).

33. SHULL, C.G., STRAUSER, W.A. and WOLLAN, E.O., Phys. Rev. 83, 333 (1951).

34. BURZO, E. and URSU, T., Sol. St. Comm. 9, 2289 (1971).

35. ARROTT, A., Phys. Rev., 108, 1394 (1957).

36. BATES, L.F., Modern Magnetism, Cambridge at the University Press (1939).

37. VAN DAM, J.E., Thesis, University of Leiden (1973).

38. TAYLOR, R.H., Thesis, (1972), University of London.

39. THOLENCE, J.L. and TOURNIER, R., J. de Phys. 35, C, 4-229 (1974).

40. KOOPMANN, G., ENGEL, U., BABERSCHKE, K. and HUFNER, B., Sol. St. Comms., 11, 1197 (1972).

41. COLES, B.R., JAMIESON, H., TAYLOR, R.H., TARI, A., J. Phys. F: Metal Phys. 5, 565 (1975).

42. SARKISSIAN, B.V.B., Thesis, University of London. (1975).

43. GRIFFITHS, D., Proc. Phys. Soc., 90, 707 (1967).

44. TAYLOR, R.H., J. Phys. F: Metal Phys. 3, L110 (1973).

45. HACKER, H., GUPTA, R. and SHEPPARD, M.L., Phys. Stat. Sol., 9,601 1972.

46. SCHAFER, W., SCHMIDT, H.K., ELSCHNER, B. and BUSCHOW, K.H.J. Phys. Lett. A, 33, 23 (1970).

47. PETER, M., SHALTIEL, D., WERNICK, J.H., WILLIAMS, J.H.,MOCK, J.B. and SHERWOOD, R.C., Phys. Rev., 126, 1395 (1962).

48. HARRIS, I.R., MANSEY, R.C. and RAYNOR, G.V., J. Less Common Metals, 9, 270 (1965).

49. BUSCHOW, K.H.J., FAST, J.F., VAN DIEPEN, A.M. and DE WIJN, H.W., Phys. Stat. Sol., 24, 715 (1967).

50. MAPLE, M.B., Thesis, University of California, (1969).

51. BENNETT, M., Private Communication.

52. HIRST, L.L., Adv. Phys. 21, 759 (1972).

53. WEISMAN, I.D., BENNETT, L.H., MCALISTER, A.J. and WATSON, R.E., Phys. Rev., B11, 82 (1975).

54. DAVIDOV, D., CHELKOWSKI, A., RETTORI, C., ORBACH, R. and MAPLE, M.B., Phys. Rev., 7, 1029 (1973).

55. SHALTIEL, D., WERNICK, J.H. and JACCARINO, V., J. Appl. Phys., 35, 978 (1964).

56. GOSSARD, A.C., KOMETANY, T.Y. and WERNICK, J.H., J. Appl. Phys., 39, 849 (1968).

57. SHULTZ, S., SHANABARGER, M.R. and PLATZMAN, P.M., Phys. Rev. Letts., 19, 749 (1967)

58. MOTT, N.F. and JONES, H., The Theory of the Properties of Metals and Alloys, Clarendon Press, Oxford (1936).

APPENDIX 1

The Magnet Current Controller.

The output transistors of the current supply for the electromagnet deliver a considerable current into an inductive load. If the output current is sharply reduced the inductive nature of the load causes a back e.m.f. across the transistors which rises to a high value while the current is still large; this takes the devices out of their safe operating area and damage may therefore occur.

To prevent the current from being quickly reduced and thereby over stressing the output transistors Dr.D.Griffiths designed and constructed a digital controller which will now be briefly described.

The basic idea is that a series of resistors, 100, 200, 400 and 800Ω, which effectively controls the current, are selected by a counter in a binary sequence giving values between 0 and 1500Ω in 100Ω steps. Zero ohms corresponds to zero current and 1500 to a current of 7.5 A. The output current is linearly dependent on the resistance therefore the 100Ω steps give ½ amp increments. Each resistor has a relay in parallel and this is switched on/off by the counter. The counter is a 191 reversible up/down counter, the outputs of which directly drive the reed relays.

The rate at which the steps can be made is regulated by an internal clock (essentially a 555 timer). The delay time which is used for switching the relays depends on the power supply and load; it was found that delays of 1 s per step was sufficient to prevent over stressing of the output transistors.

With the up/down pin of the 191 at 0 the unit counts from 0000 to 1111 at its data output. A 1111 ouput opens all the relays (0 closed) and hence the current has a maximum value. The up/down signal can be

generated manually or automatically. When 0000 or 1111 is reached an up/down switch must be changed to enable the unit to count in the reverse direction; the so-called "lock-up" condition is indicated by an l.e.d. The state of the relays at a given time and hence the magnitude of the current passing through the magnet, is indicated by a set of four l.e.d's.

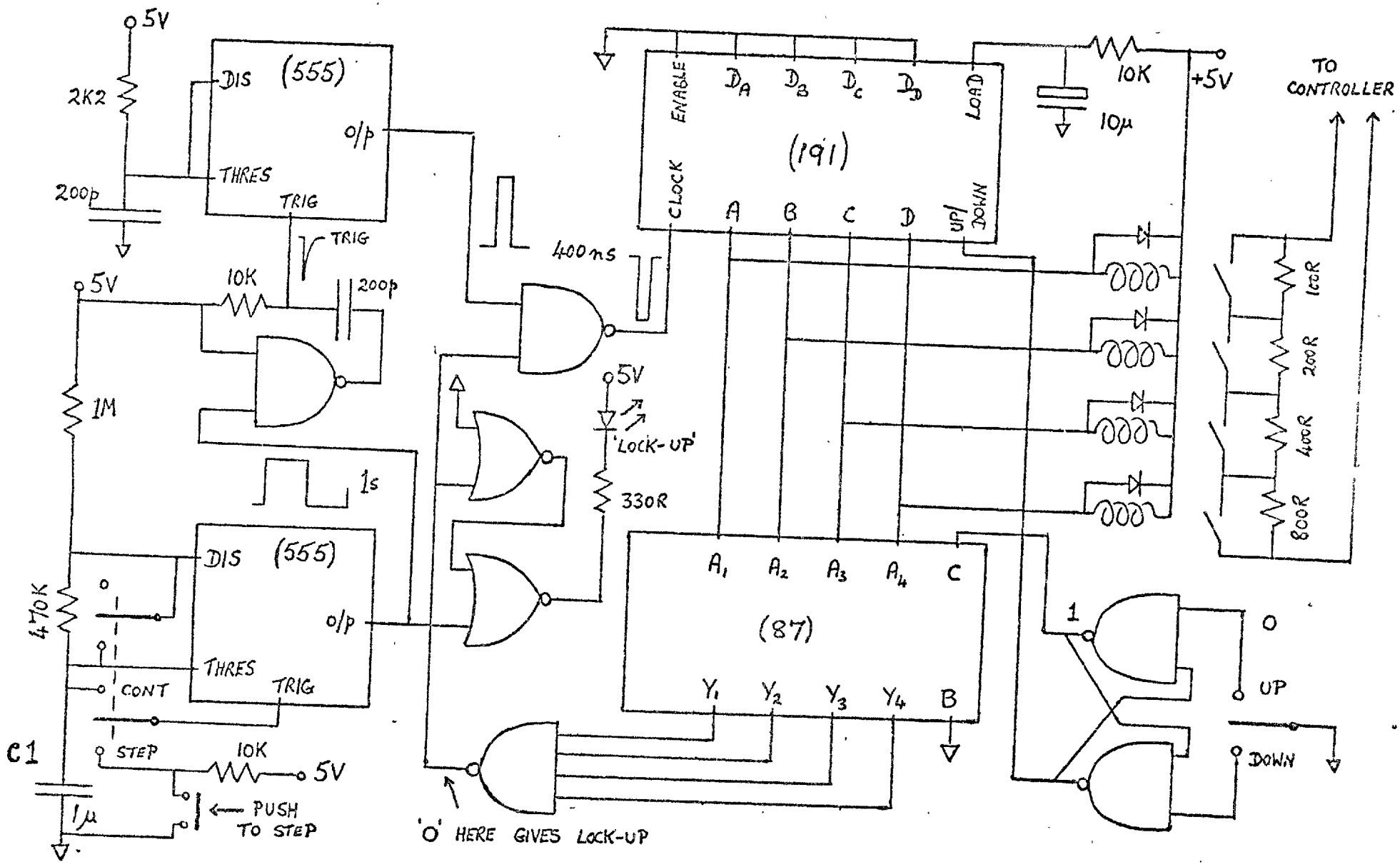
5V
2K2
200p
DIS
(555)
O/P
THRES
TRIG
TRIG
400ns
10K
200p
5V
1M
1s
DIS
(555)
O/P
THRES
TRIG
CONT
STEP
10K
5V
PUSH TO STEP
C1
1µ
470K
'O' HERE GIVES LOCK-UP
5V
'LOCK-UP'
330R
ENABLE
D_A D_B D_C D_D
LOAD
(191)
CLOCK
A B C D
UP/DOWN
10K
10µ
+5V
TO CONTROLLER
100R
200R
400R
800R
A_1 A_2 A_3 A_4 C
(87)
Y_1 Y_2 Y_3 Y_4 B
1
0
UP
DOWN

FIG.1

APPENDIX 2.

FIG.1. Correction for ΔH.

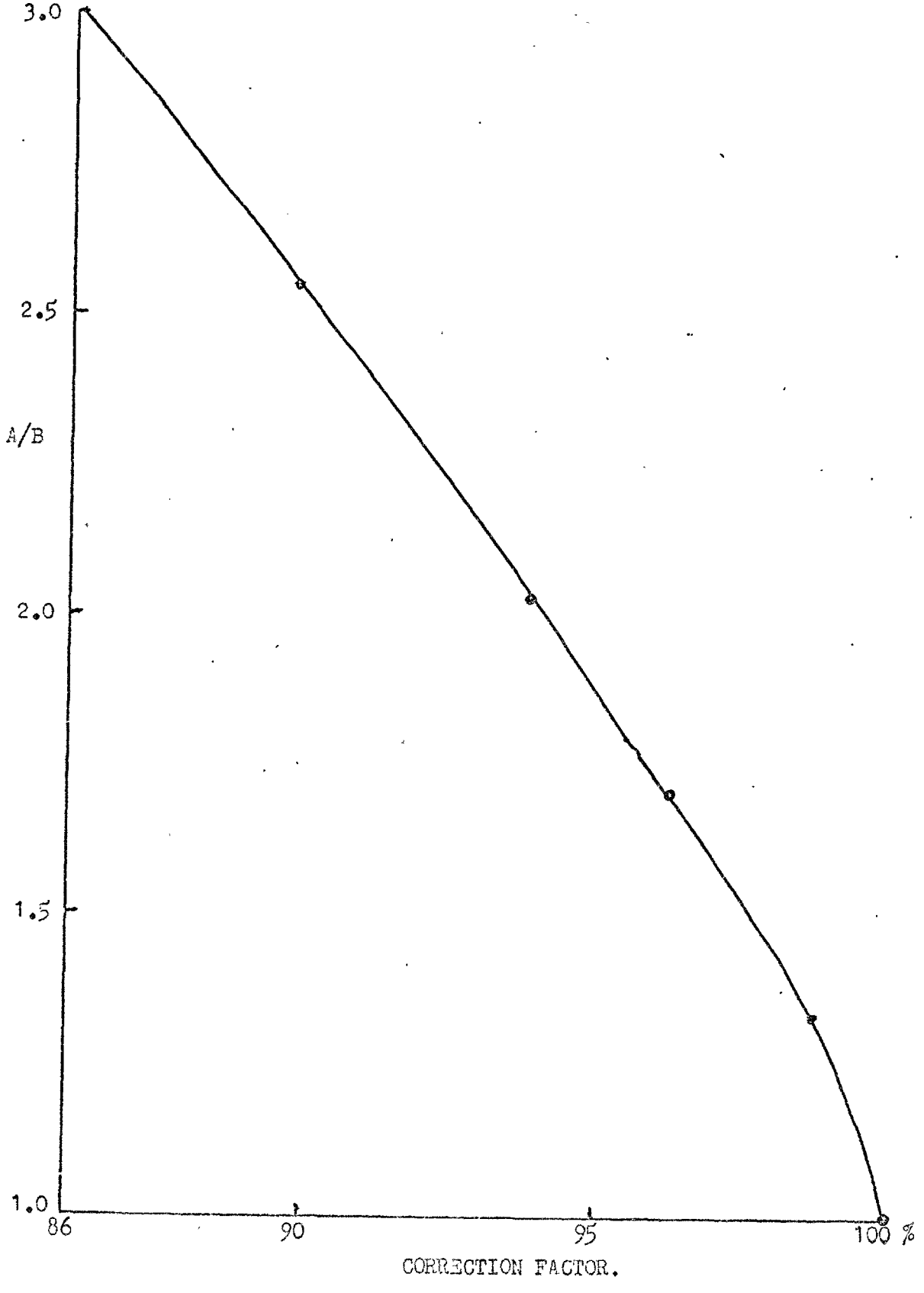

FIG.2. Correction for H_x.

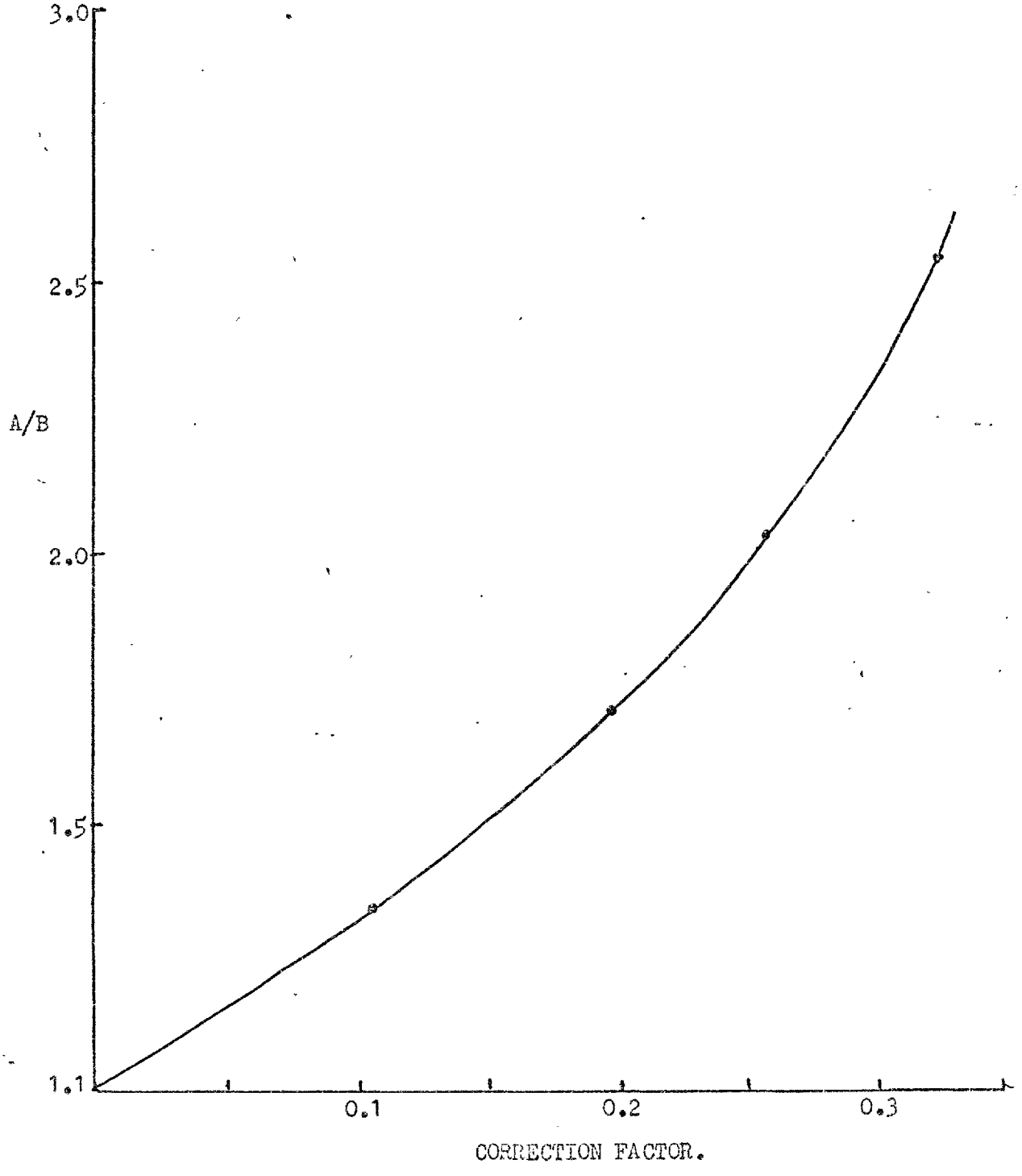

J. Phys. F: Metal Phys., Vol. 5, March 1975. Printed in Great Britain.

LETTER TO THE EDITOR

Electron spin resonance in $LaNi_5$–Gd alloys—absence of dynamic effects in the bottleneck

S E Male and R H Taylor

Department of Physics, Imperial College, London, SW7

Received 19 November 1974

Abstract. The linewidth and g-shift as a function of temperature has been studied for various concentrations of $Gd(4f^7)$ in the intermetallic compound $LaNi_5$. Both parameters show a strong temperature dependence which has previously been ascribed to dynamic effects in the electron spin resonance bottleneck. We show that this temperature dependence can be better explained by considering the effects of magnetic ordering in the compounds.

The electron spin resonance behaviour of localized moments in metals depends critically upon the strength of thermal contact between the local moment, condution electrons and lattice. Hasegawa (1959) showed theoretically that a weak coupling between the conduction electrons and the lattice would lead to a suppression of the g-shift for an s-state ion and a strong reduction in the slope of the linewidth as a function of temperature in the paramagnetic regime.

This effect, known as the electron spin resonance bottleneck, has been widely observed. The archetypal systems are Mn in Cu and Ag (Gossard *et al* 1967) but it has also been observed in a variety of other systems such as Gd in $LaAl_2$ (Taylor 1973) Gd in YAl_2 (Schafer *et al* 1972) Gd in YAg (Weimann *et al* 1972) $Eu(4f^7)$ in Ca (Schmidt 1972) and $Eu(4f^7)$ in $LaAl_2$ (Koopman *et al* 1972).

The treatment of Hasegawa leads to an expression for the observed g-shift at a given temperature and concentration of the form

$$\Delta g = \frac{(\delta_{sL})^2 \, \Delta g_0}{(\lambda \gamma \chi_i H)^2 + (\delta_{sL} + \delta_{sf})^2} \tag{1}$$

where δ_{sL} is the conduction electron–lattice relaxation rate, δ_{sf} is the conduction electron-local moment relaxation rate, γ is the gyromagnetic ratio (assumed to be the same for conduction electrons and local moments), λ is a molecular field coupling constant, H is the applied field, χ_i is the susceptibility of the Gd ions and Δg_0 the full g-shift in the absence of a bottleneck.

In many cases the term $(\lambda \gamma \chi_i H)^2$ in the denominator can be neglected but as the temperature is reduced it may become comparable with $(\delta_{sf} + \delta_{sL})^2$ and this leads to a reduction in the g-shift and a strong dependence of the g-value on the applied field. It is the influence of this term which leads to the so-called dynamic effects in the ESR bottleneck. It has been suggested that such effects are responsible for the observed behaviour

of Gd in $LaNi_5$ (Davidov and Shaltiel 1968) Gd in $LaRu_2$ (Davidov *et al* 1969) and for Eu($4f^7$) in Yb (Schmidt *et al* 1972). Until very recently dynamic effects had not been observed in any other systems (although expected and carefully looked for) but recently Rettori *et al* (1974) have claimed to have observed fairly small effects at pumped ^3He temperatures for Gd in $LuAl_2$ and YAl_2.

In this letter we set out to show that in the first of the cases above, $LaNi_5$–Gd, the behaviour attributed to dynamic effects by Davidov and Shaltiel was due rather to the onset of magnetic ordering in the alloy system.

We have thus investigated the electron spin resonance behaviour of Gd substituted on to La sites in the compound $LaNi_5$. The samples were produced by melting the constituents in an argon arc furnace and each ingot was turned and melted several times to ensure homogeneity. Weight losses were negligible in all the alloys used for ESR measurements and metallographic examination of the brittle ingots showed the alloys to be single phase. X ray analysis on a number of the samples confirmed the $CaCu_5$ structure. The measurements were performed on unannealed powders (ground under acetone) on a conventional 3 cm (X-band) spectrometer. The 'true' values of the resonant field and linewidth were deduced by the normal procedures from the observed differential lineshape which was always close to the value $A/B = 2{\cdot}55$ for particles much larger than the skin depth.

Our results are shown in figures 1 and 2 and the relevant data summarized in table 1. In addition to working at a different frequency to Davidov and Shaltiel we have also extended the measurements to higher Gd concentrations.

In the lower concentration alloys ($<1\%$ Gd) the g-shifts are temperature independent and as expected for a strongly d-like host (Coles *et al* 1970) large and negative.

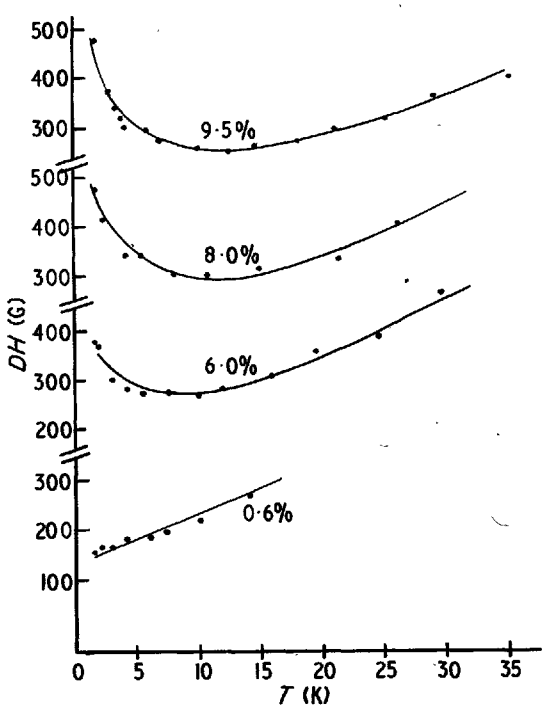

Figure 1. ESR linewidth as a function of temperature for a number of concentrations of Gd in $LaNi_5$.

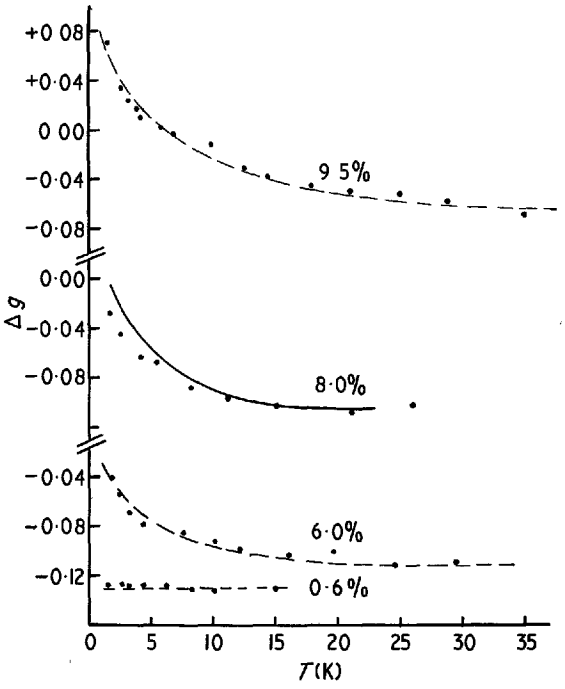

Figure 2. g-shift as a function of temperature for a number of concentrations of Gd in $LaNi_5$. The full curve for the 8% alloy shows the form of the magnetization in a field of 3 2 kG (see text).

Likewise, the linewidth as a function of temperature show no minima and are still Korringa-like until the lowest temperatures. At higher concentrations however the high temperature value of the g-shift becomes smaller (in agreement with the trend of the results of Davidov and Shaltiel) and at lower temperatures for these alloys it shows strong temperature dependence. It is this form of variation of g with temperature which Davidov and Shaltiel sought to ascribe to dynamic effects. However, we note in our data that not only is the g-shift reduced on lowering the temperature for a given alloy, but that for concentrations in excess of about 7 at % the sign of g changes at the lowest temperatures. It is clear from the form of expression (1) above that no such change of sign is admissible from bottleneck considerations. We suggest that a similar change in sign would have been observed by Davidov and Shaltiel for alloys containing higher concentrations of Gd.

Table 1. ESR data for $(La_{1-x}\,Gd_x)\,Ni_5$

x	g_{PM}	$dDH/dT\,(GK^{-1})$
0 003	1 86(5) ± 0·01	—
0·006	1·87(2) ± 0·01	10 ± 0·5
0·025	1·88(3) ± 0 01	9·3 ± 0·5
0·045	1·88(8) ± 0·01	9·6 ± 0·5
0 060	1·89(0) ± 0·01	9·2 ± 0·5
0·080	1·89(5) ± 0·01	9 5 ± 0·5
0·095	1·93(0) ± 0·01	9·0 ± 0·5

We have also attempted to fit expression (1) to the form of our data. If we take the values of the parameters used by Davidov and Shaltiel to fit their Q-band data, the full g-shift would be reduced by dynamic effects by only about one fifth for a 5% Gd alloy at 2 K in our resonant field (3·2 kOe). In fact we observed a reduction of closer to one half.

It is also clear from our data that the linewidth passes through a strong minimum as a function of temperature for Gd concentrations in excess of 1%. The temperature at which this minimum occurs corresponds roughly with the temperature at which the g-shift begins to reduce and clearly increases with increasing concentration. Similar behaviour has been observed in both the g-value and linewidth of the systems $LaAl_2$–Gd (Taylor 1973) and Pd–Gd (Taylor and Coles 1974) and both were shown to be attributable to the onset of magnetic ordering in the systems. In the latter case, the evidence suggests very strongly that the system is unbottlenecked at all concentrations and temperatures. Davidov and Shaltiel did not plot their linewidths explicitly as a function of temperature, but in their figure 2 showed the linewidth as a function of concentration at 4·2 K. They were unable to explain the form of this data consistently within the framework of their interpretation, but their plot is clearly explicable in terms of magnetic ordering (Taylor and Coles 1974, 1975).

In order to add further credence to our explanation we have measured† the magnetization of our 8% sample as a function of temperature in our resonant field value. Allowing for the effects of small amounts of free nickel in the samples and assuming an average demagnetizing factor of 2·8 (which is in very good agreement with values for this taken in previous systems such as $GdAl_2$(2·7)) (Taylor and Coles 1975) we obtain the solid curve in figure 2 which is in good agreement with our ESR data.

The compound $GdNi_5$ orders at about 31 K and it might thus be argued that the observed linewidth minima and temperature dependent g-values occur at temperatures far above the Curie point for the diluted alloys. On a naive model one might assume that a 10% Gd in $LaNi_5$ compound would order magnetically at a temperature below 3 K, whilst the anomalies observed in ESR set in at 10–20 K. Resistivity measurements on the $LaNi_5$–Gd system (to be published) show however that up to about 20% Gd there is a relatively steep rise in Curie temperature followed by a flattening out. Indeed a 10% Gd in $LaNi_5$ alloy showed signs of ordering at about 5 K. This fact, together with the clear indications in previous work (Taylor and Coles 1974, 1975) that ESR appears to be remarkably sensitive to spin correlations above the ordering temperature would appear to cover this objection.

The form of the Curie temperature as a function of concentration appears to be similar to the form of g as a function of concentration (figure 3). We believe that this may be understood as a gradual exhaustion of the response of the strongly enhanced d-band of the host. Similar curvature in both g and T_c as a function of concentration was remarked upon in the somewhat similar system Gd in Pd (Taylor and Coles 1974); here of course there will also be the added effect of band filling as Gd is added to Pd, but the above mechanism may also be important.

In conclusion, in this work we believe that we have demonstrated that dynamic effects in the ESR bottleneck are not responsible for the temperature dependence of the g-shift for Gd in $LaNi_5$, but that instead, the behaviour arises from the effects of magnetic ordering. This restores, furthermore, $LaNi_5$ to the ranks of the strongly d-like hosts

†We are indebted to Dr J B Dunlop of the University of Sheffield for performing these measurements and to Professor C Rizzuto of the Istituto di Fisica, Genoa for allowing us to use the facilities of his laboratory.

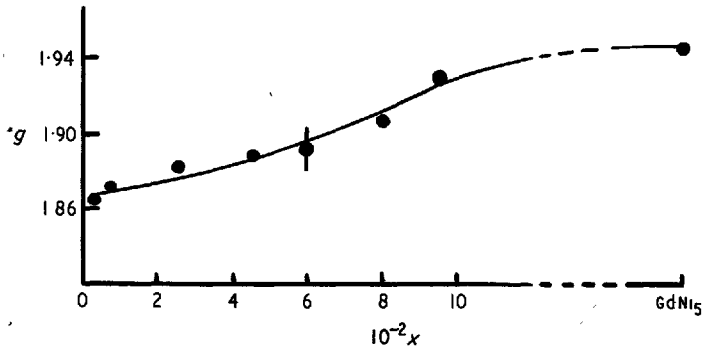

Figure 3. Paramagnetic g-shift as a function of Gd concentration across the $(La_{1-x}\ Gd_x)\ Ni_5$ system. The point for the compound $GdNi_5$ is taken from the paper of Burzo and Ursu (1971)

which do not give an ESR bottleneck on addition of s-state impurities. It would seem to us likely from the form of the data that $LaRu_2$–Gd (Davidov *et al* 1969) behaves similarly to $LaNi_5$. We would maintain, therefore, that the only unequivocal evidence obtained experimentally for the expected dynamic effects is that of Schmidt *et al* (1972) on Eu($4f^7$) in Yb, where the frequency dependence of ESR data is particularly striking. Our results show that the most convincing evidence for dynamic effects must always come from systems where while the g-shift is reduced by the bottleneck the effect of ordering is to increase it and Eu($4f^7$) in Yb is such a case.

We wish to thank Dr H E N Stone for help with the preparation of the alloys and Professor B R Coles and Dr N Rivier for useful discussions. During the course of the work one of us (SEM) was in receipt of an SRC studentship.

References

Burzo E and Ursu I 1971 *Solid St. Commun.* **9** 2289–93
Coles B R, Griffiths D, Lawin R J and Taylor R H 1970 *J. Phys.* C: *Solid St. Phys.* **3** L121–2
Davidov D, Lotem H and Shaltiel D 1969 *Phys. Lett.* **28A** 672–3
Davidov D and Shaltiel D 1968 *Phys. Rev. Lett.* **21** 1752–5
Gossard A C, Heeger A J and Wernick J H 1967 *J. Appl. Phys.* **38** 1251–5
Hasegawa H 1959 *Prog. Theor. Phys.* **21** 483–500
Koopman G, Engel U, Baberschke K and Hufner S 1972 *Solid St. Commun.* **11** 1197–200
Rettori C, Kim H M, Chock E P and Davidov D 1974 *Phys. Rev.* B **10** 1826–35
Schafer W, Schmidt H K, Elschner B and Buschow K H J 1972 *Z Phys.* **254** 1
Schmidt H K 1972 *Z. Naturf.* **27a** 191–7
Schmidt H K, Schafer W, Keller G and Elschner B 1972 *Phys. Lett.* **38A** 201–2
Taylor R H 1973 *J. Phys.* F: *Metal Phys.* **3** L110–4
Taylor R H and Coles B R 1974 *J. Phys.* F: *Metal Phys.* **4** 303–14
—— 1975 *J. Phys.* F: Metal Phys. **5** 121–42
Weinmann G, Elschner B, Buschow K H J and van Stapele R R 1972 *Solid St. Commun.* **11** 871–4